Pharmacometric modelling and simulation to optimise paclitaxel combination therapy based on pharmacokinetics, cumulative neutropenia and efficacy

Inaugural-Dissertation

to obtain the academic degree
Doctor rerum naturalium (Dr. rer. nat.)
submitted to the Department of
Biology, Chemistry and Pharmacy
of Freie Universität Berlin

by
Andrea Henrich
from Ludwigsburg

Berlin 2017

Die folgende Arbeit wurde von 2013 bis 2017 unter der Leitung von Frau Prof. Dr. Charlotte Kloft am Institut für Pharmazie der Freien Universität Berlin angefertigt.

1. Gutachter: Frau Prof. Dr. rer. nat. habil. Charlotte Kloft

2. Gutachter: Herr PD Dr. med. et phil. nat. Markus Joerger

Disputation am: 4. Dezember 2017

Meinen Eltern und
meinem Bruder
für ihre Liebe
und Unterstützung

Table of content

Abbreviations and symbols

Parameters in italics

AC	Adenocarcinoma
AIC	Akaike Information Criterion
ALT	Alanine transaminase
AST	Aspartate aminotransferase
AUC	Area under the curve
AUC_{0-6h}	Area under the curve from time t = 0 to t = 6 h
AUC_{0-24h}	Area under the curve from time t = 0 to t = 24 h
$AUC_{0-\infty}$	Area under the curve from time t = 0 to infinity
$AUC_{6h-\infty}$	Area under the curve from time t = 6 h to infinity
B1	Baseline method 1
B2	Baseline method 2
$BASE_1$	Baseline of proliferating cells not affected by time-dependent depletion
$BASE_2$	Baseline of proliferating cells affected by time-dependent depletion
$BASE_{tot}(t)$	Total baseline of proliferating cells at time t in Model A
$BASE_{tot}(t_0)$	Total baseline of proliferating cells at time t = 0 in Model A
BILI	Bilirubin concentration
BL_i	Individually measured baseline value
BME	Bone marrow exhaustion
BQL	Below lower limit of quantification
BSA	Body surface area
BSL	Neutrophil concentration at baseline
BSL_{SD}	Baseline tumour size (sum of diamters)
$C(t_j)$	Concentration of a drug at observation time t_j

CBC	Complete blood count
Central	Central paclitaxel compartment
CEPAC-TDM	CESAR (Central European Society for Anticancer Drug Research) study of Paclitaxel Therapeutic Drug Monitoring
Circ	Circulating neutrophil cell compartment
$Circ(t)$	Concentration of circulating neutrophils at time t
$Circ(t_0)$	Concentration of circulating neutrophils at time t = 0
C_{6h}	Drug concentration at time t = 6 h
C_j	Drug concentration at observation j
C_{j+1}	Drug concentration at observation j + 1
Corr	Pearson correlation coefficient
CT	Computed tomography
CTC AE	Common Terminology Criteria for Adverse Events
cov	Covariate
$C_{Carbo}(t)$	Plasma concentration of carboplatin at time t
$C_{Cis}(t)$	Plasma concentration of cisplatin at time t
CL_{lin}	Clearance of paclitaxel in the linear phase of the saturable elimination
$C_{PTX}(t)$	Paclitaxel plasma concentration at time t
$C_{Platin}(t)$	Plasma concentration of carboplatin or cisplatin at time t, respectively
CrEL	Cremophor EL
CL_{CR}	Creatinine clearance
$cumhaz(t)$	Cumulative hazard at time t
$CV, \%$	Coefficient of variation
CYP	Cytochrome P450 enzyme
d_0	Sphere with tumour diameter at time t = 0
d_{1h}	Sphere with tumour diameter at time t = 1 h
df_k	Degrees of freedom for parameter k
Emax	Maximum effect

EBE	Empirical Bayes Estimates (individual PK or PD parameter estimates)
$EC_{50\,INT}$	Concentration of paclitaxel and carboplatin at which interaction was half INT
ECOG	Eastern Cooperative Oncology Group
$E_{drug}(t)$	Drug effect at time t inhibiting k_{prol} in Model A – C and k_{stem} in Model C
E_{drug2}	Additional time-dependent drug effect affecting $Base_2$ in Model A
E_j	Drug effect at observation j
E_{j+1}	Drug effect at observation j + 1
f	Function of mathematical model
FB	Feedback
FO	First-order estimation method
FOCE	First-order conditional estimation method
F_{prol}	Fraction of proliferating cells entering maturation chain and not entering quiescent cell cycle in Model B
frB	Fraction of $BASE_{tot}(t_0)$ not affected by depletion in Model A
ftr	Fraction of input in Prol via replication in Model C
g	Group covariate value
G3+, %	Percentage of patients with grade ≥ 3 neutropenia
G4, %	Percentage of patients with grade 4 neutropenia
G-CSF	Granulocyte colony-stimulating factor
GFR	Glomerular filtration rate
GM-CSF	Granulocyte macrophage colony-stimulating factor
GOF	Goodness-of-fit
H_0	Null hypothesis
$h(t)$	Hazard function
i	Individual (for i in 1,… N)
ID	Patient identification
INT	Maximal interaction
IPP	Sequential analysis method conditioned on the individual PK parameters

IPRED	Individual prediction
IQR	Interquartile range
IRES	Individual residuals
IWRES	Individual weighted residuals
j	Observation time point (for j in 1,… J)
k	Number of parameters estimated in a model
k	Model parameter (for k in 1,… K)
k_{13}	Distribution rate constant between Central and Per2
k_{21}	Distribution rate constant between Central and Per1
k_{31}	Distribution rate constant between Per2 and Central
k_{cycle}	Circulation rate constant within quiescent cell cycle in Model B
k_{depl}	Depletion rate constant of E_{drug2} in Model A
k_g	Zero-order tumour growth rate constant
k_{g0}	Exponential tumour growth rate in the Simeoni *et al.* [1] model
Km_{EL}	Paclitaxel concentration at half VM_{EL}
Km_{TR}	Paclitaxel concentration at half VM_{TR}
k_{prol}	Proliferation rate constant of cells in Prol
k_{stem}	Proliferation rate constant of cells in Stem
k_{tr}	Transition rate constant of maturation chain
LDH	Lactate dehydrogenase
LLOQ	Lower limit of quantification
LLN	Lower limit of normal
LT-HSC	Long-term haematopoietic stem cell
m	Simulation (for m in 1,… M)
M&S	Modelling and simulation
$MARPE_p$	Median absolute relative prediction error for parameter p
MID3	Model informed drug discovery and development

MDR	Multi-drug resistance
MMT	Mean maturation time
$MRPE_p$	Median relative prediction error for parameter p
N	Total number of individuals
NLME	Nonlinear mixed-effects
NPDE	Normalised prediction distribution errors
NSCLC	Non-small cell lung cancer
o	Occasion (for o in 1,… O)
OD, %	Percentage of patients overdosed ($T_{C>0.05}$ ≥ 31 h)
OFV	Objective function value
OFV_{current}	Objective function value for the current population
OFV_{prior}	Prior objective function value (penalty term)
OFV_{post}	Posterior objective function value
OS	Overall survival
pcVPC	Prediction-corrected visual predictive check
$pcY_{i,j}$	Prediction-corrected value of $Y_{i,j}$
PD	Pharmacodynamic(s)
$pde_{i,j}$	Prediction distribution error of individual i at observation j
Per1	1st peripheral compartment of paclitaxel
Per2	2nd peripheral compartment of paclitaxel
PFS	Progression-free survival
$P_{i,o,optimised}$	Parameter of individual i, at occasion o, obtained by optimised PK model
$P_{i,o,original}$	Parameter of individual i, at occasion o, obtained by original PK model
$P_{i,o,re-est}$	Parameter of individual i, at occasion o, obtained by *post-hoc* re-estimation
$P_{i,o,sim}$	Parameter of individual i, at occasion o, obtained by simulation
PK	Pharmacokinetic(s)
PPP	Sequential analysis method conditioned on fixed population PK parameter

PRED	Population prediction
$\overline{PRED}_{bin}$	Median of the population prediction of all observations in the respective bin
$PRED_{i,j}$	Population prediction for individual i and observation j
Prol	Proliferating cell compartment
Q	Intercompartmental clearance between Central and Per2
Q1	1st quiescent cell compartment in Model B
Q2	2nd quiescent cell compartment in Model B
R	Hessian matrix
R^{-1}	Fisher information matrix
R^2	Coefficient of determination
RECIST	Response evaluation criteria in solid tumours
r_{effect}	Ratio of efficacy parameters for carboplatin and paclitaxel (β_{carbo} and β_{PTX}, respectively)
RES	Residuals
$RPE_{p,i,o}$	Relative prediction error of parameter p, for individual i, at occasion o
RS_8	Relative change in tumour size at week 8
$RSE, \%$	Relative standard error
$RSE_k, \%$	Relative standard error of parameter k
$RSE_{{\omega_k}^2,CV}, \%$	Relative standard error of the interindividual variability of parameter k reported as $CV, \%$
S	Cross product gradient matrix
$S(t)$	Survival function
SCC	Squamous-cell carcinoma
SD	Standard deviation
SE_{ω_k}	Standard error of ${\omega_k}^2$
SE_k	Standard error of k
sh_ε	ε-shrinkage
$sh_{\eta,k}$	η-shrinkage of parameter k

$sh_{\kappa,k}$	κ-shrinkage of parameter k
SL	Slope factor of linear drug effect of paclitaxel
SL_{Carbo}	Slope factor of linear drug effect of carboplatin
SL_{Cis}	Slope factor of linear drug effect of cisplatin
SL_{Platin}	Slope factor of linear drug effect of platinum-based drugs
ST-HSC	Short-term haematopoietic stem cell
Stem	Stem cell compartment in Model C
T	Event time, in this work survival time
t	Time
TA	Tumour assessment
$T_{C>0.05}$	Time $C_{PTX}(t)$ above 0.05 µmol/L in respective cycle
TEI	Time efficacy index
TEI_{carbo}	Time efficacy index of carboplatin
TEI_{PTX}	Time efficacy index of paclitaxel
t_j	Time point of observation j
t_{j+1}	Time point of observation j + 1
T_{median}	Median survival time
TNM	TNM staging system based on tumour size (T), involvement of nearby lymph nodes (N) and the presence of metastasis (M)
Transit	Transit compartment of maturation chain (3 for Model A – C)
TS	Tumour size
TS_{max}	Maximal tumour size
TTE	Time-to-event
TTP	Time to progression
UD, %	Percentage of patients underdosed ($T_{C>0.05}$ < 26 h)
ULN	Upper limit of normal
V	Volume of distribution
V_1	Central volume of distribution

V_3	Volume of distribution of Per2
$\mathrm{V(t)}$	Tumour volume at time t
VM_{EL}	Maximum elimination capacity
VM_{TR}	Maximum transport capacity
VPC	Visual predictive check
WBC	Wight blood count
WRES	Weighted residuals
X	Vector of design variables
$X_{i,j}$	Vector of individual design parameters at observation j
$Y_{i,j}$	Individual prediction at observation j
$Y_i(t)$	Model prediction for individual i at time t
Y_j	Model prediction for the typical patient at time t_j
y	Observed PK or PD data
$y_{i,j}$	Individually observed concentration at observation j

α	Significance level
β	Efficacy parameter in tumour growth inhibition model
β_{carbo}	Efficacy parameter of carboplatin in tumour growth inhibition model
β_{PTX}	Efficacy parameter of paclitaxel in tumour growth inhibition model
Γ	Variance-covariance matrix for parameter precision
γ	Exponent of feedback function
ΔOFV	Difference in OFV between two investigated models
$\delta_{i,j,k}$	0 or 1 if the decorrelated simulated value is greater or smaller than the decorrelated observed one, respectively
$\varepsilon_{i,j}$	Residual individual parameter for individual i at observation j
$\eta_{BL,i}$	Interindividual variability parameter on baseline for individual i
η_i	Interindividual variability parameter for individual i
$\eta_{k,i}$	Interindividual variability parameter for parameter k and individual i
$\eta_{SL,i}$	Interindividual variability parameter for SL and individual i
$\eta_{SLcarbo,i}$	Interindividual variability parameter for SL_{Carbo} and individual i
Θ	Vector of fixed-effects parameters
θ	Fixed-effects parameter
θ_{BL}	typical baseline value
$\theta_{Eff,cov}$	Parameter quantifying the influence covariate cov on E_{drug}
θ_k	Fixed-effects parameter of parameter k
$\theta_{k,cov}$	Parameter quantifying the influence covariate cov on parameter k
$\theta_{k,g}$	Typical value for parameter k and covariate value g
θ_{RV}	Fixed-effects parameter for residual variability
$\theta_{\mu,BSL}$	Parameter quantifying the influence of BSL_{SD} on μ
$\theta_{\mu,ECOG}$	Parameter quantifying the influence of ECOG performance status on μ
$\theta_{\mu,LDH}$	Parameter quantifying the influence of LDH on μ
$\theta_{\mu,PSURG}$	Parameter quantifying the influence of previous surgery on μ

$\theta_{\mu,RS8}$	Parameter quantifying the influence of RS_8 on μ
$\theta_{\mu,SEX}$	Parameter quantifying the influence of sex on μ
$\kappa_{k,i,o}$	Interoccasion variability parameter for parameter k and individual i at occasion o
λ	Time-dependent resistance parameter
λ_z	Terminal first-order elimination rate constant
μ	Mean of normal distribution of log survival times
μ_g	Mean of the distribution of logarithmised survival times for a patient group with covariates g
ξ	Individual likelihood
${\pi_k}^2$	Variance of all interoccasion variability parameters $\kappa_{k,i,o}$ for parameter k
Σ	Variance-covariance matrix assembling residual variability parameters
ξ_i	Individual likelihood ($p(y_i\|\Phi_i,\Sigma)\cdot \mathrm{p}(\Phi_i\|\Theta,\Omega)$)
ρ^2	Variance of normal distribution of log survival times
σ^2	Variance of all residual variability parameters $\varepsilon_{i,j}$
υ	Shape factor for logistic tumour growth
Φ	Vector of structural model parameters
Φ_i	Vector of the structural model parameter for individual i
$\phi_{BL,i}$	Model prediction of individual baseline
$\phi_{k,i}$	Structural model parameter of parameter k and individual i
$\hat{\phi}_{k,i}$	True individual parameter k of individual i
$\phi_{k,i,o}$	Structural model parameter of parameter k and individual i at occasion o
Ω	Variance-covariance matrix assembling interindividual variability parameters
${\omega_k}^2$	Variance of all interindividual variability parameter $\eta_{k,i}$ for parameter k

1 Introduction

1.1 Pharmacometric modelling and simulation of pharmacokinetics, pharmacodynamics and system dynamics

1.1.1 What is pharmacometrics?

Pharmacometrics was defined as “the science of developing and applying mathematical and statistical methods to characterise, understand and predict a drug’s pharmacokinetic and pharmacodynamic behaviour” [2]. The methodologies of this science can thereby be applied in all stages of the drug life-cycle, from drug discovery to development and therapeutic use. In general, pharmacometric models are developed based on experimental data and can implement prior information. These models are used for simulations to explore questions regarding the pharmacokinetics (PK) and/or pharmacodynamics (PD) of a drug.

Putting pharmacometrics into a wider perspective (Figure 1.1), terminology in this area developed over the last decades [3]. As an umbrella term for quantitative approaches describing the pharmacokinetics (PK) and pharmacodynamics (PD) of drugs, modelling and simulation (M&S) was the first term, that was widely used. To emphasise the impact of these approaches on decision-making, the term “model-based drug development was introduced” [4]. Since this terminology might be understood in a way that modelling approaches dominate the decision-making process, the term was modified to “model-informed drug development” [5]. Finally, the term was extended to “model-informed drug discovery and development” (MID3), to highlight the applicability of the approach in all stages of the drug life-cycle [3].

Within pharmacometrics, one can distinguish two main approaches, pharmacometrics and systems pharmacology [3]. While systems pharmacology implements knowledge of the underlying biological and pharmacological system in a very mechanistic way, pharmacometric approaches are initially more empirical. Nevertheless, these pharmacometric models can increase understanding of the particular pharmacological system and can explain and quantify sources of variability.

Within the pharmacometric approach, methods characterising PK and/or PD of a single individual (individual subject methods), and methods describing PK and/or PD of a group of individuals (population approach) can be distinguished. Methods of the population approach can then be used to quantify variability between patients and explain this variability with patient characteristics (covariates). For example, renal impairment can explain reduced drug

elimination. Thus, creatinine clearance can be used as a covariate on clearance explaining parts of the interindividual variability.

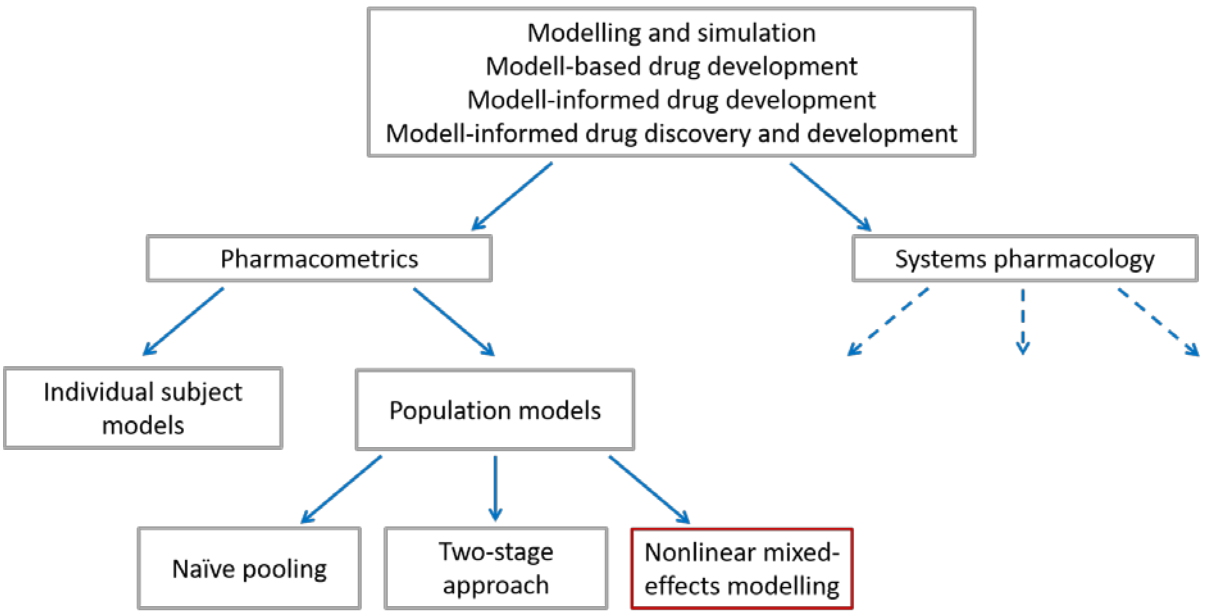

Figure 1.1: Terminology and approaches used in the area of pharmacometrics
Focus on pharmacometric approach, systems pharmacology can you the same or different methods compared to pharmacometrics (indicated by dashed arrows).

1.1.2 The population approach and its strategies

The population approach aims to describe the typical profile of the population with population parameter estimates (fixed-effects), e.g. typical value for clearance, as well as variability (random-effects). Variability is distinguished between the interindividual variability and the residual variability arising e.g. from measurement errors. Different approaches were developed and compared [6,7]:

Naïve pooled data analysis

Naïve pooled data analysis focuses on the determination of the population parameter estimates by analysing the data under the assumption that all measurements arise from a single individual. Thus, this approach ignores different sources of variability, as interindividual and residual variability, but summarises all variability in a single term [6]. It can be used in a setting in which the interindividual variability is typically small, as is in animal experiments with homogenous strains [8]. Not considering each individual can lead to misinterpretation of the available data [9] and biased parameter estimates [6]. Though, the advantage of this approach is easy implementation of different data types and fast estimation of population parameters.

Two-stage approach

As the name states, this approach has a stepwise procedure: In the first stage, parameter estimates are obtained for each individual. In the second stage, descriptive statistics are applied to describe the distribution of the individual parameters. This approach is focusing on the individual parameter estimates, but point estimates of the summary statistic can be considered as estimates of the population parameter. The distribution then describes the variability across the investigated individuals, but does typically not correctly estimate interindividual variability, since it includes parameter uncertainty, e.g. arising from measurement errors, leading typically to an overestimation of the interindividual variability parameter [6]. Sufficient number of measurements (higher than the number of parameters to be estimated) for each individual is essential for this approach to reliably estimate parameters and variability.

Nonlinear mixed-effects modelling

The nonlinear mixed-effects modelling (NLME) approach was developed in 1972 by Sheiner *et al.* [10] and is characterised by simultaneous estimation of population parameters (fixed-effects) and variability parameters (random-effects). Nonlinear is referring to the nonlinearity in the observed data, i.e. a nonlinear regression is performed.

Using NLME, fixed- and random-effects parameters can be estimated more precisely than for the naïve pooled data analysis and the two-stage approach [6,7]. Random-effects can be differentiated into interindividual and residual variability. In addition, interindividual variability can be explained by covariates, as described in section 1.1.1. The differentiation of variability and the effect of covariates can guide dosing decisions, e.g. reduced dose for patients with renal impairment.

Another advantage of this approach compared to the two-stage approach is the possibility to handle sparse data per individual due to the simultaneous estimation of fixed- and random-effects [11]. This allows the usage of the NLME approach in therapeutic areas in which only a limited number of blood samples have been taken as for routine sampling or in paediatrics.

The NLME approach was applied in the here presented work and is explained in more detail in section 2.1.1.1.

1.1.3 pharmacometric modelling and simulation: Purpose, options and impact

1.1.3.1 Possibilities in NLME model development

Considering the number of possibilities and options within the modelling process, it is important to focus on the questions to be assessed with the model, and develop a model that is “fit-for-purpose”.

Model development in NLME modelling mainly depends on the of quality (and quantity) of available data. The richer and more detailed the data, the more detailed and precise can the model be. NLME models describe the effect of an independent variable and design variables on the dependent variable. The independent variable is typically time, while design variables include e.g. the administered dosing regimen, sampling time points as well as patient-specific factors (covariates). Dependent variables are drug concentrations in a PK analysis, or toxicity, efficacy or biomarkers in a PD analysis.

NLME modelling can handle different types of dependent variables such as continuous data (e.g. concentration measurement of the drug in plasma), categorical data (e.g. grades of toxicity) or time-to-event data (e.g. survival time). The data situation of the dependent variable can be rich or sparse in terms of the number of patients and in terms of the number of measurements per patient. Both sparse situations can be handled with the NLME approach, since the whole population and each individual are considered simultaneously.

Many aspects of the modelling approach are determined by the available data as described above. Various further categorisations on the model can be done [12], e.g. the differentiation of linearity versus nonlinearity. Here, nonlinearity refers to processes that have a nonlinear correlation to the dependent variable, as e.g. a saturable clearance; not to be confused with nonlinearity in the term “nonlinear mixed-effects modelling”, which refers to the data described by the model over the independent variable.

Further, one can contrast between mechanistic, semi-mechanistic and empirical models. The more mechanistic a model, the more we can learn about the underlying biological system, the disease and its answer to drug exposure. Furthermore, mechanistic approaches, as in systems pharmacology, allow more reliable extrapolations e.g. of drug exposure. On the contrary, empirical models are only data driven, without considering prior knowledge, and follow the parsimonious principle allowing for parameter estimation and the application of the NLME approach. Moreover, empirical models can give reliable predictions if their assumptions and limitations are considered. Empirical models can be used for large populations with sparse sampling and result in reasonable estimation times. A compromise between these two extremes are semi-mechanistic models that implement a less detailed description of the biological system compared to mechanistic systems biology models, and still allow for

application of the NLME approach. To conclude, the balance between an empirical and mechanistic model has to be chosen based on the available information and the purpose of the model [13].

As seen in this section, the model depends on the available data. Nevertheless, sparse data can still be handled in NLME by implementation of prior knowledge gained from laboratory experiments or clinical trials. This knowledge can be used to inform the model structure, as in a mechanistic or semi-mechanistic model, and can further improve parameter estimation [14].

1.1.3.2 Application of NLME modelling in the drug life-cycle

The previous section gave a brief overview about the flexibility and the possibilities models can have to describe data. The flexibility in the model development also allows investigation of very diverse questions to investigate during drug development and therapeutic use. Examples of applications were recently collected and summarised by Marshall *et al.* [3] and spread over all therapeutic areas, different populations and all stages of drug life-cycle. Thus, modelling can impact internal decision making of pharmaceutical companies as well as decision making of the health authorities [15]. Further, modelling can help to improve and individualise therapy for patients [16–18]. The impact of population analysis can be also seen in the increasing number of publications applying this approach [19].

Learning and confirming

In 1997, Lewis Sheiner [14] introduced the principle of “learning and confirming” into clinical drug development. In this theory, learning studies (e.g. phase I and IIB) investigate many different dosing regimens in a small population. On the contrary, confirmatory studies (e.g. phase IIA and III/IV) examine only few regimens in a larger population. While confirmatory studies are analysed by descriptive statistics and statistical tests, as patients were assigned to the study (“intention to treat”) aiming for a yes/no answer by rejecting or accepting the null hypothesis, learning studies aim to increase the understanding of the drug behaviour and effect in dependency of the patient characteristics and the dosing regimen. Both questions can be addressed by pharmacometric PK/PD modelling. Furthermore, the developed models can inform the study design of the confirmatory studies. Finally, even confirmatory studies can be used for learning using pharmacometric PK/PD modelling, especially in phase II/IV studies, in which typically many patients with some heterogeneity are included.

Application in oncology

Modelling and simulation approaches in oncology can give guidance in two areas: drug development and therapeutic use. The former is needed since probability of final approval for oncologic drugs in phase I and II was shown to be the lowest compared to other therapeutic

areas [20]. The latter one is of specific interest, since classical cytotoxic drugs typically combine a narrow therapeutic window with high interindividual variability, leading to an increased risk of under- or overdosing [21] (see section 1.5.1). Further, anticancer therapy typically is a combination therapy leading to an increased complexity of the pharmacodynamic response: It can be explored by modelling and simulation to guide dosing of all drugs [22]. PK/PD modelling has been frequently applied in the therapeutic area of oncology and can help to optimise treatment by balancing toxicity and efficacy [23].

1.2 Non-small cell lung cancer and its therapy

1.2.1 Non-small cell lung cancer

Cancer comprises a variety of diseases in which abnormal cells grow uncontrolled. Cancer is a major cause of death worldwide, especially in the economically developed countries in which cancer is the second leading cause of death after cardiovascular diseases [24]. For Germany, an increase of the incidence of 20% is expected between 2010 and 2030, due to the increasing age in the population [25]. Within cancer, lung cancer has the highest incidence in men, and at least the third highest incidence in women [25–28]. Furthermore, mortality of lung cancer is high, which makes it the leading cause of death within cancer diseases [25–28]. Smoking is the main risk factor for lung cancer and causes about 70% – 80% of the lung cancer cases [29,30]. Due to different smoking habits, this also explains the different incidences between men and women. The incidence rate of lung cancer was approximately 60.7/100,000 for men and 26.5/100,000 for women in 2010, which resulted in mortality rates of 49.9/100,000 and 19.8/100,000 for men and women in Germany, respectively [25]. With about 83%, non-small cell lung cancer (NSCLC) accounts for the majority of lung cancers, compared to small cell lung cancer, the second most common subtype with 13% [31]. Within NSCLC, squamous-cell carcinoma, adenocarcinoma, and large cell carcinoma are the three main histological types.

At diagnose, the severity of the cancer is evaluated and classified using the TNM staging system, ranging from stage I to IV. The criteria are tumour size (T), involvement of nearby lymph nodes (N) and the presence of metastasis (M). In the study analysed in this work, patients with advanced NSCLC were enrolled, explicitly, stage IIIB (TNM categories: any T, N3, M0 or T4, any N, M0) or IV (TNM categories: any T, any N, M1).

1.2.2 General treatment strategies for cancer and application in non-small cell lung cancer

1.2.2.1 General cancer treatment strategies

The three major treatment options in cancer therapy, which are often combined, are surgery, radiotherapy and chemotherapy. In radiotherapy, ionising radiation is applied to damage DNA and thereby cause cell death. Within chemotherapy, classical cytotoxic agents are distinguished from targeted non-cytotoxic agents [32]. While non-cytotoxic drugs target cancer-specific characteristics [33,34], cytotoxic drugs are affecting the cell cycle. Thus, cytotoxic drugs affect all dividing cells, especially tissues with high proliferation, which is a characteristic of cancer tissue, but also of certain healthy tissues, leading to a variety of adverse events.

Typical adverse events caused by classical cytotoxic chemotherapy include alopecia, since the hair follicle contain rapidly diving cells responsible for the growth of hair. Further, mucosa cells are affected leading to painful inflammations in the mouth and along the gastro-intestinal tract. Another, often dose-limiting adverse event, results from the damage of the blood cell building system in the bone marrow leading to anaemia, thrombocytopenia and reduced leucocyte concentrations.

Adverse events are graded by the Common Terminology Criteria for Adverse Events (CTC AE), classifying in grade 1 – 5 [35]:

- Grade 1: Mild symptoms
- Grade 2: Moderate symptoms
- Grade 3: Severe symptoms
- Grade 4: Life-threatening symptoms
- Grade 5: Death related to adverse event

Since cancer therapy is a high burden for the patient and often constrains quality of life, the intensity of the therapy depends on the aim of the therapy, which can on a high level be curative or palliative to reduce disease symptoms and maintain or improve quality of life.

The treatment strategy for the patient further depends on the general health status including the ability for self-care, physical ability and daily activity, and is staged by the Eastern Cooperative Oncology Group (ECOG) performance status [36]:

- ECOG performance status 0: Fully active, able to carry on all pre-disease performance without restriction
- ECOG performance status 1: Restricted in physically strenuous activity but ambulatory and able to carry out work of a light or sedentary nature

- ECOG performance status 2: Ambulatory and capable of all self-care but unable to carry out any work activities; up and about more than 50% of waking hours
- ECOG performance status 3: Capable of only limited self-care; confined to bed or chair more than 50% of waking hours
- ECOG performance status 4: Completely disabled; cannot carry on any self-care; totally confined to bed or chair
- ECOG performance status 5: Dead

In future, decision about the treatment will be also based on molecular profiling, which examines the gene expression of cancer tissue. This better understanding of the cancer can then guide diagnosis and treatment by having a better prediction of the tumour growth and response to the therapy [37].

1.2.2.2 Treatment of non-small cell lung cancer

Different criteria determine the treatment strategy of NSCLC including tumour stage, tumour histology, localisation of the primary tumour, lymph nodes and metastasis as well as the general condition of the patient (ECOG performance status) and comorbidities. Generally, in early stages of NSCLC (stage I – II) surgical resection is the first choice in therapy [38–40]. In later stages (II-IIIA), adjuvant cisplatin-based chemotherapy is typically recommended [39]. Unresectable stage IIIB patients should be treated with a combination of radiotherapy and chemotherapy, which typically contains cisplatin in combination with etoposide or vinca alkaloids [41]. Depending on the patient-specific conditions, also paclitaxel-carboplatin combination therapy is applied for those patients [41]. For 35% – 40% of the NSCLC patients, diagnosis is not made before progression to stage IV, which leads to palliative treatment intention for the majority of these patients [38]. For stage IV, NSCL cancer patients, first-line treatment contains cisplatin- or carboplatin-based chemotherapy in combination with paclitaxel, gemcitabine or pemetrexed and can be further expanded by adding bevacizumab [30]. In this thesis, the combination of cisplatin or carboplatin and paclitaxel was investigated for patients with advanced stages of NSCLC.

1.2.3 Chemotherapeutic agents of interest in this thesis

1.2.3.1 Paclitaxel

Paclitaxel was originally isolated from *Taxus brevifolia* as a cytotoxic agent. Nowadays it is produced by a partial synthesis from Baccatin III after extraction from *Taxus baccata*. Paclitaxel is a antimitotic drug which was the first compound found enhancing and stabilising the polymerisation of microtubules [42]. These are hollow filaments built by two subunit

proteins, α- and β-tubulin, contributing to the heterodimer. Microtubules are essential for the separation of sister chromatids during mitosis by forming the spindle apparatus. Thus, paclitaxel inhibits mitosis in late G_2 or M phase of the cell cycle [43].

Paclitaxel has a good activity against ovarian, mammary and lung tumours, but not against other kinds of solid tumours, such as kidney or colon carcinomas and various sarcomas [44]. In platinum-based combination therapy, paclitaxel is used as first-line treatment against NSCLC [30]. This combination is not indicated for patients with an ECOG performance status > 2. No consensus on the scheduling (dosing interval and infusion duration) of paclitaxel was found yet. *In vitro* studies indicate, that the cytotoxic effect on tumour cells is higher when prolonging the exposure than increasing the dose [45]. On the other hand, it was found in patients that toxicity, but not efficacy of paclitaxel, is dependent on the duration of the infusion. Thus, 3 h infusion (instead of 24 h infusion) is recommended [46]. There is some evidence, that the weekly administration (67 – 100 mg/m² dose) has less toxic effects (reduced rate of patients experiencing grade 3 or 4 neutropenia) by having equal efficacy compared to the three-weekly administration (175 – 200 mg/m² dose) [47]. Nevertheless, three-weekly administration is still used, especially in the treatment of NSCLC.

The dose-limiting toxicity of paclitaxel chemotherapy is haematotoxicity, especially neutropenia. In addition, neurotoxicity, muscular and cardiac toxicity were seen in various trials [48]. Different mechanisms of resistance have been studied, such as the overexpression of the multi-drug resistance (MDR-1) gene, which is coding for the efflux pump P-glycoprotein [49]. Other mechanisms investigated are related to tubulin, the target of paclitaxel [42].

Cremophor EL

Paclitaxel is a poorly soluble drug; therefore, it is marketed within a formulation including cremophor EL (CrEL) as a carrier for intravenous infusion (Taxol®).

CrEL is a solubilising and emulsifying agent for the human and veterinary pharmaceutical industries. The amount of CrEL in the paclitaxel formulation is high compared to other drug formulations (CrEL included in a paclitaxel dose of 240 mg/1.77 m² BSA: 20.9 g; in a teniposide dose of 292 mg/1.77 m² BSA: 14.6 g; in a cyclosporine dose of 460 mg/m² BSA: 6.0 g) [50] and can cause hypersensitivity reactions up to anaphylactic reactions during or directly after infusion. The risk of these can be reduced by prolonging the infusion time [51] and premedication with glucocorticoids and H_1/H_2-antihistaminic agents. CrEL is suggested to form micelles with a lipophilic interior, in which paclitaxel is encapsulated and finally transported through the systemic circulation. This encapsulation leads to a reduced absorption

of paclitaxel in cells and modification of distribution processes, e.g. reduced plasma/blood concentration ratio [52]. CrEL is also known to decrease paclitaxel elimination [53], due to a reduced free drug concentration. The enclosure can also effect other lipophilic drugs and increases the risk of drug-drug interactions, e.g. anthracycline drugs [54].

Paclitaxel pharmacokinetics

As discussed, the pharmacokinetics of paclitaxel are modified by CrEL [55]. Thus, this paragraph as well as the following analysis describes the pharmacokinetics as a result of this formulation. High volumes of distribution have been reported (Table 4.2). Increasing drug doses in the three-hour infusion result in disproportionally increased maximum plasma concentrations and drug exposure, hence non-linearity is suggested [56]. Passive diffusion is considered to be the main uptake mechanism of paclitaxel into cells [57,58]. 99.8% of intracellular drug molecules are bound to cellular components and a predominant saturable and an additional non-saturable binding has been suggested [58].

Plasma protein binding was investigated in different studies, all indicating a high binding affinity of approximately 90%, independent of the paclitaxel concentration [59–62]. Nevertheless, plasma protein binding depends on CrEL concentrations; higher CrEL concentrations lead to lower unbound fractions [59,62]. In blood, paclitaxel binds additionally to erythrocytes and with even higher affinity to thrombocytes [63]. The latter binding is saturable [63]. In this thesis, paclitaxel plasma concentration denote total plasma concentrations unless otherwise stated.

Only 2% – 9% of the administered paclitaxel is excreted unchanged via the kidneys [56,64,65]. For hepatic elimination, paclitaxel is transported into hepatic cells via a liver-specific organic anion transporting polypeptide. This saturable process can be inhibited by CrEL [66]. In the cells, paclitaxel is metabolised in a phase I oxidation to the major metabolite 6α-hydroxypaclitaxel and the minor metabolites 3'p-hydroxypaclitaxel [67] and 6α, 3'p-dihydroxypaclitaxel [68]. 3'p-hydroxypaclitaxel has cytotoxic activity, but considerably lower than paclitaxel (*in vitro* half maximal inhibitory concentration (IC_{50}) on bone marrow cells approximately 15 times larger) [69]. Metabolism is catalysed by the cytochrome P450 (CYP) enzymes CYP2C8 and CYP3A4/5 (Figure 1.2). The metabolism rate depends on the liver function [70,71] and might be altered by allele variations in CYP2C8 and CYP3A4 [72,73] which potentially contribute to the interindividual variability of paclitaxel pharmacokinetics.

In summary, paclitaxel in the CrEL formulation shows nonlinear, schedule-dependent pharmacokinetics with high interindividual variability [56].

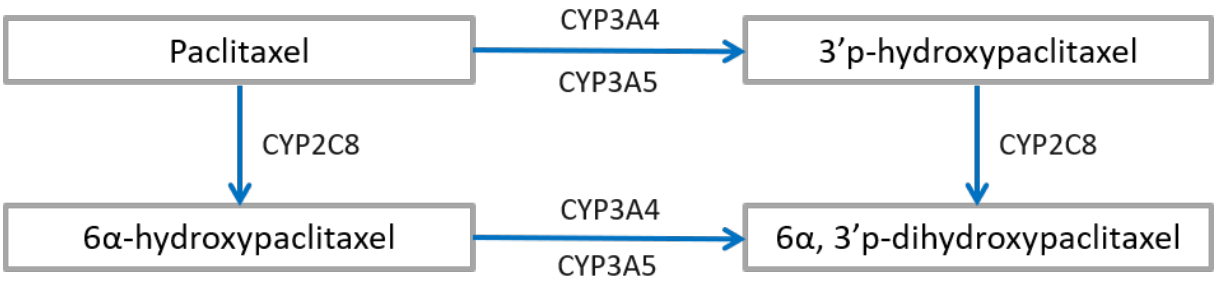

Figure 1.2: Paclitaxel metabolism (adapted from [66]).
CYP: cytochrome P450 enzyme.

1.2.3.2 Platinum-based drugs: Carboplatin and cisplatin

Cisplatin

Cisplatin was the first platinum-based drug discovered. It crosses membranes mainly via passive diffusion. Due to the decreased chloride concentration in cells compared to plasma, cisplatin is hydrolysed to the active aqua complexes cis-$[Pt(NH_3)_2Cl(OH_2)]^+$ and cis-$[Pt(NH_3)_2(OH_2)_2]^{2+}$. These highly nucleophilic active complexes platinise DNA strands (mainly at N7 atoms of guanine) resulting in inter- and intra-strand cross-links. Replication and transcription are restrained by the platinisation, which ultimately leads to cell death. Additionally, platinum is also bound to RNA, amino acids and proteins affecting among others cell membranes.

Cisplatin is used to treat different types of cancer including sarcomas, cancers of soft tissue, bones, muscles, and blood vessels. It is commonly administered intravenously every 3 to 4 weeks (50 – 100 mg/m²). Dose-limiting toxicities are nephro-, neuro- and ototoxicity.

Cisplatin is transformed in cells and in plasma by conjugation to sulfhydryl groups. Cisplatin is rapidly eliminated (half-life: 0.383 h (unbound cisplatin) [74] – 0.801 h (unbound platinum) [75]), this process takes place primarily via the kidneys by glomerular filtration and tubular secretion [76]. Cisplatin is highly bound to plasma proteins to a high extent with increased binding over time and concentration 64.8% – 97.3% [77].

Paclitaxel administered before cisplatin leads to less profound neutropenia than the alternate sequence [78].

Carboplatin

Carboplatin is a second-generation platinum analogue, for which the two chloride ligands are replaced by a bidentate malonate ligand; this modification leads to a reduced reactivity. As all platinum-based drugs, carboplatin has to be activated to an aqua complex by ligand exchange.

Due to the reduced reactivity and several intermediate steps, this process is slower than the activation of cisplatin leading to the same pharmaceutically active complexes although differences in DNA binding kinetics are discussed [79].

Carboplatin is used in different solid tumours as ovarian, cervical and lung cancer. Usually it is administered as a short intravenous infusion. The target area under the curve (AUC) concept aims to administer doses resulting in a certain drug exposure (target AUC = 4 – 7 mg • min/L), given by the Calvert formula (Eq. 1.1) [80], with GFR being the glomerular filtration rate [80]. GFR is typically estimated by the Cockcroft-Gault formula [81]. Dose-limiting toxicity is myelosuppression, in particular thrombocytopenia.

$$dose\ [mg] = target\ AUC \cdot (GFR\ [mL/min] + 25) \qquad \textbf{Eq. 1.1}$$

Carboplatin shows linear pharmacokinetics within the dose range used in clinical practice [82]. It is easily distributed within body fluids [83]. Highest concentrations are reached in liver, kidneys, skin and tumours (especially lung and liver tumours) [84]. The plasma protein binding is lower than for cisplatin but chose similar concentration- and time-dependency, with minimal binding at the beginning of infusion and up to 87% after 24 h [85–88]. The administered platinum is mainly excreted renally (50% – 75% within the first 24 h), but different to cisplatin, without tubular secretion [84].

Comparison of cisplatin and carboplatin

For the treatment of advanced NSCLC, cisplatin shows superior survival in comparison to carboplatin [89]. But the two drugs also show different profiles of adverse events: while cisplatin-based chemotherapy shows more digestive adverse events, neuro-, nephro- and ototoxicity, while carboplatin-based chemotherapy leads more often to haematotoxicity [30].

When cisplatin is given in advance of paclitaxel, the clearance of paclitaxel is reduced by 25%, leading to an increased toxicity [78]. In contrast, no evidence of sequence dependency was observed for the combination of carboplatin and paclitaxel, although increased 6α-hydroxypaclitaxel concentrations were measured when paclitaxel is administered after carboplatin [90].

The sequence-dependency of cisplatin might be due to CrEL, which inhibits the uptake of cisplatin in peripheral blood leukocytes and bone marrow cells, but not into solid tumour cells [91]. However, it was also hypothesised that cisplatin reacts immediately with DNA, forming interstrand and intrastrand cross-links leading to an S-phase arrest, whereas

carboplatin has, due to its slower activation, a delayed activity (approximately 12 h) with regard to the formation of platinum-DNA adducts [92]. Cells in S-phase arrest are less susceptibleto paclitaxel, which is acting in G_2/M phase of the cell cycle. This may cause that there is no sequence-dependent toxicity for carboplatin, but for cisplatin [90].

1.3 Neutropenia: Dose-limiting adverse event of paclitaxel

Neutropenia is a pathophysiologically low concentration of neutrophil granulocytes in the blood, which can lead to life-threatening immune-deficiencies. Grades of neutropenia are defined by neutrophil concentrations (Table 1.1) [35]. If, in addition to the neutrophils, other blood cells are decreased, myelosuppression is diagnosed.

Table 1.1: Common Terminology Criteria of Adverse Events definition of neutropenia [35]**.**

Grade of neutropenia	*Concentration of neutrophils*
1 – mild	< LLN – 1.5 • 10^{-9} cells/L
2 – moderate	< 1.5 – 1.0 • 10^{-9} cells/L
3 – severe	< 1.0 – 0.5 • 10^{-9} cells/L
4 – life-threatening	< 0.5 • 10^{-9} cells/L

LLN: lower limit of normal.

1.3.1 Haematopoiesis of blood cells

The blood building system (Figure 1.3) origins from long-term haemopoietic stem cells, which are pluripotent and have self-renewal activity. All blood cells origin from these stem cells. Further, the cells develop to short-term haemopoietic stem cells with reduced self-renewal capacity [93]. In human, haematopoietic stem cells replicate very slowly, approximately once every 40 – 50 weeks [94–96].

After the stage of stem cells, development to oligopotent progenitor cells takes place, meaning that they can no longer develop to all kinds of blood cells, but that they are lineage specific. Two main lineages are defined, the lymphoid lineage, from which T-, B-, and natural killer cells arise, and the myeloid lineage, from which granulocytes, mast cells, macrophages, thrombocytes and erythrocytes originate from. Progenitor cells account for the main proliferation taking place with a proliferation rate of approximately 0.3 $days^{-1}$ [97]. During the progenitor phase, cells are differentiating over the different progenitor cell stages to the different sub-lineages, with an overall transit time through the progenitor phase of approximately 5 days [98].

Next, the cells are further differentiating during the stages of precursor cells until they are mature cells which are released to the blood, where they can be quantified in routine measurements. Precursor cells are lineage-specific and do not further proliferate. The transit time through the precursor cell stages is about 6.6 days [99]. Via the whole process of granulopoiesis, $8.5 \bullet 10^8$ neutrophils/kg body weight are produced every day in healthy adults [99] and released to the blood, from where they migrate to tissue with a half-life of approximately 6.7 h [100].

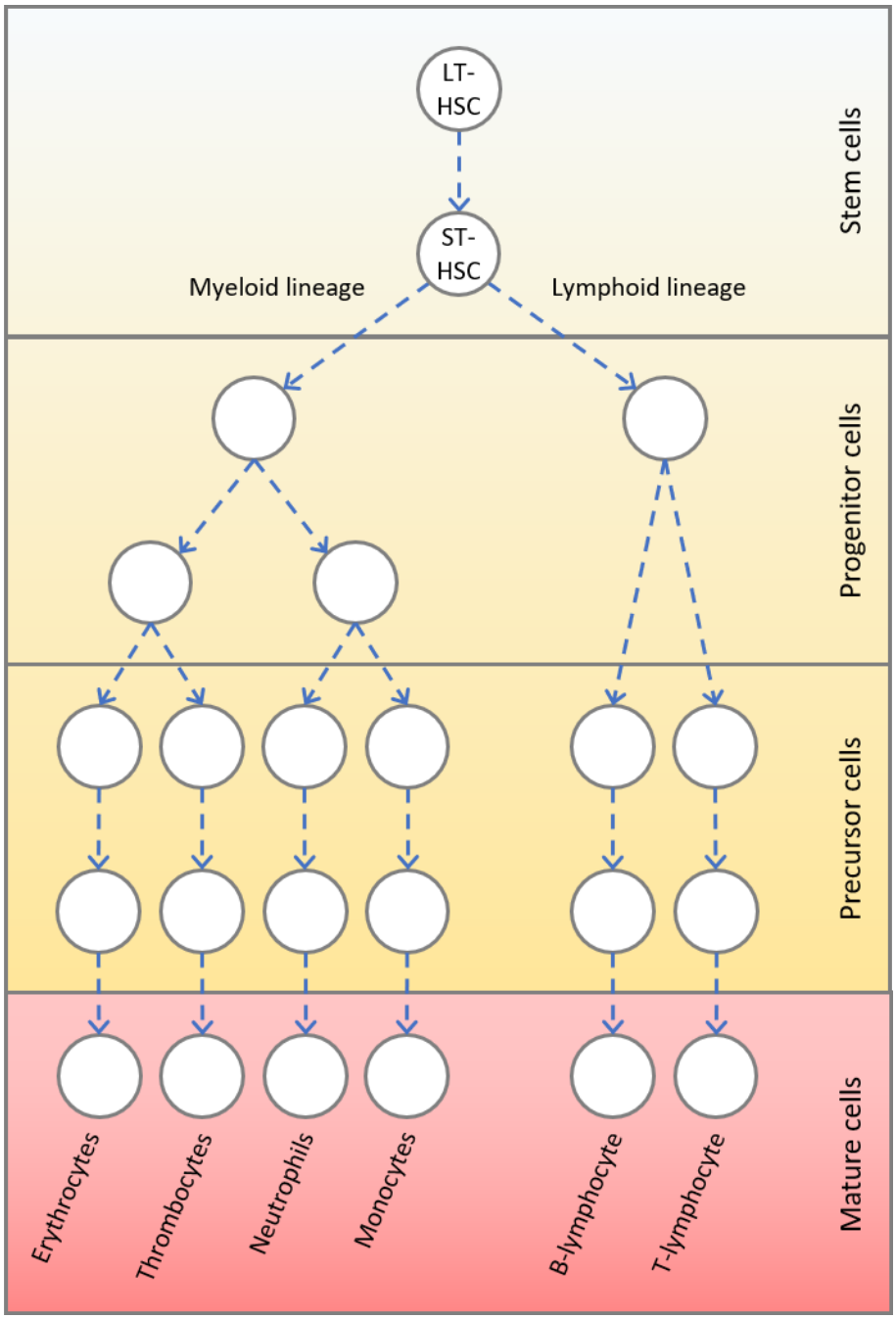

Figure 1.3: Simplified representation of the hierarchical structure of the haematopoietic system (adapted from [101])
LT-HSC: long-term haematopoietic stem cell, ST-HSC: short-term haematopoietic stem cell, dashed arrows: several interim stages exist, but are not shown here.
Yellow background: development in the bone marrow; red background: cells circulating in the blood.

Different cytokines regulate the proliferation and differentiation of the haematopoiesis as well as the release of cells into the blood. These cytokines are therefore responsible for elevated lymphocytes in case of an infectious disease and for the recovery in case of neutropenia. While stem cells are mainly influenced by the stem cell factor and fms-related tyrosine kinase 3 ligand, the lineage responsible for the building of neutrophils is mainly enhanced by granulocyte colony-stimulating factor (G-CSF) and granulocyte macrophage colony-stimulating factor (GM-CSF) [102].

1.3.2 Time-course, cumulative effect and treatment of neutropenia

Neutropenia, as well as other haematologic adverse events resulting from cytotoxic drug administration, follow a characteristic time-course (Figure 1.4): Neutrophil concentrations decrease with a delay of a few days. Since cytotoxic drugs mainly affect rapidly dividing cells, these drugs are primarily disturbing progenitor cells within the haematopoietic system. However, only neutrophil concentrations and not progenitor or precursor cells, are quantified in the blood, explaining the time-delay in the response. After the delay, neutrophil concentrations are rapidly declining until the nadir as lowest neutrophil concentration is reached. Then, neutrophil concentrations recover, which might result in a rebound effect with an increased concentration compared to baseline.

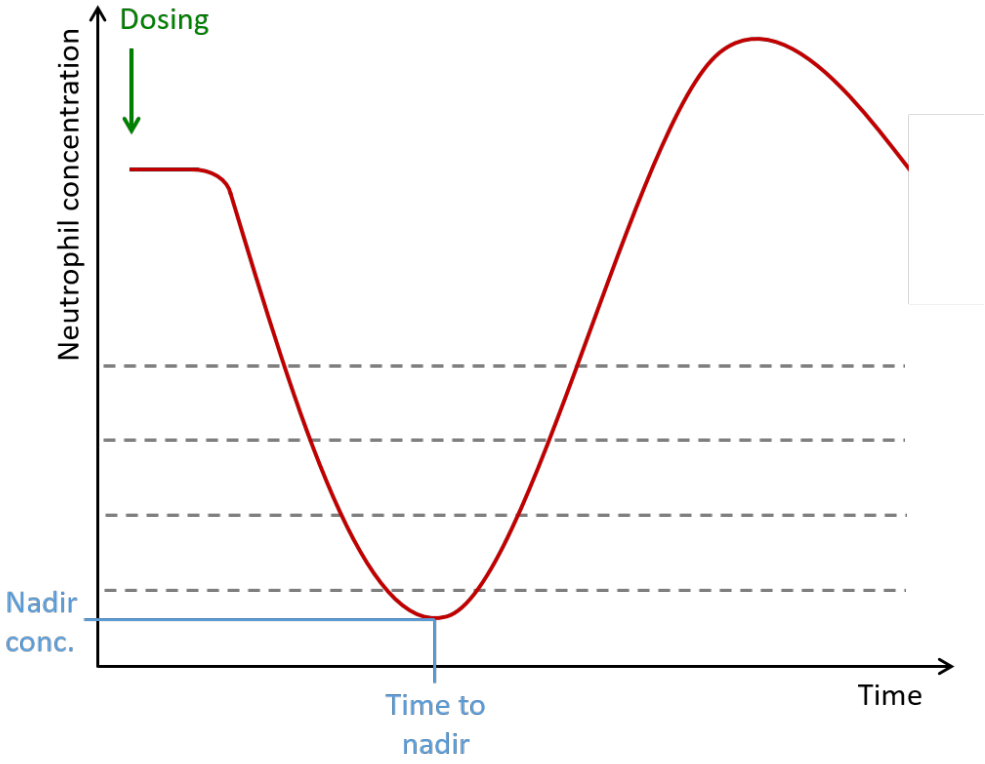

Figure 1.4: Typical time course of neutropenia after single dose of cytotoxic drug (adapted from [103,104])**.**
Blue: nadir concentration and time to nadir; green: time of single dose administration; grey dashed lines: thresholds for grading neutropenia from grade 0 to 4; red line: typical time course of neutropenia.

The time-course of neutropenia depends on the administered cytotoxic drug and the administered dosing schedule as well as patient-specific factors. For example, methotrexate and vinblastine have a shorter delay of the response of the blood cell concentrations after drug administrations compared to other drugs [105]. Dosing regimens also often include drug therapy over several days before a drug-free period, which also influences the neutrophil concentration-time profile.

For repeated treatment cycles, cumulative neutropenia was observed for different drugs [106–110], including the combination therapy of paclitaxel and carboplatin [90]. Cumulative neutropenia is a worsening of the nadir concentration over the treatment cycles. In addition, maximum neutrophil concentrations before or shortly after drug administration do not recover to baseline but decrease, as well. Different hypotheses were generated about the reasons for the cumulative nature of the toxicity [111]. The most prominent one is that the cytotoxic effect of the anticancer drugs on haematopoietic stem cells, or early and slowly proliferating progenitor cells, causes a decreased ability of long-term recovery [103,105,111,112]. This theory was defined as bone marrow exhaustion (BME) hypothesis in this thesis.

Neutropenia leads to immune deficiencies and causes infections known as febrile neutropenia. Beside of the treatment of the infections itself, recombinant G-CSF and GM-CSF are used to prevent or decrease the duration of neutropenia. Nevertheless, it is discussed that due to the G(M)-CSF, the proliferation of stem and progenitor cells is increased, leading to more severe toxicity of the chemotherapeutic drug on those cells, which further reduces the ability of long-term recovery [113]. Therefore, supportive G(M)-CSF is not given regularly in most anticancer regimens.

1.3.3 Pharmacometric models describing myelosuppression

As described in section 1.1.3.1, empirical, semi-mechanistic and mechanistic models can be developed to describe neutropenia or haematotoxicity in general. Since empirical models have limited ability for simulations, and mechanistic model are very complex and not appropriate for the available clinical data for this work, semi-mechanistic models were of interest. Those models have been reviewed by Friberg *et al.* [114]:

While four out of five semi-mechanistic haematotoxicity models included a zero-order rate constant for the synthesis of proliferating cells [115–118], the model developed by Friberg *et al*. [119], which is currently used as the gold standard model to describe neutropenia, included a first-order process. Further differences contained the implementation of the delayed onset of neutropenia, which was either included using a lag-time [115] or, more physiological transit compartments [116–119]. Another major difference was the implementation of a feedback mechanism in only two of the reviewed models [117,119], which

describes the physiological activity of G-CSF and other cytokines. Overall, the gold standard model was the most physiological and was applied in literature several times. It was also used to predict haematological toxicity for humans from animal data [120]. The advantage of the gold standard model is furthermore, that it distinguishes between drug-related parameters (describing the effect of the drug on the haematopoietic system) and system-related parameters (describing the haematopoietic system itself), which were in a comparable range across different drugs [119]. Since the gold standard model was also used in this thesis, the model is described in more detail in section 2.4.1.

However, cumulative neutropenia has been only rarely described with semi-mechanistic PK/PD models. Two models describing the cumulative pattern [121,122] were developed, even though describing cumulative haematological toxicity was not primarily intended by one of them [122]. Both of them were further investigated in this thesis and are described in section 2.4.2.1. Their physiological plausibility is discussed in section 4.2.2.

1.4 Treatment efficacy: Modelling of tumour size and survival

1.4.1 Evaluation of treatment efficacy

1.4.1.1 Response evaluation criteria in solid tumours

Response evaluation criteria in solid tumours (RECIST) [123] uses tumour size measurements to evaluate treatment response. Tumour size is typically measured in a computed tomography (CT) scan. For this evaluation, up to five target lesions are defined prior to the therapy. Their longest diameter is measured and the sum of these diameters is calculated. All additional lesions are non-target lesions and diameters are not necessarily measured at each tumour assessment, but their presence is controlled. Target and non-target lesion can include lymph nodes, but the shortest diameter of these lesions is used for evaluation and for the sum of diameters. Based on the response of target lesions, non-target lesions and on the appearance of new lesions, response is graded into categories for each of the three criteria and are then combined to an overall categorisation:

- Complete response (for target lesions: disappearance of all target lesions and any pathological lymph nodes < 10 mm)
- Partial response (for target lesions: ≥ 30% decrease in sum of diameters compared to baseline)
- Stable disease (for target lesions: between < 30% decrease and > 20% increase in sum of diameters compared to smallest sum on study)

- Progressive disease (for target lesions: ≥ 20% increase in the sum of diameters compared to smallest sum on study, absolute increase of at least 5 mm; appearance of new lesions)

1.4.1.2 Time-to-event outcome

Besides the measurement of tumour size, time to certain events is commonly used for evaluating treatment outcome:

- Time to progression: length of time from the start of treatment until disease progression
- Overall survival: length of time from start of treatment until the patient dies
- Progression-free survival: length of time from start of treatment that a patient lives with the disease, which does not get worse

Alternatively, time of diagnose can be used instead of treatment start to define time to progression and overall survival, but was not done in this thesis. Disease progression in this thesis was defined based on RECIST criteria.

1.4.2 Pharmacometric models of treatment efficacy

1.4.2.1 Pharmacometric models for tumour growth inhibition

While in preclinical trials more mechanistic models are applied, human data on tumour size is typically sparse, since CT scans are a burden for patients. Furthermore, the lack of placebo study arms, due to ethical reasons, is further complicating the development of tumour growth inhibition models. Published models were reviewed recently [124,125] and showed that tumour growth inhibition models typically consist of two terms: one term describing the net growth of the tumour without drug influence and the second one describing the drug-induced shrinkage of the tumour size. In addition, terms dealing with resistance which is often seen in clinical practice were added [126]. Models developed for non-small cell lung cancer in particular were summarised by Suleiman *et al.* [127].

1.4.2.2 Pharmacometric models for overall survival

In general, three methods describing survival times are available: parametric, semi-parametric and non-parametric survival analyses. While the parametric analysis assumes a distribution of the survival times, such an assumption is not made in the non-parametric and the semi-parametric analyses. An example for a non-parametric analysis is the Kaplan-Mayer analysis. The disadvantage of this analysis is that without assumptions of a distribution of survival times, simulations are difficult. Further, influential factors can only be evaluated by stratification and might soon lead to low patient numbers which limits the informative value. Nevertheless, Kaplan-Mayer analyses are regularly performed to statistically compare treatment outcome

between different study arms or patient groups. Semi-parametric models, such as the Cox Proportional Hazard Model, do not assume a distribution of the survival times, as the non-parametric models, but parameters quantifying the influential of covariates are estimated. Finally, parametric models, estimate parameters of an assumed distribution of the survival times and further estimate parameters for the covariate influence. Hence, parametric modelling is the most suitable approach for simulations, which was the ultimate aim in the here presented work (Project 4).

1.5 Dose optimisation/individualisation strategies in cancer therapy

1.5.1 General possibilities and clinical practice of dose individualisation

Classical cytotoxic drugs typically have a narrow therapeutic window, since on the one hand high doses are needed to achieve maximal efficacy and on the other hand high toxicity is caused by the unspecific mode of action. In addition, most anticancer drugs show high interindividual variability in the pharmacokinetics [21,128] increasing the risk of exceeding and falling below the narrow therapeutic window. Hence, dose individualisation is needed to prevent life-threatening toxicity, but obtain efficient treatment.

The most common approach is dosing based on body surface area (BSA), e.g. used for paclitaxel and cisplatin dosing. This strategy was developed in the 1950s and arose from extrapolation from animal data to humans [128]. The use of BSA-adjusted dosing has been intensively discussed and it can be concluded that for most cytotoxic drugs, variability in the PK was not reduced [21,128–130]. However, for some drugs BSA-adjusted dosing can reduce interindividual variability, as for 5-fluorouracil [131], troxacitabine [132] and paclitaxel [133]. To conclude, BSA-adjusted dosing is an opportunity for dose individualisation of some drugs, but is used for many drugs for which evidence for reduced PK variability is missing. Furthermore, BSA-adjustment, even if it reduces interindividual variability, might not be sufficient for all patients to achieve exposure within the therapeutic window.

Besides the BSA-adjusted dosing, individualisation based on other covariates, such as renal function (e.g. carboplatin, see section 1.2.3.2) or genotype of metabolising enzymes, can be done. Those covariates can be investigated using modelling and simulation, as described in section 1.1.2. In addition, therapeutic drug monitoring can be used [23,134,135], i.e. drug concentrations are measured during therapy to adapt following doses based on the gained individual PK information.

1.5.2 Towards an optimal paclitaxel therapy: Steps taken prior to this work to optimise paclitaxel therapy

Paclitaxel is one of the drugs with high interindividual variability in the PK (see section 1.2.3.1). BSA-adjustment, was correlated with exposure and clearance and volume of distribution [133,136,137] and lead to a reduction of interindividual variability in AUC of total paclitaxel by 44.2% [133]. However, high variability in drug exposure and life-threatening toxicity are still observed in clinical trials. Hence, further steps are needed to individualise paclitaxel treatment.

With this aim, Joerger *et al.* [138] developed a PK/PD model describing the paclitaxel concentration-time profiles and the resulting neutropenia (PK/PD model described in section 2.3.1 and 2.4.1). This PK/PD model was based on pooled data from two clinical trials which included dense PK sampling. Further, Joerger *et al.* developed a dose individualisation algorithm to optimise the 3-weekly dosing schedule of paclitaxel in combination with carboplatin (Figure 1.5). According to this dosing algorithm, the first dose (dose in cycle 1) is adjusted based on age, sex and BSA as those factors were significant covariates on the elimination of paclitaxel. In the first cycle, according to the algorithm, only young (< 46 years) men receive the standard dose of 200 mg/m² BSA, but women and older people receive lower doses (down to 150 mg/m² BSA). In the following cycles, the dose is adjusted based on toxicity (grade of neutropenia) and drug exposure ($T_{C>0.05}$ determined by a single PK measurement). Thus, the dosing algorithm was considering therapeutic drug monitoring and, in addition, toxicity. However, the dosing algorithm did not consider efficacy, but exposure and toxicity can be seen as surrogate parameters [130]. The algorithm aimed for a target range of $26 \leq T_{C>0.05} < 31$ h. Hence, doses should be only increased in case of low drug exposure (< 26 h) and low toxicity (grade of neutropenia ≥2). To not risk life-threating toxicity, doses should always be reduced in case of grade 4 neutropenia, even if low exposure was observed.

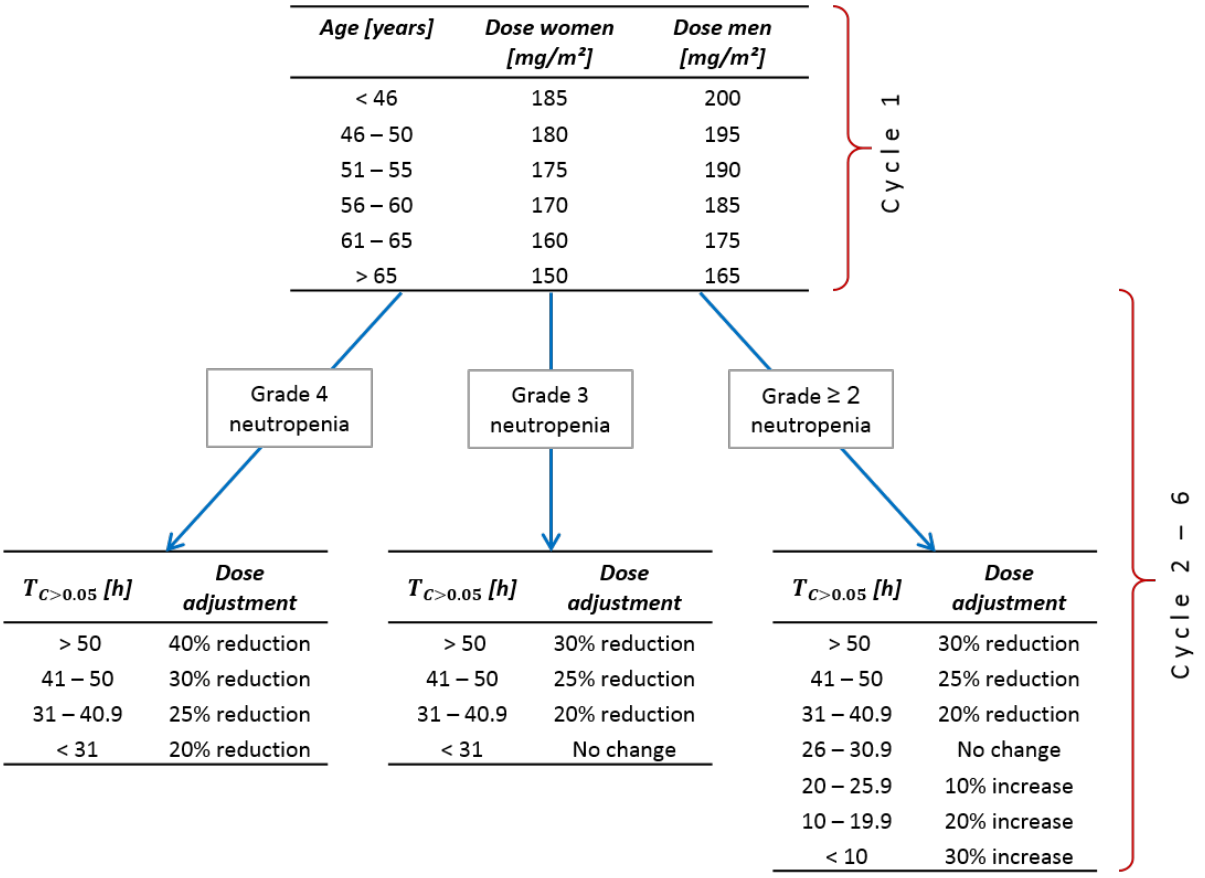

Figure 1.5: Dosing algorithm suggested by Joerger *et al.* [138]**.**
$T_{C>0.05}$: Time of paclitaxel plasma concentration > 0.05 µmol/L.

The developed dose individualisation algorithm was recently investigated in a clinical trial, the *CESAR* (Central European Society for Anticancer Drug Research) *study of Paclitaxel Therapeutic Drug Monitoring* (CEPAC-TDM). The aim of this trial was to compare the dosing algorithm with the standard BSA-adjusted dosing and investigate whether the dosing algorithm can reduce toxicity (primarily grade 4 neutropenia) and maintain efficacy at the same time.

The CEPAC-TDM study showed a significant reduction of grade ≥3 neutropenia but not the life-threating grade 4 in the patients dosed with the algorithm [139]. No significant differences were observed in terms of progression-free and overall survival, despite significantly lower doses in the experimental treatment arm as a result from dose individualisation. This clinical trial was an important step towards an optimal and individualised paclitaxel treatment, but also showed that further steps are needed to improve toxicity for the patients.

1.6 Objectives

The aim of the here presented work was to improve model-informed treatment of the combination therapy of paclitaxel and carboplatin/cisplatin for patients with advanced non-

small cell lung cancer (NSCLC). As seen in the previous sections, the burden of NSCLC is high and might further increase. Thus, a treatment that combines efficacy with tolerable toxicity in a larger proportion of patients is urgently needed. The first-line treatment against the severe advanced stage of NSCLC is currently paclitaxel in combination with platinum-based drugs. As typical of cytotoxic anticancer drugs, this therapy has a narrow therapeutic window with neutropenia as the dose-limiting toxicity. Furthermore, cumulative neutropenia was observed for the therapy of paclitaxel in combination with carboplatin. The risk of exceeding/falling below the narrow therapeutic window is high due to the high interindividual variability of paclitaxel PK.

Important steps towards dose individualisation of the paclitaxel treatment have been taken forward. A PK/PD model and a dose individualisation algorithm, which was based on this PK/PD model, was developed (Figure 1.6, beginning from the upper left part: “Clinical trials”, “PK/PD model”, “Dosing algorithm”). This algorithm was recently investigated in the CEPAC-TDM study (Figure 1.6, “Clinical trial (CEPAC-TDM)”), but failed to reduce grade 4 neutropenia. Even though efficacy was not reduced in this trial, further steps should consider efficacy carefully, since dose reductions needed for patients with severe toxicity potentially result in reduced survival or early tumour progression.

To account for all these different aspects of the paclitaxel combination therapy, the following project strategy for this thesis was developed (Figure 1.6): The data from the CEPAC-TDM study was investigated from a pharmacometric modelling and simulation perspective. In the first step, the aim was to evaluate the original PK/PD model for its applicability on the CEPAC-TDM study data (Figure 1.6, “Model evaluation”). Potential misspecifications shall be identified that could explain why the model-based dosing algorithm did not reduce grade 4 neutropenia as expected. In a next step, the PK/PD model shall be optimised based on the results of the model evaluation (Figure 1.6, “Model optimisation”). Further, cumulative neutropenia shall be implemented in the PK/PD model, since the original model was using the gold standard neutropenia model, which did not account for this behaviour. To cover both sides of the therapeutic window, a tumour growth inhibition model and overall survival model shall be developed to describe efficacy (Figure 1.6, “Efficacy modelling”). Further, the developed PK/PD models shall distinguish between the effect of paclitaxel and carboplatin, since the original model did not account for the platinum-based component of the therapy, which might also affect neutropenia. Finally, all developed models shall be used to simulate different dosing scenarios to investigate whether dose reduction or increase of the dosing interval is the better option in terms of toxicity and efficacy for patients with severe neutropenia (Figure 1.6, “Simulations”, “Dosing algorithm”).

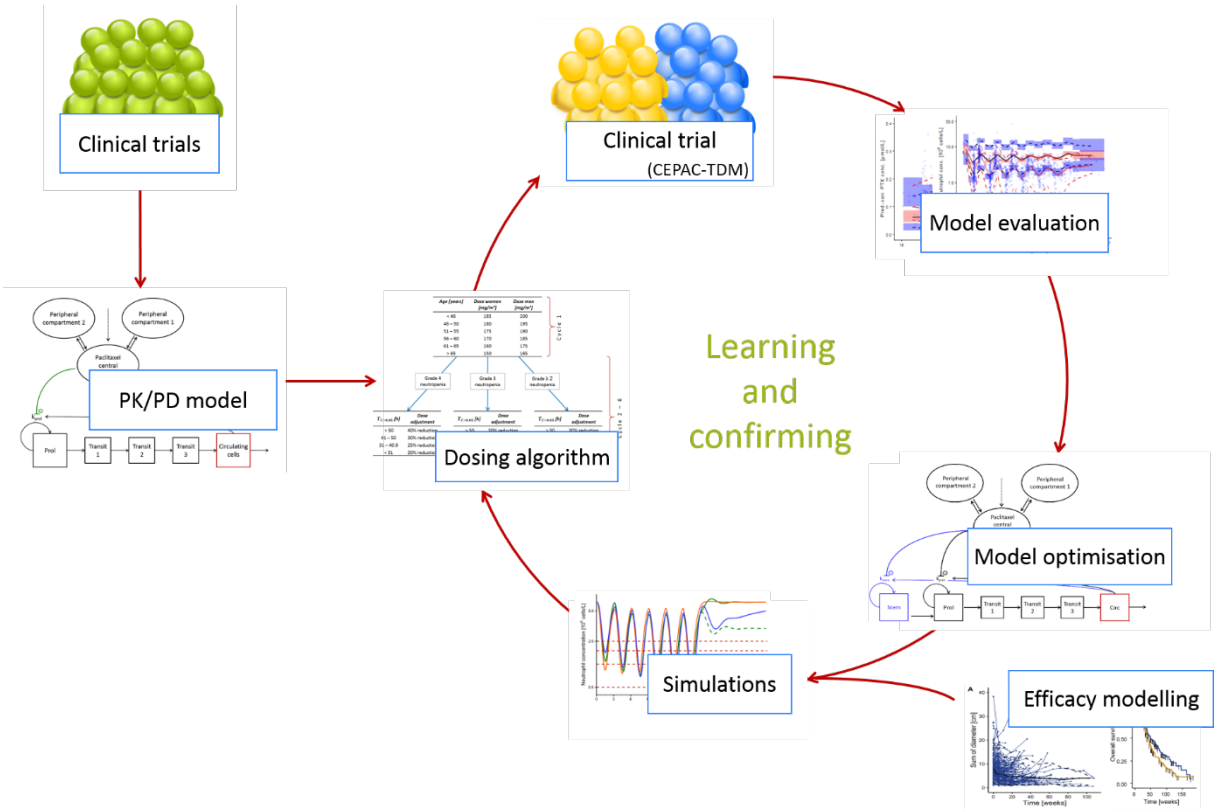

Figure 1.6: Project strategy (modified from [140])**.**
CEPAC-TDM: CESAR (Central European Society for Anticancer Drug Research) study of Paclitaxel Therapeutic Drug Monitoring; PK/PD: pharmacokinetics/pharmacodynamics.

These steps were separated into four projects:

Project 1: Pharmacokinetics

The aim of Project 1 was to externally evaluate the original PK model with the data from the CEPAC-TDM study. Potential misspecifications found in this step, shall be corrected in a PK model optimisation. In this step, the prior information of the original model shall be considered, since the original study included denser sampling than the CEPAC-TDM study. Furthermore, the aim was to evaluate whether the sequential modelling approach used in Project 2 was sufficient as input for the neutropenic effect. This step shall be performed, since individual predictions depend on the PK data for the respective patient, which was only one sample per treatment cycle.

Project 2: Neutropenia

Similar to Project 1, the objective in Project 2 was to first evaluate the original model and account for potential misspecifications in the model optimisation. Since cumulative neutropenia was expected, the aim was to identify and analyse reported models and if necessary further to develop a mechanistically plausible PK/PD model describing this behaviour. Mechanistic plausibility shall be an important model selection criterion, since the model shall be used for

simulations of different dosing scenarios. Finally, differentiation between the drug effect of paclitaxel and carboplatin was intended, since dose adaptations of one drug do not necessarily influence the effect of the concomitant drug.

Project 3: Efficacy

In Project 3, the aim was the development of a tumour growth inhibition model and an overall survival model, since these two aspects are of major importance evaluating treatment efficacy. Further, the two models should be able to predict informative drop-outs from the study treatment, since patients with diagnosed tumour progression the treatment is typically stopped, since it is assumed that resistance against the treatment was developed.

Project 4: Simulations

Finally, the models developed in Project 1 – 3 shall be used to explore different dosing scenarios. Therefore, the effect of fixed-dosing, the dosing algorithm and fixed doses with increased cycle length shall be investigated on the paclitaxel PK, neutropenia, tumour size development, overall survival and drop-out. The effect of dose reduction resulting from the dosing algorithm or increased dosing intervals on the risk of grade 4 neutropenia should be characterised. Further, it shall be investigated whether the treatment suggestions maintain tumour size reduction and overall survival.

2 Patients, methods and materials

2.1 Population pharmacometric modelling and simulation

The aim of pharmacometric modelling and simulation is to describe the pharmacokinetic (PK) and/or pharmacodynamic (PD) behaviour as well as the and dynamics of the physiological system of a population by a mathematical model. These models can then be used for simulations, which shall answer questions or investigate hypotheses arising in drug discovery and development, as well as in clinical practice and shall therefore help to optimise therapy. This overall aim leads to the following scientific workflow often applied in modelling and simulation: First, models to describe the PK and PD profiles over time are developed based on data from a clinical or preclinical trial. Different tools are used to evaluate a model for its predictive performance and applicability for the questions to be answered. If an appropriate model is identified, simulations of different patient populations or dosing regimens can be performed to investigate these questions.

2.1.1 Development of nonlinear mixed-effects models

2.1.1.1 Framework of nonlinear mixed-effects modelling

Nonlinear mixed-effects (NLME) modelling is a special nonlinear regression analysis, which combines a description of the typical patient with the variability within the population of patients. To be able to analyse the data of the whole population while considering differences between the individuals at the same time, population parameters are estimated. “Mixed-effects” means that the model contains fixed-effects parameters, such as the typical value for clearance, that are constant over the observations and independent of the design variables [141]. Further, the model contains random-effects parameters, which describe the variability of the parameters and the residual variability within the population. NLME models contain the structural submodel, covariate submodel and the pharmacostatistical submodel (Figure 2.1). The statistical submodel can be further differentiated into different hierarchical levels of variability, e.g. interindividual and residual variability. To describe PK or PD with this approach, only little information is required from an individual patient, e.g. with sparse sampling, since additional information can be “borrowed” from the population [142].

In the projects presented in the following, a PK or PD variable (dependent variable) varying over time (independent variable) was described. Thus, the following sections will focus on this approach although other independent variables are generally possible. The software NONMEM in combination with PsN (see section 2.1.5) was used for model building, thus the

following sections are related to the implementation of the NLME framework in these software tools.

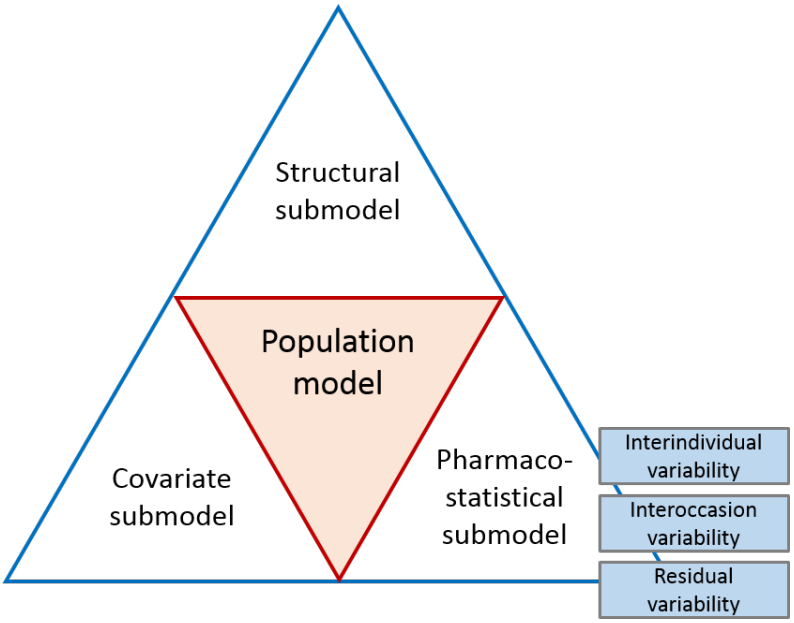

Figure 2.1 Hierarchical structure of nonlinear mixed-effects models (modified from Frank [143])**.**

Structural submodel

The aim of this submodel is to describe the general tendency in the observed PK or PD data y (dependent variable) at observation time point j (for j in 1,… J). The structural model thus is a mathematical function f (Eq. 2.1), including design variables X and structural model parameters Φ, such as the elimination rate constant λ_z or volume of distribution V in a one-compartment model. For the typical patient, these structural model parameters are the fixed-effects parameters θ, which are elements of the vector Θ. Thus, the concentration Y_j for a typical patient can be described by Eq. 2.2. The plasma concentration of a drug at observation time t_j ($C(t_j)$) for example can be described by a one-compartment structural model and would result in Eq. 2.3 after a single intravenous injection of a $Dose$, which would be a design variable.

$$Y_j = f(\Phi, X) \qquad \textbf{Eq. 2.1}$$

$$Y_j = f(\Theta, X) \qquad \textbf{Eq. 2.2}$$

$$C(t_j) = \frac{Dose}{V} \cdot e^{-\lambda_z \cdot t_j} \qquad \textbf{Eq. 2.3}$$

Pharmacostatistical submodel: Interindividual variability

Interindividual variability is added to describe the concentration-time profile not only for the typical patient, but also for each individual i (in 1,… N). The individual concentration-time profile ($Y_i(t)$) is described by Eq. 2.4, where Φ_i is a vector of the individual values of each structural model parameter $\phi_{k,i}$ (for k in 1,… K) and $X_{i,j}$ is the vector of the individual design parameters at observation j, e.g. dose administered to this patient.

$$Y_{i,j} = f(\Phi_i,\ X_{i,j}) \qquad \textbf{Eq. 2.4}$$

For an additive model, $\phi_{k,i}$ is the sum of the fixed-effects parameters θ_k and the individual variability parameter $\eta_{k,i}$ (Eq. 2.5). The parameter $\eta_{k,i}$ of all individuals is assumed to be normally distributed with mean of 0 and a variance ${\omega_k}^2$, which is a random-effects parameter. Different functional models describing the interindividual variability are possible, as e.g. in Eq. 2.6 where an exponential model is shown, leading to a log-normal distribution of $\phi_{k,i}$, since $\eta_{k,i}$ is always assumed to be normally distributed. A log-normal distribution has the advantage, that individual parameters are limited to positive values, which is typically physiologically plausible, as e.g. for clearance or volume of distribution.

$$\phi_{k,i} = \theta_k + \eta_{k,i} \quad \eta_{k,i} \sim \mathcal{N}(0,\ {\omega_k}^2) \qquad \textbf{Eq. 2.5}$$

$$\phi_{k,i} = \theta_k \cdot e^{\eta_{k,i}} \quad \eta_{k,i} \sim \mathcal{N}(0,\ {\omega_k}^2) \qquad \textbf{Eq. 2.6}$$

For the additive interindividual variability model, the standard deviation of $\phi_{k,i}$ is independent of θ_k [144], thus the standard deviation ω_k is reported. For the exponential model on the other side, ω_k is the standard deviation on the logarithmic domain and is approximately equal to the coefficient of variation on the standard domain [145]. Thus, the coefficient of variation ($CV, \%$, Eq. 2.7) is independent of θ_k and is reported when assuming an exponential model. In this way, the parameter estimates of the typical value and the interindividual variability can be interpreted independently from each other.

$$CV, \% = \sqrt{{\omega_k}^2} \cdot 100 \qquad \textbf{Eq. 2.7}$$

The variances of all interindividual variability parameters ${\omega_k}^2$ can be assembled into the so-called variance-covariance matrix Ω. The off-diagonal elements of this matrix Ω describe the covariance between the interindividual variability parameters. In the projects presented below, only the diagonal elements (${\omega_k}^2$) of Ω due to the sparse data situation and the complexity of the models were estimated, thereby assuming that the ${\omega_k}^2$ are independent of each other.

Pharmacostatistical submodel: residual variability

The residual variability, resulting from e.g. measurement imprecision or inadequate model structure, is described as the discrepancy between the individual prediction at observation j ($Y_{i,j}$) and the measured dependent PK and/or PD variable ($y_{i,j}$). In Eq. 2.8, where an additive residual variability model is assumed, $\varepsilon_{i,j}$ is this discrepancy for each individual i at each observation j. $\varepsilon_{i,j}$ is, similar to the interindividual variability, assumed normally distributed with mean 0 and variance σ^2, which is again a random-effects parameter.

$$y_{i,j} = Y_{i,j} + \varepsilon_{i,j} \quad \varepsilon_{i,j} \sim \mathcal{N}(0, \sigma^2) \qquad \textbf{Eq. 2.8}$$

Again, different residual error models are possible. An exponential model can be achieved by log-transforming the observed data and applying the additive function [146]. Another way of describing the additive residual variability is by estimating the variance as a fixed-effects parameter (Eq. 2.9), where the random-effects parameter is fixed to 1, but then multiplied with the respective fixed-effects parameter (θ_{RV}), resulting in a variance of $\sigma^2 = {\theta_{RV}}^2$. Optionally, more than one residual variability term can be estimated, then the random-effects parameters are summarised in the variance-covariance matrix Σ, but this was not done in the here presented work.

$$y_{i,j} = Y_{i,j} + \theta_{RV} \cdot \varepsilon_{i,j} \quad \varepsilon_{i,j} \sim \mathcal{N}(0, 1) \qquad \textbf{Eq. 2.9}$$

The same concept as for interindividual variability applies for residual variability in terms of the reporting of the variability. Thus, for an additive error model the standard deviation is reported, while for an exponential model the coefficient of variation is stated (Eq. 2.10).

$$CV, \% = \sqrt{\sigma^2} \cdot 100 \qquad \textbf{Eq. 2.10}$$

Pharmacostatistical submodel: interoccasion variability

Optionally, further levels of variability can be added as e.g. interstudy or interoccasion variability. Interoccasion variability is frequently used, also in the PK model of paclitaxel in this work. Dependent on the research question and study design, an occasion is defined differently, here it was defined as one chemotherapeutic cycle. It describes the random variability within one patient between different occasions/drug administrations. The individual parameters ($\phi_{k,i,o}$) are thus allowed to change with each occasion o (for o in 1,… O), where the discrepancy in the individual parameters between occasion is described by $\kappa_{k,i,o}$. $\kappa_{k,i,o}$ is again normally distributed with mean 0 and the variance ${\pi_k}^2$ as random-effects parameter. Different

implementations are possible for interoccasion variability, Eq. 2.11 shows the exponential implementation used in this work.

$$\phi_{k,i,o} = \theta_k \cdot e^{\eta_{k,i}+\kappa_{k,i,o}} \quad \kappa_{k,i,o} \sim \mathcal{N}(0,\ {\pi_k}^2) \qquad \textbf{Eq. 2.11}$$

Covariate submodel

Covariates, most often patient-specific factors, are used to explain interindividual variability. Covariates are typically added after the development of the base model (structural plus pharmacostatistical model). Covariates can be continuous (e.g. body weight) or categorical (e.g. sex). Once more, different implementations are possible. Eq. 2.12 and Eq. 2.13 give the implementation in a linear and a power function, respectively, of a continuous covariate cov on a parameter k as it was done in this work. The parameter $\theta_{k,g}$ is the typical value of the parameter θ_k for a group of patients for whom the covariate value g was measured. The mathematical implementation and the fixed-effects parameter $\theta_{k,cov}$ defines the relationship between the parameter $\theta_{k,g}$ and the measured covariate. Both implementations are centred to the median of the covariate measurements within the observed population ($median(cov)$).

$$\theta_{k,g} = \theta_k \cdot \left(1 + \theta_{k,cov} \cdot (g - median(cov))\right) \qquad \textbf{Eq. 2.12}$$

$$\theta_{k,g} = \theta_k \cdot \left(\frac{g}{median(cov)}\right)^{\theta_{k,cov}} \qquad \textbf{Eq. 2.13}$$

For categorical covariates, θ_k is typically taken as reference for the most frequent group (e.g. females) and the deviation for other groups is then defined by $\theta_{k,cov}$. Eq. 2.14 and Eq. 2.15 give two possible implementations of a dichotomous covariate as sex, with g being the covariate group (e.g. if encoded as 0 for females and 1 for males). The second option (Eq. 2.15) can be extended to covariates with more than two covariate groups.

$$\theta_{k,g} = \theta_k \cdot {\theta_{k,cov}}^{g} \quad \text{resulting in: } \theta_{k,g} = \begin{cases} \theta_{k,female} & if\ g = 0 \\ \theta_{k,male} & if\ g = 1 \end{cases} \qquad \textbf{Eq. 2.14}$$

$$\theta_{k,g} = \theta_k \cdot \theta_{k,cov} \quad \text{with } \theta_{k,cov} = \begin{cases} 1 & if\ g = 0 \\ 1 + \theta_{k,cov1} & if\ g = 1 \end{cases} \qquad \textbf{Eq. 2.15}$$

For selection of covariates to be implemented in the model, the first step is to preselect potential covariates based on physiological plausibility, i.e. prior knowledge about the underlying mechanisms or correlations that were reported in literature between a covariate and a population parameter θ_k. Further, a graphical screening based on the base model (structural and pharmacostatistical submodel) is performed to evaluate the shape and extent of the potential influences. These graphical evaluations comprised for continues covariates scatter

plots and for categorical covariates Box-and-Whisker plots of $\phi_{k,i}$ or $\eta_{k,i}$ versus the potential covariate. These plots are influenced by η-shrinkage (see section 2.1.2.2), which can hide true relationships or indicate false relationships, if η-shrinkage is greater than 20% – 30% [147]. To avoid misleading conclusions due to η-shrinkage, significant covariates identified in the modelling process should be investigated on all other parameters as well. Thus, considering η-shrinkage, only covariates that showed a correlation in the visual evaluation were investigated further. For selection of significant covariates of those remaining after graphical exploration, different approaches are available such as the stepwise covariate model-building procedure (SCM) [148] and the lasso method [149]. The ones applied are described in section 2.1.2.6.

2.1.1.2 Estimation methods

NLME modelling aims to estimate the set of population parameters (Θ, Ω, Σ), that best describes the population and individual PK or PD data. For estimation, the maximum likelihood approach is applied. In this approach, the aim is to determine the set of parameters, that maximises the probability that the observed data arises from the model, called the likelihood of the parameters. This is done in an iterative procedure in which first the likelihood is evaluated for a set of parameters. Then, a gradient method "moves" the parameter values in the direction where the likelihood improves most and the parameter set is updated. The next iteration starts with evaluating the likelihood for the new set of parameters. This process is repeated until the parameter set is found, for which the likelihood is maximal. For mathematical reasons, the estimation algorithms aim to minimise twice the negative log-likelihood, which is also called the objective function value (OFV).

If the parameters were known, the likelihood would be given by equation Eq. 2.16. The likelihood is the product of the likelihood of each individual i evaluated, with N being the total number of individuals.

$$likelihood(\Theta, \Omega, \Sigma) = \prod_{i=1}^{N} p(y_i|\Phi_i, \Sigma) \cdot p(\Phi_i|\Theta, \Omega) \qquad \textbf{Eq. 2.16}$$

Thereby, $p(y_i|\Phi_i, \Sigma)$ is the conditional probability density of y_i given Φ_i and Σ, and comparably, $p(\Phi_i|\Theta, \Omega)$ is the conditional probability density of Φ_i given Θ and Ω. For simplification $p(y_i|\Phi_i, \Sigma) \cdot p(\Phi_i|\Theta, \Omega)$, the individual likelihood will be abbreviated with ξ_i. For mathematical reasons, the logarithm of the likelihood is used (log-likelihood). Since in the nonlinear mixed-effects modelling approach the individual parameters Φ_i are random, ξ_i has to be integrated over the parameter space. This marginal distribution cannot be computed analytically, since the structural model is nonlinear. Therefore, the log-likelihood has to be approximated. Two

approaches for a linearization based on Taylor series approximation were used in the thesis presented here: The first-order (FO) estimation method and the first-order conditional estimation (FOCE) method.

While the FO method linearises $log(\xi_i)$ at Θ, the FOCE methods linearises $log(\xi_i)$ for each individual at the individual's maximum likelihood. With this linearisation, the resulting likelihood approximation can be computed analytically. Thus, the FOCE method is more precise, especially in case of a larger degree of nonlinearity, but also more time-consuming [150]. Estimation can be further improved by using the interaction option, which means that the dependency of the residual variability on the interindividual variability is considered during estimation.

Estimates of the individual parameters ($\phi_{k,i}$, compared to the true and unknown value $\hat{\phi}_{k,i}$) are obtained by *post-hoc* estimation, which is performed in each iteration step of the FOCE method, but optional after successful minimisation with the FO method. These estimates are obtained by maximising the empirical Bayes posterior density of $\eta_{k,i}$, resulting in the name empirical Bayes estimates (EBEs) [151]. The name *post-hoc* arises from the estimation after the population parameters are obtained.

More methods are available for parameter estimation [152], but FO and FOCE (with and without interaction) are the ones most frequently used. More detailed information, including derivation of estimation methods applied in NLME modelling, can be found in literature [153,154].

2.1.1.3 Pharmacokinetic/pharmacodynamic modelling

Modelling of pharmacodynamic data as effect of the pharmacokinetics, so called PK/PD modelling, can be complex and different approaches can be applied depending on the data situation and the model [144]. Typically, the PK model is build first, then the PK/PD model can be developed in a simultaneous approach, where all PK and PD parameters are estimated at the same time, or in a sequential analysis. Furthermore, there are situations where no PK data is available, thus a previously developed model can be utilised and used in the development or evaluation of the PD part of the PK/PD model.

Simultaneous PK/PD modelling approach

In the simultaneous PK/PD modelling approach, all population parameters from the PK and PD part of the model are estimated simultaneously. This model is seen as the "best-case" performance, i.e. parameters are estimated with the lowest bias and the highest precision compared to the sequential analysis approaches [155,156]. On the other hand, this method is computationally expensive and time-consuming and was therefore not applied in this work

considering the sparse data situation, the complex PK and PK/PD models and the long convergence times.

Sequential analysis – conditioned on the individual PK parameters

Different sequential approaches are available considering the PK information to a different extent. The method conditioned on the individual PK parameters (IPP) uses the EBEs from the PK analysis to inform the pharmacodynamic response. Thus, the individual concentration-time profile is considered, but no error in these parameter estimates is assumed, which can lead to an underestimation of the imprecision of the PD parameters [155]. Further methodological developments account for the imprecision in the EBEs [157], but were not considered in the work for the aforementioned reasons.

Sequential analysis – without PK data available

This project faced two situations where no PK data were available. First, no concentration measurements were performed for the concomitant medication of carboplatin and cisplatin in the CEPAC-TDM study. To be still able to consider their effect on the PD, PK models from literature were utilised, only considering the population prediction. Consequently, no interindividual variability and parameter imprecision was allowed in the PK which probably led to an overestimation of the interindividual variability of the parameters linking PK and PD.

The second situation where no PK data were available, appeared for the conventional study arm of the CEPAC-TDM study (see section 2.2.1), where no paclitaxel PK data were measured. Thus, patients in Arm A were not considered in PK/PD model building, but in model evaluation. Here, population PK and PD parameters were fixed and *post-hoc* estimation was performed only based on the PD data, similar to the fixed population PK parameter (PPP) approach [158]. Even though this approach performs less well for estimation of population PD parameters [155], it was therefore possible to allow for variability in the PK and PD for model evaluation.

2.1.1.4 Baseline models

Baseline response is frequently measured in PK or PD, when endogenous substances are observed. Different methods were described by Dansirikul *et al.* [159]. The methods investigated in this thesis are shortly described in the following paragraphs.

Baseline method 1 (B1)

In the baseline method 1 (B1), the typical baseline (θ_{BL}) value is estimated as a population parameter. The individual baseline ($\phi_{BL,i}$) is then determined by assuming interindividual variability ($\eta_{BL,i}$) around the population value. Typically, a log-normal distribution is assumed

as in Eq. 2.6. This method is preferable if the residual variability is considerably higher than the interindividual variability on the baseline [159].

Baseline method 2 (B2)

Baseline method 2 (B2) uses the individually measured baseline value (BL_i) and allows deviation from this value with the same distribution as for the residual variability. Thus, the residual variability has to be estimated as a fixed-effects parameter (θ_{RV}), as e.g. described in Eq. 2.9. The same principle is then applied for the interindividual variability term (η_{BL}), for which variance is fixed to 1 and scaled by θ_{RV} (Eq. 2.17). Hence, no assumption is made about the distribution of the baseline values in the population.

$$\phi_{BL,i} = BL_i \cdot e^{\theta_{RV} \cdot \eta_{BL,i}} \quad \eta_{BL,i} \sim \mathcal{N}(0,\ 1) \qquad \textbf{Eq. 2.17}$$

2.1.1.5 Use of prior information for parameter estimation

Prior information can be used for the model structure by implementing knowledge of the underlying physiological mechanism or previously developed model structures. Further, the parameter estimates of such previously developed models can be used. This can be done in cases where the study data, on which the previous model was developed, is not available or to stabilise the estimation process, if there was only sparse sampling performed in the study to analyse.

In principle there are three methods to implement prior knowledge for parameter estimation [160]:

- Both datasets of the previous and current analysis can be merged and estimation includes all information simultaneously. This process can increase convergence time and is of course only possible if the previous dataset is available.
- The second approach is to fix some (or all) parameter estimates to the value of the prior analysis. If biased estimates are taken for the analysis, this can also lead to bias of the remaining newly estimated parameter [161]. Nevertheless, this approach can be useful for sampling regimens where no information about e.g. the absorption phase is included in the study data.
- Finally, the frequentist prior approach was developed [160], which includes the parameter estimates of the prior analysis, but also accounts for their uncertainty. In this approach, parameters are estimated but restricted by a penalty term that decreases the likelihood of parameters highly deviating from the prior ones. This method was applied in the here presented work and will be described more detailed in the following paragraphs.

Frequentist prior approach

In this frequentist prior approach, the overall posterior objective function value (OFV_{post}) that is minimised during estimation is the sum of i) the objective function value considering the current data and the population parameter estimates (OFV_{current}), as described in section 2.1.1.2, and ii) the penalty term (OFV_{prior}). This penalty term is based on the parameter estimates of the prior study and their uncertainty and is supposed to mimic the objective function, that would arise from to the prior study data. Hence, the minimisation has to balance the two objective function terms, meaning that the estimated parameters cannot differ too much from the prior ones, since it would increase OFV_{prior} even though it might decrease OFV_{current} to some extent.

To derive the penalty term, first a multidimensional distribution is built based on the fixed-effects parameters and their uncertainty described with the diagonal (and optimally the off-diagonal elements) of the variance-covariance matrix Γ (see section 2.1.2.2). In parallel an inverseWishart distribution is assumed for the random-effects parameters and their respective uncertainty. The uncertainty of a random-effects parameter ω_k is taken into account expressed as degrees of freedom (df_k) and can be seen as the number of patients/samples with full information in the prior analysis for interindividual and residual variability, respectively. Thus, the degrees of freedom should always be smaller than the number of patients/samples in the prior analysis. Eq. 2.18 was suggested for the calculation of the degrees of freedom for interindividual variability parameters [162].

$$df_k = 2 \cdot \left(\frac{{\omega_k}^2}{SE_{\omega_k}} \right)^2 + 1 \qquad \textbf{Eq. 2.18}$$

Finally, the product of the two distributions (multivariate normal for the fixed-effects parameters and inverseWishart for the random-effects) is built resulting in a normal-inverseWishart distribution. Twice the logarithm of the density of this distribution is then the penalty term OFV_{prior}. Other distributions than the normal-inverseWishart can possibly be assumed, but were not applied in this work.

This methodology is based on Bayesian statistics, however, due to the assumption that a true, but unknown value for each model parameter exists, the wording “frequentist prior” was established in literature [160].

2.1.1.6 Time-to-event modelling

In time-to-event (TTE) modelling, the dependent variable is not continuous, instead, it is dichotomous, i.e., whether the event has occurred or not. Hence, instead of optimising

likelihoods of PK and/or PD variables as described in section 2.1.1.2, the probability or probability density of having an event at a certain time is optimised. TTE analysis can also accommodate events that can occur more than once per patient, e.g. certain adverse events, which then requires a repeated TTE analysis. In this thesis TTE analysis was used to describe overall survival, thus, no repeated TTE analysis was required and the following will focus on non-repeated TTE. Further, this work focused on parametric survival analysis, since semi-parametric and non-parametric models are less suitable of simulations of different study designs (see section 1.4.2.2).

Some similarities between PK and TTE analysis can be seen, i.e. the hazard ($h(t)$) can be compared with an elimination rate in PK [163]. More precisely, the hazard is the instantaneous rate at which events occur. The survival function ($S(t)$), the time course of the probability of surviving at least up to time t, can be computed from the cumulative hazard at time t ($cumhaz(t)$) (see Eq. 2.19). Further, based on this, the distribution of survival times (probability density function, $pdf(t)$, see Eq. 2.20) can be derived.

$$S(t) = e^{-cumhaz(t)} \quad \textbf{Eq. 2.19}$$

$$pdf(t) = S(t) \cdot h(t) \quad \textbf{Eq. 2.20}$$

Distribution of survival times

Different distributions can be assumed for the distribution of survival times, e.g. exponential or Weibull distribution. In this work, a log-normal distribution for the event times (T) was assumed as suggested in [164], with mean θ and variance σ^2 (Eq. 2.21). The probability density function of event times is given by Eq. 2.22 and the survival function in Eq. 2.23.

$$log(T) = \theta + \varepsilon \quad \varepsilon_{i,j} \sim \mathcal{N}(0, \sigma^2) \quad \textbf{Eq. 2.21}$$

$$pdf(t) = \frac{1}{\sqrt{2 \cdot \pi \cdot \sigma^2} \cdot t} \cdot e^{-\frac{1}{2}\left(\frac{\log(t)-\theta}{\sigma}\right)^2} \quad \textbf{Eq. 2.22}$$

$$S(t) = 1 - \int_0^t pdf(t)dt \quad \textbf{Eq. 2.23}$$

For implementation of covariates in this TTE model, an accelerated failure time model can be used as in Eq. 2.24. In this approach, covariates are implemented in an additive manner on the mean of the log-normal distribution of event times, allowing for an easy interpretation of the covariate effect $\theta_{k,cov}$.

$$\theta = \theta_k + \theta_{k,cov} \cdot cov \quad \textbf{Eq. 2.24}$$

Censoring

In TTE analysis, censoring of events is a common methodological challenge, which means that the exact time of the event is not known or not recorded for some or all patients. Two different types of censoring can occur: (i) right censoring if not for all patient the event might have been observed during the time the patient was enrolled in the study and (ii) interval censoring if the event is recorded but exact time of the event is unknown (e.g. in the analysis of time to tumour progression, since tumour size is typically evaluated once every few weeks). The day the patients died is typically reported precisely, thus interval censoring is usually not of relevance in an overall survival analysis. However, patients dropped out without having an event or patients who had no event until database lock. For these right censored events, the probability of not having had an event at the time they were last observed is optimised during parameter estimation.

2.1.2 Model evaluation and selection

Model evaluation is an important step during model development. Model evaluation is used to assess whether the model predicts the data sufficiently well and for comparison and selection of different models during model development. Different techniques based on statistical methods, diagnostic plots and also a simulation-based analysis can be performed. Beside of these techniques, it is also important to evaluate the physiological plausibility which determines the applicability of the model for extrapolations, as discussed in section 1.1.3.1. In addition, the parsimony principle has to be considered, which aims for the lowest complexity of a model, thus, the lowest number of parameters. Hence, model evaluation does not necessarily need to find the model describing the data best, but has to find the balance considering the quality of the prediction, the purpose of the model, the physiological plausibility and the parsimony principle.

2.1.2.1 Strategies of model evaluation

One can distinguish between internal and external model evaluation strategies. The internal strategy uses the data from one study for model development and for the evaluation of the final model, while the external evaluation uses datasets from different studies.

External model evaluation is the most stringent method for investigating a developed model [165]. Nevertheless, obtaining new experimental data for model evaluation is especially in the clinical setting not always possible. Using data splitting, only parts of the data are used for model development (index dataset) and the remaining usually smaller part is used for model evaluation (validation dataset). The possibility to apply data splitting is also limited in cases of small study size or sparse sampling, since it increases the prediction error [166]. Therefore, it

is recommended to merge both datasets in the end of the analysis and re-estimate the parameters, based on the full information for both the internal data splitting evaluation [167] and the external model evaluation technique [165].

However, internal and external model evaluation apply the same techniques that will be described below. For external and data splitting, individual parameter estimates (EBEs) can be obtained by *post-hoc* estimation, without changing the population parameters. Thus, evaluation of the individual predictions is also possible.

2.1.2.2 Numerical and statistical methods

Objective function value and Akaike information criterion

The objective function value (OFV) is twice the negative log-likelihood (section 2.1.1.2). For two nested models, twice the logarithm of the ratio between their likelihoods is approximately χ^2 distributed [12]. The degree of freedom in this distribution is the difference in the number of estimated parameters between two models. Hence, a drop of 3.84 in the OFV can be considered superior with a significance level of α = 0.05 for a nested model with one additional parameter (degrees of freedom = 1). This significance test is called the likelihood ratio test and is used in model development to judge, whether e.g. an additional compartment or covariate improves the model prediction significantly.

Since comparison of OFV, and thus the likelihood ratio test, is only applicable for nested models, another criterion accounting for the difference in the number of estimated parameters is needed. For these situations (models that are not nested), the Akaike information criterion (AIC) is used. AIC is calculated as the OFV plus twice the number of parameters estimated, penalising models with more parameters. A drop in AIC cannot be statistically interpreted, but a threshold of 2 is often considered for decision in favour or against a model [168] otherwise, the simpler model is chosen (parsimony principle). Both criterions OFV and AIC can only be compared for models based on the same dataset.

Parameter precision

Standard errors and confidence intervals are used to evaluate the precision of the population parameter estimation. Standard errors can be computed from the variance-covariance matrix of the parameter estimates Γ (as square root of the diagonal elements). In NONMEM this variance-covariance matrix Γ is by default derived from the estimate of $R^{-1}SR^{-1}$ with R being the Hessian matrix (second derivative of the objective function at the maximum likelihood estimate), R^{-1} being the inverse matrix of R (Fischer information matrix) and S being the cross product gradient matrix. In case of numerical difficulties, an estimation of the parameter precision based only on S is possible [12].

The relative standard error ($RSE, \%$) is calculated for better comparison. For a fixed-effects parameter (θ_k) Eq. 2.25 is applied, while for a random-effects parameter ${\omega_k}^2$, reported as coefficient of variation ($CV, \%$) Eq. 2.26, is applied. The factor 2 in the denominator of Eq. 2.26 derives from the transformation from the variance to the standard deviation scale, which is needed when considering $CV, \%$ [144]. Confidence intervals can be computed based on the standard errors assuming normal distribution.

$$RSE_k, \% = \frac{SE_k}{\theta_k} \cdot 100 \qquad \textbf{Eq. 2.25}$$

$$RSE_{{\omega_k}^2,CV}, \% = \frac{SE_{{\omega_k}^2}}{2 \cdot {\omega_k}^2} \cdot 100 \qquad \textbf{Eq. 2.26}$$

Another method frequently applied to determine parameter precision is the bootstrap analysis. In this method, a large number (e.g. 1000) datasets are created by "sampling with replacement" of the individuals from the original dataset. Thus, a series of bootstrap datasets is generated, each including the same number of patients as the original one. Parameter estimation is performed for each of the bootstrap datasets and percentiles of the resulting parameter estimates serve as confidence intervals [8]. The convergence rate is defined as the proportion datasets with which parameter estimation was successful. A bootstrap should only be accepted if certain convergence rate was achieved, since a low convergence rate reduces the number of bootstrap estimations and therefore limits its value.

Finally, confidence intervals can be determined by log-likelihood profiling. In this method, no assumption on the distribution of the parameter values and therefore of the symmetry of the confidence intervals is made. The estimation is repeated several times fixing the parameter of interest each time to a different value but close to the one estimated previously. All other parameters are estimated in each run and the OFV is obtained. Since the evaluated models are nested to the investigated one, the parameter values that lead to an increase in the OFV of 3.84 are the lower/upper bound of the 95% confidence interval.

Shrinkage

Shrinkage happens in sparse data situations when only little information is available on the individual parameter estimates (the EBEs). In these situations, the variance of the EBEs shrinks towards zero. This observation is called η-shrinkage ($sh_{\eta,k}$) for parameter k. Similarly, ε-shrinkage (sh_ε) appears when the distribution of the individual weighted residuals (IWRES, see section 2.1.2.3) shrinks towards zero, due to the sparse data situation which leads to an "overfitting" [147,169]. η- and ε-shrinkage are defined in Eq. 2.27 and Eq. 2.28, respectively, where SD is the standard deviation. Shrinkage of interoccasion variability (κ-shrinkage, sh_κ)

Eq. 2.29 was derived based on the definition of η-shrinkage. Shrinkage greater than 20% - 30% can have substantial influence of diagnostics based on individual parameter estimates and can thus lead to misinterpretations [147,169].

$$sh_{\eta,k} = 1 - \frac{SD(\eta_{k,i})}{\omega_k} \quad \textbf{Eq. 2.27}$$

$$sh_{\varepsilon} = 1 - SD(IWRES) \quad \textbf{Eq. 2.28}$$

$$sh_{\kappa,k} = 1 - \frac{SD(\kappa_{k,i,o})}{\pi_k} \quad \textbf{Eq. 2.29}$$

Condition number

The condition number quantifies the degree of collinearity of parameter estimates, which can arise form correlations between independent variables or from a few influential observations. It is calculated as the ratio between the largest and the smallest eigenvalue of the variance-covariance matrix Γ. A high condition number indicates that the parameter estimates are very sensitive to the dataset, based on which the estimation was performed [12]. Thus, the condition number is a useful tool to identify ill-conditioning or overparameterisation of a model, although different cut-off values are used to judge ill-conditioning based on the condition number, ranging from 200 to 10 000 [144].

2.1.2.3 Standard goodness-of-fit plots

Standard goodness-of-fit (GOF) plots comprise certain graphical analyses, that is used to determine the “fit of the model to the respective observed data” and examine potential misspecifications of the model. These plots are based on the observed, the predicted and the residuals resulting from those:

The population prediction (PRED) is the predicted PK or PD measurement considering the independent variables, like time and dosing, but not the random effects. The individual prediction (IPRED) on the other hand considers in addition the individual parameter estimates (EBEs). The residuals (RES) and individual residuals (IRES) are calculated as the difference between the observed data and the population- and individual prediction, respectively. For computation of the weighted residuals (WRES) and individual weighted residuals (IWRES), a certain weighing scheme is applied to RES and IRES, respectively (regimens were applied as described in [144], page 132 – 133). While WRES and IWRES, are approximated using the FO method, conditional weighted (individual) residuals are calculated using the FOCE method [170].

Using these elements, the following plots were generated and evaluated for potential misspecifications:

- Measured PK or PD versus the respective population prediction
- Measured PK or PD versus the respective individual prediction
- Conditional weighted residuals versus time (or time after last dose)
- Conditional weighted residuals versus population prediction
- Individual weighted residuals versus time (or time after last dose)
- Individual weighted residuals versus population prediction

2.1.2.4 Visual predictive checks

The visual predictive check (VPC) is a simulation-based evaluation method to evaluate the predictive performance of a model. For this analysis, the underlying study including the design variables (e.g. dose, sampling time, covariates) are simulated stochastically (typically 1000 times, see section 2.1.3.2), using the model of interest and its parameter estimates. These simulated PK and/or PD profiles are then visually compared to the observed data. For this comparison, the 5^{th}, 50^{th} and 95^{th} percentiles are computed for the observations and simulations, respectively. Based on the percentiles of each of the simulated datasets the 90% confidence interval, around the simulated percentiles are typically shown as shaded areas. Simulated percentiles and their confidence intervals are finally compared with the percentiles of the observed data, indicating a sufficient prediction if the percentiles of the observed data are within the range of the confidence intervals of the simulated percentiles.

Binning

In clinical trials, sampling time points between individuals can vary for different reasons e.g. if the patient is not seeing the physician the day he/she is supposed to or due to organisation of the clinical routine. Thus, observations are often available not for distinct time points, but within a sampling window. In the VPC analysis, binning is used to summarise observations/simulations and percentiles are calculated for a time interval (bin). Binning allows to evaluate a smooth time course which is better to interpret. The number and boundaries of the bins should be set with respect to the sampling windows and should result in a balanced and reasonable number of observations in each bin, to calculate percentiles and their confidence intervals. In this thesis bins were set manually.

Prediction-corrected visual predictive check

VPCs can be misleading in cases of a wide range of a covariate in the population or in cases of adaptive dosing [169,171,172] as performed in the CEPAC-TDM study. For these cases, prediction-corrected visual predictive checks (pcVPC) can be performed, in which the

observed and simulated data are normalised using the population prediction (Eq. 2.30) [173]. $Y_{i,j}$ and $pcY_{i,j}$ denote here the simulated data of the jth observation for the ith individual and the respective prediction-corrected value. The parameter $PRED_{i,j}$ is the population prediction considering the independent and design variables and sampling time j of the ith individual. $\overline{PRED}_{bin}$ in contrast is the median of the population prediction of all observations in the respective bin. The same prediction-correction is applied for the observed measurements ($y_{i,j}$).

$$pcY_{i,j} = Y_{i,j} \cdot \frac{\overline{PRED}_{bin}}{PRED_{i,j}} \qquad \textbf{Eq. 2.30}$$

2.1.2.5 Normalised prediction distribution errors

Analysis of normalised prediction distribution errors (NPDE) is another simulation-based technique typically applied for external model evaluation. In contrast to the VPC/pcVPC, NPDE analysis is not (or not only) based on visual inspection and is thus less subjective. Calculation of the NPDEs is done in the following steps [174,175].

1. The study is stochastically simulated (including interindividual, interoccasion and residual bariability) M times (m = 1, ..., M; again typically M = 1000 simulations, see section 2.1.3.2).
2. Decorrelation is performed for the observed and simulated data to correct for the correlation of data within one individual.
3. Prediction distribution errors ($pde_{i,j}$) are computed (Eq. 2.31). For this calculation, $\delta_{i,j,k}$ can take the values 0 or 1 if the decorrelated simulated value is greater or smaller than the decorrelated observed one, respectively.

$$pde_{i,j} = \frac{1}{M} \cdot \sum_{m=1}^{M} \delta_{i,j,k} \qquad \textbf{Eq. 2.31}$$

4. Finally, normalisation is performed by applying the inverse cumulative distribution function. Thus, the resulting normalised prediction distribution errors are normally distributed with mean = 0 and variance = 1 (standard normal distribution), if the null hypothesis (H_0) that the data can be described by the model, holds true.
5. H_0 is evaluated by the following statistical tests:
    a. t-test to investigate whether the mean is significantly different from 0
    b. Fisher variance test to investigate whether variance is significantly different from 1
    c. Shapiro–Wilk test of normality to investigate whether the distribution is significantly different from a normal distribution

6. A global adjusted p-value is built based on all the three statistical testes and can be used for decision making.
7. Further graphical evaluation can be performed based on quantile-quantile plots, histograms and scatter plots over time and prediction of the NPDEs.

2.1.2.6 Model selection criteria

Selection of the structural model

Selecting between different structural models in this thesis was based on different criteria:

- Physiological plausibility: physiological plausibility was an important factor for model selection, since it is a requirement for reasonable extrapolations in simulations.
- Drop in OFV/AIC: Based on OFV/AIC it can be judged which model describes the data better. For nested models, a significance level of α = 0.05 in the likelihood ratio test models was used for decision making. If this criterion was not fulfilled the simpler model was chosen. In case of non-nested models, AIC was considered and a drop of ≥ 2 was needed to decide for the more complex models.
- Parameter precision: models with fixed-effects parameters estimated with a relative standard error of > 30 were not accepted.
- Condition number: Models with a condition number > 1000 were not chosen.
- Graphical evaluation based on Goodness-of-fit plots and pcVPCs: Only models improving the prediction based on the graphical analysis were chosen.

All different criteria were considered during base model development. All criteria had to be fulfilled to decide for a more complex model. Otherwise, based on the parsimony principle, the simple model was chosen.

Inclusion/exclusion of interindividual variability parameters

It is physiologically plausible to describe interindividual variability on all model parameters. However, estimation of all interindividual variability parameters is often not reliably possible, e.g. due to a sparse data situation. Thus, it was only included when it had a relevant extent ($CV, \%$ of at least 10%), improved the model prediction (decrease in OFV of ≥ 10, see section 2.1.2.2) and enough information was available for estimation (relative standard error < 50%, η-shrinkage < 50%, see section 2.1.2.2).

Covariate selection

Covariate model building was performed in Project 2 (neutropenia model) and 3 (tumour growth inhibition model and overall survival model). In all projects, physiological plausibility was a mandatory criterion for selection of a covariate-parameter relation. Further, graphical

evaluation of the base model was performed and only covariates that showed a trend in this visual inspection were investigated (details described in the respective project). Since additional therapy with chemotherapeutics, radiotherapy or G-CSF was typically not present at start of study therapy, these influences were evaluated by implementation in the model and the respective drop in OFV, in case the covariate-parameter relation was considered physiologically plausible, independent of the graphical exploration (which uses baseline values).

The stepwise covariate model-building procedure (SCM) [148] was followed in the respective projects. In the first step of SCM (forward inclusion), the preselected covariates were investigated in a univariate manner, i.e. one covariate is investigated at a time. The covariate decreasing the OFV most and at least with a significance level of α = 0.05 (ΔOFV = 3.84 for one additional parameter) in the likelihood ratio test was included. Then, again all remaining covariates were added one at a time. This procedure was repeated until no further significant covariates were found. The resulting model is called the “full covariate model”. As additional criterion in this thesis, interindividual variability in none of the parameters must have been increased due to inclusion of a covariate.

The second step, the backwards deletion, was used to account for multiple testing and thus uses a stricter significance level (α = 0.005, ΔOFV = 7.88 for one additional parameter). In this step, covariates were removed from the full covariate model one at a time, if not fulfilling the significance criterion.

The covariates resulting from the backwards deletion step were further analysed for their clinical relevance and removed from the model if not considered clinical relevant. Clinical relevance was fulfilled if the effect of the covariate causes a change in the group parameter $\theta_{k,g}$ compared to the typical value θ_k of ≥ 30% [176]. For continuous covariates, the minimum and maximum of the covariate in the study population was used to evaluate clinical relevance. Finally, it was evaluated whether sufficient information was available to estimate the covariate effect $\theta_{k,cov}$, meaning that the 95% confidence interval of a covariate parameter based on $RSE, \%$ or log-likelihood profiling must not include the value, which would mean no effect (e.g. 0 for a covariate implementation as in Eq. 2.13 or 1 as in Eq. 2.14, respectively). Deviations of this general procedure are stated in the respective project section.

2.1.3 Simulations

Simulations are, on the one hand, used for model evaluation as described in the previous section. On the other hand, simulations can be used to explore certain aspects of the model and increase thus the understanding of the system. Further, simulations are used to assess relevant questions about study design, for decision making during development and market

authorisation and for dose individualisation as discussed in section 1.1.3. Simulations give the possibility to ask “what if” questions by investigating different scenarios, e.g. different dosing regimens or special patient populations. For these purposes, we distinguish between deterministic and stochastic simulations:

2.1.3.1 Deterministic simulations: The typical profile

Deterministic simulations are used to simulate the typical concentration-time profile considering the design variables as e.g. dosing and covariates. Random-effects are not considered in this type of simulations. Hence, deterministic simulations do not reflect the range of PK or PD profiles that can result from a given scenario. Nevertheless, deterministic simulations can be useful to explore model properties.

2.1.3.2 Stochastic simulations: The population

Stochastic simulations, also called Monte Carlo simulations, on the other hand, consider interindividual and, if included, interoccasion variability. Therefore, it is sampled from the distributions defined by these random-effects parameters and based on the resulting individual parameters, the individual PK and/or PD profile is simulated. Thus, for this type of simulations the range of expected PK and/or PD outcomes can be examined. This approach is therefore useful to examine e.g. response in terms of toxicity or efficacy and evaluate the percentage of patients, that would profit from a certain dosing regimen. Hence, this is the approach applied e.g. for trial simulations or for investigation of dosing regimens. Depending on the question to examine, considerations about population, trial design to be simulated as well as the analysis of the simulation results have to be made [144].

2.1.4 Descriptive statistics

Generally statistical methods are described in the respective project as well as the previous parts of this section 2.1. To descriptively describe tendencies, the median was used, if not otherwise stated. Variability in the population was described by standard deviation, variance or coefficient of variation. Further, descriptive statistics that was performed for the exploratory analysis of the CEPAC-TDM study data is described in section 2.3.3.

For linear regression, the coefficient of determination (R^2), which is the squared Pearson correlation coefficient (Corr) was computed to quantify the correlation.

Statistical tests were performed with applying a significance level of α = 0.05, if not otherwise stated.

2.1.5 Software

Model development and stochastic simulations were performed using NONMEM (ICON Development Solutions. Ellicott City, USA. Version 7.3.0. http://www.iconplc.com/innovation/nonmem/) in combination with PsN (M. Karlsson, A. Hooker, R. Nordgren, K. Harling and S. Freiberga, Uppsala Universitet. Uppsala, Sweden. Version 4.4.0. https://uupharmacometrics.github.io/PsN/). Since the models of Project 1 and 2 were computationally expensive, a high-performance computing cluster (Soroban cluster https://www.zedat.fu-berlin.de/HPC/EN/Soroban) was used and parallelisation was performed, if possible. A run summary was created using Pirana (Pirana Software & Consulting. Version 2.9.4. http://www.pirana-software.com/) to maintain an overview of the modelling activities. Deterministic simulations were performed with Berkeley Madonna (R.I. Macey and G.F. Oster. University of California, Berkeley, USA. Version 8.3.18. http://www.berkeleymadonna.com/). Dataset preparation and plotting during explorative data analysis and model evaluation was performed in R (The project for statistical computing. Vienna, Austria. Version 3.3.0. https://www.r-project.org/) in combination with RStudio (Version 0.99.902. https://www.rstudio.com/). For plotting, the R package ggplot2 (version 2.1.0) was utilised, while for the evaluation of the simulation-based diagnostics the R packages vpc (Version 0.1.1) [177] and npde (Version 2.0) [175] were used. NONMEM model codes of the chosen models of Project 1 – 3 are given in the appendix (see section 10.3).

2.2 Data management of the CEPAC-TDM study data

2.2.1 Study design of the CEPAC-TDM study

Study objective

The objective of the CEPAC-TDM study was to evaluate, whether it is possible to reduce severe toxicity, namely grade 4 neutropenia, by applying the developed dose individualisation algorithm without compromising efficacy in terms of overall and progression-free survival. This investigator initiated trial was sponsored by the Central European Society for Anticancer Drug Research – EWIV (CESAR). It was a prospective, open-label, randomised, parallel-group study that was carried out in 10 study centres in Germany and Switzerland.

Study population, inclusion, exclusion criteria

Patients newly diagnosed with advanced NSCLC (stage IIIB-IV) were included with palliative intention. The inclusion criteria selected patients from both sex, age between 18 and 75 years and ECOG performance status of maximum 2. Additional criteria to be met were:

- Absolute neutrophil concentration $> 1.5 \bullet 10^9$ cells/L, which corresponds to grade ≤ 1 neutropenia
- Thrombocyte concentration $> 100 \bullet 10^9$ cells/L, which corresponds to grade 0 thrombocytopenia
- Plasma concentration of total bilirubin ≤ 2 • upper limit of normal (ULN = 1 – 1.5 mg/dL)
- Plasma concentration of aspartate aminotransferase (AST) and alanine aminotransferase (ALT) ≤ 2.5 • upper limit of normal, corresponding to grade ≤ 1 in the respective laboratory test or ≤ 5 • upper limit of normal in case of liver metastases (ULN = 40 U/L), corresponding to grade ≤ 2 in the respective laboratory test
- Creatinine clearance (according to Cockcroft-Gault formula [81]) ≥ 30 mL/min, corresponding to grade ≤ 1 chronic kidney disease; for patients planned to receive cisplatin: ≥ 60 mL/min, corresponding to grade 0 chronic kidney disease

Patients must have not received prior treatment with paclitaxel or cisplatin or carboplatin and must not have pre-existing neuropathy > grade I. The complete list of in- and exclusion criteria can be found in the study protocol (https://clinicaltrials.gov/ct2/show/NCT01326767).

Study treatment

An overview of the study is visualised in Figure 2.2. At baseline, disease status of the patients was evaluated (diagnosis, histology, tumour size, prior cancer treatment). In addition, demographics (e.g. age, body weight, body height, sex), medical history, complete blood count and ECOG performance status (among other parameters) were documented at baseline for each patient. Then, patients received paclitaxel treatment in combination with a platinum-based drug (cisplatin or carboplatin) for up to six cycles (cycle length: 3 weeks). After completion of the treatment phase, patients underwent an end of treatment visit and entered then the follow-up observation phase until death or until the overall study ended. For treatment, patients were randomised into two study arms:

- Arm A (conventional treatment arm): standard dosing of paclitaxel (200 mg/m² every three weeks)
- Arm B (experimental treatment arm): dose individualisation according to the published dosing algorithm (described in section 1.5.2, Figure 1.5).

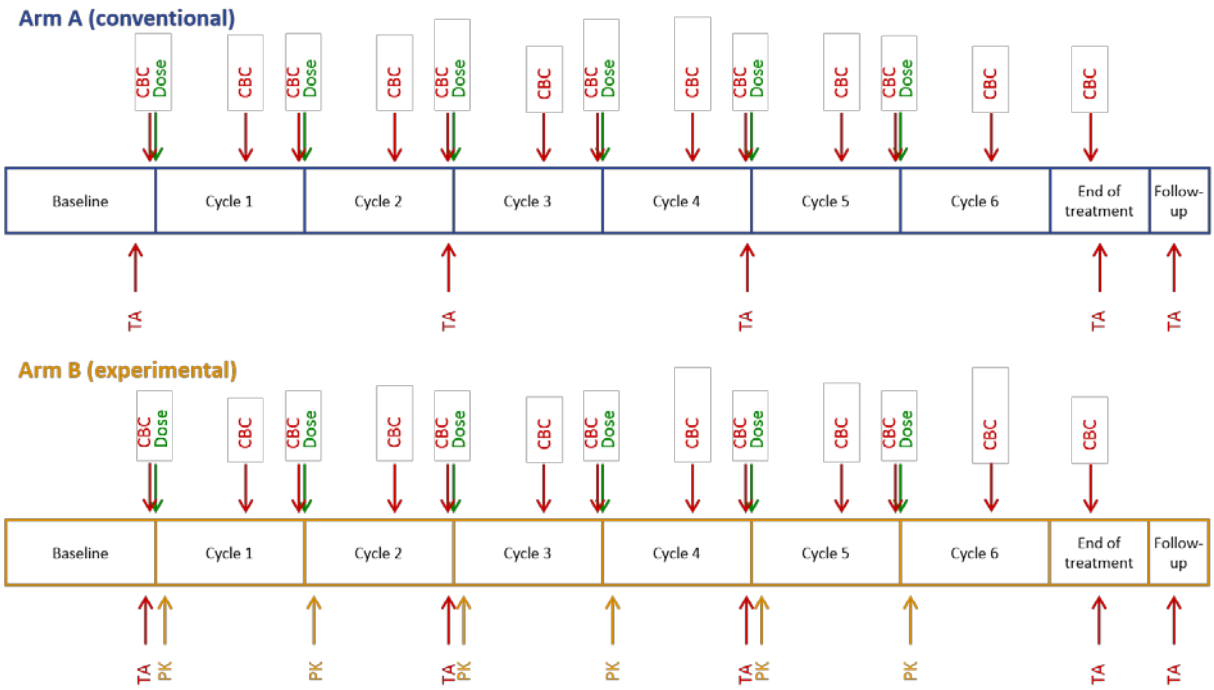

Figure 2.2: Study design of the CEPAC-TDM Study.
CBC: complete blood count; PK: pharmacokinetics; TA: tumour assessment.

Paclitaxel was administered at the beginning of each cycle, i.e. every 3 weeks. For patients in the conventional study Arm A, dose was based on body surface area (BSA) and was standardised to 200 mg/m² BSA. In Arm B, patients received the paclitaxel dose adapted to the described dosing algorithm, i.e. the 1st dose was based on age, sex and BSA. The following doses for these patients were then further adapted based on drug exposure and experienced grade of neutropenia in the previous cycle. Additionally, after the paclitaxel infusion, either cisplatin (80 mg/m² on day 1 or 40 mg/m² on day 1 and 2) or carboplatin (target AUC: 6 mg • min/L) was administered. Infusion duration was 3 h for paclitaxel, and 0.5 h and 2 h for carboplatin and cisplatin, respectively. Further dose or therapy adaptions of all 3 drugs were undertaken in case of toxicity (Table 2.1). To avoid hypersensitivity reactions to the paclitaxel formulation, premedication of dexamethasone and H_1- and H_2-antihistaminic drugs was ensured.

Table 2.1: Dose adaptations exceeding the dosing algorithm.

Drug	*Dose adaption in Arm A*	*Dose adaption in Arm B*
Paclitaxel	**Neutropenia grade 4**: reduction by 20%.	
	Peripheral neuropathy grade ≥ 2: reduction by 20% (if patient receives cisplatin, first switched to carboplatin, and only if neuropathy persists, paclitaxel should be reduced).	
	Non-haematological toxicity grade ≥ 3: reduction by 20%.	
Carboplatin	**Renal function:** dose is adapted every cycle according to the Cockcroft-Gault formula.	
	Thrombocytopenia grade ≥ 3: dose reduction by 75%.	
Cisplatin	**Peripheral neuropathy grade ≥ 2:** persisting at the start of the subsequent cycle: cisplatin is changed to carboplatin.	
	Nephrotoxicity: if glomerular filtration rate (GFR) drops to < 60 mL/min: cisplatin is changed to carboplatin.	
	Ototoxicity: cisplatin is changed to carboplatin.	

Dose adaptation due to toxicity was recommended in the same way for both study arms, beside of paclitaxel dose reduction due to neutropenia, since this was specified in the dosing algorithm for study Arm B.

Evaluation of drug exposure, toxicity and efficacy

For patients in study Arm B, the paclitaxel plasma concentration was determined 24 h after infusion. Paclitaxel concentrations were centrally measured for all study sides using high-performance liquid chromatography with ultraviolet detection as described in [178] with a lower limit of quantification (LLOQ) of 0.015 mg/L and precision and accuracy within the requirements of the EMA guideline [179].

This single plasma sample per cycle was utilised to determine the individual, cycle-specific $T_{C>0.05}$ as marker for drug exposure by *post-hoc* estimation with the published PK model [138]. $T_{C>0.05}$ was then used for dose adaption in the following cycle according to the algorithm. Thus, the *post-hoc* estimation was performed in each cycle with the information available until then, e.g. for cycle 3 the samples from cycle 1 and 2 were considered in addition.

A complete blood count (CBC) with white blood cell (WBC) differentiation to determine neutropenia and other haematologic toxicities, was evaluated at baseline, on day 1 and 15 ± 2 of each cycle and finally at the end of treatment visit. These analyses were performed at each of the study sites for the respective patients. Primary G-CSF prophylaxis was not allowed by

the protocol, but therapeutic G-CSF administration was allowed in patients experiencing prolonged grade 4 neutropenia (for at least 7 days), febrile neutropenia or grade 4 neutropenia after at least one prior dose reduction of paclitaxel (secondary prophylactic).

Evaluation of further toxicities, beside of neutropenia, according to the CTC AE criteria were observed during the whole treatment period. In addition, ECOG performance status was evaluated at the beginning of each cycle as well as in screening/baseline and end of treatment visit. Treatment was stopped in case of intolerable toxicity, decided on an individual basis.

Efficacy was evaluated based on the RECIST criteria of tumour growth. These criteria report a minimum size of 0.10 cm for tumour lesions and 0.15 cm for malignant lymph nodes to be measurable for assessment via a computed tomography (CT) scan [123]. Radiological assessment of tumour size was performed at baseline after cycle 2 and 4, after end of treatment and in the follow-up phase. Study therapy was ended as soon as tumour progression was detected. Besides the tumour size analysis, survival status was examined regularly, at least every 3 months.

2.2.2 Data management and dataset preparation

Raw data from the CEPAC-TDM study was processed and re-constructed in a NONMEM® readable format. This step was a critical step that was needed before modelling activities could be performed. All following steps are based on the created table file, thus careful thought about assumptions, changes and imputation of missing values are of importance. In addition, all steps done in the dataset preparation had to be well documented to achieve reproducibility and correct interpretation of the results. A summary of the created columns of the dataset, the interpretation of their content as well as modifications or imputations performed can be found in the appendix (see section 10.1). All dataset preparations were performed in R (see section 2.1.5), so that the script serves as documentation as well. To assure quality of the dataset preparation, the R script was proof-read by other working group members not involved in the project.

Generally, a NONMEM dataset contains information in columns about dosing, dependent variables (e.g. plasma concentration of paclitaxel for the PK analysis or neutrophil concentration/tumour size for the PD analysis) and independent variables (e.g. time, patient-specific covariates). In addition, NONMEM specific variables specifying e.g. the type of event of a row (i.e. dosing event or measurement) had to be specified.

Only data before the database lock on the 11th November 2015 were used for the analysis. Follow-up visits with additional information about tumour progression and survival performed after this date were not considered. This can result in discrepancies between the statistical analysis of the data performed in [139] and here presented work, when analysing time to

progression, progression-free survival and overall survival (252 vs 296 reported death in the here presented analysis compared to [139], respectively).

Missing information of independent and dependent variable

Treatment of missing data depends on the type of the unavailable information, i.e. missing data of the time point (independent variable), the result of the PK or PD measurements or the covariate information have to be treated differently.

Regarding missing information about the time point of an event, some events in the dataset only had the month and the year reported, then the middle of the month was assumed. This was for example the case for some adverse events or the start of co-medication, but never for dosing or measurement of the PK or PD variable used in this thesis, thus it was not a critical assumption. Further, clock time was only reported for paclitaxel dosing and PK sampling. Since the other variables (e.g. neutrophil concentrations, tumour size and covariates) do not change in considerable magnitudes within one day, the imputation performed here (10:00 o'clock was assumed for all events, since it was the most frequent clock time in the dataset) was also not crucial. Nevertheless, also some dosing or PK sampling events contained missing or implausible information, the performed changes can be found in the appendix (see section 10.1, Table 10.1 – Table 10.3) for the respective columns.

For missing information of the evaluated PK or PD variable, two potential documentations were observed: either reported as missing or as 0, meaning that the measurement was below the lower limit of quantification (BQL). Since the number of BQL data for the PK, as well as for the neutrophil concentrations and tumour size, was very low (see section 3.1.1), they were considered to be missing and no imputation was performed. On the other hand, missing PK and neutrophil samples were more frequent but no reason was documented, therefore these samples were assumed to be missing completely at random and were not considered in the following analysis. Imputation of missing times of tumour size measurements was not possible, since the protocol was not strict about the measurement times, especially in the follow-up. Further, additional measurements were performed that were not asked for in the protocol. Hence, also for the PK, the missing measurements were assumed to be missing completely at random. If for tumour size one lesion was not measurable, it was assumed that this lesion is in complete response and does therefore not contribute to the sum of diameters.

Finally, missing covariate information had to be considered. For the analysis with NONMEM covariate information has to be complete for all time points for each patient. Thus, if no information was available at all for a patient the median of the whole population or a subgroup (if dependence of the covariate on a subgroup was known from literature, e.g. females/males) was imputed. For the time between covariate measurements, the method "last observation

carried forward" was applied, so that the information of the last measurement was used until a new measurement was performed. For bilirubin concentrations (BILI), which was a covariate of the PK model linear interpolation was performed instead, i.e. a linear regression was performed for the time between two measurements. This was done, since the changes between two measurements were high for some patients and a more realistic approach was aimed for. Still linear interpolation was not performed within the NONMEM analysis, but the standard approach (next observation carried backwards) was used.

Outliers and implausible values

The dataset was evaluated for implausible values and outlies in each column. These were investigated by graphical evaluation and physiological plausibility. In general, outliers were only manipulated in case of implausibility, as e.g. implausible values of tumour size diameter of lymph nodes of > 16 cm were assumed to be reported in mm instead of cm. Further, for some events implausible dates were reported that were probably caused by a typographical mistake in the year. All changes were marked in the dataset, with a so-called "flag", which is a column that describes the respective event the change or imputation performed. A summary of the changes, their underlying assumptions and their flagging is reported in the appendix (see section 10.1).

2.2.3 Exploratory analysis: Numerical, statistical and graphical analysis

The objective of the exploratory analysis was, on the one hand, to assess the plausibility and detect possible inconsistencies and outliers. On the other hand, the aim was as well to explore the data to inform the modelling strategy, e.g. baseline behaviour, delays in the PK or the PD response [180,181]. The following plots were created and analyses performed:

- Cross-column checks of the dataset: this step ensures that the requirements of NONMEM are fulfilled by checking that certain conditions in one column result in certain condition in another column. E.g. that dosing and measurement information are provided in separate rows and that in case of a paclitaxel dosing the time after last dose is set to 0.
- Outliers in the dependent variable were detected in index plots of the data variables against the patient identification (ID).
- To analyse potential covariates, a summary of patient characteristics was created and the distribution of the covariates was visualised in histograms and bar charts for continuous and categorical covariates respectively.
- In addition, correlations between covariates were analysed:

  - For correlation between two continuous covariates, scatter plots of one covariate against another were created and correlation coefficient (Corr) was calculated (see section 2.1.4).
  - For correlation between two categorical covariates, stacked bar charts were prepared.
  - For correlation between a continuous and a categorical covariate, Box-and-Whisker plots were generated.
  - Tabular summary of previous therapy, concomitant therapy and supportive G-CSF therapy.
- Adherence to the dosing algorithm and cycle length was analysed.
- Finally, an exploratory graphical analysis was performed applying different stratifications (e.g. by sex or study arm) for comparison. If needed, variables were transformed to log-scale to focus on the lower value range. In this step, the following aspects were visualised:
  - Dose evolution over time
  - Development of the $T_{C>0.05}$ determined during the study over the treatment cycles
  - Paclitaxel concentration-time profile
  - Neutrophil concentration over time as well as other blood cell concentrations
  - Tumour growth over time
  - Time to tumour progression, overall and progression-free survival were visualised in Kaplan-Mayer plots
  - Maximum number of study cycles patients received and reasons for not finishing the 6 treatment cycles were explored

2.3 Project 1: Pharmacokinetic modelling of paclitaxel

2.3.1 Original paclitaxel PK model and its external model evaluation

In this project, a published paclitaxel PK model (original/published PK model) developed by Joerger *et al.* [138] was utilised. This PK model was the origin for the developed dosing algorithm (see section 1.5.2) and was applied during the CEPAC-TDM study (see section 2.2.1) to compute the individual $T_{C>0.05}$ (see section 2.2.1), which was then determining the dose of the next cycle for patients in the experimental study Arm B. Further, the resulting individual concentration-time profiles were used to determine the drug effect on the pharmacodynamics in terms of neutropenia in the here presented work.

The pharmacokinetics of paclitaxel in the original model were described by a three-compartment (one central and two peripheral compartments) model with nonlinear distribution to the 1st peripheral compartment and nonlinear elimination (Figure 2.3). The following structural parameters were used to describe this model:

- Central volume of distribution (V_1)
- Volume of distribution of the 2nd peripheral compartment (V_3)
- Maximum transport capacity (VM_{TR})
- Paclitaxel concentration at half VM_{TR} (Km_{TR})
- Distribution rate constant between central and 1st peripheral compartment (k_{21})
- Intercompartmental clearance between central and 2nd peripheral compartment (Q)
- Maximum elimination capacity (VM_{EL})
- Paclitaxel concentration at half VM_{EL} (Km_{EL})

For the here presented work, the metabolite concentrations described in the original model were neglected, since their formation did not influence the rest of the PK and these metabolite concentrations were not available in the study data.

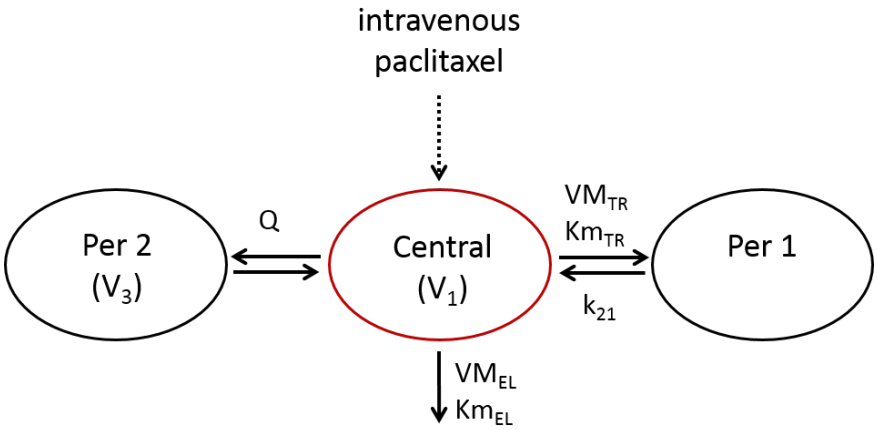

Figure 2.3: Original PK model of paclitaxel (modified from [138,140])**.**
Compartments: Central: central paclitaxel compartment; Per1 and Per2: 1st and 2nd peripheral compartment of paclitaxel, respectively.
k_{21}: distribution rate constant between Central and Per1; Km_{EL}: paclitaxel concentration at half VM_{EL}; Km_{TR}: paclitaxel concentration at half VM_{TR}; Q: intercompartmental clearance between Central and Per2; V_1: central volume of distribution; V_3: volume of distribution of Per2; VM_{EL}: maximum elimination capacity; VM_{TR}: maximum transport capacity.

As covariates explaining parts of the interindividual variability, BSA, sex, age and total bilirubin concentration (BILI) were implemented on the maximum elimination capacity (VM_{EL}) using power functions (Eq. 2.32), in which θ_{BSA}, θ_{SEX}, θ_{AGE} and θ_{BILI} were the respective fixed-effects parameters to describe the covariate effects and BSA, SEX, AGE and $BILI$ were the individually measured covariates (for SEX: 0 corresponds to females and 1 to males). The parameter $\theta_{VM_{EL}}$

specifies the typical value of VM_{EL} for a patient with typical BSA (1.8 m²), sex (female), age (56 years) and BILI (7 µmol/L) to which the equation was centred.

$$VM_{EL} = \theta_{VM_{EL}} \cdot \left(\frac{BSA}{1.8\ m^2}\right)^{\theta_{BSA}} \cdot {\theta_{SEX}}^{SEX} \cdot \left(\frac{AGE}{56\ years}\right)^{\theta_{AGE}} \cdot \left(\frac{BILI}{7\ \mu mol/L}\right)^{\theta_{BILI}} \quad \textbf{Eq. 2.32}$$

Interoccasion variability was incorporated on the central volume of distribution (V_1) and on VM_{EL}. To describe interindividual, interoccasion and residual variability, an exponential model was assumed. Since the PK data was log-transformed, the exponential residual variability model was implemented by using a linear function (see section 2.1.1.1). First-order conditional estimation (FOCE) was used as estimation method. The parameter estimates are reported in Table 3.5 (left column).

The published PK model described above was externally evaluated, using the data from the CEPAC-TDM study. For this and all following steps in Project 1, only patient data from the experimental study Arm B was utilised, since only here PK concentrations were measured. A *post-hoc* estimation was performed to obtain the individual parameter estimates and the individual concentration-time profiles without re-estimating the population parameters. Further, 1000 simulation of the study population were performed. Based on these results the following evaluations were performed including stratifications on the implemented covariates:

- Basic goodness-of-fit plots of individual- and population prediction and residuals (see section 2.1.2.3)
- Evaluation of shrinkage and distribution of the individual parameters (see section 2.1.2.2)
- Prediction-corrected visual predictive checks (pcVPC) (see section 2.1.2.4)
- NPDE analysis (see section 2.1.2.5)

2.3.2 Model optimisation combining prior knowledge and the CEPAC-TDM data

For optimisation of the PK model to account for the population of the CEPAC-TDM study, the population parameters were re-estimated, considering the prior information from the original model. Thus, the frequentist prior approach using the Normal-InverseWishart distribution [160] was implemented, extracting the final PK parameter estimates and their precision (see section 2.1.2.2) from the NONMEM output of the original PK model. Precision of the fixed-effects parameters was determined by the diagonal elements of the variance-covariance matrix Ω (Model I). In addition, the off-diagonal elements of this matrix were used in Model II. Precision of the interindividual variability parameters was described by the degrees of freedom (df_k, Eq. 2.18), representing the number of patients with full information for the respective parameter in the original study. The degrees of freedom for estimating the residual

variability were set to 1000, which was the lowest value which resulted in successful and stable estimation on the one hand and flexibility on the other hand. Interoccasion variability was not estimated but, assumed to be the same as published, since only one PK measurement per cycle (= occasion) was available.

To compare the model parameters in the linear part of saturable maximum effect (Emax) function, clearance for low concentrations CL_{lin} was calculated (Eq. 2.33), as well as the parameters k_{13} (Eq. 2.34) and k_{31} (Eq. 2.35, respectively), which are the rate constants for the linear distribution to the 2nd peripheral compartment and back to the central compartment, respectively.

$$CL_{lin} = VM_{EL}/Km_{EL} \quad \textbf{Eq. 2.33}$$

$$k_{13} = Q/V_1 \quad \textbf{Eq. 2.34}$$

$$k_{31} = Q/V_3 \quad \textbf{Eq. 2.35}$$

2.3.3 Evaluation of the impact of the optimised model

The two optimised PK models using the prior approach (with (Model II) and without (Model I) use of the off-diagonal element of the variance-covariance matrix of the fixed-effects parameters) were evaluated and compared to the original model on the individual and population level. Thus, the influence of the new parameter set on the predicted concentration-time profile was evaluated.

While in the CEPAC-TDM study $T_{C>0.05}$ was obtained by *post-hoc* estimation (see section 2.1.1.2) from the available information in the respective cycle, $T_{C>0.05}$ in the following steps was determined from the full information of all treatment cycles so far for each patient and was even determined for cycles without PK measurement. Therefore, the number of patients per cycle and the individual parameter value itself can differ between the ones presented in the exploratory data analysis and the ones determined in Project 1.

PK model evaluation and comparison – population level

For model evaluation of the optimised PK model, a bootstrap analysis [182] (1000 bootstraps) was performed to retrieve the 95% confidence intervals of the parameter estimates (see section 2.1.2.2). For comparison, the confidence intervals of the original model were calculated based on the standard error (retrieved from the original NONMEM output) assuming normal distribution.

Further, a deterministic simulation (see section 2.1.3.1) was performed with the original and the optimised PK parameter sets, to explore the differences in the behaviour of the models. In

addition, goodness-of-fit plots and pcVPCs were generated, to evaluate potential improvements of the model prediction.

PK model evaluation and comparison – individual level

Individual parameter estimates were again obtained by *post-hoc* estimation for the original and the optimised PK model (only performed for Model I) and disagreements of the two models were quantified as bias and imprecision for different parameters p (Eq. 2.36, Eq. 2.37 and Eq. 2.38) [183]. These parameters p are the EBEs on the one hand and the exposure parameters $T_{C>0.05}$ and AUC on the other.

$$RPE_{p,i,o} = \left(P_{i,o,original} - P_{i,o,optimised}\right)/P_{i,o,optimised} \quad \textbf{Eq. 2.36}$$

$$MRPE_p = median\left(RPE_{p,i,o}\right) \quad \textbf{Eq. 2.37}$$

$$MARPE_p = median\left(\left|RPE_{p,i,o}\right|\right) \quad \textbf{Eq. 2.38}$$

In which $P_{i,o,original}$ and $P_{i,o,optimised}$ were the parameter value of individual i at occasion o (if interoccasion variability was applicable) based on the original and the optimised model, respectively; $RPE_{\mathrm{p,i,o}}$ was the relative prediction error of the original parameter from the optimised of parameter p; $MRPE_p$ was the median relative prediction error expressing bias and $MARPE_p$ was the absolute (unsigned) value of the relative prediction error expressing imprecision for each parameter, taking as reference the optimised parameters.

Evaluation of the impact of the optimised model on the study outcome

The clinical impact of the new parameter set of Model I for the CEPAC-TDM study was further evaluated for $T_{C>0.05}$. $T_{C>0.05}$ was obtained firstly by *post-hoc* estimation for the original and the optimised PK model for each patient in study Arm B. Secondly, 1000 stochastic simulations of the patient population were performed for patients in Arm B and in Arm A using the optimised PK model. $T_{C>0.05}$ obtained via the two approaches (*post-hoc* estimation and simulation) for the different study arms was compared using Box-and-Whisker plots over the treatment cycles. Thus, the target attainment of $T_{C>0.05}$ being in the therapeutic window was comparted between the two approaches and study arms.

2.3.4 Evaluation of limited sampling strategy applied in the CEPACT-TDM study

Since the individual PK concentration-time profile determines the drug effect on neutropenia in the PK/PD model (Project 2), the PD parameter estimation depends on the quality of the individual PK prediction. Therefore, the feasibility of the sequential PK/PD modelling approach was evaluated, considering the spare PK sampling during the CEPAC-TDM clinical trial. For

this purpose, the precision of the EBEs and exposure parameters were investigated by simulation and *post-hoc* re-estimation:

- Simulation step: The PK model with the optimised parameters (Model I) was used to stochastically simulate 100 different datasets using the patient characteristics, the dosing information and the sampling time points of the patients in Arm B from the CEPAC-TDM study. The simulated parameters (PK and exposure parameters) ($P_{\mathrm{i,o,sim}}$) and the simulated concentrations at the study sampling time point were recorded and treated as reference.
- *Post-hoc* re-estimation step: As in the CEPAC-TDM study, a *post-hoc* estimation was performed based on the simulated single plasma sample per cycle. The individual parameters ($P_{\mathrm{i,o,re-est}}$) were obtained for each patient of each of the simulated datasets.
- Comparison: For calculation of bias and imprecision, the relative prediction errors $RPE_{p,i,o}$ were computed as in Eq. 2.39 and bias and imprecision were obtained by applying Eq. 2.37 and Eq. 2.38.

$$RPE_{p,i,o} = \left(P_{i,o,re-est} - P_{i,o,sim}\right)/P_{i,o,sim} \qquad \textbf{Eq. 2.39}$$

2.4 Project 2: Modelling of paclitaxel-induced long-term neutropenia

2.4.1 Original PK/PD model to describe neutropenia and its external model evaluation

Originally, Joerger *et al.* [138] described paclitaxel-induced neutropenia with the gold standard Friberg *et al*. [119] structural model, which described the proliferation and maturation process of the granulopoiesis with a chain of compartments. This chain started with a proliferation compartment (Prol) mimicking the rapidly dividing progenitor cells. Cells in this compartment replicated with a proliferation rate constant (k_{prol}). In the next step, cells were maturating over a chain of transit compartments (Transit1 – Transit3) until they reached the state of circulating neutrophils (Circ), from where cells were finally eliminated (Figure 2.4).

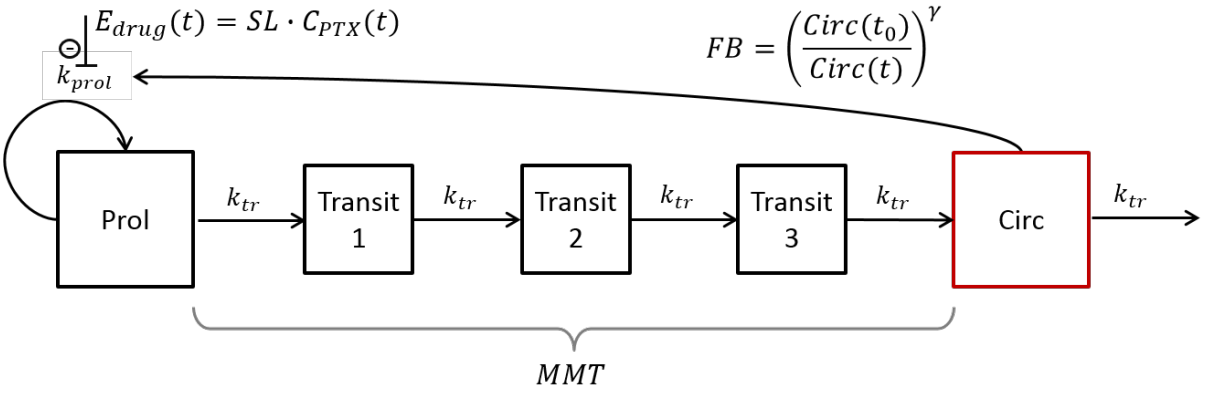

Figure 2.4 Structure of the gold standard PK/PD model describing neutropenia resulting from paclitaxel therapy (modified from [104,119])**.**
Compartments: Circ: circulating neutrophil cell compartment; Prol: proliferating cell compartment; Transit1-Transit3: transition compartments.
Parameters: $Circ(t)$ and $Circ(t_0)$: concertation of circulating cells at time t and at baseline, respectively; $C_{PTX}(t)$: paclitaxel concentration at time t; $E_{drug}(t)$: drug effect on k_{prol} at time t; FB: feedback; k_{prol}: proliferation rate constant of cells in Prol; k_{tr}: transition rate constant of maturation chain; MMT: mean maturation time; SL: slope factor of paclitaxel; γ: exponent of feedback function.
Colour: red: observation compartment.

Due to homeostasis, the transition rate constant (k_{tr}) was assumed to be equal to k_{prol}. Further, the elimination rate of the circulating cells was assumed to be equal to k_{tr} as well. The transition rate constant k_{tr} was derived via the estimated mean maturation time (MMT), with n being the number of transit compartments (Eq. 2.40). For this project, n was assumed to be 3 as in the original model.

$$MMT = (n+1)/k_{tr} \qquad \textbf{Eq. 2.40}$$

To enable the system to recover after being disturbed by chemotherapy, a feedback mechanism (FB) was included in the model, which was mimicking the physiological system of cytokines as G-CSF that induce the proliferation of progenitor cells. FB was defined as the ratio between the concentration of circulating cells at time t ($Circ(t)$) and at baseline ($Circ(t_0)$) to the power of the feedback exponent γ (Eq. 2.41). The proliferation rate constant k_{prol} was multiplied by FB. Thus, FB increased or decreased the effective proliferation depending on the neutrophil concentration $Circ(t)$. Further, $Circ(t_0)$ was used to initialise all PD compartments (Prol, Transit1 – 3, Circ) at baseline (time t = 0).

$$FB = \left(\frac{Circ(t)}{Circ(t_0)}\right)^{\gamma} \qquad \textbf{Eq. 2.41}$$

A linear effect of the paclitaxel plasma concentration at time t ($C_{PTX}(t)$) on k_{prol} was assumed, in which the slope factor (SL) defined the sensitivity of the physiological granulopoiesis system to the drug (Eq. 2.42). This drug effect (E_{drug}) was inhibiting the proliferation (cytostatic effect)

and could even lead to a net loss of cells from the proliferation compartment (cytotoxic effect), if E_{drug} was greater than 1 since k_{prol} was multiplied by (1 - E_{drug}).

$$E_{drug} = SL \cdot C_{PTX}(t) \qquad \textbf{Eq. 2.42}$$

In the original model [138], the baseline method B2 (see section 2.1.1.4) was used to describe $Circ(t_0)$. Thus, only the system-related parameters MMT and γ and the drug-related parameter SL were originally estimated as fixed-effects parameters. An exponential interindividual variability model was assumed for MMT and SL. For the residual variability, an exponential model was assumed by logarithmic transformation of the dependent variable (neutrophil concentration), as described in Eq. 2.9.

A sequential modelling approach was applied (see section 2.1.1.3), using the individually estimated PK parameters (from the optimised PK model in Project 1) to describe the concentration-time profile of paclitaxel ($C_{PTX}(t)$) for each patient. Parameter estimates of the original model are given in Table 3.7 (column “Gold standard (original)”).

This published PK/PD model was externally evaluated, as described for the PK model in section 2.3.1, using basic goodness-of-fit plots, pcVPCs and NPDE analysis. In line with the original model, the FO estimation algorithm was used for the external model evaluation.

2.4.2 Model optimisation to describe long-term toxicity

2.4.2.1 Base model development for cumulative neutropenia

Parameters of the structural gold standard neutropenia model, described in the previous section, were re-estimated using the data of the CEPAC-TDM study. Further, three different structural models were investigated (Model A – C, described in the following paragraphs), of which two (Model A and B) were adapted from literature. For all model optimisation steps, the estimation algorithm was changed from FO to FOCE with interaction. Moreover, it was investigated whether the model prediction could be improved by applying baseline method B1 (see section 2.1.1.4). Additionally, the need of the interindividual variability on MMT was examined. For all investigated PK/PD models, the PD compartments were initialised with the individual value of $Circ(t_0)$ as in the original model, except for some compartments in Model B (see following paragraphs).

Model A: Modification of the feedback function

Model A (Figure 2.5), had been developed to describe thrombocytopenia in patients treated with trastuzumab emtansine [121]. The rational of this model was that parts of the proliferating cells are depleted due to the cytotoxic drug. This was implemented by dividing the baseline

concentration $BASE_{tot}(t_0)$ into two parts $BASE_1$ and $BASE_2$. On $BASE_2$, a second linear drug effect (E_{drug2}) was implemented with a depletion rate constant k_{depl} describing the relation between drug exposure and E_{drug2}. This additional drug effect led to a reduction of the overall baseline over time ($BASE_{tot}(t)$) until $BASE_{tot}(t) \approx BASE_1$, which thus reduced the feedback FB and finally the extent of proliferation in Prol. Originally, the average concentration of trastuzumab emtansine in each cycle was used as drug exposure parameter [121]. For the CEPAC-TDM data, not the average concentration but $T_{C>0.05}$ of paclitaxel was implemented in the PK/PD model as drug exposure parameter determining E_{drug2}.

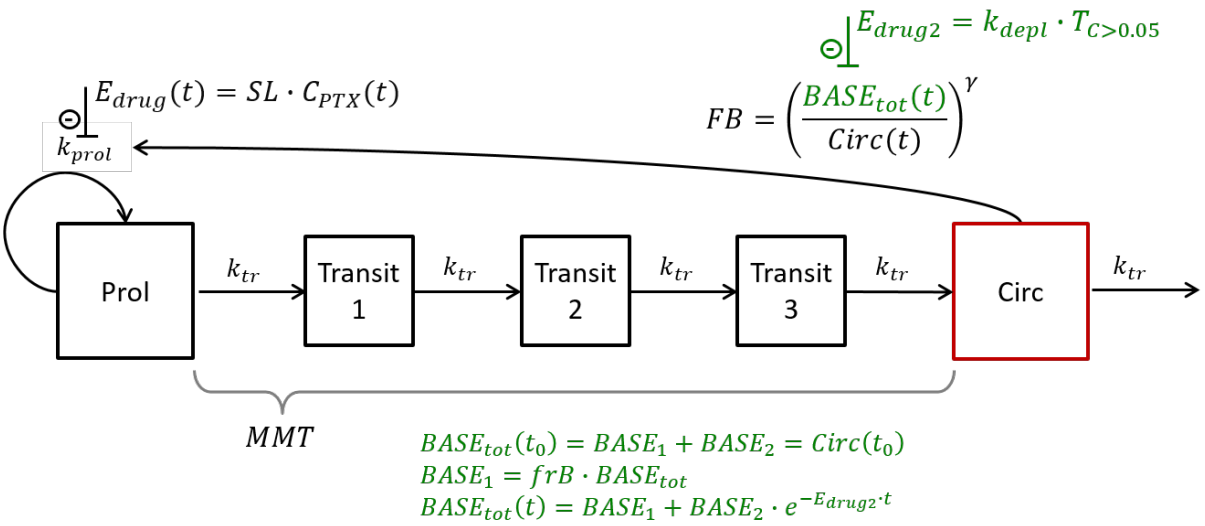

Figure 2.5: Structure of Model A (modified from [121,140])**.**
Compartments: Circ: circulating neutrophil cell compartment; Prol: proliferating cell compartment; Transit1-Transit3: transition compartments.
Parameters: $BASE_1$: baseline of proliferating cells not affected by depletion; $BASE_2$: baseline of proliferating cells affected by depletion; $BASE_{tot}(t)$ and $BASE_{tot}(t_0)$: total baseline of proliferating cells at time t and at time t = 0, respectively; $Circ(t)$ and $Circ(t_0)$ concentration of circulating neutrophils at time t and at time t = 0, respectively; $C_{PTX}(t)$: paclitaxel plasma concentration at time t; $E_{drug}(t)$: drug effect on k_{prol} at time t; E_{drug2}: additional drug effect on $BASE_2$; FB: feedback; frB: fraction of $BASE_{tot}(t_0)$ not affected by depletion; k_{prol}: proliferation rate constant of cells in Prol; k_{tr}: transition rate constant of maturation chain; MMT: mean maturation time; SL: slope factor of paclitaxel; $T_{C>0.05}$: time of C_{PTX} > 0.05 µmol/L; γ: exponent of feedback function.
Colour: red: observation compartment; green: changes from gold standard model.

Originally, k_{depl}, the depletion rate constant for the second drug effect and $BASE_1$ were estimated in addition to the parameters implemented in the Friberg *et al.* model (MMT, γ and SL) [121]. In this work, the model was re-parametrised to achieve a better interpretability of the parameters: frB, the fraction of circulating cells at baseline not affected by the second drug effect, was estimated instead of $BASE_1$.

Model B: Implementation of quiescent cell cycle

Model B (Figure 2.6) was based on a model, that was originally developed to describe neutropenia after different doses of diflomotecan [122]. The physiological rationale for the

altered model structure was the hypothesis, that not all potentially proliferating cells in the bone marrow are proliferating and that these resting quiescent cells are not affected by the chemotherapy. Two additional compartments (Q1 and Q2) were implemented in the gold standard structural model [119] which accounted for these quiescent cell in a cell cycle. Two additional parameters describing the circulation between the proliferation compartment and the quiescent stages were estimated: F_{prol} which was the fraction of cells proliferating and not transiting to the quiescent state, and k_{cycle} the transition rate constant for the circulation of the quiescent cells.

The compartments Prol, Q1 and Q2 were not initialised by $Circ(t_0)$ as for all other remaining compartments, but with $Circ(t_0)/F_{prol}$ for the proliferation compartment and with $(1 - F_{prol})/F_{prol} \bullet Circ(t_0)$ for Q1 and Q2 in the quiescent cell cycle.

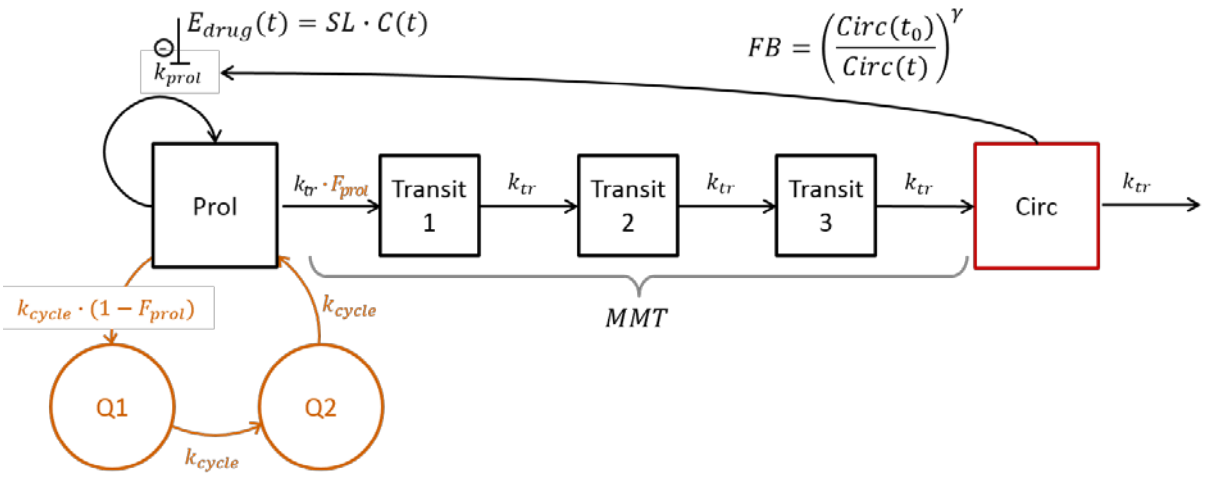

Figure 2.6: Structure of Model B (modified from [122,140])**.**
Compartments: Circ: circulating neutrophil cell compartment; Prol: proliferating cell compartment; Q1 and Q2: 1st and 2nd quiescent cell compartment; Transit1-Transit3: transition compartment.
Parameters: $Circ(t)$ and $Circ(t_0)$ concentration of circulating neutrophils at time t and at time $t = 0$, respectively; $C_{PTX}(t)$: paclitaxel plasma concentration at time t; $E_{drug}(t)$: drug effect on k_{prol} at time t; FB: feedback; F_{prol}: fraction of proliferating cells entering maturation chain; k_{cycle}: circulation rate constant within quiescent cell cycle; k_{prol}: proliferation rate constant of cells in Prol; k_{tr}: transition rate constant of maturation chain; MMT: mean maturation time; SL: slope factor of paclitaxel; γ: exponent of feedback function.
Colour: red: observation compartment; orange: changes from gold standard model.

Model C: Implementation of slowly proliferating stem cells

The physiological rationale for the development of a new model, Model C (Figure 2.7), was hierarchy of the haematopoietic system, where pluripotent stem cells are the origin of the progenitor cells. Those cells were not considered in the gold standard model, but were implemented in Model C as stem cell compartment (Stem). A smaller proliferation rate constant (k_{stem}) was implemented for the stem cell compartment and the influence of the drug effect and the feedback mechanism on this parameter was kept. To ensure equilibrium of the haematopoietic system without therapy, k_{prol} was estimated as a fraction of the transition rate

constant k_{tr}. This parametrisation had the advantage, that k_{tr} could still be derived from MMT, as described in Eq. 2.40, which allowed comparability to the original model and to Model A and B. The structure of Model C was defined by the following system of ordinary differential equations (Eq. 2.43 - Eq. 2.48), which all were initialise with the individual value of the baseline $Circ(t_0)$ as in the gold standard model:

$$\frac{dStem}{dt} = k_{stem} \cdot \left(1 - E_{drug}(t)\right) \cdot FB \cdot Stem - k_{stem} \cdot Stem \qquad \textbf{Eq. 2.43}$$

$$\frac{dProl}{dt} = k_{prol} \cdot \left(1 - E_{drug}(t)\right) \cdot FB \cdot Prol - k_{tr} \cdot Prol + k_{stem} \cdot Stem \qquad \textbf{Eq. 2.44}$$

$$\frac{dTransit1}{dt} = k_{tr} \cdot Prol - k_{tr} \cdot Tranisit1 \qquad \textbf{Eq. 2.45}$$

$$\frac{dTransit2}{dt} = k_{tr} \cdot Transit1 - k_{tr} \cdot Tranisit2 \qquad \textbf{Eq. 2.46}$$

$$\frac{dTransit3}{dt} = k_{tr} \cdot Transit2 - k_{tr} \cdot Tranisit3 \qquad \textbf{Eq. 2.47}$$

$$\frac{dCirc}{dt} = k_{tr} \cdot Transit3 - k_{tr} \cdot Circ \qquad \textbf{Eq. 2.48}$$

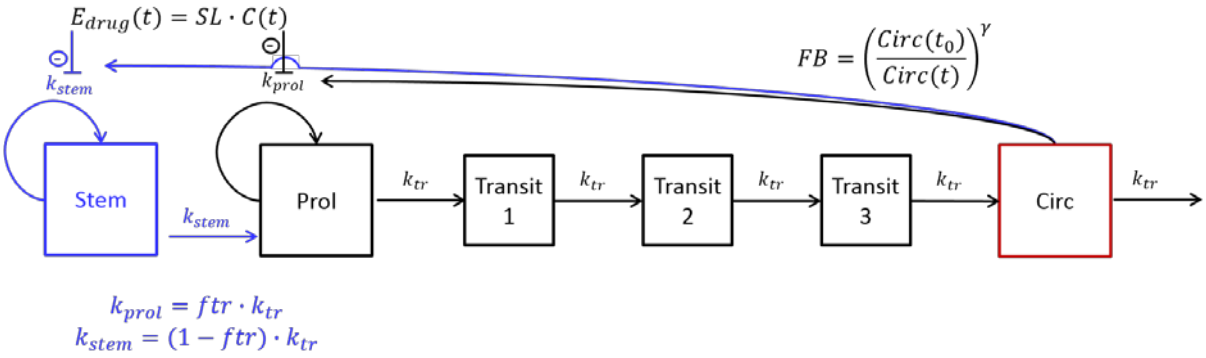

Figure 2.7: Structure of Model C (modified from [140])**.**
Compartments: Circ: circulating neutrophil cell compartment; Prol: proliferating cell compartment; Stem: stem cell compartment; Transit1-Transit3: transition compartment.
Parameters: $Circ(t)$ and $Circ(t_0)$ concentration of circulating cells at time t and at time t = 0, respectively; $C_{PTX}(t)$: paclitaxel plasma concentration at time t; $E_{drug}(t)$: drug effect on k_{prol} at time t; FB: feedback; ftr: fraction of input in Prol via replication; k_{prol}: proliferation rate constant of cells in Prol; k_{stem}: proliferation rate constant of cells in Stem; k_{tr}: transition rate constant of maturation chain; MMT: mean maturation time; SL: slope factor of paclitaxel; γ: exponent of feedback function.
Colour: red: observation compartment; blue: changes from gold standard model.

Evaluation and comparison of the performance of Model A – C

Model evaluation and selection was based on:

- Physiological plausibility to ensure reliable extrapolations for the simulations needed to investigate different dosing regimens
- Akaike Information Criterion (since the implemented models were not nested)
- Condition number
- Parameter precision (relative standard error, RSE)
- Goodness-of-fit plots of individual predictions, population predictions and weighted residuals
- pcVPCs

Model A – C were further explored by deterministic simulations for a typical patient (sex: male, age: 56 years, BILI: 7 µmol/L, BSA: 1.8 m², baseline neutrophil concentration: 6.48 • 10^9 cells/L (median of the baseline of the male population in Arm B of the CEPAC-TDM study)) after administration of 3-weekly dosing of 185 mg/m² over 6 cycles using the typical parameter estimates of each PK/PD model. Neutrophil concentrations in the circulating cell compartment and all other compartments were explored. Model A was assuming a constant second drug effect (E_{drug2}) during the cycles and an assumption had to be made for the behaviour of E_{drug2} after end of therapy. Two strategies were explored: firstly, E_{drug2} was only active until the end of the last cycle (3 weeks after the last dose administration) and secondly, the effect did continue until the end of the observed time period. For each of the three models the highest (peak) and the lowest value (nadir) from the 1st to the 6th cycle was calculated based on this deterministic simulation (Eq. 2.49 and Eq. 2.50, respectively) to quantify cumulative neutropenia.

$$\text{Relative change in peak value, \%} = 100 - \left(\frac{peak\ concentration\ in\ the\ beginning\ of\ cycle\ 6}{baseline\ concentration} \cdot 100\right) \quad \textbf{Eq. 2.49}$$

$$\text{Relative change in nadir value, \%} = 100 - \left(\frac{nadir\ concentration\ in\ the\ 6^{th}\ cycle}{nadir\ concentration\ in\ the\ 1^{st}\ cycle} \cdot 100\right) \quad \textbf{Eq. 2.50}$$

2.4.2.2 Differentiation of drug effects between paclitaxel and the platinum-based drugs

Two different approaches were investigated to distinguish between the drug effect of paclitaxel and the one of the platinum-based drug within Model C: Either an additive effect with paclitaxel

was assumed or the framework of the general pharmacodynamic interaction model [184] was applied.

Carboplatin and cisplatin literature PK models

To account for both platinum-based drugs, two published structural and covariate PK models [75,185] were implemented. Since no concentration measurements were available for any of the two drugs, variability was neglected, as described in section 2.1.1.3. Based on these two PK models, the typical concentration-time profiles of carboplatin and cisplatin were retrieved considering individual dosing and covariates.

Both models were based on ultrafiltrated plasma concentrations, i.e. unbound concentrations, quantified by flameless atomic absorption, i.e. not the drug concentration but the platinum concentrations were measured. Since this method cannot distinguish between parent drug and different subsequently formed platinum complexes, the platinum concentration was assumed to represent the pharmacological active concentration of carboplatin/cisplatin and their subsequently formed platinum complexes. In the following, this concentration will be referred to as carboplatin/cisplatin concentration, considering the differences in the molecular mass between platinum and carboplatin/cisplatin.

In the utilised information for carboplatin by Lindauer *et al.* [185], the concentration-time profile of carboplatin ($C_{Carbo}(t)$) was described by a linear two-compartment model. This model originally described the platinum concentration. As described above, the carboplatin concentrations were corrected by the difference in molecular mass, thus, changing of PK model parameters was not necessary. Several covariates were implemented as power functions to explain the interindividual PK variability of carboplatin within the population:

- Body weight on the central volume of distribution
- Age and body height on the intercompartmental clearance
- Creatinine clearance and body height on clearance

The concentration-time profile of cisplatin ($C_{Cis}(t)$) was described by de Jongh *et al*. [75] with a one-compartment model. This model was directly describing the cisplatin concentration with the underlying assumptions described above. Also in this model, the unexplained interindividual variability was reduced by the implementation of the covariate body surface area in a linear relationship on clearance and volume of distribution.

Additive drug combination effect

Two slope factors for carboplatin and cisplatin (SL_{Carbo} and SL_{Cis}, respectively) were estimated and an additive drug effect of paclitaxel and the platinum-based drugs was assumed. Since only one of the two platinum-based drugs was administered per cycle for each patient, E_{drug}

was given by Eq. 2.51, where SL_{Platin} and $C_{Platin}(t)$ are the slope factors of the linear drug-concentration effect and drug concentration of the platinum-based drug administered, respectively. The combined drug effect was the sum of each of the drugs calculated as the product of the respective slope factor and the drug concentration for each of the three drugs.

$$E_{drug} = SL_{Platin} \cdot C_{Platin}(t) + SL_{PTX} \cdot C_{PTX}(t) \qquad \textbf{Eq. 2.51}$$

In a deterministic simulation for a typical male patient (age: 56 years, bilirubin concentration: 7 µmol/L, weight: 70 kg, height: 176 cm, creatinine clearance: 103.1 mL/min, resulting in a body surface area of 1.86 m²), the virtual patient was treated with doses typical for the CEPAC-TDM study (paclitaxel: single dose, 3 h infusion; 187.5 mg/m^2; carboplatin: 2 h infusion started after end of paclitaxel infusion, dose based on Calvert formula [80] to achieve an AUC of 6 mg • min/L; cisplatin: 1/2 h infusion started after end of paclitaxel infusion, 80 mg/m²). The AUC of the drug effect was calculated for each drug until 24 h after start of the paclitaxel infusion (AUC_{0-24h}), using the trapezoidal rule (Eq. 2.52), were j was the observation, t was the time and E was the respective drug effect. The analysis was performed using time intervals of $t_{j+1} - t_j$ = 0.1 h. Time t = 0 was set at the start of paclitaxel infusion for all drugs, even though carboplatin/cisplatin infusion started 3 h later, to represent 24 h of day one of a cycle.

$$AUC_{0-24h} = \frac{1}{2}\sum_{j=1}^{j-1}(E_{j+1} + E_j) \cdot (t_{j+1} - t_j) \qquad \textbf{Eq. 2.52}$$

General pharmacodynamic interaction model

As an alternative approach, describing the combination therapy of paclitaxel with carboplatin the general pharmacodynamic interaction modelling approach [184] was evaluated. This approach gives the opportunity to identify and quantify the interaction in terms of synergism and antagonism. Since the number of patients treated with cisplatin as concomitant mediation was low (see section 3.1.1), this approach was only investigated for carboplatin, while for cisplatin an additive effect was assumed as described above.

Since all patients received combination therapy of paclitaxel with one of the platinum-based drugs, estimation of mono-therapeutic effects was not possible with the available data from the CEPAC-TDM study. Thus, to apply the general PD interaction approach, slope factors for paclitaxel and carboplatin describing the drug effect on neutropenia with monotherapy were taken from literature (in which they were estimated with the structure of the gold standard model): For paclitaxel SL was fixed to 2.21 L/µmol [119] and for carboplatin SL_{Carbo} was fixed to 0.460 L/mg [186].

Accounting for the sparse sampling of the available neutrophil data, the same extent of interaction of paclitaxel on carboplatin and of carboplatin on paclitaxel, respectively, was assumed. Therefore, E_{drug} for occasions of concomitant carboplatin administration was described by Eq. 2.53, where INT was the maximal interaction term and $EC_{50\,INT}$ was the concentration of paclitaxel and carboplatin at which interaction was half of INT. If INT is 0, additivity results. On the other hand, if INT is smaller or greater than 0, synergism or antagonism is described, respectively.

$$E_{drug} = \frac{SL \cdot C_{PTX}(t)}{1 + \frac{INT \cdot C_{Carbo}}{EC_{50\,INT} + C_{Carbo}}} + \frac{SL_{Carbo} \cdot C_{Carbo}(t)}{1 + \frac{INT \cdot C_{PTX}}{EC_{50\,INT} + C_{PTX}}} \qquad \textbf{Eq. 2.53}$$

Due to numerical difficulties, $EC_{50\,INT}$ had to be fixed to a very small value $1 \cdot 10^{-6}$ mg/L and $1 \cdot 10^{-6}$ µmol/L for the first and second term of the sum in Eq. 2.53. Different units of $EC_{50\,INT}$ arose from the different units of the paclitaxel and carboplatin concentration, but can be neglected for such low concentrations. The low concentration of $EC_{50\,INT}$ resulted in an on-off effect, i.e. as soon as a low concentration of both drugs were present, the full interaction occurred, as it can be seen in the resulting approximation in Eq. 2.54. Further, due to the numerical difficulties in the estimation process, parameter precision was computed using the S matrix only (see section 2.1.2.2).

$$E_{drug} = \frac{SL \cdot C_{PTX}(t)}{1 + INT} + \frac{SL_{Carbo} \cdot C_{Carbo}(t)}{1 + INT} \qquad \textbf{Eq. 2.54}$$

2.4.2.3 Covariate model development

The additive combination model (Eq. 2.51) was investigated for the influence of potential covariates. First, in a graphical exploration trends in the plots of the individual $\eta_{k,i}$ over the covariates were investigated. Scatter plots were used for continuous covariates and Box-and-Whisker plots for categorical covariates, respectively. The following covariates were investigated on both parameters SL and SL_{carbo}:

- Continuous covariates: BSA, age, body height, body weight, creatinine clearance, bilirubin concentration, aspartate aminotransferase, alanine aminotransferase, gamma-glutamyl transpeptidase, alkaline phosphatase, total plasma protein concentration, tumour histology, tumour stage.
- Categorical covariates: Sex, smoking status, ECOG performance status, previous anticancer therapy and more specific, previous chemotherapy, pervious radiotherapy and pervious surgery.

In this visual inspection, it was investigated whether the influence of the covariate exceeded a change of 20% in the respective parameter estimate and only those exceeding this 20%

threshold were further investigated. More precisely, for continuous covariates, it was investigated at the minimum and maximum of the covariate observed in the study population, whether the linear regression of $\eta_{k,i}$ over the covariate exceeded that threshold. For categorical covariates, it was investigated whether at least one category exceeded that threshold. The level of 20% was chosen to be less restrictive than the clinical relevance criterion of 30% (see section 2.1.2.6) and therefore avoided the exclusion of potentially relevant covariates in this step. Continuous covariates were investigated with a linear covariate model.

Due to the low number of patients receiving previous chemotherapy or radiotherapy, the previous therapy was dichotomised and summarised to one covariate effect, not differentiating whether chemotherapy or radiotherapy had been administered.

In the next step, covariates identified during the visual inspection were evaluated in a SCM analysis (see section 2.1.2.6). In addition, concomitant chemo-/radiotherapy (summarised as one dichotomous covariate as for previous therapy), supportive G-CSF therapy and comedication that could lead to neutropenia (see Table 10.9 in the appendix for more information on how comedication was evaluated) were investigated in the SCM analysis. For previous therapy, concomitant therapy, supportive therapy and comedication, the covariate effect was investigated on the combined drug effect (E_{drug}). Categorical covariates on E_{drug} were investigated in two ways: additive or multiplicative implementation (see Eq. 2.55 and Eq. 2.56, respectively).

$$E_{drug} = SL_{Platin} \cdot C_{Platin}(t) + SL \cdot C_{PTX}(t) + \theta_{Eff,cov}{}^{g} \qquad \textbf{Eq. 2.55}$$

$$E_{drug} = \left(SL_{Platin} \cdot C_{Platin}(t) + SL \cdot C_{PTX}(t)\right) \cdot \theta_{Eff,cov}{}^{g} \qquad \textbf{Eq. 2.56}$$

The additive covariate effect (Eq. 2.55) assumes that the drug effect is affected during the concomitant/supportive therapy/comedication is active, independent of the drug effect of the study therapy. Thus, a drug effect only caused by concomitant/supportive therapy/comedication might occur even though no paclitaxel or platinum-based drug are present in the system. On the other hand, the multiplicative (Eq. 2.56) implementation is enhancing the drug effect caused by paclitaxel and the platinum-based drug.

2.4.3 PK/PD model evaluation of the developed model using the conventional CEPAC-TDM study arm

A method similar to the data splitting method (see section 2.1.2.1) was applied to evaluate the prediction of the additive effect model including covariates (see section 2.4.2.3). The evaluation dataset in this approach was the data of study Arm A. A *post-hoc* estimation was

performed allowing for interindividual variability in the PK and PD parameters. Strictly, the applied approach is not in accordance with the data splitting method, since the individual were not randomly assigned to the index and validation dataset. However, for simplification, the term will be used in the following for the applied approach.

Further, a prediction-corrected visual predictive check was generated for which the simulations included interindividual variability on the PK and the PD parameters, as for the *post-hoc* estimation.

2.4.4 Impact of the optimised PK/PD model on the CEPAC-TDM study results

The impact of the newly developed PK/PD model on the interpretation of the CEPACT-TDM study was evaluated by extracting the time to nadir and the nadir itself from the *post-hoc* estimation of this PK/PD model for both study arms and comparing these values to the actual sampling times and day 15 ± 2 neutrophil concentrations, respectively.

2.5 Project 3: Efficacy modelling: Tumour size and overall survival

2.5.1 Tumour growth inhibition modelling

Similar to the development of the neutropenia PK/PD model, the tumour growth inhibition PK/PD model was developed considering patients from Arm B only, while Arm A was used for the final evaluation. As in Project 2, first the paclitaxel effect alone was considered, then the differentiation between the drug effect of paclitaxel and carboplatin was introduced. Since it was seen in Project 2 that the cisplatin effect was not estimable, these patients were not included in the tumour growth inhibition model development. Further, tumour growth measurements > 30 weeks were not considered, since the aim was to predict individual change in tumour size at week 8 to inform overall survival. Additionally, patients with concomitant or follow-up chemo-/radiotherapy or surgery were excluded from the analysis starting from the day the additional treatment began (Figure 3.29).

2.5.1.1 Development of structural tumour growth inhibition model

The development of the tumour growth inhibition model was based on the review from Ribba *et al.* [124], which summarised approaches to describe the change in tumour size (TS) over time in differential equations. In general, the change in tumour size was described as the difference of tumour net growth and drug-induced net decay (Figure 2.8 for equations). Three models were investigated describing the net growth: linear model, exponential model and generalised logistic model. All net growth models included a growth rate constant, k_g, which

can be a zero-order (linear growth) or first-order (exponential and generalised logistic growth) rate constant. The general logistic growth model further included two additional parameters, describing the maximum tumour size to that the cancer can grow (TS_{max}) and a shape parameter υ.

For this investigation, the drug-induced decay was exposure-driven with a linear drug effect, described by the drug-effect parameter β, similar to the slope factor in the neutropenia model (Project 2). After the optimal net growth model was selected, an additional resistance term within the drug effect term was evaluated. This resistance is a time-dependent effect which exponentially reduces the decay over time. The parameter λ is the rate constant shaping the resistance.

In all models, baseline method B2 (see section 2.1.1.4), using the individual measured baseline but allowing for residual variability, was applied to describe individual tumour size at time t = 0. Model selection was based on the comparison of OFV, relative standard errors, condition numbers and diagnostic plots between competing models as described in section 2.1.2.6.

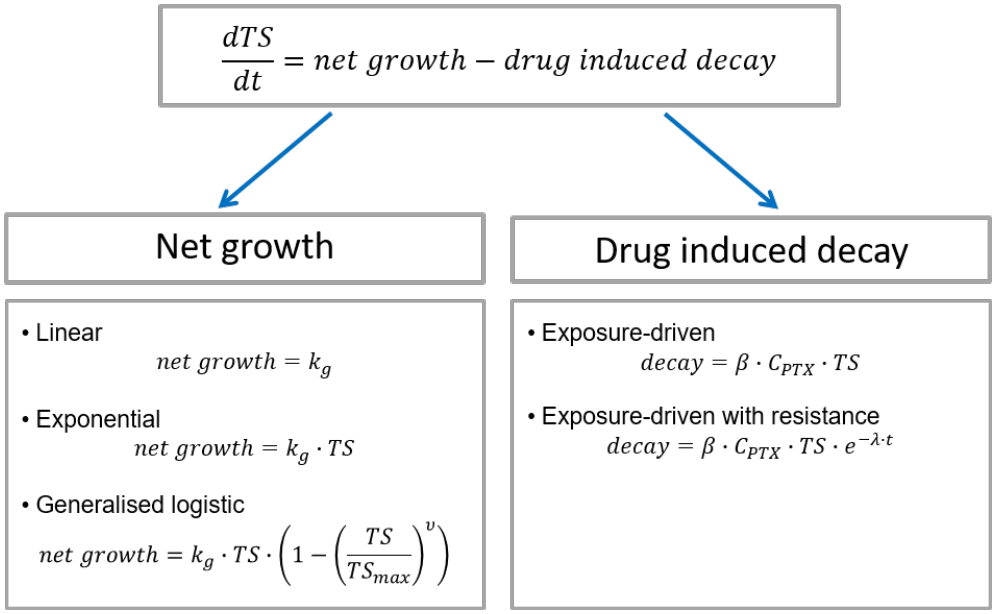

Figure 2.8: Investigated structural models to describe tumour growth inhibition dynamics (modified from [124])**.**
k_g: tumour growth rate constant; TS: tumour size; TS_{max}: maximal tumour size; β: efficacy parameter; λ: time-dependent resistance parameter; υ: shape factor for logistic tumour growth.

2.5.1.2 Differentiation between drug effect of paclitaxel and carboplatin

Since two efficacy parameters for paclitaxel and carboplatin were not estimable, a fixed ratio r_{effect} between the two drug effects was assumed which then resulted in an additive model (Eq. 2.57 and Eq. 2.58) as in Project 2.

$$\beta_{carbo} = r_{effect} \cdot \beta_{PTX} \quad \textbf{Eq. 2.57}$$

$$\frac{dTS}{dt} = k_g - (\beta_{PTX} \cdot C_{PTX} + \beta_{carbo} \cdot C_{Carbo}) \cdot TS \quad \textbf{Eq. 2.58}$$

The ratio of the efficacy parameters for carboplatin and paclitaxel (β_{carbo} and β_{PTX}, respectively), r_{effect}, was derived from reported *in vivo* studies from literature. Herbst *et al.* [187] had compared the effect of paclitaxel (36 mg/kg, on day 7 – 11 after tumour cell implantation) and carboplatin (50 mg/kg, on day 7 after tumour cell implantation) on lung cancer in mice (lung cancer types arising from mice).

Further, these researchers [187] had investigated the pharmacokinetics in different tissues, e.g. in tumour. Concentration-time profiles of both drugs in the tumour tissue were digitalised and the area under the curve for the whole concertation-time profile ($AUC_{0-\infty}$) was computed (Eq. 2.59 – Eq. 2.61). Similar to Eq. 2.52, the trapezoidal rule was used to calculate the AUC for the first 6 hours (AUC_{0-6h}), using the time interval of observation j and j + 1 ($t_{j+1} - t_j$) and the drug concentrations at the respective time points (C_j and C_{j+1}). The terminal first-order elimination rate constant (λ_z) was approximated by linear a regression and used to calculate the AUC for the terminal phase, thus the time between 6 h and infinity ($AUC_{6h-\infty}$), based on the last observed drug concentration at t = 6 h (C_{6h}). To account for the multiple drug administrations, $AUC_{0-\infty}$ of a single paclitaxel administration was multiplied by the number of doses that had been administered by Herbst *et al.* [187] (5 doses). The proportion of the extrapolated part $AUC_{6h-\infty}$ from the total $AUC_{0-\infty}$ was 61.7% and 9.42% for paclitaxel and carboplatin, respectively.

$$AUC_{0-6h} = \frac{1}{2}\sum_{j=1}^{j-1}(C_{j+1} + C_j) \cdot (t_{j+1} - t_j) \quad \textbf{Eq. 2.59}$$

$$AUC_{6h-\infty} = \frac{C_{6h}}{\lambda_z} \quad \textbf{Eq. 2.60}$$

$$AUC_{0-\infty} = AUC_{0-6h} + AUC_{6h-\infty} \quad \textbf{Eq. 2.61}$$

Herbst *et al.* [187] further reported the tumour growth delay that they had been observing for each drug, when comparing the time needed to reach a certain tumour size (here 500 mm³) for treated mice compared to mice without treatment. This tumour growth delay (in the linear tumour growth phase) had been also defined as time efficacy index (TEI) by Simeoni *et al.* [1]. The reported time efficacy indices of paclitaxel and carboplatin were TEI_{PTX} = 4.6 days and TEI_{carbo} = 4.2 days, respectively.

Simeoni *et al.* [1] had developed a preclinical tumour growth inhibition model, incorporating the time efficacy index as defined in Eq. 2.62, with efficacy parameter β, of the respective drug and an exponential tumour growth rate, k_{g0}. Since the tumour growth rate k_{g0} describes a pathophysiological process, it was assumed to do not change between drugs. Hence, r_{effect} can be calculated as described in Eq. 2.63.

$$TEI = \frac{\beta \cdot AUC_{0-\infty}}{k_{g0}} \qquad \textbf{Eq. 2.62}$$

$$r_{effect} = \frac{\beta_{carbo}}{\beta_{PTX}} = \frac{TEI_{carbo} \cdot AUC_{0-\infty,PTX}}{AUC_{0-\infty,carbo} \cdot TEI_{PTX}} \qquad \textbf{Eq. 2.63}$$

2.5.1.3 Covariate model development

A full covariate analysis was performed for (patho)physiological covariates. All covariates were investigated on both parameters, k_g and β_{PTX}. Continuous covariates were investigated assuming a linear relationship (Eq. 2.12) and categorical covariates were implemented as explained in Eq. 2.15. The following covariates were investigated:

- Continuous covariates: age, body weight, body surface area, concentration of lactate dehydrogenase, number of lesions (sum of target and non-target lesions)
- Categorical covariates: sex, tumour stage (stage IIIB or IV), tumour histology (adenocarcinoma, squamous-cell carcinoma, unknown (including one patient with bronchioalveolar carcinoma)), smoking status (current, former, never), previous therapy (chemo-/radiotherapy or surgery), ECOG performance status, existence of brain lesions

As described in section 2.1.2.6, a stepwise covariate model-building procedure (SCM) was performed evaluating the drop in OFV, decrease in interindividual variability, clinical relevance and parameter precision for covariate selection.

Standard goodness-of-fit plots and (stratified) pcVPCs were generated for the base model with and without carboplatin effect, for the covariate model and for subsequent steps if needed for decision-making. Further, the data splitting method (section 2.1.2.1) was applied to compare the model prediction with the observed tumour size measurements in study Arm A using pcVPCs. As discussed for Project 2 (see section 2.4.3) the terminology “data splitting” is not exactly correct, since the individuals are not randomly distributed to the index and evaluation dataset, but will be used for simplification.

2.5.2 Investigating tumour size as predictor of overall survival

For the analysis of survival times, the model developed by Wang *et al.* [164] was utilised. PK was not directly influencing overall survival compared to the previously developed PK/PD models. Thus, it was possible to merge the data from both study arms, with and without PK measurements, and all patients were analysed, independent of additional therapy (concomitant/supportive therapy and comedication) beyond the study medication. As in [164], a normal distribution of logarithmised survival times ($\log(T)$) with mean μ and variance ρ^2 was assumed (see Eq. 2.64 and section 2.1.1.6). The median survival time T_{median} on normal scale is then given by Eq. 2.65.

$$\log(T) \sim \mathcal{N}(\mu, \rho^2) \qquad \textbf{Eq. 2.64}$$

$$T_{median} = e^{\mu} \qquad \textbf{Eq. 2.65}$$

For the covariate analysis, a full model approach was used, i.e. all potential covariates were implemented at once and then a backwards deletion step was conducted, thus omitting the forward step, as described in section 2.1.2.6. The covariates previously identified to be significant by Wang *et al.* [164] for patients with non-small cell lung cancer, treated with paclitaxel and carboplatin combination therapy, were implemented in the full model on μ:

- ECOG performance status
- Concentration of lactate dehydrogenase at baseline (LDH)
- Relative change in tumour size at week 8 (RS_8)
- Sex
- Prior surgery
- Baseline tumour size (BSL_{SD})

6-month weight loss was not considered in the analysis, even though it was a significant covariate in [164], since it is determined approximately at the end of therapy and is therefore not a prognostic marker. The mean of the distribution of survival times for a patient group with a set of covariate values g (μ_g), is given by Eq. 2.66, which shows that all covariate effects were additive. The parameters for the covariate relations in this equation were: $\theta_{\mu,ECOG}$, $\theta_{\mu,LDH}$, $\theta_{\mu,SEX}$, $\theta_{\mu,PSURG}$, $\theta_{\mu,RS8}$ and$\theta_{\mu,BSL}$ for the respective covariates. Continuous covariates (LDH, RS_8 and BSL_{SD}) were implemented normalised on the median of the study population using a linear model.

$$\mu_g = \mu + \theta_{\mu,ECOG} + \theta_{\mu,LDH} \cdot \left(LDH - 230\frac{U}{L}\right) + \theta_{\mu,SEX} + \theta_{\mu,PSURG} + \qquad \textbf{Eq. 2.66}$$

$$\theta_{\mu,RS8} \cdot (RS_8 - 69.3\%) + \theta_{\mu,BSL} \cdot (BSL - 7.90\ cm)$$

$$\theta_{\mu,ECOG} = \begin{cases} \theta_{\mu,ECOG<2} & if\ ECOG < 2 \\ \theta_{\mu,ECOG=2} = 0 & if\ ECOG = 2 \end{cases}$$

$$\theta_{\mu,SEX} = \begin{cases} \theta_{\mu,female} & if\ SEX = 0 \\ \theta_{\mu,male} = 0 & if\ SEX = 1 \end{cases}$$

$$\theta_{\mu,PSURG} = \begin{cases} \theta_{\mu,without} = 0 & if\ PSURG = 0 \\ \theta_{\mu,with} & if\ PSURG = 1 \end{cases}$$

2.6 Project 4: Evaluation of dosing strategies to optimise paclitaxel cancer therapy

2.6.1 Representative patient population

The virtual population was based on the CEPAC-TDM study population and was created as described in Figure 2.9, considering the correlations between patient characteristics identified in section 3.1.2 and Figure 10.1. Sex, tumour size at baseline and LDH were randomly sampled from the population of the CEPAC-TDM study. Bilirubin, creatinine concentration and ECOG performance status were based on sex sampled from the CEPAC-TDM study population. Similarly, neutrophil concentration at baseline and tumour histology were sampled considering the ECOG performance status. Age was sampled based on ECOG performance status and sex, due to the correlation observed (Figure 10.1). Weight and height were sampled from the same patient due to the high correlation considering patient sex and ECOG performance status. Finally, creatinine clearance and BSA were calculated using the Cockcroft-Gault formula and the Dubois-Dubois formula, respectively. Patients were assumed to not receive supportive G-CSF therapy. Based on this workflow 1000 virtual patients were generated.

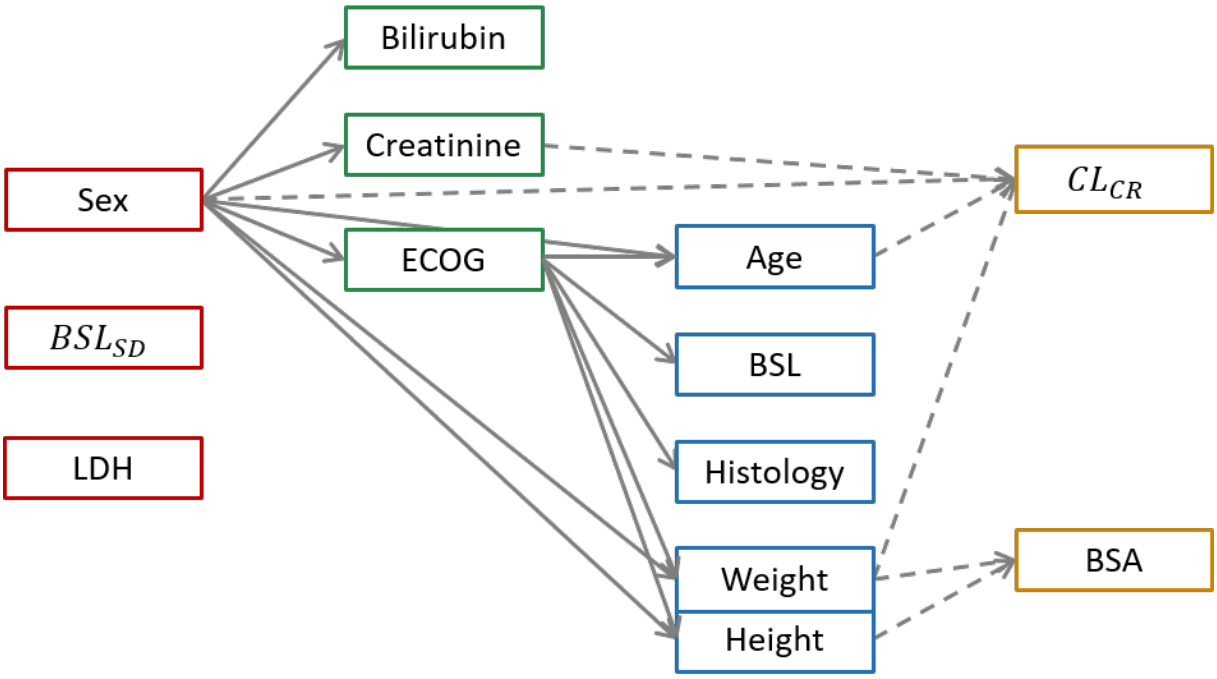

Figure 2.9: Schematic representation on the generation of the simulated population.
Sex, BSL_{SD} and LDH were sampled randomly from the population of the CEPAC-TDM study.
Solid line arrows: one covariate was sampled from the population of the CEPAC-TDM study based on the covariate from which the arrow originates from. Weight and Height were sampled together from the same patient due to their strong correlation.
Dashed arrows: covariate was *calculated* based on the ones from which the arrow originates from; weight and height were taken from the same individual of the CEPAC-TDM study.
BSA: body surface area; BSL: neutrophil concentration at baseline; BSL_{SD}: baseline tumour size; CL_{CR}: creatinine clearance; LDH: lactate dehydrogenase concetration.

2.6.2 Simulated dosing scenarios for pharmacokinetics, neutropenia and efficacy

The following dosing scenarios were deterministically simulated using the developed models for pharmacokinetics (Model I, section 2.3.2), neutropenia (Model C (section 2.4.2.1) including additive combination effect of paclitaxel and the platinum-based drug (section 2.4.2.2) and G-CSF as additive covariate on the drug effect (section 2.4.2.3)), tumour growth inhibition (see section 2.5.1) and overall survival (see section 2.5.2) as described in Project1 – 3 (respective model code can be found in the appendix (section 10.3)):

- Scenario 1 – No dose adaptation across cycles: This dose was adjusted based on sex, age and BSA as suggested by the dosing algorithm for the first cycle but without adaptations in later cycles (6 cycles with length 3 weeks, dosing on first day of each cycle).
- Scenario 2 – Dose adaptation across cycles: The doses were derived from the dosing algorithm. Thus, the first dose was the same as in Scenario 1, but the following doses were adjusted based on the grade of neutropenia (simulated nadir, not day 15 as

originally) and $T_{C>0.05}$. The cycle length was unchanged (3 weeks) with dosing on the first day of each cycle.

- Scenario 3 – Increased dosing interval without dose adaptation across cycles: The same fixed dose as in Scenario 1 was administered, but the dosing interval was increased to:
    - Scenario 3A: 3 weeks + 3 days
    - Scenario 3B: 3 weeks + 5 days
    - Scenario 3C: 3 weeks + 7 days

For all dosing scenarios, 6 cycles were simulated and the dose of carboplatin was kept constant with target AUC dosing of 6 mg • min/L (see section 1.2.3.2). In sequential steps, the simulated paclitaxel concentration-time profile informed neutropenia and tumour growth inhibition and the later informed overall survival (Figure 2.10). Further, the analysis considered drop-out for patients as soon as death occurred or tumour size increased compared to the previous measurement. For this step, it was assumed that tumour size was measured every 6 weeks as it was done in the CEPAC-TDM study. On the other hand, tumour growth was not considered for drop-out in the overall survival analysis, since typically survival is evaluated for all patients in the follow-up independently of tumour progression.

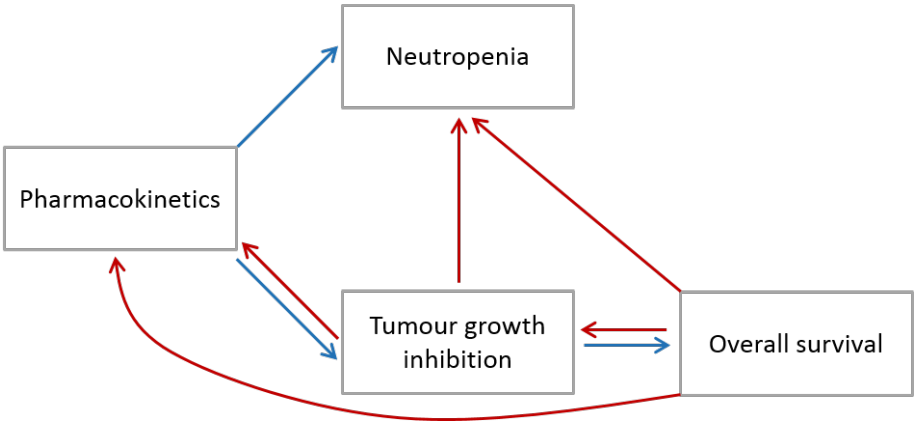

Figure 2.10: Schematic representation of the simulation strategy.
Blue arrows indicate that the model was informed by results of the other model; red arrows indicate that drop-out in a model was considered based on results of the other one.
I.e., simulations of neutropenia and tumour growth inhibition were dependent of the results of the simulated pharmacokinetics. Further, overall survival was dependent on the result from the simulations of tumour growth inhibition. For evaluation of the simulation results, drop-out for different reasons was considered. Simulated patients that died were excluded from all analysis from the simulated day of death on. Patients with simulated tumour progression were excluded from the pharmacokinetic and neutropenia analysis from the simulated day observation of progression on.

3 Results

3.1 Exploratory analysis of CEPAC-TDM study data: Numerical, statistical and graphical analysis

The CEPAC-TDM study included 365 patients. These patients were randomised equally into the two study arms, with 183 patients randomised to Arm B (experimental arm). The majority of patients were males (67%). Median age was 63 years and 88% of the patients were former or current smokers. A full summary of patient characteristics is reported in [139].

3.1.1 Numerical and graphical exploration of dosing, pharmacokinetics and pharmacodynamics

Dose evolution over time

In total, patients received 734 and 720 paclitaxel treatment cycles in combination with a platinum-based drug for Arm A and B, respectively. Dose adaptions were performed differently for the two study arms (see section 2.2.1), resulting in median paclitaxel doses of 368 mg in Arm A (range: 208 - 520 mg) and 285 mg in Arm B (range: 111 - 505 mg). In Arm B, paclitaxel dose was adapted according to the published dosing algorithm [138] and toxicity, resulting in a more profound dose reduction and an increased range of doses (Figure 3.1).

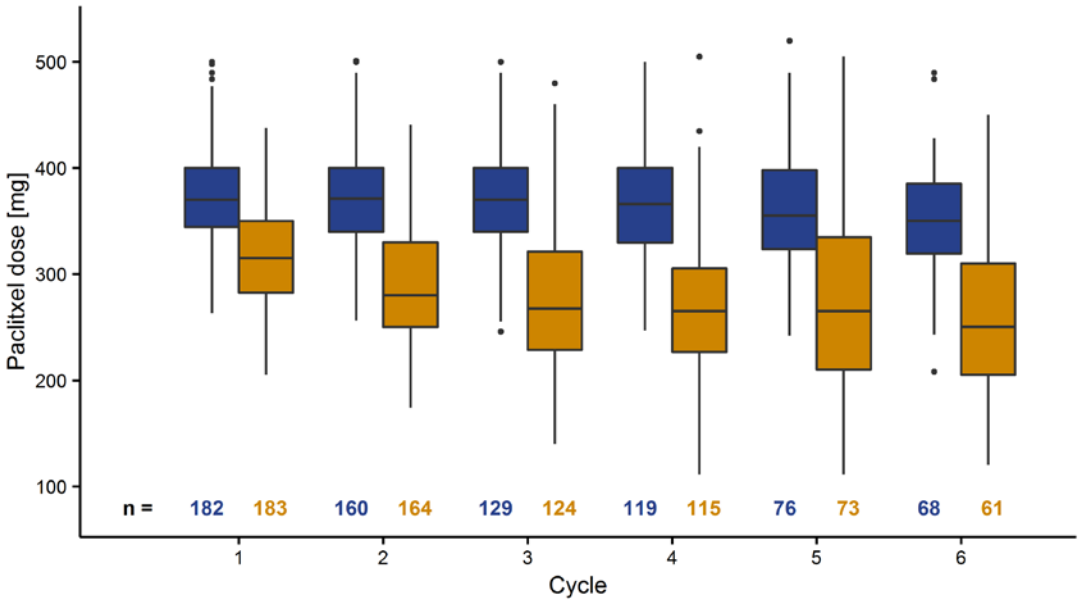

Figure 3.1 paclitaxel dose evolution over the treatment cycles.
Boxes: interquartile range (IQR), including median; whiskers: range from box hinge to highest/lowest value within 1.5•IQR; points: data beyond whiskers.
Colour: blue: Arm A; orange: Arm B.
n: number of patients.

Regarding the concomitant platinum-based drug, carboplatin was administered for the majority of patients starting with the 1st cycle (149 vs 33 in Arm A and 153 vs 30 in Arm B). For 9 of the 63 patients receiving cisplatin in the 1st cycle, platinum-based combination therapy was changed to carboplatin over time, due to cisplatin-related toxicity.

Adherence to the dosing algorithm

Adherence to the dosing algorithm was evaluated (Table 3.1) to examine the validity of the study outcome. If patients would not have received the dose suggested by the protocol, statistical analysis with the assumption "intention to treat" (see section 1.1.3.2) would be misleading. Therefore, the relative deviation from the planned dose including the dosing algorithm (for paclitaxel in Arm B) and toxicities was evaluated, distinguishing between the 1st cycle, where dose was based on covariates (BSA, CL_{CR}, …) and cycle 2 to 6, where drug exposure and toxicities from the last cycle were influential.

For paclitaxel, doses in both study arms were administered according to the protocol for the first study cycle. In the following cycles, a trend to overdosing can be seen for both study arms, but stronger for patients in Arm A (Table 3.1).

Similarly, carboplatin doses in the 1st cycle were in line with the protocol. Later, underdosing occurred in approximately the same extent (~ 10%) in both study arms. For cisplatin, the highest deviation from the protocol dose was observed. In both study arms, approximately 30% of the doses were more than 20% higher than suggested from the protocol. Further examination revealed that most of these patients were treated with 100 mg/m² instead of 80 mg/m².

Table 3.1: Adherence to the dosing algorithm for paclitaxel and the platinum-based drugs stratified by study arm (number of doses over-/underdosed).

	Overdosed in cycle 1		***Underdosed in cycle 1***		***Overdosed in cycle 2 - 6***		***Underdosed in cycle 2 - 6***	
	Arm A	***Arm B***	***Arm A***	***Arm B***	***Arm A***	***Arm B***	***Arm A***	***Arm B***
Paclitaxel	0%	0.546%	0.549%	0%	27.9%	15.1%	1.09%	0.931%
	n = 182	n = 183	n = 182	n = 183	n = 552	n = 537	n = 552	n = 537
Carboplatin	1.34%	0.654%	4.03%	4.58%	5.54%	6.54%	12.4%	9.59%
	n = 149	n = 153	n = 149	n = 153	n = 451	n = 459	n = 451	n = 459
Cisplatin	36.4%	33.3%	3.03%	0%	33.7%	33.3%	5.94%	0%
	n = 33	n = 30	n = 33	n = 30	n = 101	n = 78	n = 101	n = 78

Over- and underdosing considered doses that deviated more than 20% from the protocol dose including the published dosing algorithm and further toxicities as described in Table 2.1.
n: total number of doses considered.

The adherence regarding the cycle length was overall good, the median cycle length was 21 days (5^{th} percentile: 20 days; 95^{th} percentile: 28 days). Reduced cycle lengths were rarely undertaken (4.13% of the cycles were shorter than 20.0 days). Nevertheless, increased cycle length was more common (26.3% of the cycles were longer than 22.0 days).

Paclitaxel concentration-time profile

A total of 660 PK samples were analysed from Arm B (no PK measurements available from Arm A). Two of these analysed PK samples were LLOQ, but the value was reported, while for two other samples the measured value was not reported. The former samples were included in the analysis, while the latter (0.303%) were ignored and considered as missing completely at random due to their low number. The missing samples (8.33%) were also assumed to be missing completely at random and thus not considered in the analysis.

The planned sampling time was 24 h after start of the paclitaxel administration. Eventually, sampling times ranged from 16.2 h to 29.3 h. This range in the sampling time allows to generate a plot of the measured paclitaxel concentrations over time after last dose (Figure 3.2). This plot reports that samples were taken in the terminal phase of the concentration-time profile, recognisable by the linear behaviour on semi-logarithmic scale, and close to the threshold of 0.05 µmol/L.

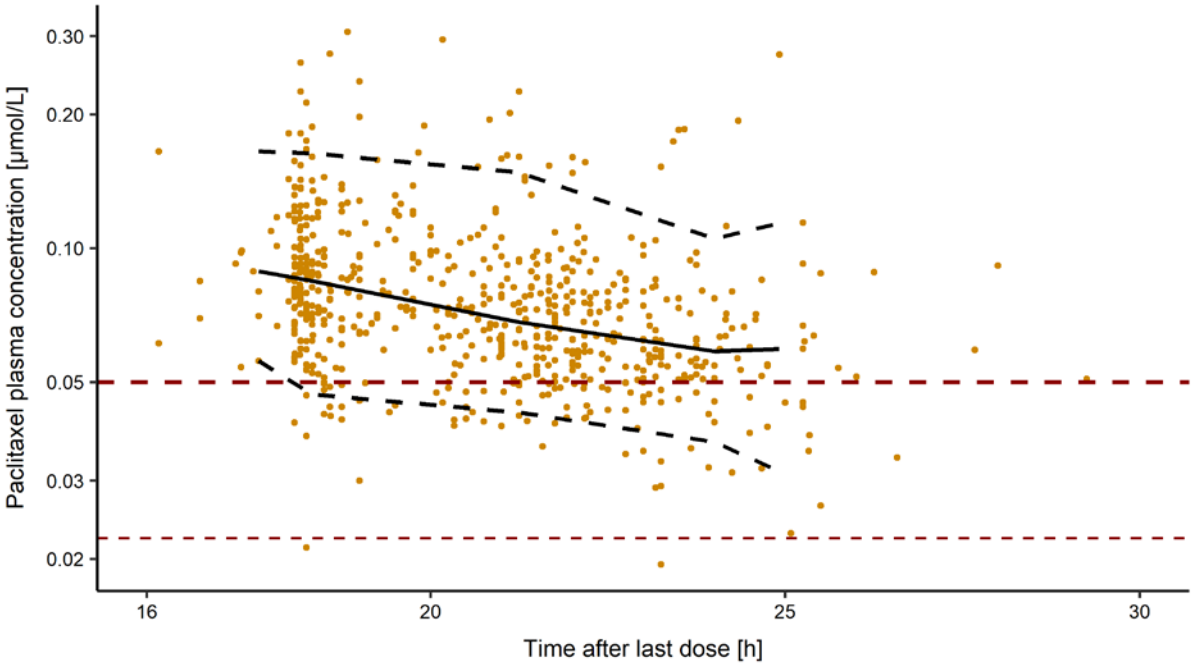

Figure 3.2: Paclitaxel concentration measurements of patients in Arm B over time after last paclitaxel dose.
Bold red dashed line: threshold of 0.05 µmol/L; thin red dashed line: lower limit of quantification (19 ng/mL = 0.0223 µmol/L); black solid line: median concentration-time profile, black dashed lines: 5th and 95th percentile.

Development of the $T_{C>0.05}$ over the treatment cycles

Time above the threshold of 0.05 µmol/L ($T_{C>0.05}$) was determined during the study, using the published PK model to define the next dose for patients in Arm B. This evaluation was based on a single paclitaxel plasma concentration sample. The targeted time range was ≥ 26 h to < 31 h. For the first cycle, for which the dose was only based on the covariates (BSA, age and sex), the median lay within this target range (Figure 3.3). However, 66.3% of the patients were over- or underdosed regarding the target range. For cycle 3 onwards, the median $T_{C>0.05}$ decreased below the lower bound of the target range, leading to underdosing for > 50% of the patients. The highest percentage of patients within the target range was achieved for the 2nd cycle (46.2%).

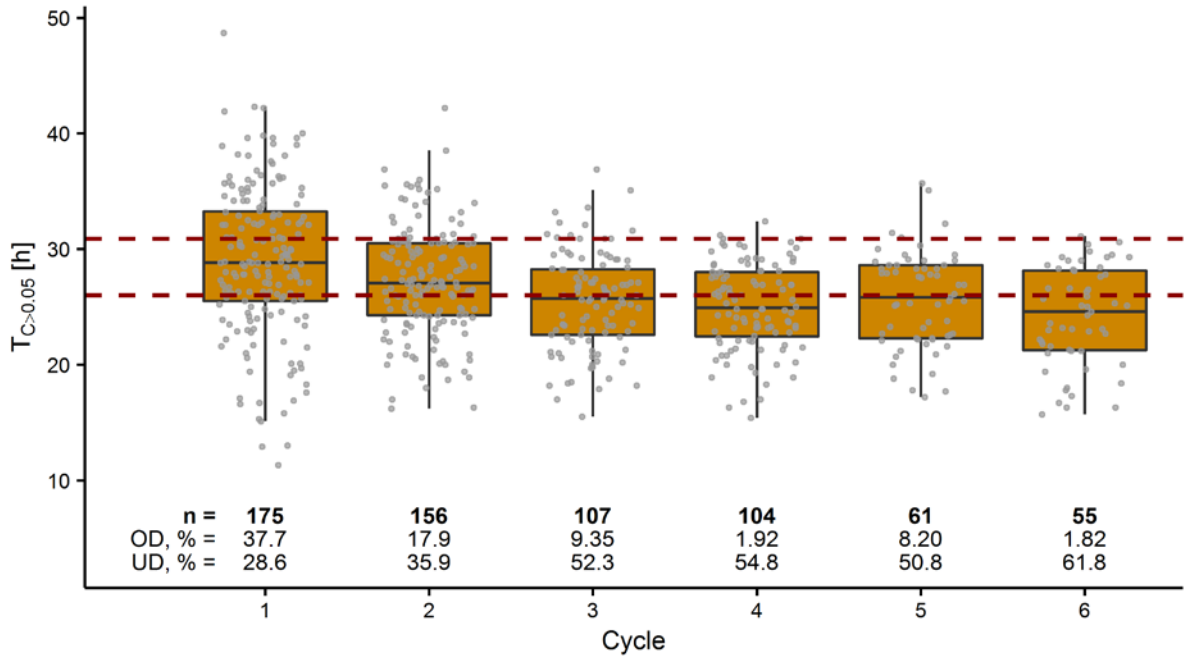

Figure 3.3: Time above the threshold of 0.05 µmol/L ($T_{C>0.05}$) over the treatment cycles.
Boxes: interquartile range (IQR), including median; whiskers: range from box hinge to highest/lowest value within 1.5•IQR; points: all $T_{C>0.05}$ determined in the study; red dashed lines: target range 26 – 31 h; n: number of observations; OD, %: percentage of patients overdosed ($T_{C>0.05}$ ≥ 31 h); UD, %; percentage of patients underdosed ($T_{C>0.05}$ < 26 h).

Concentration of neutrophils and other blood cells over time

Altogether, 3325 (missing: 8.60%) neutrophil concentrations were measured, while for day 15, 14.1% of the samples were missing. In total, 0.966% of the PD samples were below the lower limit of quantification. Those samples as well as the missing samples were considered to be missing completely at random and thus not considered for the following modelling activities.

Figure 3.4 (Panel A and B) shows the development of the neutrophil concentration over time. It reveals a trend of decreasing neutrophil concentrations over the repeated treatment cycles for both study arms and for the measurements on day 1 and day 15 of the cycle. This pattern is called cumulative neutropenia. The cumulative pattern was also observed for the thrombocyte concentration as well as for the erythrocyte concentration (Figure 3.5). Comparing the two study arms (Figure 3.4, Panel C), grade 4 and grade ≥3 neutropenia was slightly reduced for patients in Arm B. Nevertheless, the statistical analysis performed by Joerger *et al.* found no significant difference even for grade 4 neutropenia between the study arms [139], despite the substantial decrease in dose in Arm B (Figure 3.1). Even though

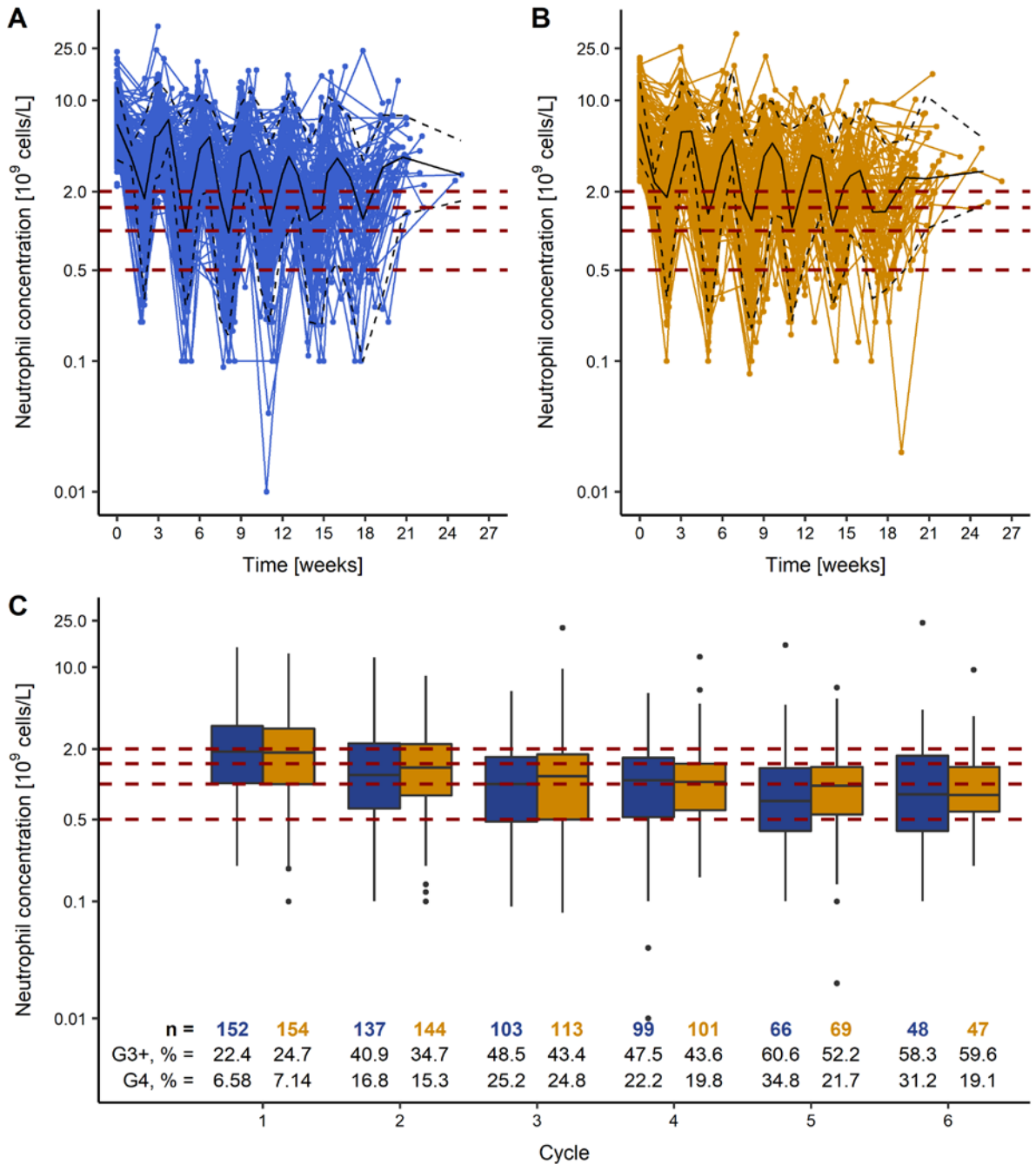

Figure 3.4: Neutrophil concentrations over time on semi-logarithmic scale, stratified by study arm.
Panel A and B: neutrophil concentrations for patients in Arm A and B, respectively; red dashed lines: thresholds for grading neutropenia from grade 0 to 4; black solid line: median concentration-time profile: dashed black lines: 5th and 95th percentile of the concentration-time profile.
Panel C: neutrophil concentrations on day 15 ± 2; blue and orange boxes: interquartile range (IQR), including median for Arm A and B, respectively; whiskers: range from box hinge to highest/lowest value within 1.5•IQR; points: data beyond whiskers; red dashed lines: thresholds for grading neutropenia from grade 0 to 4; n: number of observations; G3+, %: percentage of patients with grade ≥ 3 neutropenia; G4, %: percentage of patients with grade 4 neutropenia.

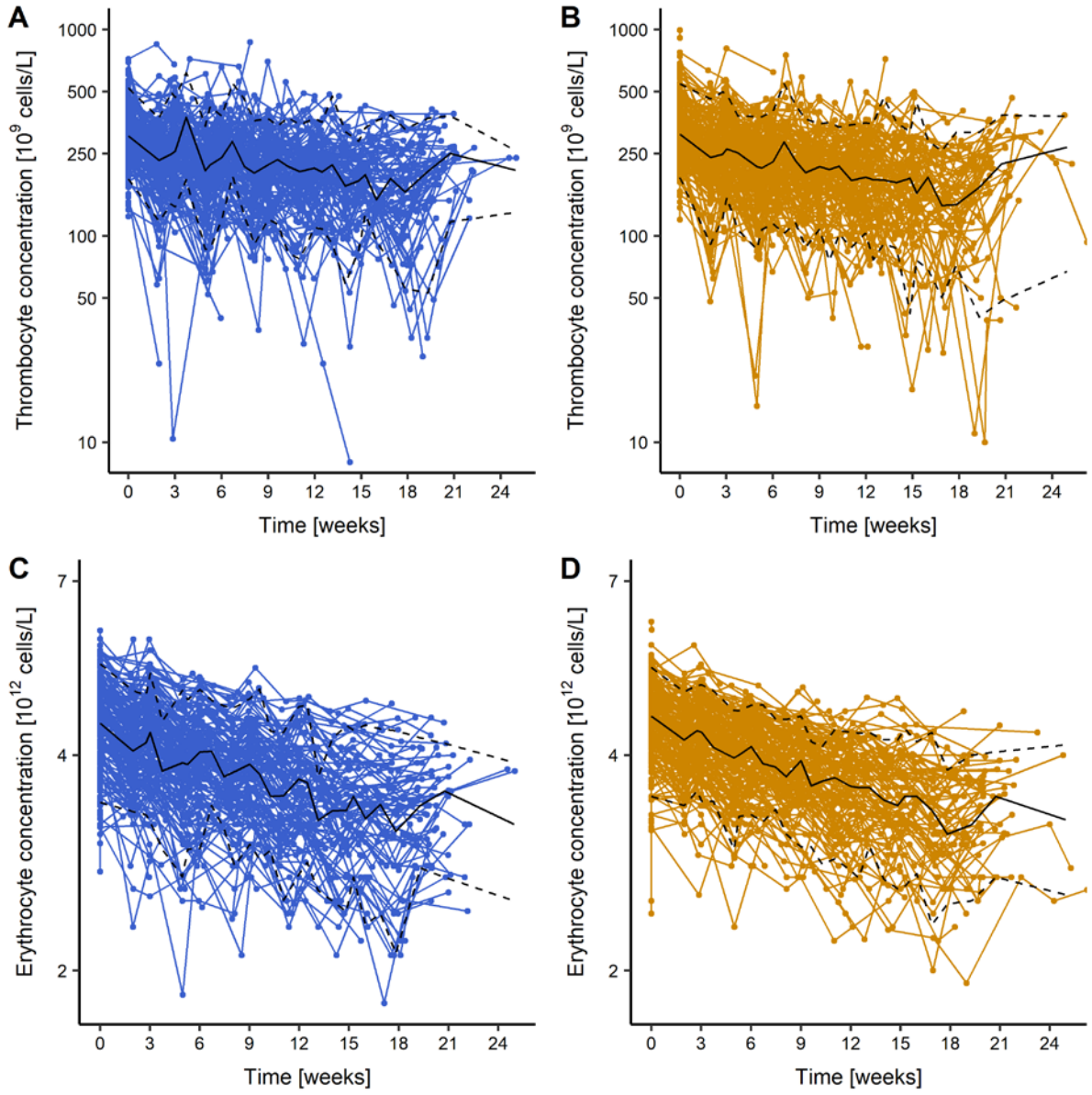

Figure 3.5: Thrombocyte and erythrocyte concentrations over time on semi-logarithmic scale, stratified by study arm.
Panel A and B: thrombocyte concentrations for patients in Arm A and B, respectively; Panel C and D: erythrocyte concentrations for patients in Arm A and B, respectively.
Black solid line: median concentration-time profile: dashed black lines: 5th and 95th percentile of concentration-time profile.

In total, 20 patients (11 patients (6.04%) in Arm A and 9 patients (4.92%) in Arm B) received G-CSF during the study therapy to treat severe neutropenia. Besides of two patients, this treatment was only applied during one treatment cycle.

Tumour growth over time

Sum of diameters was reported 1323 times. Of these, 11 measurements were reported with 0 and assumed to be missing completely at random due to the low number (0.831%) and thus not considered in the following analysis. In addition, for 40 occasions the diameter was not reported for all target lesions. In these cases, the sum of diameters of the remaining target

lesions was calculated and used as sum of diameters, assuming that the not measurable lesions were in complete response.

Tumour sum of diameters, according to the RECIST criteria, for both study arms showed an initial response for the median profile (Figure 3.6). Evaluating the median profile over time, misinterpretation must be avoided by considering the decreasing number of patients evaluated, since patients with progressive disease have a higher risk of death. Thus, the summary statistics (median, 5th and 95th percentile) showed a stabilising of the disease, which was caused by a selection bias. However, it can be seen in the individual profiles, that many patients develop tumour regrowth after initial response. This might be either due to resistance or end of treatment.

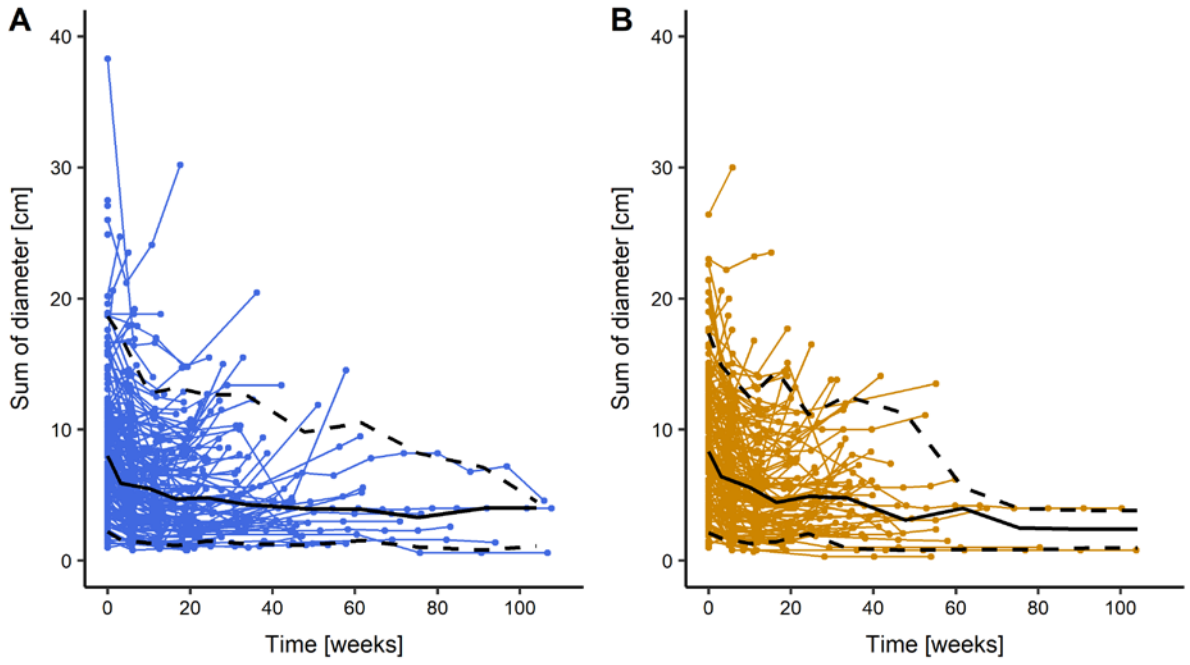

Figure 3.6: Sum of diameters according to RECIST criteria over time.
Panel A: patients in Arm A; Panel B: patients in Arm B.
Black solid line: median tumour size development: dashed black lines: 5th and 95th percentile of tumour size development.

Time to tumour progression, overall and progression-free survival

Efficacy was further evaluated in terms of time to progression (TTP), overall survival (OS) and progression-free survival (PFS) using Kaplan-Mayer plots (Figure 3.7). In the visual inspection, a difference between the two study arms was only found for OS but not for TTP and PFS. Nevertheless, the statistical analysis did not find a significant difference for any of the three efficacy markers when analysing all follow-up visits [139].

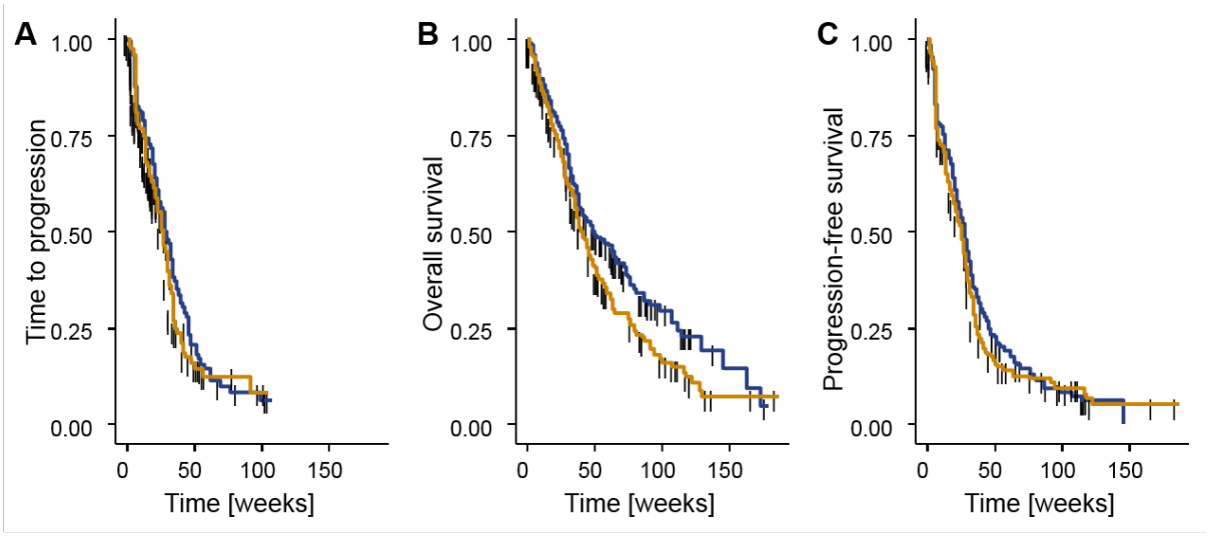

Figure 3.7: Kaplan-Mayer plots of time to progression, overall survival and progression-free survival.
Panel A: time to progression; Panel B: overall survival; Panel C: progression-free survival.
Blue: Arm A; orange: Arm B; vertical lines: censored events.

Maximum number of study cycles patients received

The fact that the number of patients decreases over the treatment cycles (Figure 3.8), does not necessarily imply that the patients dropped out, but that study treatment was stopped for these patients. Patients were still observed in the follow-up and could have received other treatment regimens. Notably, there are two occasions when the number of patients treated with the study medication decreased stronger, namely after the 2nd and the 4th cycle, when tumour assessment was planned and patients diagnosed with progressive disease were further excluded from study treatment. More precisely, considering all cycles, 39.0% of the patients not undergoing the 6 cycles ended study treatment due tumour progression. Another 10.6% of these patients died during the study therapy. For 50.4% of the patients, end of study treatment was for unknown or other reasons as e.g. adverse events or global deterioration of health.

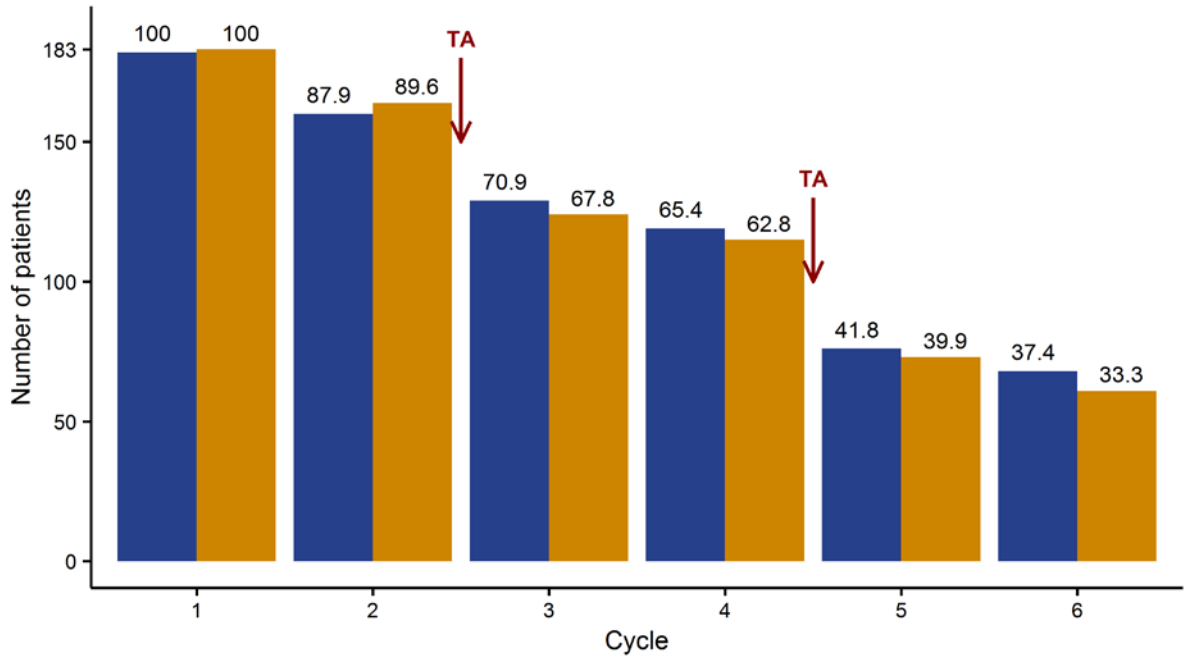

Figure 3.8: Number of patients treated in the respective treatment cycle.
Blue: Arm A; orange: Arm B; numbers: percentage of patients treated compared to cycle 1; TA: arrows mark the planned tumour assessments.

3.1.2 Exploration of covariates

This section only focuses on the covariates finally selected in at least one of the models presented in Project 1 – 3, and therefore needed to be considered for the virtual population in Project 4.

Distribution and correlation of continuous covariates

Evaluation of the distribution and correlation between continuous covariates (Figure 3.9) showed a weak correlation ($0.3 \leq Corr < 0.5$) between age and creatinine clearance as well as between body height and creatinine clearance. Further, a strong and expected correlation ($Corr \geq 0.5$) was found between:

- BSA, weight and body height
- Creatinine clearance and BSA/weight
- Creatinine clearance and creatinine

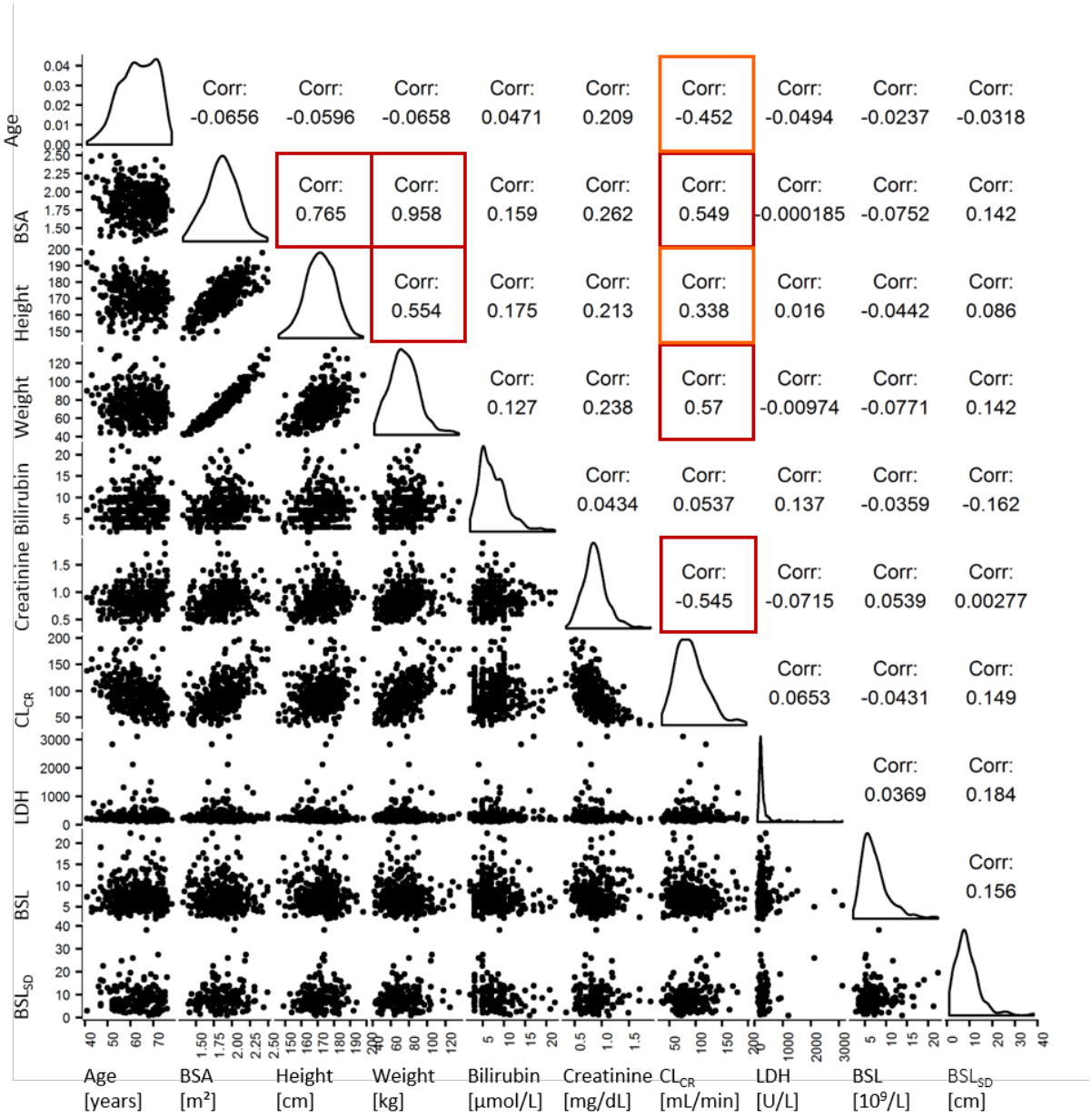

Figure 3.9: Distribution of continuous covariates and correlations between them.
Diagonal elements: distribution of covariates; lower panels of off-diagonal elements: scatter plots of continuous covariates; upper panels of off-diagonal elements: Pearson correlation coefficient (Corr) between the respective covariates.
BSA: body surface area; CL_{CR}: Creatinine clearance; LDH: lactate dehydrogenase; BSL: neutrophil concentration at baseline; BSL_{SD}: baseline tumour size.
Orange boxes: weak correlation (0.3 ≤ Corr < 0.5); red boxes: strong correlation (Corr ≥ 0.5).

Distribution and correlation of categorical covariates

Visual analysis of the distribution of categorical covariates and their correlations revealed a correlation between tumour histology and ECOG performance status (Figure 3.10), which was thus considered for the virtual population in Project 4 (see section 2.6.1)

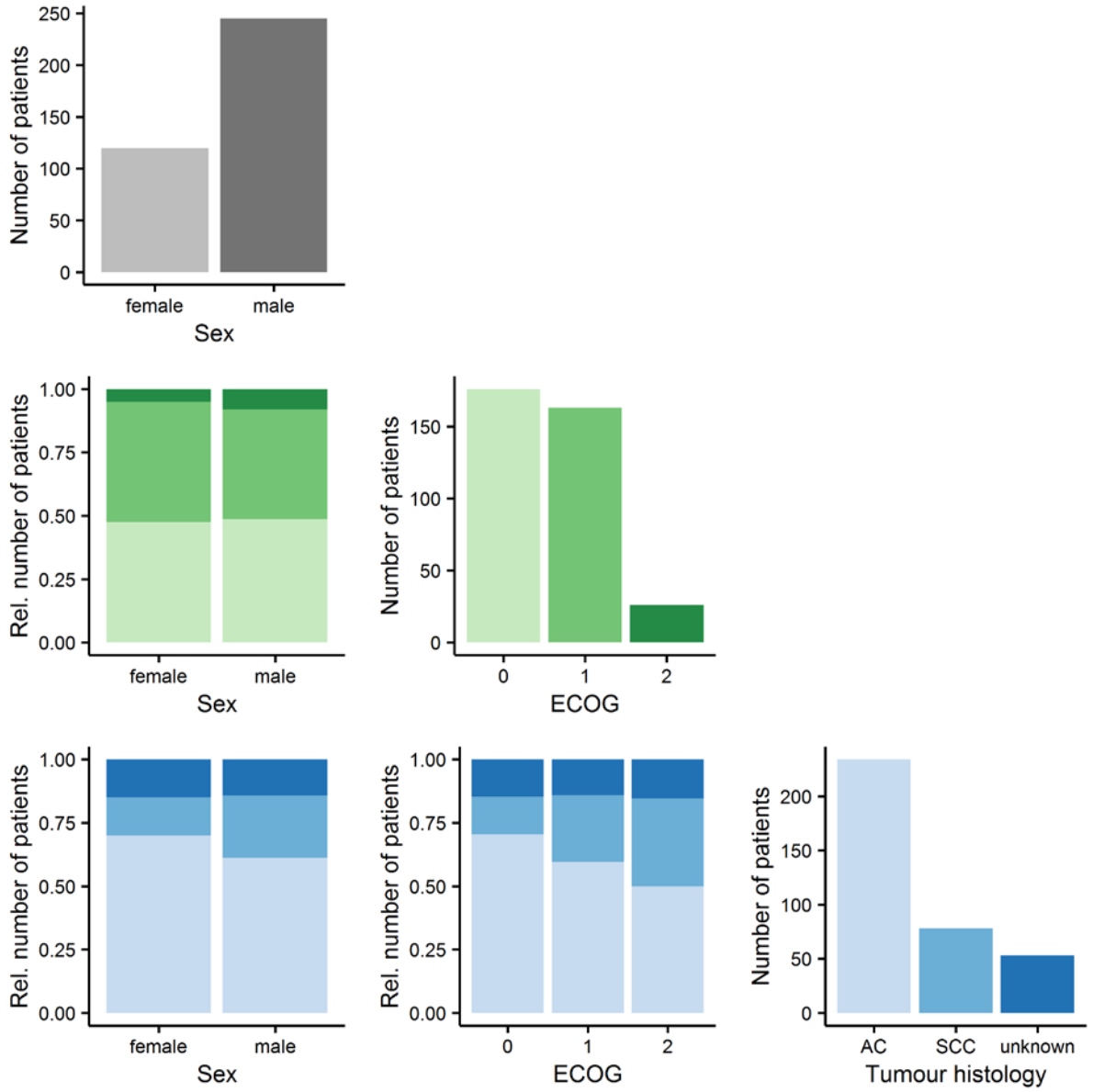

Figure 3.10: Distribution of categorical covariates and correlations between them.
Diagonal elements: distribution of categorical; off-diagonal elements: stacked bar carts of categorical covariates.
Dark grey: male; light grey: female; dark green: ECOG performance status = 2; middle green: ECOG performance status = 1; light green: ECOG performance status = 0; dark blue: unknown tumour histology; middle blue: squamous-cell carcinoma (SCC); light blue: adenocarcinoma (AC).

Correlation between a continuous and a categorical covariate

Correlations between continuous and categorical covariates were analysed using Box-and-Whisker plots (Figure 10.1, in the appendix). This visual analysis showed a correlation between:

- Sex and bilirubin concentration
- Sex and creatinine concentration
- ECOG performance status and age
- ECOG performance status and baseline neutrophil concentrations

- ECOG performance status and the body size descriptors weight body, height and BSA

Evaluation of previous therapy and concomitant therapy

Since previous therapy before the CEAPC-TDM study or concomitant therapy outside the study medication can potentially influence the development of neutropenia, as well as tumour size, these factors were evaluated independently of their implementation in any of the models presented in this work. Overall, 40 of the 365 patients (11.0%) received an anticancer therapy before start of the CEPAC-TDM study (Table 3.2). The majority of these previous therapies were radiotherapies, followed by chemotherapies and surgery.

Table 3.2: Number of patients receiving previous therapy before the CEPAC-TDM study.

Treatment	*Arm A*	*Arm B*	*Total study*
Any therapy	26	14	40
Chemotherapy	13	4	17
Radiotherapy	18	8	26
Surgery	14	6	20

Any therapy is not the sum of chemotherapy, radiotherapy and surgery, since some patients received multiple therapies.

In total, 215 patients (58.9%) were treated with concomitant therapy during the CEPAC-TDM study (Table 3.3). For evaluation of the concomitant therapy it is important to distinguish between patients who received therapy only in the follow-up phase and patients who already received concomitant therapy in parallel to the study medication of the CEPAC-TDM study (Table 3.4). The number of patients who received additional therapy parallel to the study therapy was low (25 patients, 6.85%). While overall, the majority of patients who received further treatment at any time of the study received chemotherapy, during the CEPAC-TDM study treatment the majority of concomitant therapies were radiotherapies. Chemotherapy and radiotherapy potentially decrease neutrophil concentrations and were thus investigated as covariate on the drug effect in the neutropenia model in Project 2 (see section 2.4.2.3). PK interactions are potentially possible but were not investigated due to the diversity of the concomitant therapy and the sparse paclitaxel PK information. Surgery was only rarely performed (overall 4 times, one of this during study treatment period).

Table 3.3: Concomitant therapy at any time of the study including follow-up.

Treatment	*Arm A*	*Arm B*	*Total study*
Any therapy	110	105	215
Chemotherapy	94	86	180
Radiotherapy	52	43	95
Surgery	3	1	4

Any therapy is not the sum of chemotherapy, radiotherapy and surgery, since some patients received multiple therapies.

Table 3.4: Concomitant therapy during study treatment.

Treatment	*Arm A*	*Arm B*	*Total study*
Any therapy	15	10	25
Chemotherapy	6	4	10
Radiotherapy	8	6	14
Surgery	1	0	1

Any therapy is not the sum of chemotherapy, radiotherapy and surgery, since some patients received multiple therapies.

3.2 Project 1: Pharmacokinetic modelling of paclitaxel

3.2.1 External PK model evaluation using the CEPAC-TDM data

An external PK model evaluation was performed by comparing predictions of the published PK model [138] with the PK data from the CEPAC-TDM study. For this evaluation, different types of analyses were performed.

First, a *post-hoc* estimation was performed to obtain the individual and population predictions. These individual predictions were compared to the observed data (Figure 3.11, Panel A and B) and showed a good prediction, i.e. the data points were equally distributed around the line of identity and did not differ much from this line. Though, high shrinkage was observed in this step for interindividual variability (η-shrinkage: VM_{EL}: 47.4%; Km_{TR}: 92.9%; VM_{TR}: 92.3%; k_{21}: 97.6%; V_3: 58.5%; Q: 52.8%), interoccasion variability (κ-shrinkage: V_1: 98.6%; VM_{EL}: 57.2%) and residual variability (ε-shrinkage: 97.4%), which points towards an "overfitting" (see section 2.1.2.2).

In the next step, the population prediction was compared to the observed data, as done for the individual prediction (Figure 3.11, Panel C and D). Here, the prediction was inferior compared

to the individual prediction. In general, an underprediction of the concentrations by the PK model was observed which was more severe for males. Further, the conditional weighted residuals revealed a small trend of the overpredictions being more severe for higher concentrations in the beginning of the observed time period.

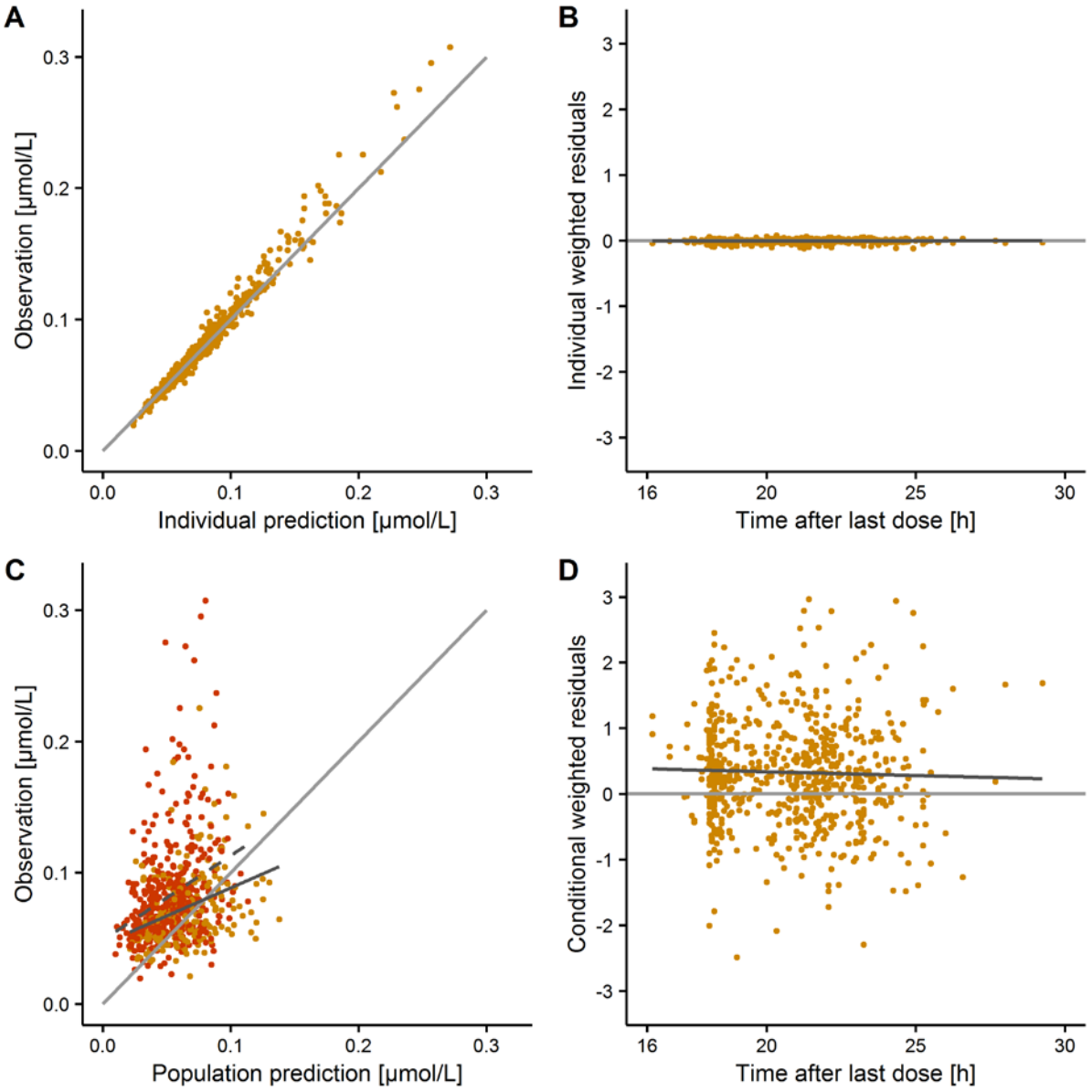

Figure 3.11: Goodness-of-fit plots for the external PK model evaluation using the paclitaxel concentrations measured in the CEPAC-TDM study and the original PK model.
Panel A: paclitaxel concentrations of the CEPAC-TDM study over the individual prediction obtained by *post-hoc* estimation.
Panel B: individual weighted residual over time after last dose.
Panel C: paclitaxel concentrations of the CEPAC-TDM study over the population prediction obtained stratified by sex: red: males, orange: females.
Panel D: conditional weighted residual over time after last dose.
Light grey line: line of identity; dark grey line: linear regression, for Panel C: dashed: males, solid: females.

Further, simulation-based model evaluations were performed in terms of pcVPCs and NPDE analysis. The pcVPC (Figure 3.12) confirmed the observations of the analysis of the population predictions in the Goodness-of-fit plots. In the pcVPC, again the underprediction was obvious as well as the trend that this underprediction reduced over the time after last dose. The NPDE analysis resulted in global adjusted p-value of $2.21 \bullet 10^{-36}$, i.e. the H_0 hypothesis, that the measured paclitaxel concentrations can be described by the PK model, was rejected.

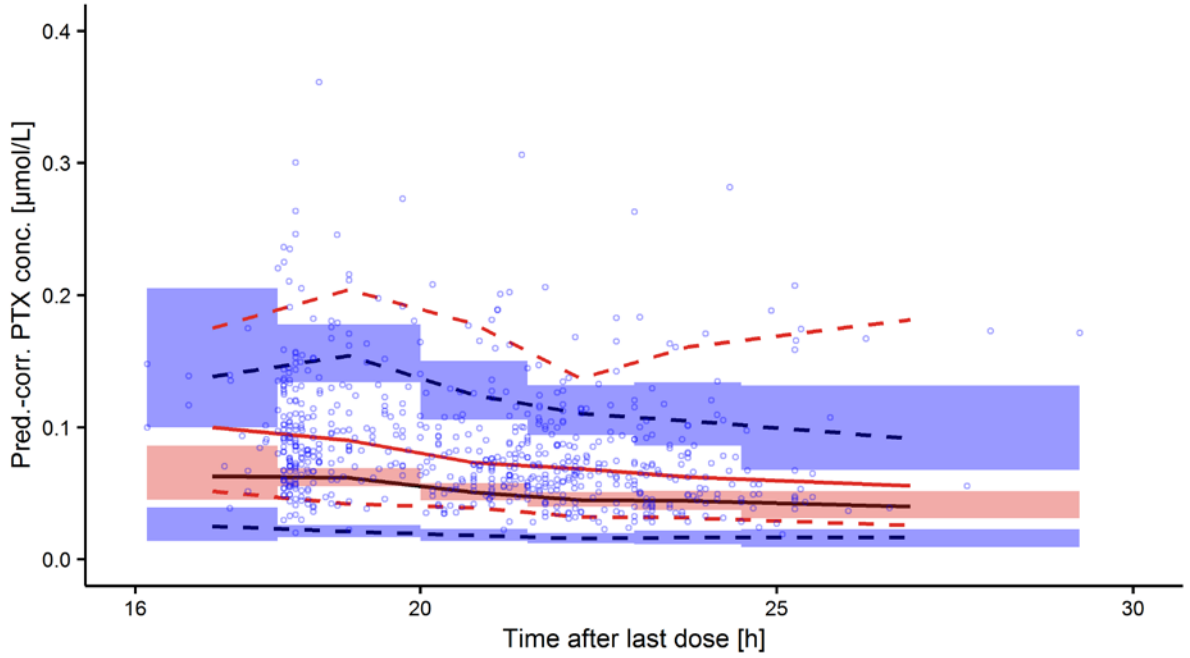

Figure 3.12: Prediction-corrected visual predictive check of the external PK model evaluation using the paclitaxel concentrations measured in the CEPAC-TDM study and the original PK model.
Blue circles: observed neutrophil concentrations; red lines: median (solid), 5th, 95th percentiles (dashed) of observations; black lines: median (solid), 5th and 95th percentiles (dashed) of simulations; shaded areas: 90% confidence intervals of simulated percentiles.

3.2.2 PK model optimisation and evaluation of the optimised model

Due to the results of the external model evaluation, the PK model was optimised by applying the frequentist approach (see section 2.1.1.5). Thus, the prior knowledge, comprising the model structure and the parameter estimates of the published PK model, were combined with the information contained in the PK samples of the CEPAC-TDM study. Two approaches were compared using either the diagonal- or the diagonal- and off-diagonal elements of the variance-covariance matrix Γ to determine the uncertainty of the fixed-effects parameters for the penalty function (Model I and Model II, respectively).

PK model evaluation and comparison – population level

By applying the frequentist prior estimation, population parameters did not change significantly for neither of the two approaches, Model I and II (Table 3.5). Nevertheless, the changes in the

fixed-effects parameters resulted in a decreased clearance (CL_{lin}) for both models, but the decrease was stronger for Model I (13.8% compared to 5.47% for Model II). Further changes were observed for the linear distribution to the 2nd peripheral compartment evaluated based on k_{13} and k_{31}: Model I resulted in an increased distribution to this compartment and a decreased distribution back to the central compartment. Model II, on the other hand, showed a stable value for the distribution to the 2nd peripheral compartment, while the back-distribution to the central compartment was increased. Further, both models described the covariates to be less influential, with lower absolute values for the respective parameter estimates. Only the effect of age was increased in Model II. Regarding the random-effects parameters, Interindividual variability was slightly reduced (relative change below 10%) for all model parameters in both models, as well as residual variability.

Table 3.5: Parameter estimates of the original PK model compared to the PK parameters from re-estimation using the original PK parameters as prior information (modified from [140])**.**

Parameter	***Parameter estimate (95% confidence interval)***		
	Original PK model [138]*****	***Optimised PK Model I*****	***Optimised PK Model II******
Fixed-effects parameters			
V_1 [L]	10.8 (9.99 – 11.6)	10.8 (10.7 – 10.8)	11.4 (9.73 – 11.5)
V_3 [L]	275 (245 – 305)	301 (292 – 311)	265 (212 - 274)
Km_{EL} [µmol/L]	0.576 (0.49 – 0.662)	0.667 (0.645 – 0.687)	0.640 (0.587 – 0.655)
VM_{EL} [µmol/h]	35.8 (32.5 – 39.1)	35.9 (35.1 – 36.6)	37.6 (35.8 – 38.3)
Km_{TR} [µmol/L]	1.43 (1.19 – 1.67)	1.44 (1.38 – 1.48)	1.35 (0.0684 – 1.43)
VM_{TR} [µmol/h]	177 (166 – 188)	175 (174 – 176)	178 (176 - 191)
k_{21} [h^{-1}]	1.11 (1.04 – 1.18)	1.12 (1.11 – 1.13)	1.13 (1.10 – 1.14)
Q [L/h]	15.6 (14.0 – 17.2)	16.8 (16.5 – 17.1)	16.5 (16.1 – 18.2)
BSA on VM_{EL}	1.30 (1.05 – 1.55)	1.14 (1.06 – 1.25)	1.09 (0.989 – 1.32)
Sex on VM_{EL}	1.16 (1.07 – 1.25)	1.07 (1.03 – 1.10)	1.07 (1.02 – 1.11)
Age on VM_{EL}	-0.449 (-0.630 – -0.268)	-0.447 (-0.525 – -0.367)	-0.517 (-0.592 – -0.405)
BILI on VM_{EL}	-0.160 (-0.223 – -0.0973)	-0.0942 (-0.124 – -0.0648)	-0.0877 (-0.154 – -0.0623)
CL_{lin} [L/h] [#]	62.2	53.8	58.8
k_{13} [1/h][#]	1.44	1.56	1.45
k_{31} [1/h] [#]	0.0567	0.0558	0.0623
Interindividual variability parameters			
V_3; CV, %	46.2 (39.4 – 53.0)	42.2 (41.5 – 43.0)	42.1 (41.5 – 46.7)
VM_{EL}; CV, %	17.8 (14.6 – 21.0)	16.0 (15.1 – 16.9)	16.4 (15.3 – 19.6)
Km_{TR}; CV, %	69.8 (58.2 – 81.4)	68.9 (68.7 – 69.5)	69.4 (67.9 – 71.6)
VM_{TR}; CV, %	28.7 (24.4 – 33.0)	28.3 (28.3 – 28.4)	28.4 (27.8 – 28.5)
k_{21}; CV, %	9.31 (-1.18 – 19.8)	8.94 (8.85 – 9.06)	9.05 (8.26 – 9.13)
Q; CV, %	45.8 (40.4 – 51.2)	42.5 (41.9 – 43.3)	42.1 (42.7 – 46.0)
Interoccasion variability parameters			
V_1; CV, %	37.3 (34.0 – 40.6)	37.3 (fixed)	37.3 (fixed)
VM_{EL}; CV, %	15.2 (13.0 – 17.4)	15.2 (fixed)	15.2 (fixed)
Residual variability parameters			
Exponential model; CV, %	18.2 (18.1 – 18.3)	17.8 (17.8 – 17.8)	17.8 (17.7 – 18.2)

CV, %: coefficient of variation; V_1: central volume of distribution; V_3: volume of distribution of 2nd peripheral compartment; Km_{EL}: paclitaxel concentration at half VM_{EL}; VM_{EL}: maximum elimination capacity; Km_{TR}: paclitaxel concentration at half VM_{TR}; VM_{TR}: maximum transport capacity; k_{21}: distribution rate constant between central and 1st peripheral compartment; Q: intercompartmental clearance between the central and the 2nd peripheral compartment; BSA: body surface area [m²]; BILI: Bilirubin concentration [µmol/L]; CL_{lin}: clearance of paclitaxel in the linear phase of the saturable elimination; k_{13}: distribution rate constant between central and 2nd peripheral compartment; k_{31}: distribution rate constant between 2nd peripheral and central compartment.

* Confidence intervals based on standard errors of original model, assuming normal distribution.

** Confidence intervals determined by bootstrap analysis (1000 runs, convergence rate 96.5%).

*** Confidence intervals determined by bootstrap analysis (700 runs, convergence rate 89.1%).

[#] Parameter was not estimated but derived from the fixed-effects parameters (see Eq. 2.33 – Eq. 2.35).

Deterministic simulations of the three models were performed to explore the difference in the typical concentration-time profile resulting from the new sets of parameters (Figure 3.13). When investigating these deterministic simulations on a linear scale, no obvious differences were seen. When transformed to a semi-logarithmic scale, changes in the terminal phase of the concentration-time profile were observed. Thereby, Model I showed a greater difference to the original model than Model II. Both models led to an increased $T_{C>0.05}$ for the typical patient simulated (increase $T_{C>0.05}$ of 8.0 h for Model I and 4.7 h for Model II).

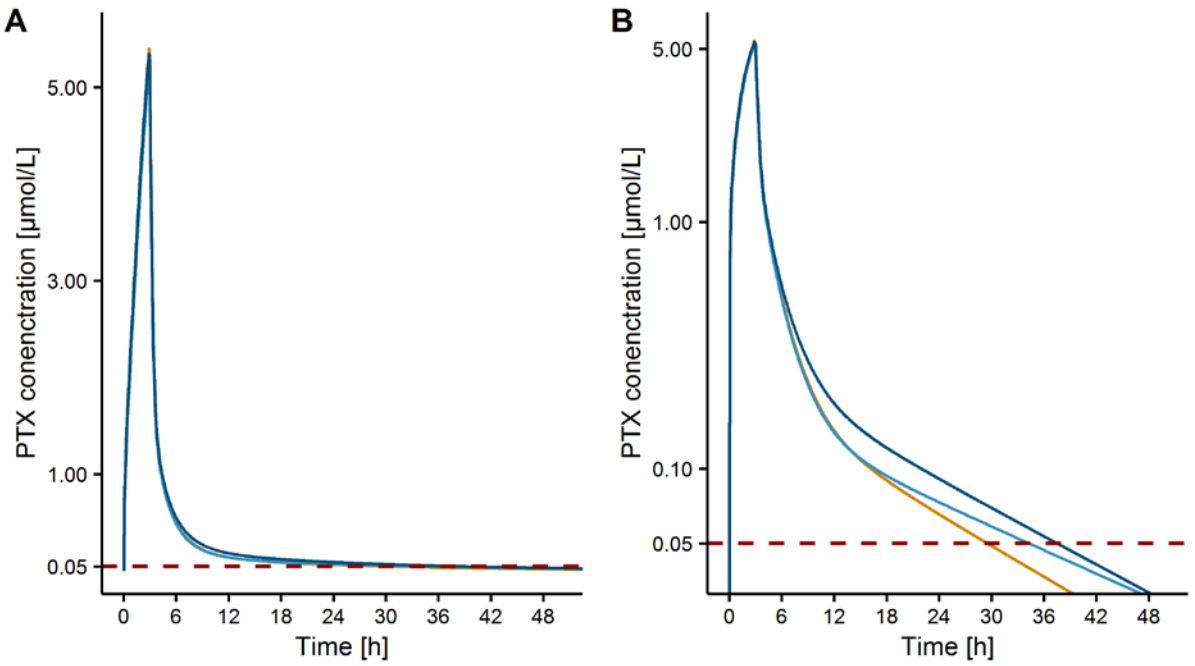

Figure 3.13: Deterministic simulation using the original and optimised PK model.
Deterministic simulation of a typical patient: male, age: 56 years, bilirubin concentration: 7 µmol/L, body surface area: 1.8 m² receiving a single 3 h infusion of 200 mg/m² paclitaxel.
Panel A: linear scale; Panel B: semi-logarithmic scale.
Orange line: original model; dark blue line: optimised PK Model I (see section 2.3.2); light blue line: optimised PK Model II (see section 2.3.2); red dashed line: threshold paclitaxel concentration of 0.05 µmol/L.

Parameter precision, determined by bootstrap analysis, was good for both models, but the resulting confidence intervals were narrower for Model I. Further, the estimation of Model I was more stable, which was reflected in the higher convergence rate of the bootstrap analysis (96.5% and 89.1% for Model I and II, respectively). Both models (Model I and Model II) were evaluated and compared using goodness-of-fit plots (Figure 3.14, Panel A – B) and pcVPCs (Figure 3.14, Panel C – D), since OFV and AIC were not applicable for comparison due to the different derivation of the penalty function influencing these values. For both models, the individual prediction was, as in the original model, very good (data not shown), while the population predictions still indicated some misspecification, even though the prediction was improved. No significant difference was observed between the two models in

the goodness-of-fit plots. However, pcVPCs indicated a better prediction for Model I, which was thus chosen for the following analysis.

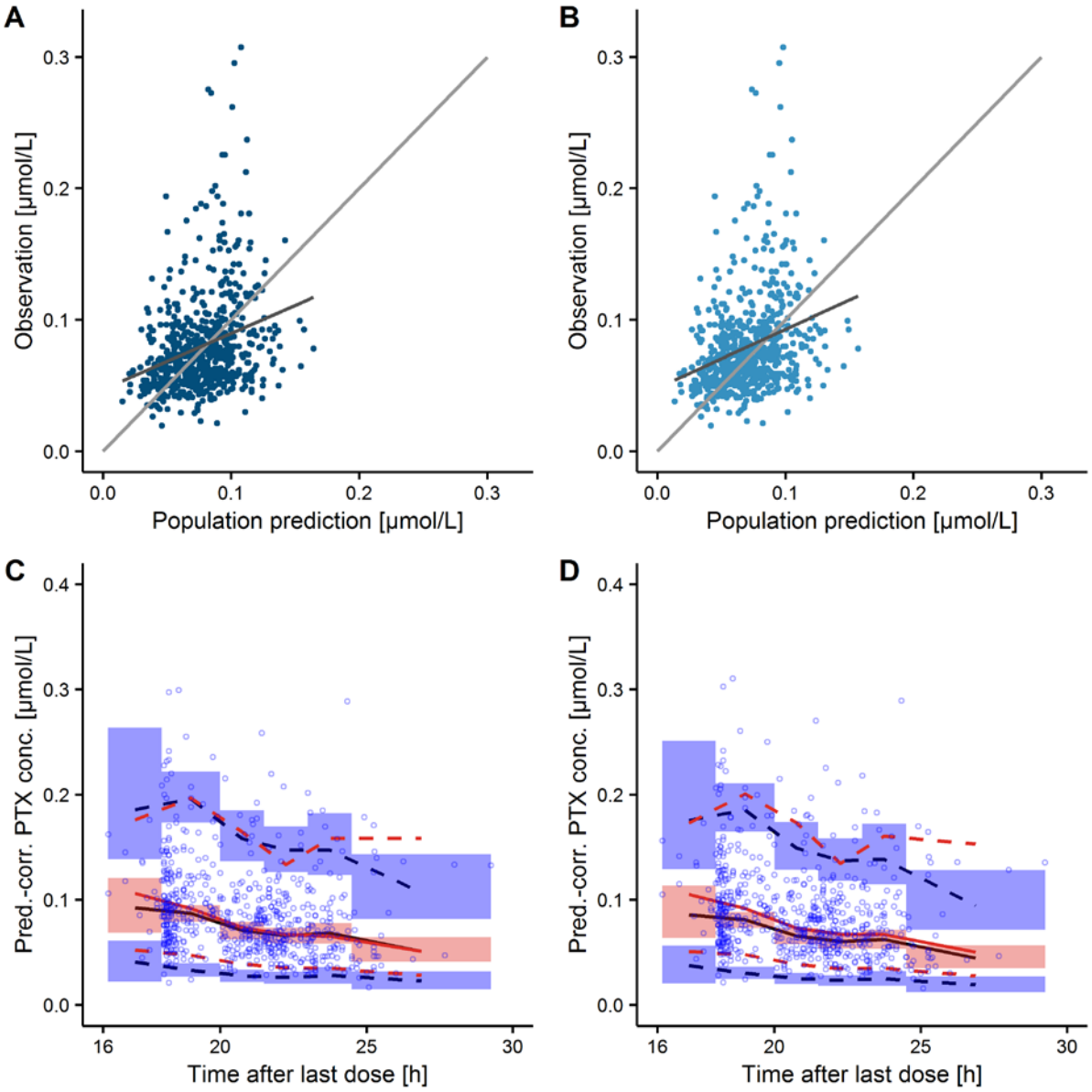

Figure 3.14: Evaluation of PK models considered in model optimisation (modified from [140])**.**
Panel A (dark blue): optimised PK Model I (see section 2.3.2); Panel B (light blue): optimised PK Model II (see section 2.3.2).
Light grey line: line of identity; dark grey line: linear regression.
Panel C and D: prediction-corrected visual predictive checks of Model I and II, respectively.
Blue circles: observed paclitaxel concentrations; red lines: median (solid), 5th, 95th percentiles (dashed) of observations; black lines: median (solid), 5th and 95th percentiles (dashed) of simulations; shaded areas: 90% confidence intervals of simulated percentiles.

PK model evaluation and comparison – individual level

To further evaluate the impact of the new set of parameters, the differences of the EBEs and exposure parameters resulting from the *post-hoc* estimation of the original model and optimised Model I were compared (Figure 3.15). Thereby, the highest change in the EBEs was

observed for V_3 and Q ($MRPE_p$: -14.7% and 6.05%, respectively), which were also the parameters with the highest change in the estimation of the fixed-effects parameters. The change in the EBE of VM_{EL} ($MRPE_p$: -3.33%, $MARPE_p$: -3.82%) is mainly caused by the change in covariate effect, since the parameter in the original model was only 1.00% smaller compared to the new parameter set of Model I. Further, higher individual estimates of the drug exposure parameters $T_{C>0.05}$ and AUC ($MRPE_p$: -5.82% and -4.28%, respectively) were observed.

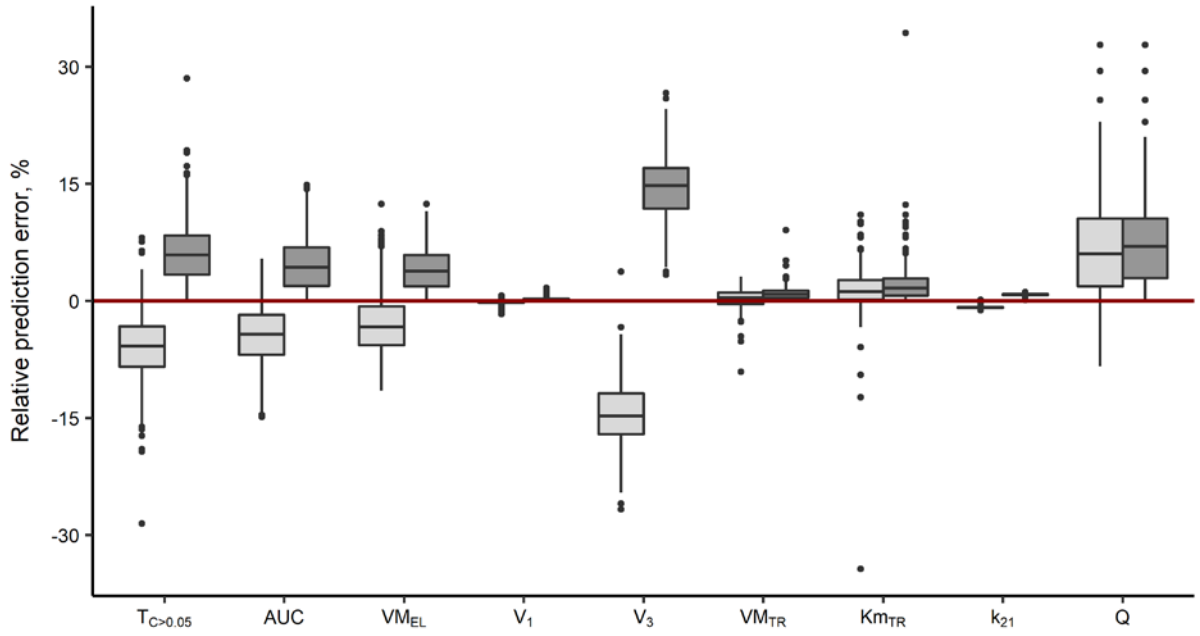

Figure 3.15: Relative deviation of the Empirical Bayes Estimates and PK parameters of the original PK model compared to Model I [140]**.**
Box-Whisker plot of individual relative prediction error ($RPE_{p,i,o}$, light grey, accounting for precision) and absolute value of $RPE_{p,i,o}$ (dark grey, accounting for bias) determined by *post-hoc* estimation from optimised PK Model I compared to the ones from original parameter set.
Boxes: interquartile range (IQR), including median; whiskers: range from box hinge to highest/lowest value within 1.5•IQR; points: data beyond whiskers.
For explanation of Model I see section 2.3.2.
$T_{C>0.05}$: Time of paclitaxel concentration > 0.05 µmol/L; AUC: area under the curve; VM_{EL}: maximum elimination capacity; V_1: central volume of distribution; V_3: volume of distribution of 2nd peripheral compartment; VM_{TR}: maximum transport capacity; Km_{TR}: paclitaxel concentration at half VM_{TR}; k_{21}: distribution rate constant between 1st peripheral and central compartment; Q: intercompartmental clearance between central and 2nd peripheral compartment.
For parameters V_3, VM_{TR}, Km_{TR}, k_{21} and Q: n = 183 (patients); for parameters $T_{C>0.05}$, AUC, VM_{EL}, V_1: n = 720 (treatment cycles).

Evaluation of the impact of the optimised model on the study outcome

Further, investigating the prediction of $T_{C>0.05}$ of the two PK models (original and Model I), the percentage of patients being overdosed was estimated higher when using the optimised PK model (Figure 3.16). The original model estimated that less than 10% of the patients were overdosed from cycle 3 on, while the optimised model estimated this percentage in a range of

20 – 30%. On the other hand, the percentage of patients underdosed decreased when applying estimation with the new model. Overall, patients not reaching the target range were estimated to be higher when applying the optimised Model I.

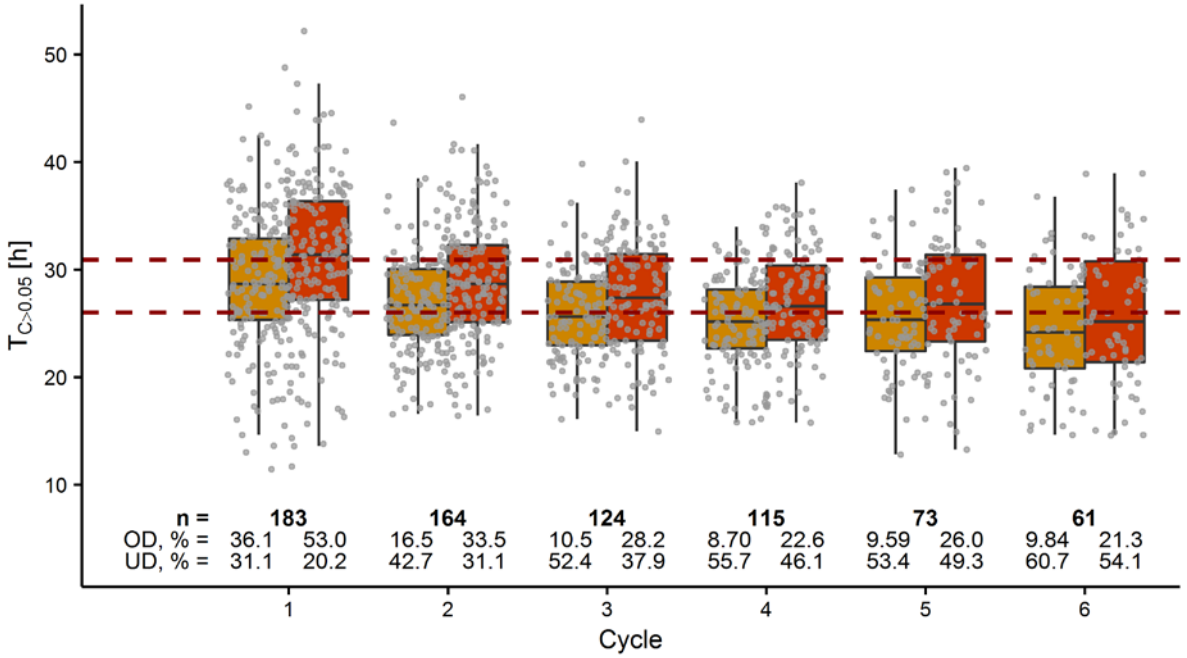

Figure 3.16: Comparison of time above the threshold of 0.05 µmol/L ($T_{C>0.05}$) obtained by *post-hoc* estimation from the original and optimised (Model I) PK model.
Boxes: interquartile range (IQR), including median; whiskers range from the hinge to the highest value within 1.5 • IQR; grey points: all individual $T_{C>0.05}$ values.
Colour: orange: original model; red: optimised Model I (see section 2.3.2).
n: number of patients in the respective cycle; OD, %: percentage of patients overdosed ($T_{C>0.05}$ ≥ 31 h); UD, %: percentage of patients underdosed ($T_{C>0.05}$ < 26 h).

To examine exposure in the two study arms, stochastic simulation using Model I of both study arms were performed and the resulting $T_{C>0.05}$ were compared with the *post-hoc* estimations of the patients in Arm B (Figure 3.17) using the optimised Model I. The simulations for Arm A showed that also the dose reductions in Arm A lead to a decreasing exposure over the cycles. However, the median $T_{C>0.05}$ for Arm A was higher than for Arm B for all treatment cycles. Within Arm B, the median of the simulations and the *post-hoc* estimations were approximately the same for the first cycle, but in the following cycles, increasing differences were observed with lower values for the simulated median $T_{C>0.05}$.

The variability in $T_{C>0.05}$ was comparable between simulations of the two study arms. The comparison within Arm B on the other hand showed, that the variability in $T_{C>0.05}$ was higher for the stochastic simulation than for the *post-hoc* estimation, which is plausible, since the simulation was not influenced by shrinkage.

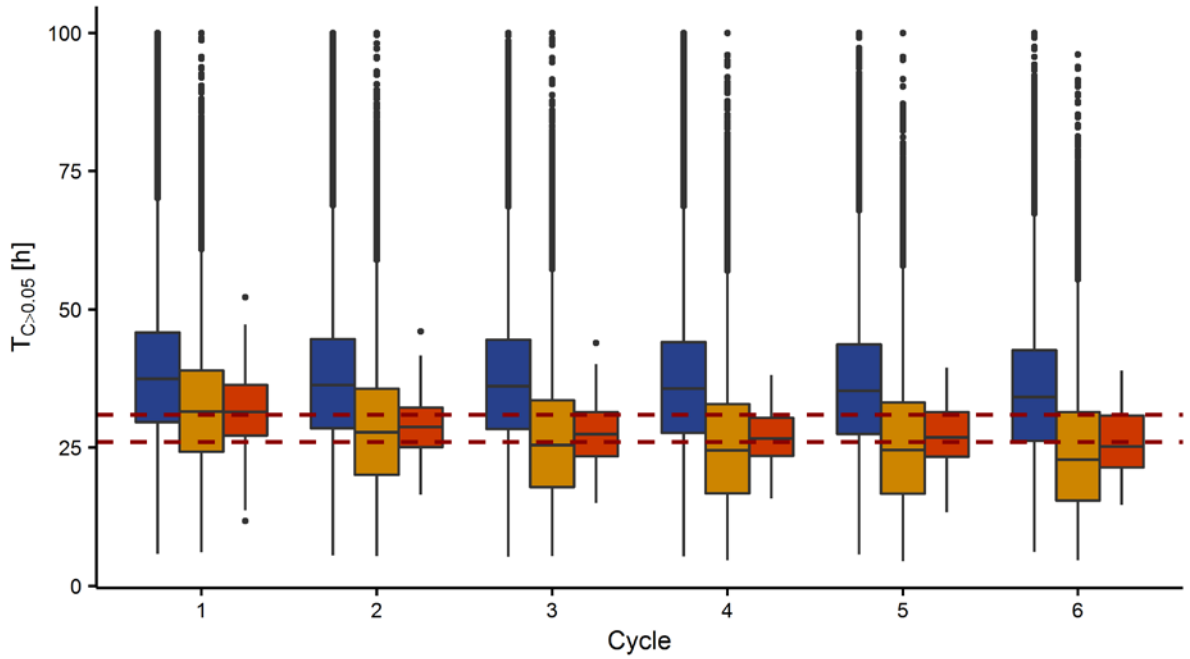

Figure 3.17: Comparison of exposure obtained by simulations between both study arms and exposure obtained by *post-hoc* estimation for patients in Arm B using Model I.
Boxes: interquartile range (IQR), including median; whiskers: range from box hinge to highest/lowest value within 1.5•IQR; points: data beyond whiskers.
For explanation of Model I see section 2.3.2.
Colours: blue: stochastic simulations of study Arm A; orange: stochastic simulations of study Arm B; red: *post-hoc* estimation of study Arm B.
$T_{C>0.05}$: time above the threshold of 0.05 µmol/L

3.2.3 Evaluation of the limited sampling strategy applied in the CEPACT-TDM study

In the CEPAC-TDM study, PK samples were only taken once per cycle, approximately 24 h after drug administration. This sparse sampling might influence the individual prediction of the paclitaxel concentration-time profile profiles, which was used to inform neutropenia (Project 2) and tumour size outcome (Project 3). Thus, precision and bias of the EBEs and the drug exposure parameters $T_{C>0.05}$ and AUC were evaluated using simulations with *post-hoc* re-estimation considering the sparse sampling performed in the CEPAC-TDM study (Table 3.6). *Post-hoc* estimation showed only slightly biased estimation (bias < ± 7%) of both EBEs and exposure parameters. On the other hand, imprecision was high (> 20%) for some parameters, as e.g. Km_{TR} and V_3. For the exposure parameters, imprecision was lower compared to most of the EBEs. In summary, *post-hoc* estimation resulted in reliable exposure parameter estimates, while individual PK parameters were shrunk to the typical value. Thus, variability in the individual concentration-time might be underestimated and might influence the PD parameter estimation in Project 2 and 3.

Table 3.6: Bias and imprecision of the EBEs and exposure parameters considering the sparse sampling strategy of the CEPAC-TDM study

Parameter	*Bias, %*	*Imprecision, %*
$T_{C>0.05}$*	-0.791	11.8
AUC*	2.06	15.8
VM_{EL}*	0.326	9.84
V_1*	0.107	24.7
V_3**	-6.73	25.7
VM_{TR}**	1.96	18.9
Km_{TR}**	3.08	43.6
k_{21}**	-0.0179	6.03
Q**	-5.02	24.0

Bias: median of individual relative prediction error $RPE_{p,i,o}$; imprecision: median of the absolute value of $RPE_{p,i,o}$.
$T_{C>0.05}$: time above the threshold of 0.05 µmol/L; AUC: area under the curve; VM_{EL}: maximum elimination capacity; V_1: central volume of distribution; V_3: volume of distribution of 2nd peripheral compartment; VM_{TR}: maximum transport capacity; Km_{TR}: paclitaxel concentration at half VM_{TR}; k_{21}: distribution rate constant between central and 1st peripheral compartment; Q: intercompartmental clearance between central and the 2nd peripheral compartment.
* n = 72 000 treatment cycles.
** n = 18 300 patients.

3.3 Project 2: Modelling of paclitaxel-induced long-term neutropenia

3.3.1 External model evaluation of the prior neutropenia model

The PK/PD model prediction combining the optimised PK model and the original PD model parameters (Table 3.7, left column), were evaluated for the newly obtained neutrophil concentration measurements of the CEPAC-TDM study. The goodness-of-fit plots (Figure 3.18) revealed a good prediction for the individual predictions. However, when stratified by treatment cycle, it was observed that the goodness-of-fit was dependent on the treatment cycle. More precisely, while in the early cycles neutrophil concentrations tended to be underpredicted, the later cycles showed an overprediction. This trend was also seen for the individual weighted residual over the study time. When investigating the population prediction, overprediction was seen for all treatment cycles. As for the individual prediction, a trend to higher overprediction with increasing cycle number was observed.

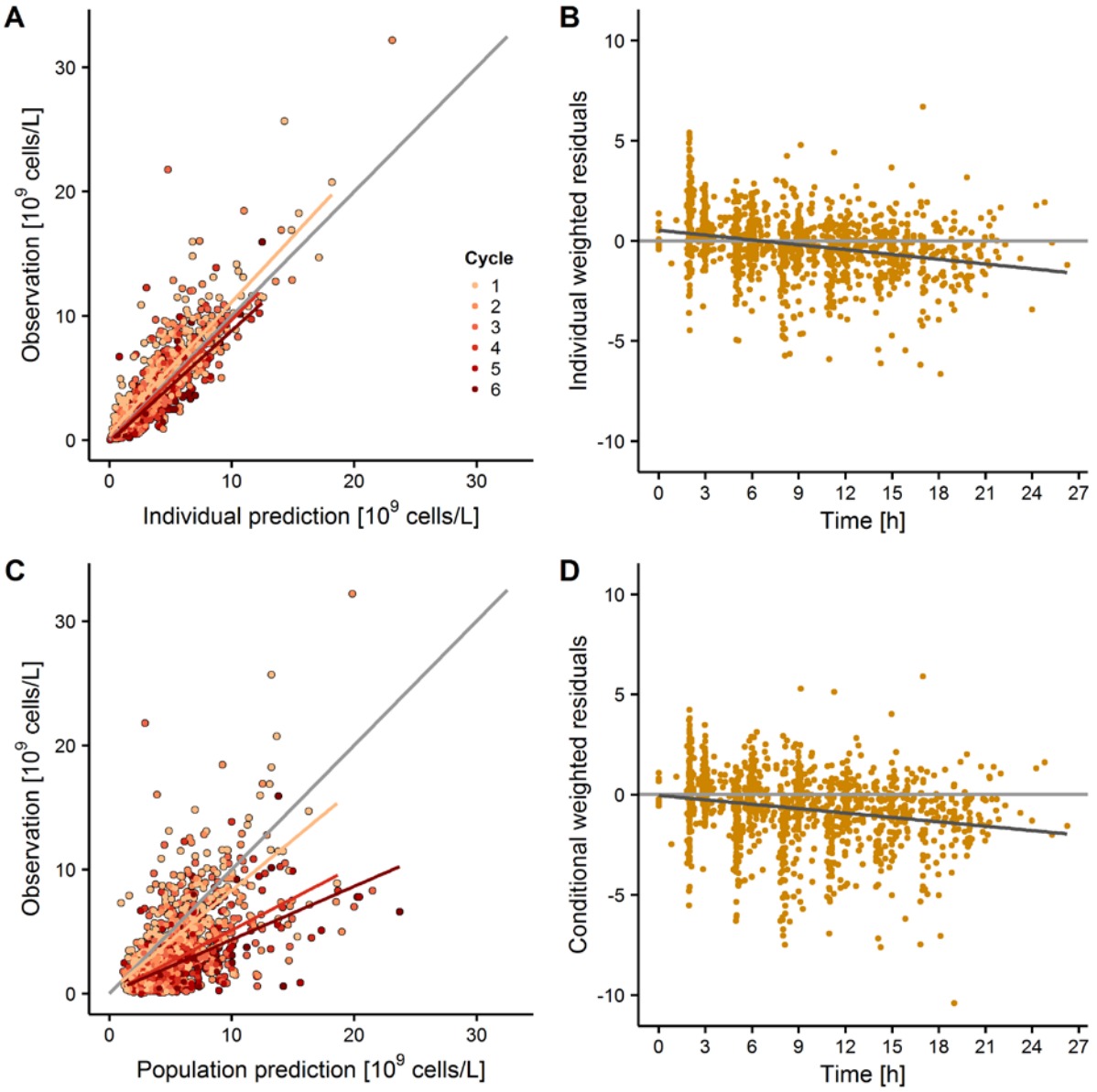

Figure 3.18: Goodness-of-fit plots for the external PK/PD model using the gold standard model and the CEPAC-TDM study data.
Panel A: neutrophil concentrations of the CEPAC-TDM study against the individual prediction obtained by *post-hoc* estimation, stratified by treatment cycle.
Panel B: individual weighted residual over time.
Panel C: neutrophil concentrations of the CEPAC-TDM study against the population prediction obtained stratified by treatment cycle.
Panel D: conditional weighted residual over time.
Light grey line: line of identity; dark grey line: linear regression; red lines in Panel A and C: regression line for treatment cycle 1, 4 and 6; orange and red colours in Panel A and C: treatment cycles corresponding to legend in Panel A.

In the simulation-based external model evaluation, the pcVPC (Figure 3.19) confirmed the trend of worsening overprediction over the study time, seen in the goodness-of-fit plots. It further disclosed some reasons of this overprediction: Firstly, day 15 ± 2 neutrophil measurements were overpredicted already in the first cycle. Secondly, while the observed neutrophil concentrations decreased over the treatment cycles, as described in section 3.1.1,

the simulated concentrations did not follow this pattern. In contrast, the simulations predicted increasing neutrophil concentrations for day 15 ± 2 measurements over time, due to the paclitaxel dose reductions. Hence, observations and simulations showed oppositional trends, leading to an increasing discrepancy between observation and model prediction over time.

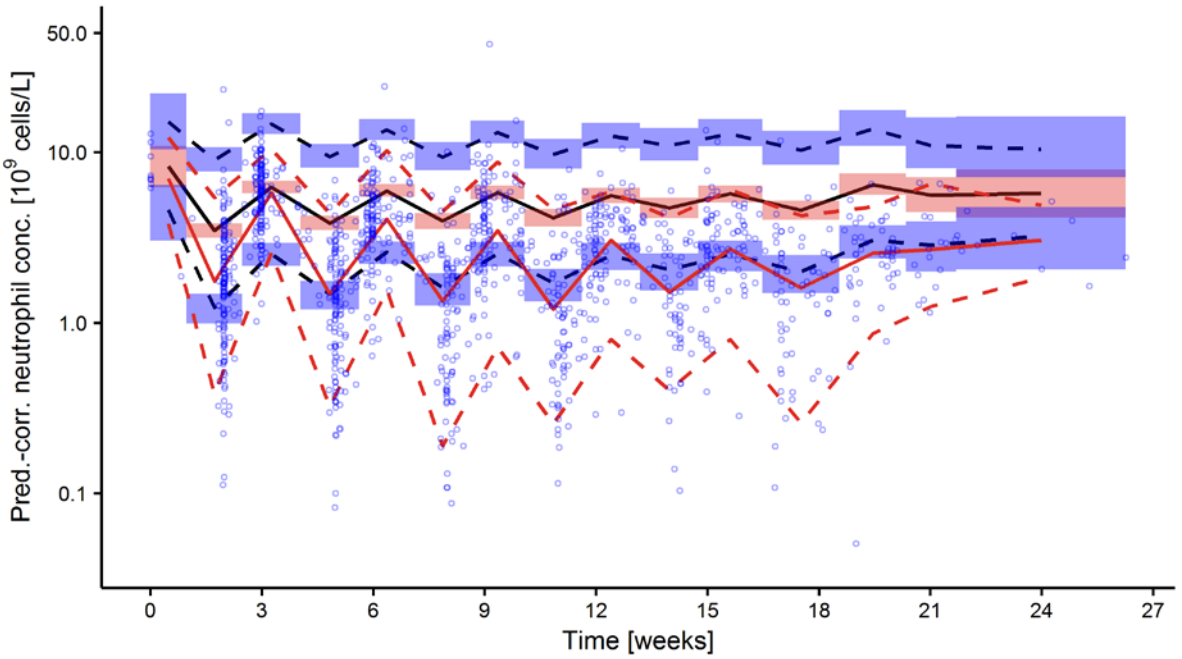

Figure 3.19: Prediction-corrected visual predictive check of the external PK/PD model evaluation using the gold standard model and the CEPAC-TDM study data [140].
Blue circles: observed neutrophil concentrations; red lines: median (solid), 5th, 95th percentiles (dashed) of observations; black lines: median (solid), 5th and 95th percentiles (dashed) of simulations; shaded areas: 90% confidence intervals of simulated percentiles.

The NPDE analysis for the external model evaluation of the PK/PD model resulted in a global adjusted p-value of approximately 0 ($< 1 \cdot 10^{-60}$), indicating a significant difference between the simulations and the observed data.

Shrinkage resulted in negative values for the interindividual variability in SL (η-shrinkage: -5.31%), $Circ(t_0)$ (η-shrinkage: -12.8%) and for the residual variability (ε-shrinkage: -52.5%). Negative η-shrinkage values occur if the variability in the EBEs is higher than it was specified by the population parameters. Only η-shrinkage of the mean maturation time was greater than 0 (35.7%).

3.3.2 Model optimisation to describe long-term toxicity

3.3.2.1 Base model development for cumulative neutropenia

The first step of the model optimisation was to re-estimate the PD model parameters with the data from the CEPAC-TDM study, not changing the model structure. Further, 3 different structural models (Model A – C) were investigated. For all models, the B1 method for

describing baseline neutrophil concentrations was investigated (see section 2.1.1.4), but did not improve the model prediction evaluated using goodness-of-fit plots. Thus, the B2 method was used for the following analysis which uses the individually measured baseline and allows for residual variability.

Model evaluation of the original model, the re-estimated gold standard model and Model A – C

The Akaike information criterion (AIC) decreased by approximately 2000 when re-estimating the model parameters (Table 3.7). However, it must be considered that the original model used the FO approximation method, while for the re-estimation and Model A – C FOCE including interaction was used. Thus, the AIC obtained with the original model (including original parameter estimates) was not statistically comparable to the AIC of the re-estimation and PK/PD Models A – C. Comparing the AIC of the parameter re-estimation with Model A – C, the highest value was observed for the re-estimation, followed by Model B, Model A and finally Model C, indicating the best prediction for the latter. The condition number was below 200 for all PK/PD models considered in the model optimisation, indicating that the models were not overparameterised.

When re-estimating the parameters of the gold standard model with the CEPAC-TDM data, the mean maturation time decreased by 9.22%, while the slope factor increased about 72.3% compared to the original model. The increase in the SL was also present for Model A – C with the highest value for Model B. The mean maturation time was similar to the re-estimated gold standard model for Model A and B, and slightly higher for Model C (increase by 13.3%). Nevertheless, due to the different model structure, comparison between values of the fixed-effects parameter can be misleading.

For Model A (Table 3.7, column “Model A”), the parameter estimate of frB denoted, that $BASE_{tot}(t)$ can decrease to approximately 50% of the original baseline over time. This decreased baseline concentration was then targeted for all compartments, including Circ, i.e. the cell concentration in all compartments would only recover to this concentration. The decline in $BASE_{tot}(t)$ followed an exponential decline (Figure 3.21, Panel B) with a half-life of approximately 15 days, resulting from the second drug effect, if $T_{C>0.05}$ was assumed to be 30 h. For Model B (Table 3.7, column “Model B”), the estimates of F_{prol} and k_{cycle} indicated that approximately 30% of the cells in Prol continued the maturation process, while 70% went into the additional circulation as quiescent cells. In this circulation, the mean transition time was 32.5 h (= 3/k_{cycle}). The parameter estimate of ftr in Model C (Table 3.7, column “Model C”) expressed that the proliferation in the proliferating cell compartment was approximately 3.7 times faster than for the cells in the stem cell compartment.

Interindividual variability on the MMT was negligible in the investigated PK/PD models, due to insufficient decrease in the OFV (< 10%), low estimates (coefficient of variation < 10%) and high η-shrinkage (> 50%). Interindividual variability on SL was estimated approximately in the same range (43.8 – 47.1 L/µmol) for all models, but for Model B, where the estimate was approximately twice as high. The residual variability for all models investigated during optimisation was significantly higher, than for the original model (increase of ≥ 63.0%). The highest residual variability was observed for the re-estimation using the gold standard structural model (increase of 90.8%). The residual variability for Model A – C was approximately in the same range (51.5% – 55.1%), with the lowest value observed for Model C.

For all models investigated during model optimisation, η-shrinkage was moderate for SL (21.6% – 25.1%). However, for $Circ(t_0)$, η-shrinkage was higher (37.5% – 42.4%). ε-shrinkage was low (≤ 12.7%) for all investigated models.

Parameter precision was high (RSE < 20%) for most of the parameters, but for two parameters in Model B (SL and k_{cycle}, RSE ≤ 26.8%).

Table 3.7: PD parameter estimates of the original PK/PD model in comparison to the re-estimation and the different model structures (Model A – C) (modified from [140])**.**

Parameter	***Parameter estimate (RSE, %) [shrinkage, %]***				
	Gold standard (original) [138]*****	***Gold standard (re-estimated)***	***Model A***	***Model B***	***Model C***
AIC	2524.839	530.682	276.340	323.703	174.577
Condition number	n.a.	11.5	26.4	128	21.3
Fixed-effects parameters					
MMT [h]	141	128 (2.03)	128 (2.04)	117 (4.80)	145 (2.65)
SL [L/µmol]	2.6	4.48 (4.55)	4.35 (4.84)	173 (26.8)	13.1 (4.56)
γ	0.2	0.231 (6.79)	0.244 (7.54)	0.615 (9.28)	0.257 (5.53)
frB	n.a.	n.a.	0.453 (4.68)	n.a.	n.a.
k_{depl} [h^{-2}]	n.a.	n.a.	$9.04 \cdot 10^{-5}$ (17.9)	n.a.	n.a.
F_{prol}	n.a.	n.a.	n.a.	0.315 (13.4)	n.a.
k_{cycle} [h^{-1}]	n.a.	n.a.	n.a.	0.0924 (26.1)	n.a.
ftr	n.a.	n.a.	n.a.	n.a.	0.787 (2.76)
Interindividual variability parameters					
MMT; CV, %	27.0 [35.7]	n.a.	n.a.	n.a.	n.a.
SL; CV, %	44.9 [-5.31]	43.8 (8.23) [25.1]	47.1 (7.57) [21.9]	97.0 (12.7) [22.7]	44.8 (6.54) [21.6]
$Circ(t_0)$******; CV, %	31.6 [-12.8]	60.3 (3.27) [37.7]	53.9 (3.53) [41.7]	55.1 (3.38) [37.5]	51.5 (3.61) [42.4]
Residual variability parameters					
Exponential model******; CV, %	31.6 [-52.5]	60.3 (3.27) [12.7]	53.9 (3.53) [6.80]	55.1 (3.38) [7.68]	51.5 (3.61) [6.92]

CV, %: coefficient of variation; RSE, %: relative standard error; AIC: Akaike information criterion, n.a.: not applicable.
For explanation of Model A – C, see section 2.4.2.1.
MMT: mean maturation time; SL: slope factor of paclitaxel; γ: exponent of feedback function; frB: fraction of total baseline of proliferating cells not affected by depletion; k_{depl}: depletion rate constant of second drug effect; F_{prol}: fraction of proliferating cells entering maturation chain; k_{cycle}: circulation rate constant within quiescent cell cycle; ftr: fraction of input in proliferating cell compartment via replication; $Circ(t_0)$: concentration of circulating neutrophils at time t = 0.
* Parameter estimates from literature; AIC and shrinkage determined in the external model evaluation.
** Baseline method B2 was applied for all models. Thus, interindividual variability of baseline neutrophil concentration (deviation from the individual measured baseline) was estimated together with the residual variability as a single parameter.

The prediction-corrected visual predictive check (pcVPC) for the re-estimated gold standard structural model showed that the prediction was significantly improved compared to the original model. However, only in cycle 1, the day 15 ± 2 neutrophil concentrations were well predicted by the re-estimated model. Later, the cumulative neutropenia pattern was not described by this model structure, leading to a worsening of the overprediction over time. On the contrary, for

Model A – C an improvement of the prediction was observed compared to the re-estimated gold standard model. All three models captured the decreasing pattern in the neutrophil concentrations over the treatment cycles. Nevertheless, Model B did not predict the neutrophil concentrations as good as Model A and C for which no considerable difference was observed.

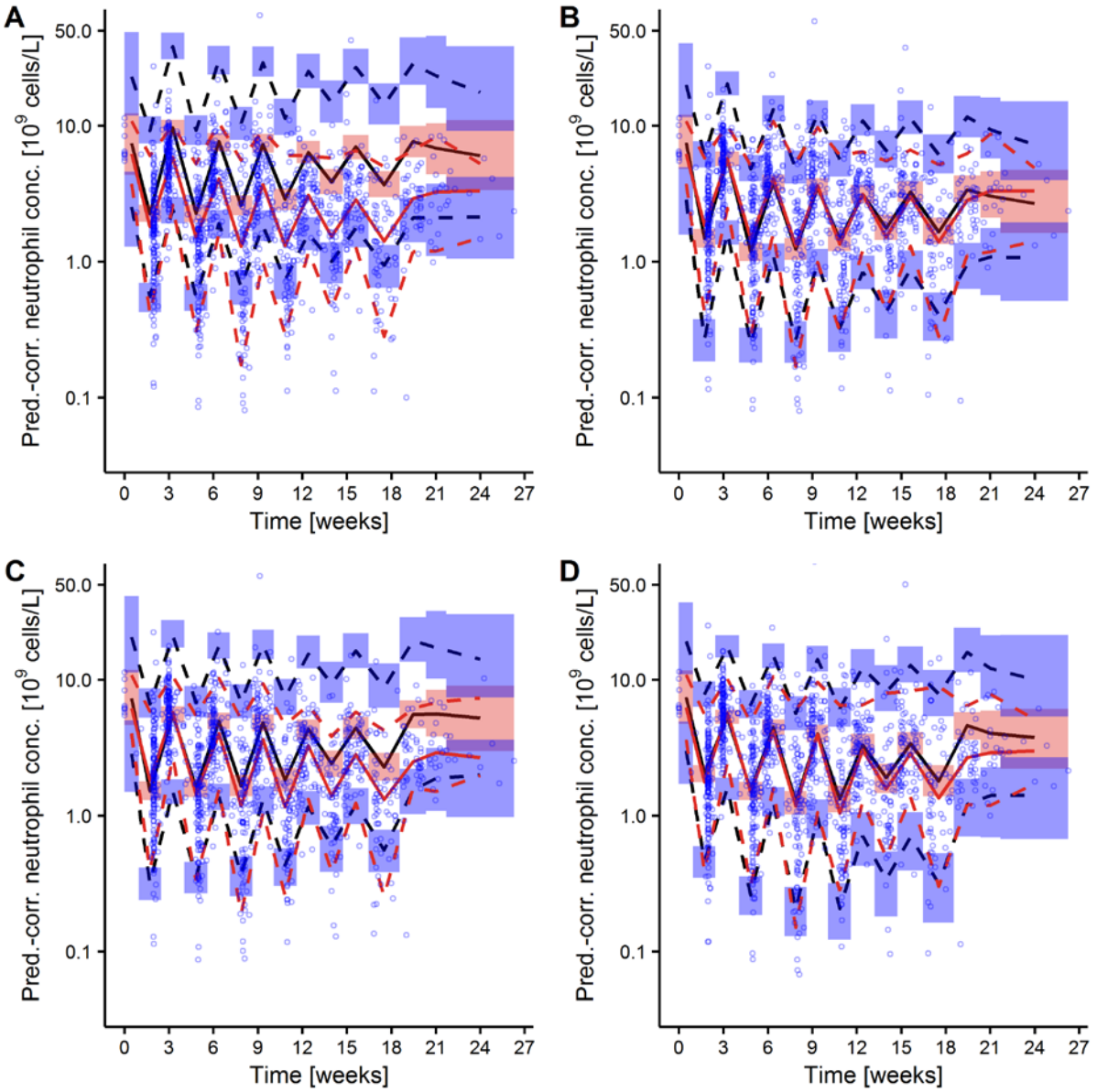

Figure 3.20: Prediction-corrected visual predictive checks of the different models investigated for PK/PD model optimisation (modified from [140])**.**
Panel A: Re-estimated gold standard model; Panel B: Model A; Panel C: Model B; Panel D: Model C. For explanation of Model A – C, see section 2.4.2.1.
Blue circles: observed neutrophil concentrations; red lines: median (solid), 5th, 95th percentiles (dashed) of observations; black lines: median (solid), 5th and 95th percentiles (dashed) of simulations; shaded areas: 90% confidence intervals of simulated percentiles.

Deterministic simulation for exploration of typical concentration-time profile

In the following step, a deterministic simulation was utilised to explore the typical neutrophil concentration-time profile of the re-estimated gold standard model and

Model A – C (Figure 3.21 and Figure 3.22). Further, the relative change in the peak and nadir value from cycle 1 to cycle 6 were compared for Model A – C (Table 3.8). The nadir was also used to grade neutropenia in this analysis. Using the gold standard model structure including the newly estimated parameters, a similar pattern for the neutrophil and proliferating cell concentrations over the cycles was observed (Figure 3.21, Panel A). Only the 1st cycle showed different behaviour for both cell types with a slightly deeper nadir and a higher peak concentration. The deeper nadir is probably caused by the higher neutrophil concentrations compared to time of the next dose administration and accordingly the reduced feedback, hence the proliferation is slower at the first dose administration, compared to the following doses. The deeper nadir then also causes the higher peak concentration, due to an increased feedback. The re-bound effect was distinct in this model, with peak values reaching 44% and 74% increase compared to the baseline value for the circulating and proliferating cells, respectively.

Model A (Figure 3.21, Panel B) showed an exponential decline in $BASE_{tot}(t)$, which was striving to $BASE_1$. After 6 weeks (≙ 3.14 times the half-life, resulting from the parameter estimate of k_{depl} (Table 3.7) and $T_{C>0.05}$ = 34.5 h) $BASE_{tot}(t)$ was approximately equal to $BASE_1$ (within ± 5% of $BASE_1$). Thus, no further visual differences in the prediction were observed from cycle 4 on. Model A further predicted approximately the same maximum neutrophil value for the 1st cycle (baseline) and the 2nd cycle. However, for the following cycles up to cycle 6, the relative change of the peak value was the highest compared to Model B and C (Table 3.8). The relative change in the nadir value on the other hand, was in-between the relative change of Model B and C, predicting grade 2 neutropenia for the 1st cycle and grade 3 for all following cycles.

Model B (Figure 3.21, Panel C) did not show a decrease in the concentration of proliferating and quiescent cells over the cycles. The concentrations in those compartments were generally higher due to the higher initial values for those compartments (20.6 and 14.1 cells/L, respectively, see section 2.4.2). However, the concentration in the circulating cell compartment was not able to recover within the cycle length of 3 weeks. Thus, the highest relative change in the peak value from for this model was observed between the 1st and the 2nd cycle (19.1%). For the following cycles, no considerable change in the peak and nadir values became obvious when comparing to cycle 2. Model B predicted the lowest degree of cumulative neutropenia for both parameters, relative change of the peak and nadir value (Table 3.8), predicting grade 3 neutropenia for all treatment cycles.

Model C (Figure 3.21, Panel D) predicted a strong decrease in the concentration in the stem cell compartment over the cycles, since they were not able to fully recover within the 3 weeks before the next dose administration. As a result, the peak concentration in proliferation compartment were low compare to the original model (Figure 3.21, Panel A) and did not

significantly exceed the baseline concentration. A slight increase in the peak proliferating cell concentration was observed from cycle 3 on, which is probably caused by an increased feedback due to the decreasing neutrophil concentrations. However, the generally low concentrations of proliferating cells finally lead to decreasing neutrophil concentration over the cycles. Model C predicted an intermediate change in the decrease for the peak value while the highest cumulative neutropenia effect for the nadir value was observed (Table 3.8), i.e. grade 2 neutropenia in the 1st cycle, grade 3 in the 2nd cycle and even grade 4 in cycle 5 and 6.

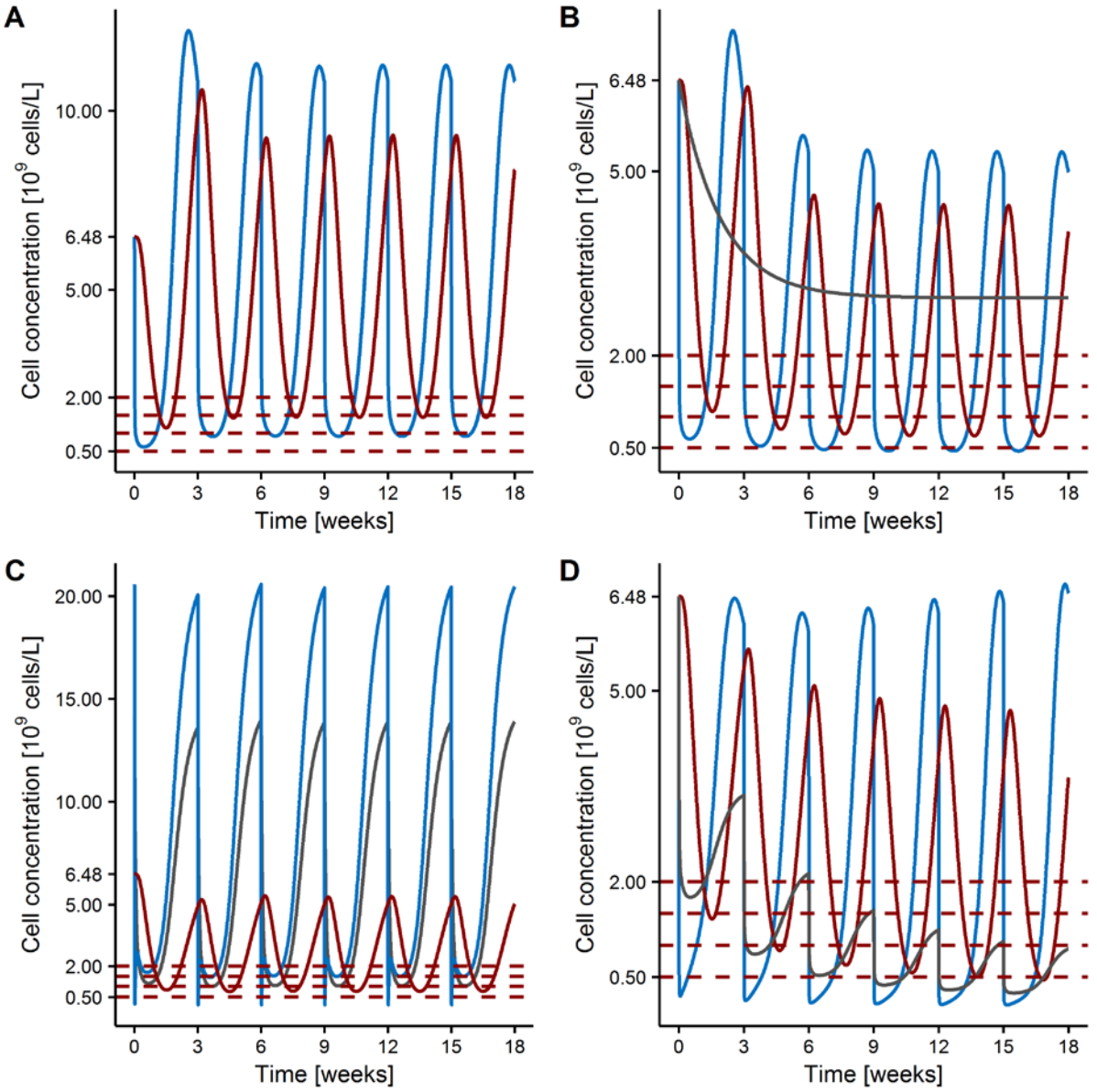

Figure 3.21: Deterministic simulation over 6 treatment cycles of different cell types of models evaluated during model optimisation.
Deterministic simulation of a typical patient (sex: male, age: 56 years, BILI: 7 µmol/L, BSA: 1.8 m², baseline neutrophil concentration: 6.48 • 10^9 cells/L) receiving 3-weekly paclitaxel (185 mg/m² in 3 h infusion) for 6 cycles.
Panel A: re-estimated gold standard model; Panel B: Model A; Panel C: Model B (due to the different initial conditions the baseline value of the proliferating cells and the cells in the 1st quiescent compartment was 14.1 • 10 and 20.6 • 10^9 cells/L, respectively); Panel D: Model C.
For explanation of Model A – C, see section 2.4.2.1.
Red dashed lines: thresholds for grading neutropenia from grade 0 to 4; red solid line: neutrophil concentration; blue line: concentration of proliferating cells; grey line in Panel B: total baseline concentration; grey line in Panel C: concentration of cells in the 1st quiescent cell compartment (Q1); grey line in Panel D: concentration of stem cells.

Table 3.8 Relative change in peak and nadir value from cycle 1 to cycle 6 for Model A – C determined by deterministic simulation.

Parameter	*Model A*	*Model B*	*Model C*
Relative change in peak value, %	31.4	7.65	27.6
Relative change in nadir value, %	36.5	17.0	67.8

Extrapolating the deterministic simulation for Model A – C beyond the end of the 6th cycle (Figure 3.22), predictions of the neutrophil concentrations strongly varied. All models, except of Model A when assuming E_{drug2} over the whole observation period, predicted that baseline would be reached at some point after the end of therapy. However, the time until full recovery was predicted differently, with the longest time for Model C (approximately half a year after the last drug administration). For Model A, two assumptions were investigated, either an immediate end of E_{drug2} after the end of the last cycle, or continuation of E_{drug2} beyond the last cycle. The assumption made influenced the prediction of the recovery of the neutrophil concentration after end of therapy substantially: While the first assumption, end of E_{drug2} after the last cycle, led to a fast recovery back to baseline, the second assumption predicted that the patient would only recover to the reduced baseline $BASE_{tot}(t)$, which approximated $BASE_1$. Model B, the model with the highest parameter estimate for the γ exponent of the feedback function, showed almost no oscillation. This might be caused by the model structure and the reduced proportion of cells entering the maturation chain. Due to the reduced oscillation in Model B, the neutrophil concentration recovered within approximately 5 weeks after the last dose.

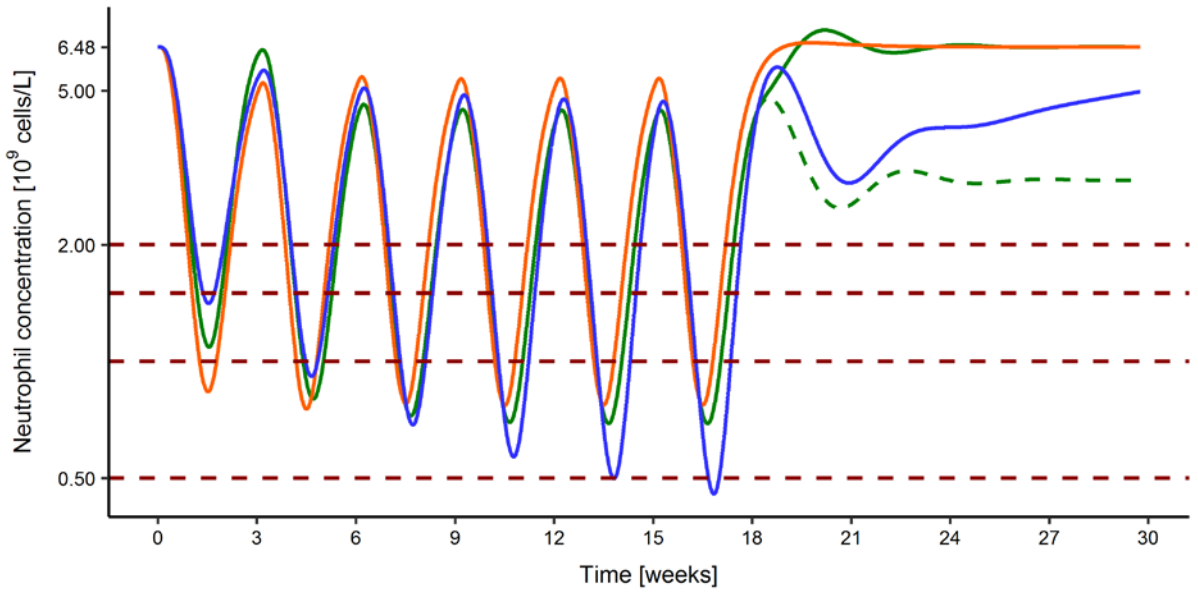

Figure 3.22: Deterministic simulation using Model A – C of a typical patient undergoing 6 cycles of paclitaxel therapy and extrapolation after end of treatment [140]**.**
Typical patient (sex: male, age: 56 years, BILI: 7 µmol/L, BSA: 1.8 m², baseline neutrophil concentration: 6.48 • 10^9 cells/L) receiving 3-weekly paclitaxel (185 mg/m² in 3 h infusion) for 6 cycles. Green: Model A; orange: Model B; blue: Model C; red dashed lines: thresholds for grading neutropenia from grade 0 to 4.
For explanation of Model A – C, see section 2.4.2.1.

3.3.2.2 Differentiation of drug effects between paclitaxel and the platinum-based drugs

Model C was further optimised by implementing the drug effects of carboplatin and cisplatin. Two approaches were investigated: assuming an additive effect and the general PD interaction model. For both modelling approaches the AIC dropped compared to Model C which was not differentiating between paclitaxel and the platinum-based drugs (Table 3.9). The condition number stayed below 200, indicating that the additional complexity caused no overparameterisation. The system-related parameters MMT and γ were estimated to be within the 95% confidence interval of Model C but ftr was outside, indicating that the system-related parameters are comparable to the gold standard model.

The estimate of the paclitaxel slope factor (SL) dropped significantly for the additive model compared to Model C. The slope factor of cisplatin (SL_{cis}) was estimated to be higher than for carboplatin. Correcting the slope factor for the plasma concentration of the respective drug, i.e. calculating the drug effect for each of the drugs over time (Figure 3.23), the drug effect of cisplatin was still estimated to be higher than the one for carboplatin (AUC_{0-24h}: 92.4 and 57.6, respectively, see Eq. 2.52). The drug effect of cisplatin was even higher than the one for paclitaxel (AUC_{0-24h}: 83.2).

For the general PD interaction model, the slope factor of cisplatin was estimated even higher than for the additive effect model. The interaction term INT was estimated to be negative and therefore quantified a synergism of 56.3%.

The residual variability was comparable between Model C and the two drug combination models. Both models were estimated with high parameter precision. Nevertheless, estimation of the relative standard error in the general PD interaction model was not possible using the full $R^{-1}SR^{-1}$ matrix but only the cross-product gradient (S) matrix (see section 2.1.2.2). Hence, relative standard errors are not fully comparable between the models and might be underestimated for the general PD interaction model.

Table 3.9: Parameter estimations of structural Model C with and without accounting for the effect of the platinum-based drugs (modified from [140])**.**

Parameter	***Parameter estimate (RSE, %) [shrinkage, %]***		
	Model C	***Additive effect***	***General PD interaction model***
AIC	174.577	132.063	134.108
Condition number	21.3	113	6.91
Fixed-effects parameters			
MMT [h]	145 (2.65)	142 (2.94)	141 (1.57)
SL [L/µmol]	13.1 (4.56)	5.18 (26.1)	2.21 (fix)
γ	0.257 (5.53)	0.274 (5.11)	0.281 (3.22)
ftr	0.787 (2.76)	0.723 (2.03)	0.700 (0.363)
SL_{carbo} [L/mg]	n.a.	0.997 (16.9)	0.46 (fix)
SL_{cis} [L/mg]	n.a.	32.1 (20.4)	44.5 (6.74)
INT	n.a.	n.a.	-0.563 (0.922)
Interindividual variability parameters			
SL; CV, %	44.8 (6.54) [21.6]	68.0 (15.4) [37.0]	80.0 (15.2) [46.5]
SL_{carbo}; CV, %	n.a.	44.4 (15.5) [50.5]	40.4 (21.2) [45.6]
$Circ(t_0)$*; CV, %	51.5 (3.61) [42.4]	50.7 (3.71) [43.1]	50.7 (1.20) [43.1]
Residual variability parameters			
Exponential model*; CV, %	51.5 (3.61) [6.92]	50.7 (3.71) [6.92]	50.7 (1.20) [6.69]

CV, %: coefficient of variation; RSE, %: relative standard error; AIC: Akaike information criterion, PD: pharmacodynamic(s), n.a.: not applicable.
For explanation of Model C, see section 2.4.2.1; for additive effect and general PD interaction model see section 2.4.2.2.
MMT: mean maturation time; SL: slope factor of paclitaxel; γ: exponent of feedback function; ftr: fraction of input in proliferating cell compartment via replication; SL_{carbo}: slope factor of carboplatin; SL_{cis}: slope factor of cisplatin; INT: maximal interaction; $Circ(t_0)$: concentration of circulating neutrophils at time t = 0.
* Baseline method B2 was applied for all models. Thus, interindividual variability of baseline neutrophil concentration (deviation from the individual measured baseline) was estimated together with the residual variability as a single parameter.

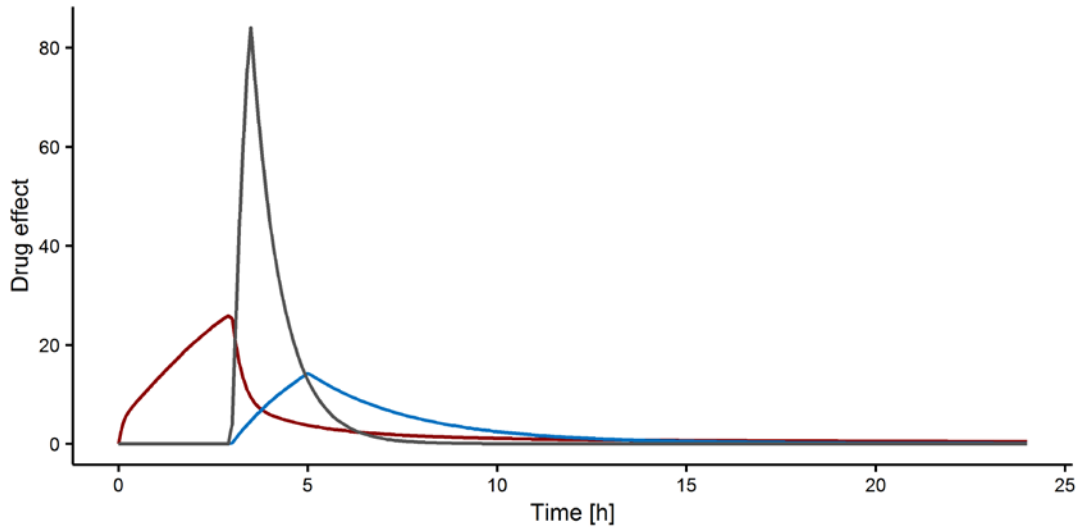

Figure 3.23: Deterministic simulation of drug effects as product of the respective drug concentration-time profile and the respective slope factor for the additive effect model.
Simulated patient: age: 56 years, bilirubin concentration: 7 µmol/L, weight: 70 kg, height: 176 cm, creatinine clearance: 103.1 mL/min, body surface area of 1.86 m².
Simulated dosing scenario: paclitaxel: single dose, 3 h infusion; 187.5 mg/m²; carboplatin: 2 h infusion started after end of paclitaxel infusion, dose based on Calvert formula to achieve an AUC of 6 mg • min/L; cisplatin: 1/2 h infusion started after end of paclitaxel infusion, 80 mg/m².
Red line: paclitaxel drug effect; blue line: carboplatin drug effect; grey line: cisplatin drug effect.
For explanation of additive effect model see section 2.4.2.2.

Visual predictive checks were performed for both models, the additive effect model and the general PD interaction model (Figure 3.24). No significant difference was found between the two models. A minor improvement of the prediction was seen for both models compared to Model C (Figure 3.20) in the median profile as well as for the 5th and 95th percentile.

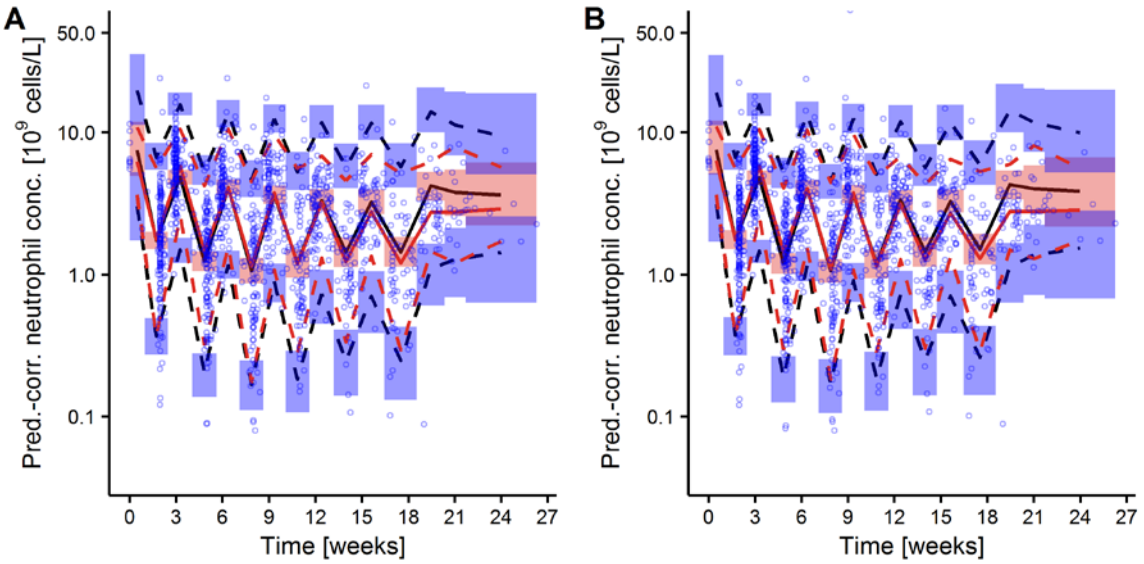

Figure 3.24: Prediction-corrected visual predictive checks of the additive effect model and the general PD interaction model (modified from [140])**.**
Blue circles: observed neutrophil concentrations; red lines: median (solid), 5th, 95th percentiles (dashed) of observations; black lines: median (solid), 5th and 95th percentiles (dashed) of simulations; shaded areas: 90% confidence intervals of simulated percentiles.
For explanation of the additive effect and general PD interaction model see section 2.4.2.2.

3.3.2.3 Covariate model development

Visual investigation of potential covariates (see Figure 10.2 and Figure 10.3, appendix) revealed a potentially clinically relevant trend only for previous therapy in general as well as for previous chemo- and radiotherapy. In general, trends (even if not considered to be potentially relevant) pointed into the same direction for both parameters (SL and SL_{carbo}). Further, these trends were more distinct for the slope factor of paclitaxel than for the slope factor of carboplatin.

Due to these results, previous chemo-/radiotherapy was investigated for their covariate effects on E_{drug} in addition to concomitant therapy, supportive G-CSF treatment and comedication. Only supportive G-CSF therapy as additive effect on E_{drug} (Eq. 2.55) significantly decreased the OFV (-22.5). This covariate effect was estimated to be -0.512 (see Table 3.10), which indicates that the drug effect is decreased by G-CSF therapy (Eq. 3.1). If no effect of paclitaxel and cisplatin/carboplatin was present, k_{prol} and k_{stem} were increased by approximately 50% compared to patients without G-CSF therapy, since these proliferation rate constants were multiplied with $(1 - E_{drug})$. The other parameter estimates did not change significantly. No relevant improvement due to this covariate was found by analysing the resulting pcVPC (Figure 3.25).

$$E_{drug} = SL_{Platin} \cdot C_{Platin}(t) + SL_{PTX} \cdot C_{PTX}(t) - 0.512^{g}$$

$$\text{with: } g = \begin{cases} g = 0 & if\ no\ G\text{-}CSF\ effect \\ g = 1 & during\ G\text{-}CSF\ effect \end{cases} \qquad \textbf{Eq. 3.1}$$

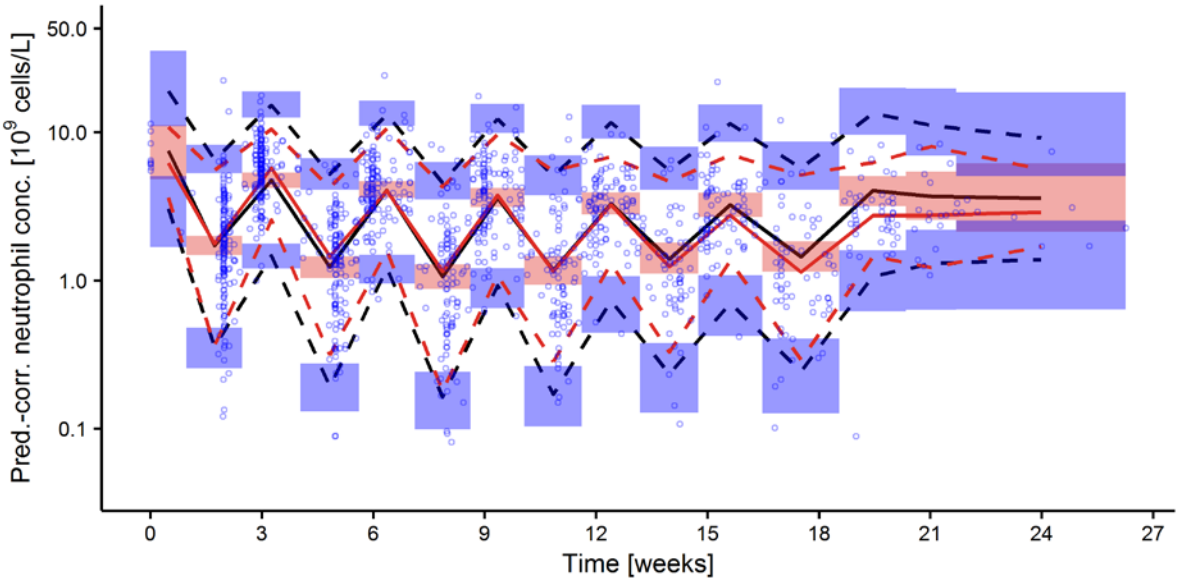

Figure 3.25: Prediction-corrected visual predictive of the full neutropenia model including combination therapy with cisplatin/carboplatin and G-CSF comedication [140]**.**
Blue circles: observed neutrophil concentrations; red lines: median (solid), 5th, 95th percentiles (dashed) of observations; black lines: median (solid), 5th and 95th percentiles (dashed) of simulations; shaded areas: 90% confidence intervals of simulated percentiles.

Table 3.10: Parameter estimates of the neutropenia model including combination therapy with carboplatin/cisplatin without and with covariate effect.

Parameter	***Parameter estimate (RSE, %) [shrinkage, %]***	
	Additive combination effect	***Full model***
OFV	115.063	92.546
Condition number	113	130
Fixed-effects parameters		
MMT [h]	142 (2.94)	140 (3.95)
SL [L/µmol]	5.18 (26.1)	5.16 (26.9)
γ	0.274 (5.11)	0.270 (5.44)
ftr	0.723 (2.03)	0.722 (2.06)
SL_{carbo} [L/mg]	0.997 (16.9)	1.01 (17.1)
SL_{cis} [L/mg]	32.1 (20.4)	32.1 (20.4)
G-CSF on $E_{drug}(t)$*	n.a.	-0.512 (26.0)
Interindividual variability parameters		
SL; CV, %	68.0 (15.4) [37.0]	67.5 (15.4) [37.0]
SL_{carbo}; CV, %	44.4 (15.5) [50.5]	43.8 (15.4) [49.9]
$Circ(t_0)$*; CV, %	50.7 (3.71) [43.1]	50.2 (3.6) [42.6]
Residual variability parameters		
Exponential model**; CV, %	50.7 (3.71) [6.92]	50.2 (3.63) [7.01]

CV, %: coefficient of variation; RSE, %: relative standard error; AIC: Akaike information criterion, n.a.: not applicable.
MMT: mean maturation time; SL: slope factor of paclitaxel; γ: exponent of feedback function; ftr: fraction of input in proliferating cell compartment via replication; SL_{carbo}: slope factor of carboplatin; SL_{cis}: slope factor of cisplatin; G-CSF: granulocyte colony-stimulating factor; $E_{drug}(t)$: drug effect at time t inhibiting proliferation rate constant of cells in proliferating cell compartment; $Circ(t_0)$: concentration of circulating neutrophils at time t = 0.
* Additive effect of G-CSF on $E_{drug}(t)$ (Eq. 2.55)
** Baseline method B2 was applied for all models. Thus, interindividual variability of baseline neutrophil concentration (deviation from the individual measured baseline) was estimated together with the residual variability as a single parameter.

3.3.3 PK/PD model evaluation of the developed model using the conventional CEPAC-TDM study arm

The prediction-corrected visual predictive check showed that the PK/PD model developed on the Arm B study data, describing neutropenia as a result of an additive effect from paclitaxel and cisplatin/carboplatin concentration, was able to well predict the neutrophil concentrations

measured in study Arm A (Figure 3.26). Nevertheless, the 5th percentile was slightly underestimated.

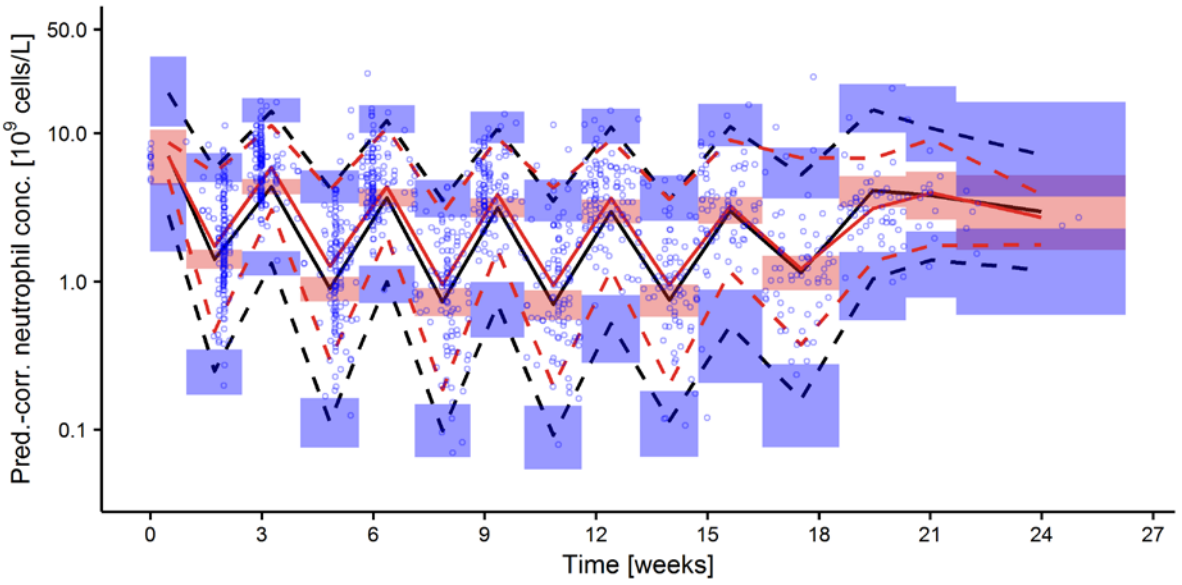

Figure 3.26: Prediction-corrected visual predictive check for study Arm A using the additive effect PK/PD model including granulocyte colony-stimulating factor as covariate.
Blue circles: observed neutrophil concentrations; red lines: median (solid), 5th, 95th percentiles (dashed) of observations; black lines: median (solid), 5th and 95th percentiles (dashed) of simulations; shaded areas: 90% confidence intervals of simulated percentiles.

3.3.4 Impact of the optimised PK/PD model on the CEPAC-TDM study results

Time to nadir was analysed for all patients and cycles in both study arms and compared to the sampling time used as surrogate for the nadir: the sample on day 15 ± 2 (Figure 3.27). For most occasions (84.6%), sampling took place between day 15 and day 17 after dose administration. However, a large variability can be seen, with planned day 15 ± 2 samples that were actually taken on day 6 or 22 (minimum and maximum, respectively) of the study cycle. Compared to the expected nadir based on the model prediction, the developed PK/PD model predicted the nadir to be approximately on day 11 (median: 11.2 days).

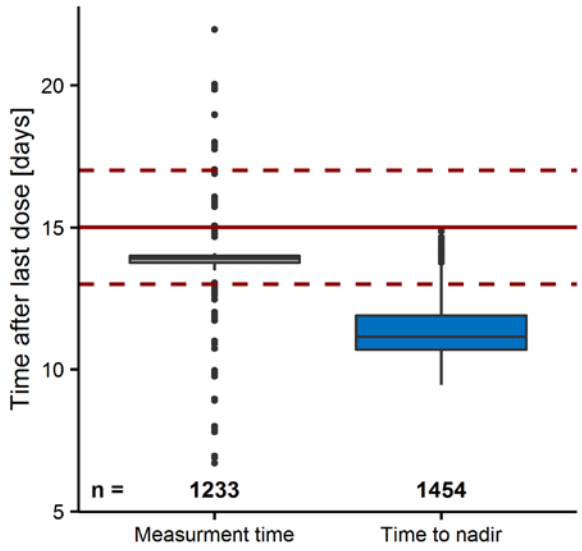

Figure 3.27: Comparison of the actual sampling time in the CEPAC-TDM study for the neutrophil concentration (scheduled on day 15 ± 2) compared to the model estimated time to nadir.
Boxes: interquartile range (IQR), including median; whiskers: range from box hinge to highest/lowest value within 1.5•IQR; points: data beyond whiskers; solid red line: planned sampling time (day 15); dashed red lines: range of the planned sampling time (day 15 ± 2).
n: number of observations.

Sampling on day 15 ± 2, which is after the nadir, but was used to grade neutropenia, underestimated the severity neutropenia for both study arms when comparing to the model predicted nadir (Figure 3.28). Further, the variability in the neutrophil concentrations was overpredicted during the study. The nadir concentrations predicted similar percentage of patients having grade 3 or 4 neutropenia for Arm A and B, respectively, in the different treatment cycles. The percentage of patients suffering from grade 4 neutropenia on the other hand was lower for Arm B for all cycles but cycle 1, for the measured neutrophil concentrations as well as for the predicted nadir concentrations.

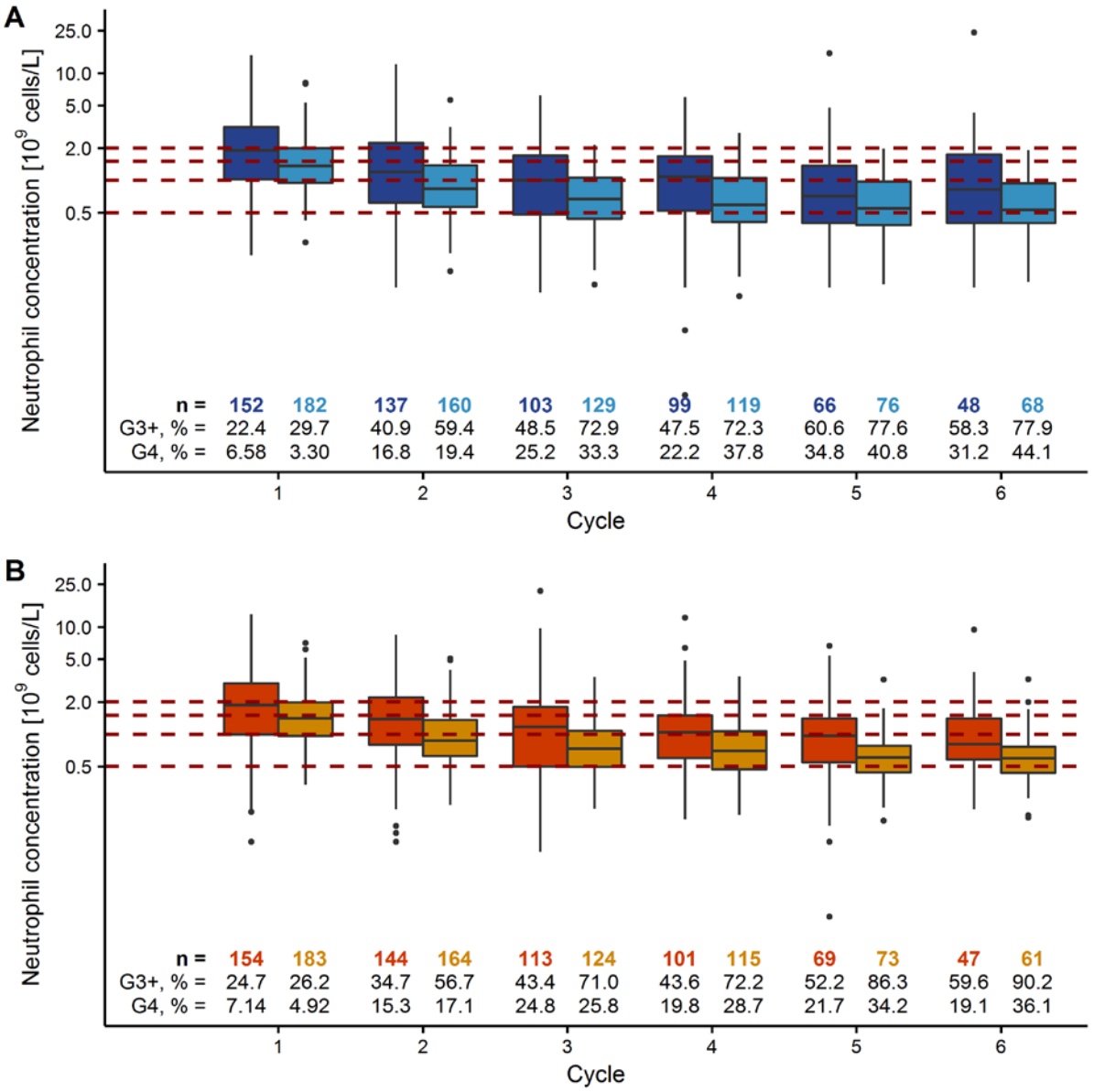

Figure 3.28: Neutrophil measurements of day 15 ± 2 compared to the model predicted nadir using the optimised PK/PD model.
Panel A: study Arm A; Panel B: study Arm B.
Boxes: interquartile range (IQR), including median; whiskers: range from box hinge to highest/lowest value within 1.5•IQR; points: data beyond whiskers; red dashed lines: thresholds for grading neutropenia from grade 0 to 4.
Colours: dark blue and red boxes: measured neutrophil on day 15 ± 2 concentration of study Arm A and B, respectively; light blue and orange boxes: nadir concentrations estimated by the optimised PK/PD model.
n: number of observations in the respective study arm and cycle; G3+, %: percentage of patients with grade ≥ 3 neutropenia; G4, %: percentage of patients with grade 4 neutropenia.

3.4 Project 3: Efficacy modelling: Tumour size and overall survival

3.4.1 Tumour size modelling

3.4.1.1 Development of structural tumour growth inhibition model

The analysis excluded measurements determined more than 30 weeks after the first dose and measurements that were potentially influenced by other therapies than paclitaxel and carboplatin. Figure 3.29 shows that most of the tumour measurements (56.7% of the excluded measurements) were excluded because they were from cisplatin patients that were not analysed due to the results of Project 2 (unrealistically high influence of cisplatin resulting probably from the low patient number treated with cisplatin). In addition, measurements after 30 weeks since first dose were excluded, since the main purpose of the tumour growth inhibition model was to predicted individual tumour sizes at week 8 to inform the overall survival model and drop-out during study treatment (up to 18 weeks). Time points later than 30 weeks did not improve prediction for these early measurements, but increased interindividual variability. Patients with additional anticancer treatment besides the study medication were excluded as soon as the additional treatment was administered. Of the remaining patients, 119 and 132 patients in Arm A and B, respectively, had evaluable tumour size measurements after baseline. For the other 29 and 21 patients in Arm A and B, respectively, only the baseline measurement was evaluable.

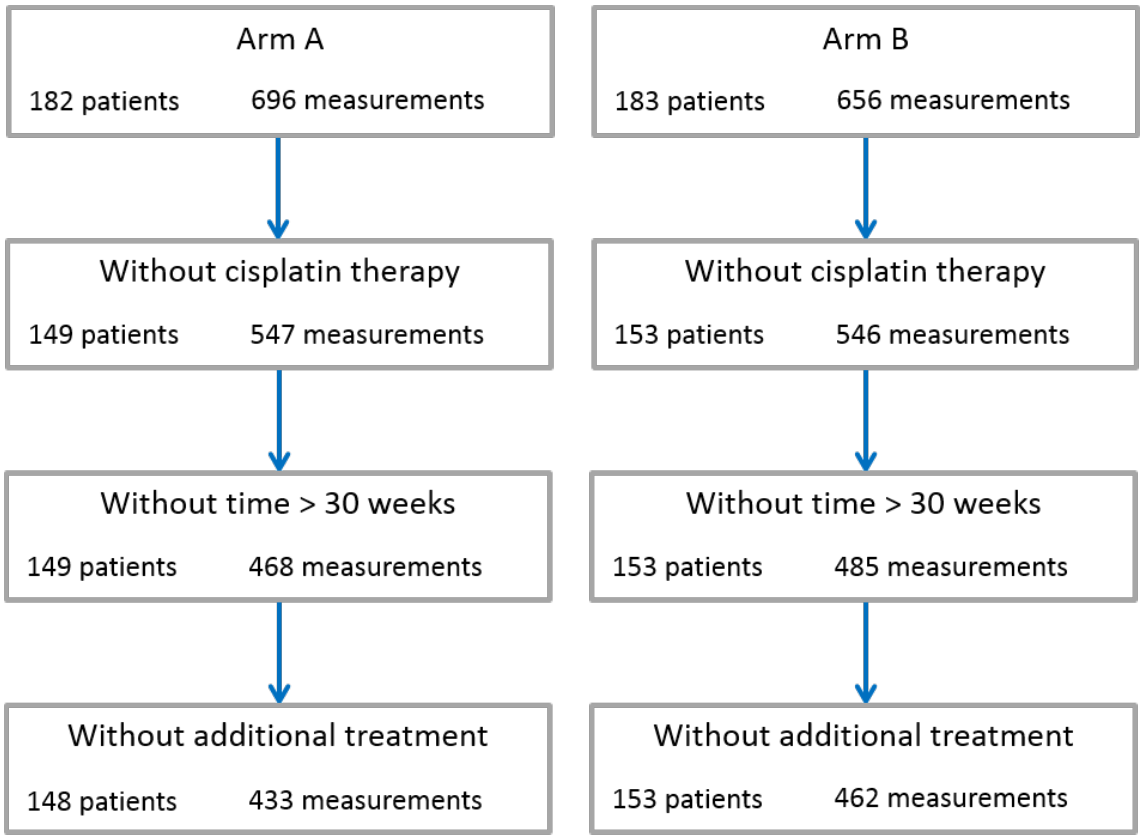

Figure 3.29: Flowchart of data excluded for tumour growth inhibition analysis.
Data was excluded stepwise for different reasons. Boxes show the remaining patients/tumour size measurements after each step. The reasons were cisplatin combination therapy (only carboplatin combination therapy was allowed), time after first dose > 30 weeks and additional treatment with chemo-/radiotherapy or surgery as soon as this additional therapy started.
Left panel: study Arm A; right panel: study Arm B.

First, a base model considering the paclitaxel effect alone was developed. A linear tumour growth model in combination with an exposure-driven drug effect, but without a resistance mechanism, was selected (Figure 2.8). An exponential or generalised logistic tumour growth model did not or not sufficiently improve the model prediction based on the OFV, Table 3.11. The incorporation of a resistance term did improve the model prediction but lead to inacceptable parameter precision (RSE > 30%).

Table 3.11: Development of structural tumour growth inhibition model.

Net growth	*Drug-induced decay*	*ΔOFV*	*Condition number*	*Max RSE,%*
Linear	Exposure-driven		12.2	25.9 for k_g
Exponential	Exposure-driven	9.499	35.4	22.6 for k_g
Generalised logistic	Exposure-driven	-5.728	35.1	28.0 for k_g
Linear	Exposure-driven with resistance	-31.724	27.7	50.6 for k_g

ΔOFV: difference in objective function value from the model with linear net growth and exposure-driven drug-induced decay; Max RSE, %: maximum relative standard error of fixed-effects parameters; k_g: tumour growth rate constant.

Parameter estimation with the base model including the paclitaxel effect alone was sufficiently precise (< 30%) (Table 3.12, column "base model paclitaxel"). The zero-order growth rate constant k_g was estimated to be 9.81 mm/week. If the drug-induced decay exceeds the growth rate, the tumour shrinks: Based on the parameter estimates of this tumour growth inhibition model and assuming a tumour size of 7.90 cm (median tumour size at baseline in the CEPAC-TDM study), tumour shrinkage appeared at paclitaxel concentrations > $7.32 \cdot 10^{-3}$ µmol/L. Interindividual variability was high (> 75%) for both structural parameters, k_g and β_{PTX}, combined with considerable η-shrinkage (> 30%). Residual variability on the other hand was low (< 20%). The pcVPC showed a good prediction of the median profile, but the 95th percentile was overpredicted (Figure 3.30, Panel A).

Table 3.12: Parameter estimates of key models describing tumour growth inhibition.

Parameter	***Parameter estimate (RSE, %) [shrinkage, %]***		
	Base model paclitaxel	***Base model combination therapy***	***Covariate model***
OFV	-427.498	-429.739	-454.174
Condition number	12.2	14.0	26.7
Fixed-effects parameters			
k_g [cm/h]	5.84 • 10^{-4} (25.9)	6.44 • 10^{-4} (25.8)	6.26 • 10^{-4} (22.0)
β_{PTX} [L/µmol/h] *	1.01 • 10^{-2} (16.0)	4.96 • 10^{-3} (15.8)	4.25 • 10^{-3} (17.1)**
r_{effect}	n.a.	0.137 (fix)	0.137 (fix)
Tumour histology (unknown) on β_{PTX}	n.a.	n.a.	1.10 (68.9)
Tumour histology (Squamous-cell carcinoma) on β_{PTX}	n.a.	n.a.	1.32 (62.9)
Age on k_g	n.a.	n.a.	-5.06 • 10^{-2} (30.2)
Interindividual variability parameters			
k_g; CV, %	78.6 (29.5) [55.3]	78.3 (27.8) [48.3]	63.2 (30.6) [53.1]
β_{PTX}; CV, %	83.7 (10.8) [37.2]	164 (11.4) [49.1]	126 (16.8) [43.7]
$TS(t_0)$*; CV, %	16.9 (9.82) [57.3]	17.0 (10.1) [59.0]	17.0 (9.23) [55.1]
Residual variability parameters			
Exponential model**; CV, %	16.9 (9.82) [32.5]	17 (10.1) [34.2]	17.0 (9.23) [30.1]

CV, %: coefficient of variation; RSE, %: relative standard error; AIC: Akaike information criterion, n.a.: not applicable.
OFV: objective function value; k_g: tumour growth rate constant; β_{PTX}: efficacy parameter of paclitaxel; r_{effect}: ratio of efficacy parameters for carboplatin and paclitaxel; $TS(t_0)$: tumour size at time t = 0
* For reference group with adenocarcinoma.
** Baseline method B2 was applied for all models. Thus, the interindividual variability of the baseline tumour size (deviation from the individual measured baseline) was estimated together with the residual variability as a single parameter.

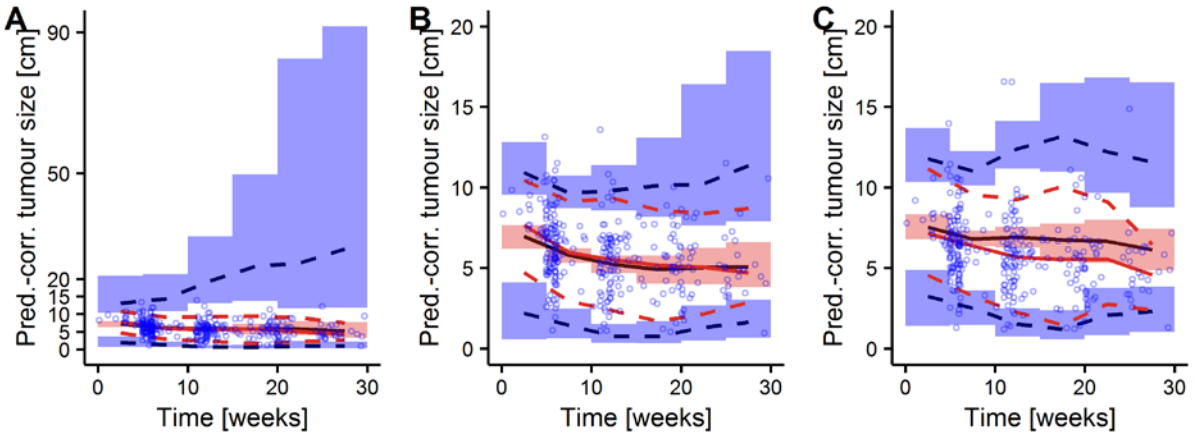

Figure 3.30: Prediction-corrected visual predictive check of tumour growth inhibition models for patients in study Arm B.
Panel A: base model with paclitaxel drug effect alone; Panel B: base model with paclitaxel and carboplatin combination therapy; Panel C: covariate model including tumour histology and age as covariates.
Blue circles: observed tumour size; red lines: median (solid), 5th, 95th percentiles (dashed) of observations; black lines: median (solid), 5th and 95th percentiles (dashed) of simulations; shaded areas: 90% confidence intervals of simulated percentiles.

3.4.1.2 Differentiation between drug effect of paclitaxel and carboplatin

In a next step, differentiation between the drug effects of paclitaxel and carboplatin was investigated. Estimation of two independent drug effect parameters was not possible, but the effect ratio between these two parameters was fixed based on *in vivo* mouse studies. This parameter, r_{effect}, was calculated to be 0.137, i.e. β_{carbo} was 86.3% lower than β_{PTX} (for the units as using in the modelling process). Comparing β_{PTX} and β_{carbo} on the same unit (L/µmol/h), β_{carbo} was 63.1% lower than β_{PTX}. The parameter r_{effect} was fixed for the estimation of the remaining parameters, which resulted in a minor improvement in OFV (ΔOFV = 2.26) with comparable parameter estimates and parameter precision (Table 3.12, column "base model combination therapy"). Only the interindividual variability of β_{PTX} was considerably higher (increase of 97.6%). Since no interindividual variability was included on β_{Carbo}, this variability was compensated by the interindividual variability on β_{PTX}. Further, the implementation of the combination therapy improved the pcVPC, especially for the 95th percentile (Figure 3.30, Panel B).

3.4.1.3 Covariate model development

Finally, in a covariate analysis using the stepwise covariate model-building procedure, tumour histology and age were significant covariates on β_{PTX} and k_g, respectively, with an overall decrease in OFV of ΔOFV = -24.4 (Table 3.12, column "covariate model"). None of the other investigated covariate relations, such as smoking status (see section 2.5.1.3) were significant and were thus not included in the model. Parameter imprecision of the covariate effects of the tumour growth was high (> 60%). More precisely, the 95% confidence interval derived from the

relative standard error assuming normal distribution included 0, which would result in no influence of the covariate. Thus, to confirm the significance of the covariate effect, the confidence intervals were determined by log-likelihood profiling. This analysis showed that the confidence intervals were not normally distributed and narrower, then assumed from the relative standard errors (Figure 3.31). The confidence intervals determined by log-likelihood profiling did not include 0 anymore.

Moreover, both covariates were considered as clinically relevance, defined as change ≥ 30% in the group parameter $\theta_{k,g}$ for a extreme covariate value compared to the typical one θ_k [176]. With each additional year of age, k_g decreases by 5.06%. This means that over the age range of 51 to 74 years (5th and 95th percentile of the population in Arm B) k_g varied between 54.5% (of the typical k_g (age of 65 years) at age 74 years) and 170% (at the age of 51 years). For patients with unknown tumour histology, β_{PTX} was increased by 110% and for patient with squamous-cell carcinoma by 132%.

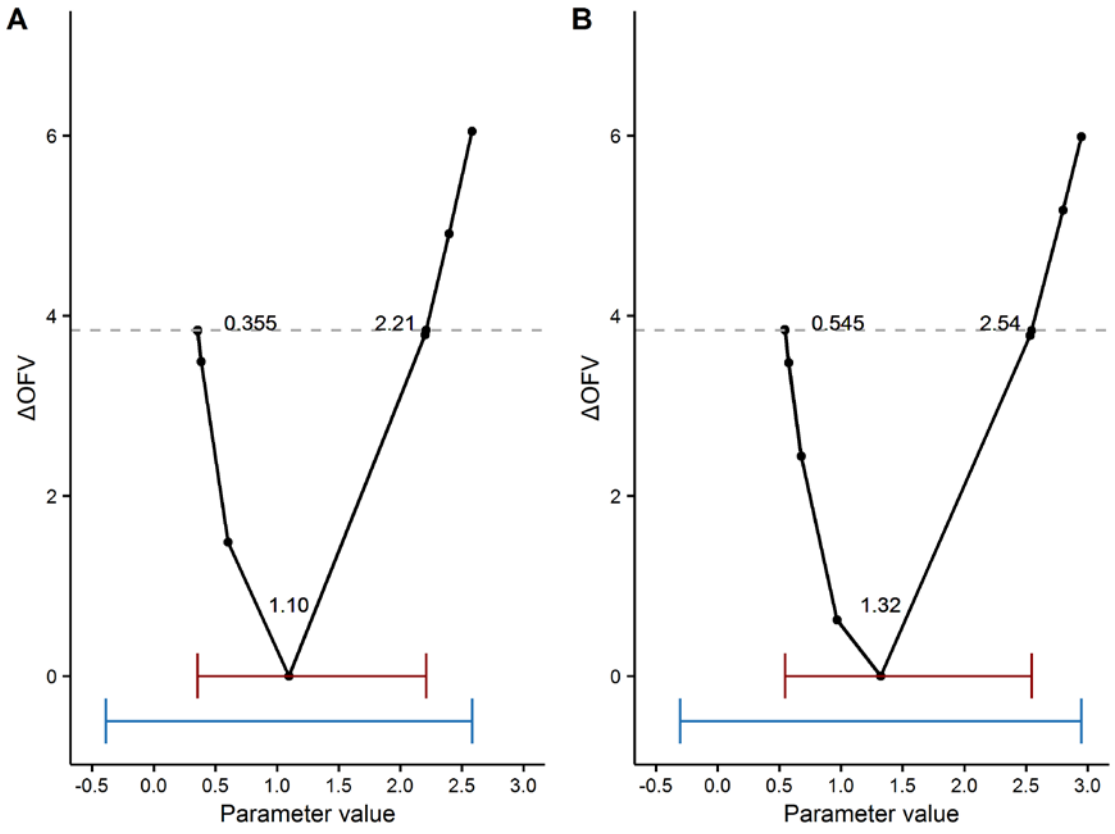

Figure 3.31 Log-likelihood profiling of the tumour histology covariate effect on the paclitaxel efficacy parameter β_{PTX}.
Panel A: covariate parameter for unknown tumour histology; Panel B: covariate parameter for squamous-cell carcinoma.
Black point: evaluated parameter values of β_{PTX}; numbers; β_{PTX} parameter value resulting in the lowest objective function value (OFV) and β_{PTX} parameter values leading to an increase in OFV of 3.84, determining the 95% confidence interval; red line: confidence interval determined by log-likelihood profiling; blue line: confidence interval derived from the relative standard error assuming normal distribution.

While the prediction, in terms of OFV, was improved by implementing age and tumour histology as covariates, the pcVPC showed an overprediction of the median profile as well as for the 95th percentile (Figure 3.30, Panel C). Nevertheless, the prediction of the 5th percentile improved. Stratification on tumour histology (Figure 3.32, Panel A - C) revealed, that tumour size for patients with unknown tumour histology or squamous-cell carcinoma were better predicted than tumour size for patients with adenocarcinoma (reference group). Nevertheless, observed median tumour size at week 8 was within the 90% confidence interval of the model prediction for each tumour histology group. Evaluating the tumour size prediction over age (Figure 3.32, Panel D), overprediction was observed over the whole age range but for patients of approximately 55 years. However, observed median tumour size for all but one age group were within the 90% confidence interval as well. Hence, the model fulfilled the purpose of the modelling approach: reliable prediction of tumour size at week 8 which can be used as predictor covariate of overall survival.

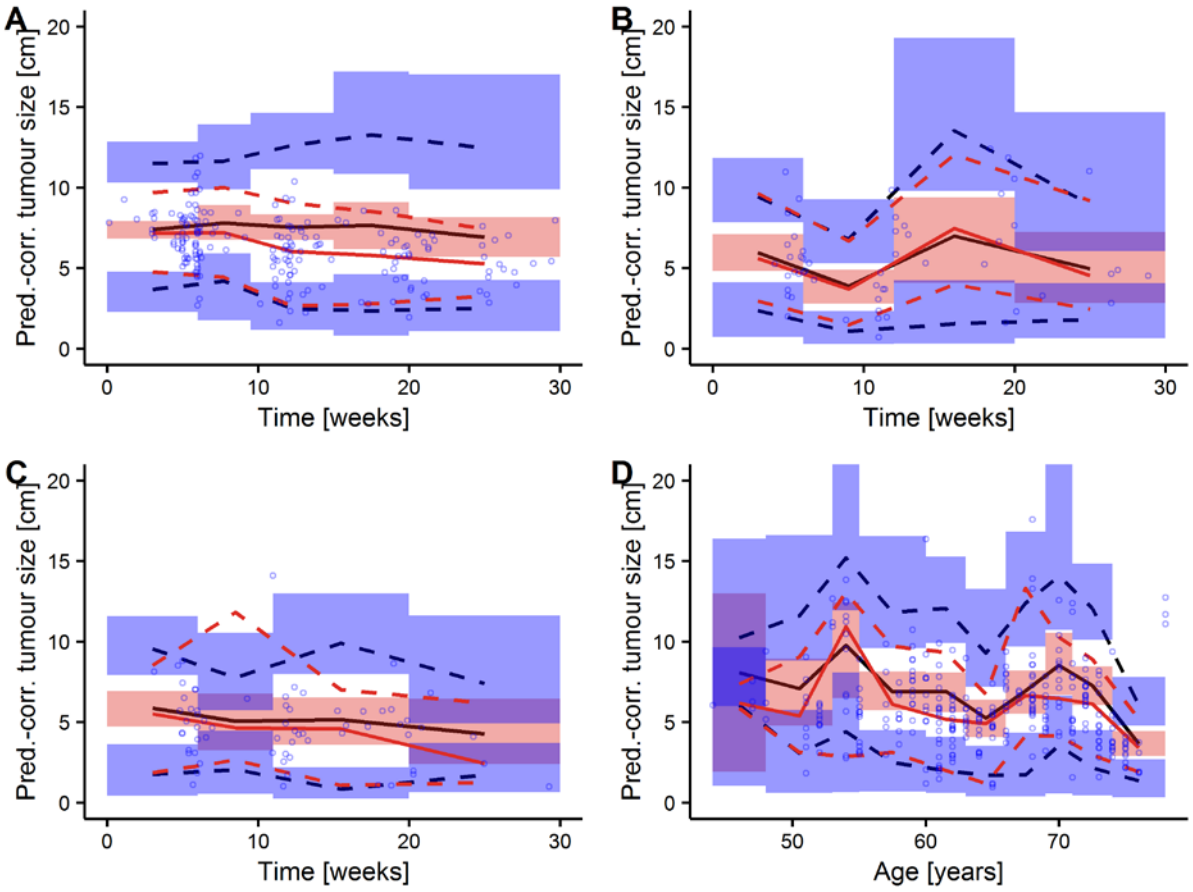

Figure 3.32: Prediction-corrected visual predictive check of the covariate tumour growth inhibition models for patients in study Arm B stratified by covariates.
Panel A: reference group adenocarcinoma (n = 84 patients); Panel B: unknown tumour histology (n = 22 patients); Panel C: squamous-cell carcinoma (n = 26 patients); Panel D: evaluation over age.
Blue circles: observed tumour size; red lines: median (solid), 5th, 95th percentiles (dashed) of observations; black lines: median (solid), 5th and 95th percentiles (dashed) of simulations; shaded areas: 90% confidence intervals of simulated percentiles.

3.4.1.4 Model evaluation using Arm A study data

Using the data splitting method, the model prediction of the covariate tumour growth inhibition model was compared to observed tumour size measurements of patients in study Arm A. Without stratification, the predicted and observed data were in good agreement with each other (Figure 3.33, Panel A). Furthermore, a good predictive performance was observed over the whole age range and for patients with adenocarcinoma (Figure 3.33, Panel B and C). It was further observed that the relation between prediction-corrected tumour size and age was more linear compared to Arm B (Figure 3.32, Panel D). On the other hand, an underprediction of tumour size was observed for the two smaller tumour histology groups of unknown histology (n = 15) and squamous-cell carcinoma (n = 27), (Figure 3.33, Panel D and E). While for the squamous-cell carcinoma patients, median observation at week 8 were within the 90% confidence interval of the prediction, this was not the case for patients with unknown tumour histology. However, only 15 patients with analysable tumour size measurements after baseline were the latter group.

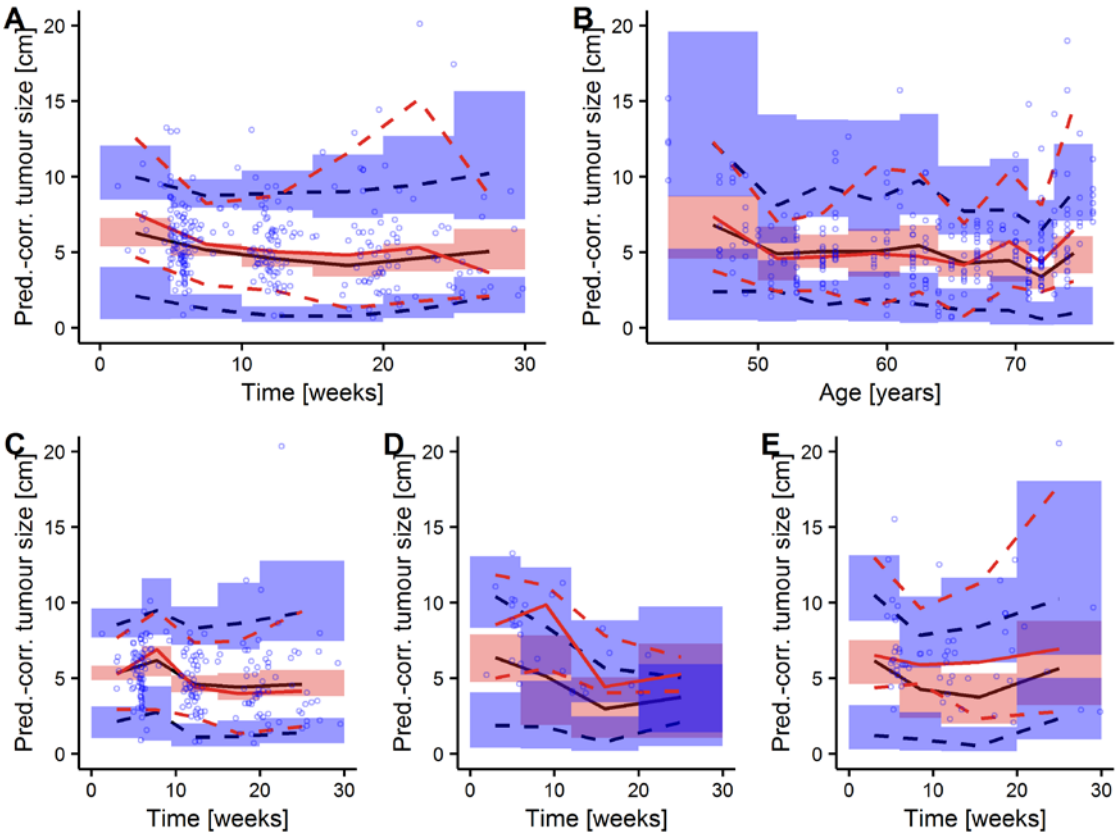

Figure 3.33: Prediction-corrected visual predictive check of the covariate tumour growth inhibition models for patients in study Arm A stratified by covariates.
Panel A: without stratification; Panel B: evaluation over age; Panel C: reference group adenocarcinoma (n = 77 patients); Panel D: unknown tumour histology (n = 15 patients); Panel E: squamous-cell carcinoma (n = 27 patients).
Blue circles: observed tumour size; red lines: median (solid), 5th, 95th percentiles (dashed) of observations; black lines: median (solid), 5th and 95th percentiles (dashed) of simulations; shaded areas: 90% confidence intervals of simulated percentiles.

3.4.2 Linking tumour size to overall survival

The parameters of the base model without covariates (Eq. 2.64 and Eq. 2.65) assuming a log-normal distribution of survival times resulted in parameters with high precision (RSE < 10%) (Table 3.13). Adding all significant covariates from Wang *et al.* [164] (ECOG performance status, LDH, sex, prior surgery, RS_8 and BSL_{SD}, Eq. 2.66) improved the model prediction based on the OFV (ΔOFV = -33.3, six additionally estimated parameters). The backwards deletion reduced the model to three significant covariates: ECOG performance status, LDH, RS_8. The performed backwards deletion step did not increase the OFV significantly (ΔOFV = 2.73, reduction of 3 parameters to be estimated). Parameter imprecision of the remaining covariate effects was high (31% – 36%), but the 95% confidence intervals (assuming normal distribution) of these parameters did not comprise 0 which would mean no influence of the respective covariate.

Table 3.13 Parameter estimates of the base model, the full model and the final covariate model describing overall survival.

Parameter	***Parameter estimate (RSE, %)***		
	Base model	***Full model***	***Covariate model***
OFV	4245.596	4212.259	4214.988
Condition number	1.08	61.7	56.2
Fixed-effects parameters			
μ	8.88 (0.837)	8.09 (3.28)	8.14 (3.26)
ρ	1.27 (6.83)	1.19 (6.53)	1.19 (6.50)
Covariate effect parameters			
ECOG on μ	n.a.	0.888 (31.9)	0.873 (31.8)
LDH on μ	n.a.	-0.00101 (35.6)	-0.00108 (32.0)
Sex on μ	n.a.	0.0684 (249)	n.a.
Prior surgery on μ	n.a.	0.321 (99.4)	n.a.
RS_8 on μ	n.a.	-0.00298 (38.6)	-0.00309 (35.9)
BSL_{SD} on μ	n.a.	-0.0183 (96.2)	n.a.

OFV: objective function value; RSE, %: relative standard error; n.a.: not applicable.
μ: mean of normal distribution of log survival times; ρ: standard deviation of normal distribution of log survival times; LDH: lactate dehydrogenase concentration [U/L]; RS_8: relative change in tumour size at week 8; BSL_{SD}: baseline tumour size (sum of diameters).

The visual predictive checks (VPCs) of base, full and covariate model (Figure 3.34) showed a good prediction of the survival curve for the first two years (104 weeks). Afterwards, the model predicted longer survival than observed but it must be considered that only very few patients

were observed beyond 2 years (24 patients, of which 12 dropped out afterwards with unknown survival and their survival status was therefore right censored). Furthermore, an unexpected high number of patients (5 patients) died between week 107 and 117 since the first drug administration. While for the first year the observed survival data was close to the 95th percentile of the simulations (indicating a tendency for underprediction of survival), the second year was predicted well for all 3 models. No significant improvement or worsening was detected between the development steps of the overall survival model.

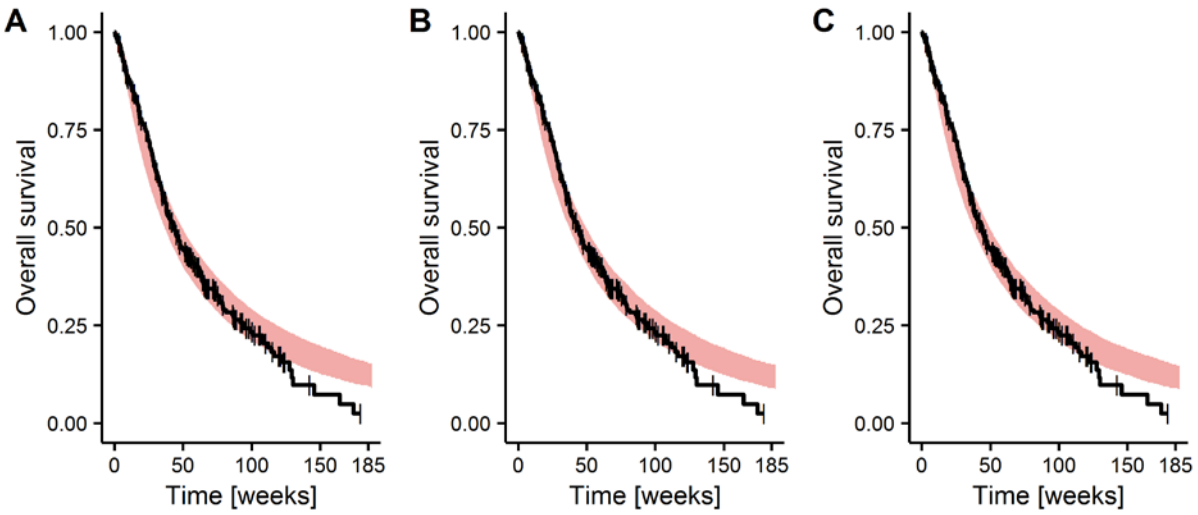

Figure 3.34: Visual predictive check of overall survival models.
Panel A: base model; Panel B: full model; Panel C: covariate model.
Black line: observed overall survival (vertical lines: right censored event); shaded areas: 90% confidence intervals of simulations.

Stratification of the VPCs by the identified covariates (Figure 3.35) showed a trend to underprediction of survival times for patient with physiological LDH concentrations (Panel C), for patients with partial or complete response at week 8 (Panel E) and partly (between 15 and 30 weeks) for patients with an ECOG performance status of < 2 (Panel A). For all other groups, the 95% prediction interval covered the observed data in the first two years.

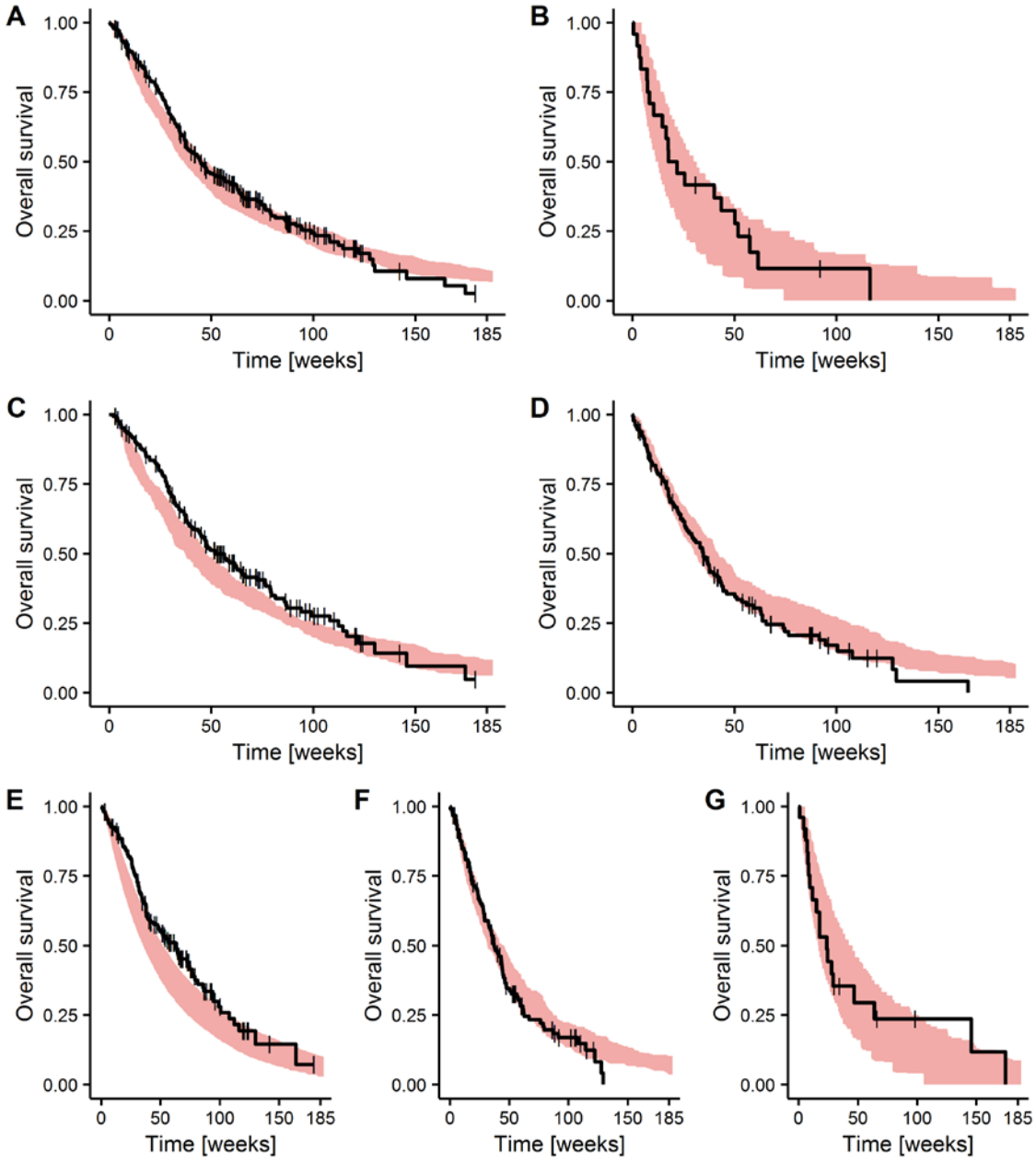

Figure 3.35: Stratified visual predictive check of the developed overall survival model.
Panel A: ECOG performance status < 2 (n = 554 patients); Panel B: ECOG performance status = 2 (n = 48 patients); Panel C: lactate dehydrogenase concentration (LDH) ≤ 240 U/L (within physiological range, 342 patients); Panel D: LDH > 240 U/L (elevated = 260 patients); Panel E: relative change in tumour size at week 8 (RS_8) ≤ 70% (partial or complete response, n = 340 patients); Panel F: 70% > RS_8 < 120% (stable disease, n = 248 patients); Panel G: RS_8 ≥ 120 (progressive disease, n = 50 patients).
Black line: observed overall survival (vertical lines: right censored event); shaded areas: 90% confidence intervals of simulations.

To evaluate the impact of the covariates on survival, the median survival time (T_{median}) and its 95% prediction interval was compared to the typical patient (Figure 3.36). Compared to the typical patient, reduced ECOG performance status (i.e. better physical condition of the patient), reduced LDH concentrations and reduced RS_8 did increase the median survival time. The influence of the covariates on the 2.5th percentile was small (at maximum +19 days for patients

with ECOG performance status < 2 and -4 days for patients with strongly elevated LDH concentrations). An ECOG performance status < 2 showed the strongest effect on median survival times with an increase of 199 days (6.5 months), while the influence of the other investigated covariates, LDH and RS_8, was rather small (± 40 days). Since the covariate relation effects the assumed log-normal distribution of survival times, the influence of the covariates on the 97.5th percentile was the highest and ranged from 1064 days (≈ 3 years) for patients with elevated LDH to 3524 days (≈ 9.5 years) for patients with ECOG performance status < 2.

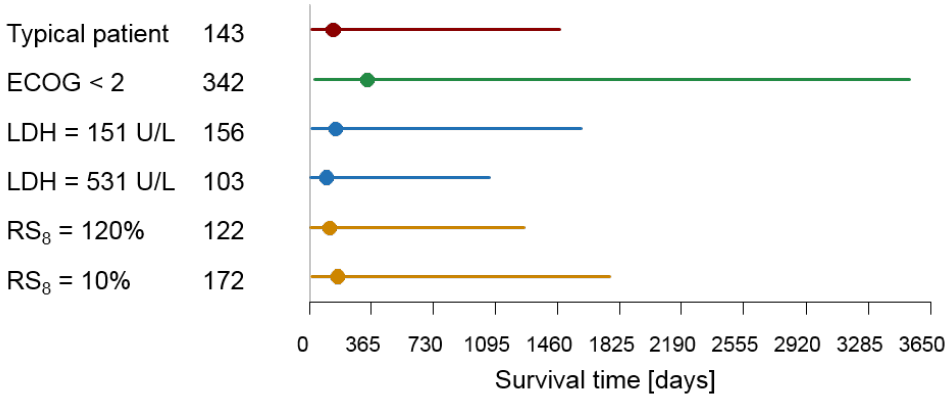

Figure 3.36: Forest plot visualising the impact of covariates on survival times using the developed overall survival model.
Points: median survival time of the respective patient group, respective value in days given in the second column; lines 95% prediction interval.
Patient groups/colours: red (top row): typical patient (ECOG = 2, LDH = 230 U/L, RS_8 = 69.3); green (2nd row): influence of ECOG performance status; blue: influence of LDH at 5th (151 U/L) (3rd row) and 95th percentile (531 U/L) (4th row), respectively; orange: influence of RS_8 at the threshold between stable (120%) and progressive disease (5th row), and close to complete response (10%) (last row).
LDH: concentration of lactate dehydrogenase at baseline [U/L]; RS_8: relative change in tumour size at week 8.

3.5 Project 4: Evaluation of dosing strategies for paclitaxel cancer therapy

3.5.1 Pharmacokinetic treatment outcome

Scenario 1 – 3 were simulated for 1000 patients investigating different dosing or cycle length strategies. In a first step, the pharmacokinetic treatment outcome was investigated, i.e. patients within and outside the PK target range (26 h ≤ $T_{C>0.05}$ < 31 h) (Figure 3.37). Since the first dose in the first cycle is the same in all scenarios, no difference was expected and observed in the first cycle. In this cycle, an overdosing, i.e. patients above the PK target range, was observed in 64.9% of the patients for all scenarios. In the following cycles (cycle 2 – 6), Scenarios 1 (no dose adaptation across cycles) and 3A – 3C (increased dosing interval without dose adaptation across cycles) did not show a significant difference either, since the same

dose was given and the different time of administration did not influence the PK target evaluation by treatment cycle, as drug concentrations did not accumulate. Minor differences arose from differences in the drop-out based on prediction of tumour re-growth or death. Scenario 2, in which dosing was adjusted as suggested by the dosing algorithm based on toxicity and drug exposure, resulted in a decreased exposure and the median $T_{C>0.05}$ was within the target range from the second cycle on. Nevertheless, the interindividual variability in $T_{C>0.05}$ was very high and thus, the proportion of patients within the target range was 23.1% in cycle 2 and 15.0% in cycle 6, while the patients outside the target range were at risk of treatment failure or severe toxicity.

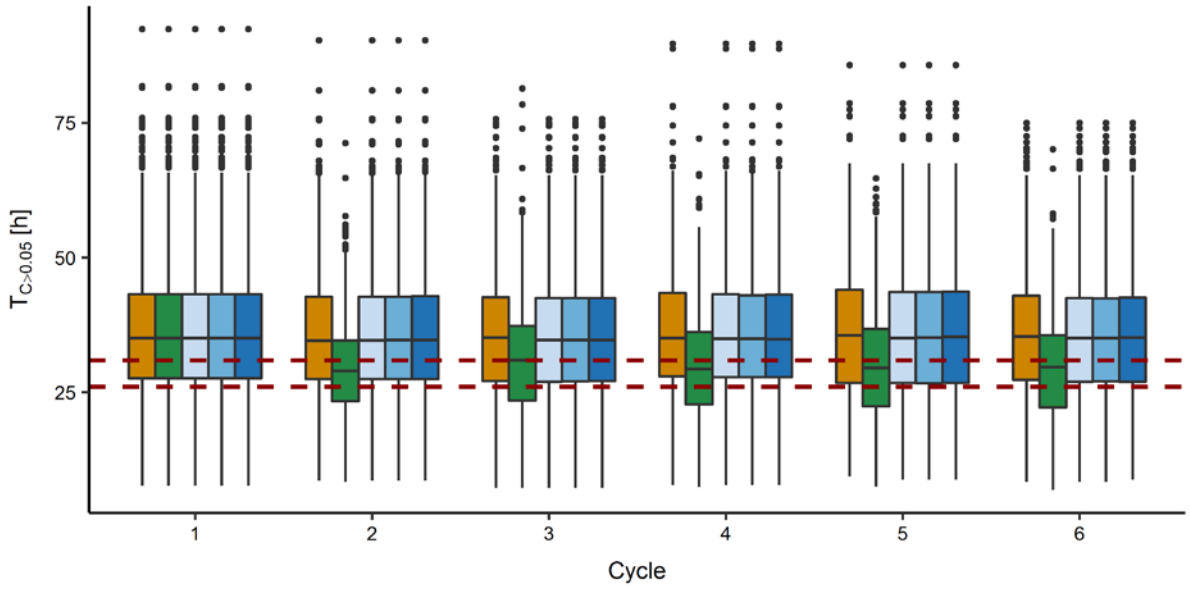

Figure 3.37: Simulated pharmacokinetic treatment outcome across different dosing scenarios.
Colours: orange: Scenario 1 (no dose adaptation across cycles); green: Scenario 2 (dose adaptation across cycles); light blue: Scenario 3A (increased dosing interval: + 3 days); middle blue: Scenario 3B (increased dosing interval: + 5 days); dark blue: Scenario 3C (increased dosing interval: + 7 days).
Boxes: interquartile range (IQR), including median; whiskers: range from box hinge to highest/lowest value within 1.5•IQR; points: data beyond whiskers; red dashed lines: target range (26 h ≤ $T_{C>0.05}$ < 31 h).
$T_{C>0.05}$: time above the threshold of 0.05 µmol/L.

3.5.2 Neutropenia treatment outcome

Nadir neutrophil concentrations were evaluated over the treatment cycles (Figure 3.38, Panel A). For the first cycle, due to the same dosing, all scenarios predicted the same proportion of patients for each of the grades of neutropenia: For all dosing scenarios, the proportion of patients with severe grade 3 or life-threatening grade 4 neutropenia increased over the treatment cycles (Table 3.14). In cycle 6, Scenario 1 showed the highest proportion of patients with grade 4 neutropenia, approximately every 2nd patient, compared to the other dosing scenarios. Scenario 2 showed a slightly lower proportion of patients with grade 4 neutropenia in the 6th cycle compared to Scenario 3A – C, instead, the proportion of patients with grade 3 neutropenia was slightly increased.

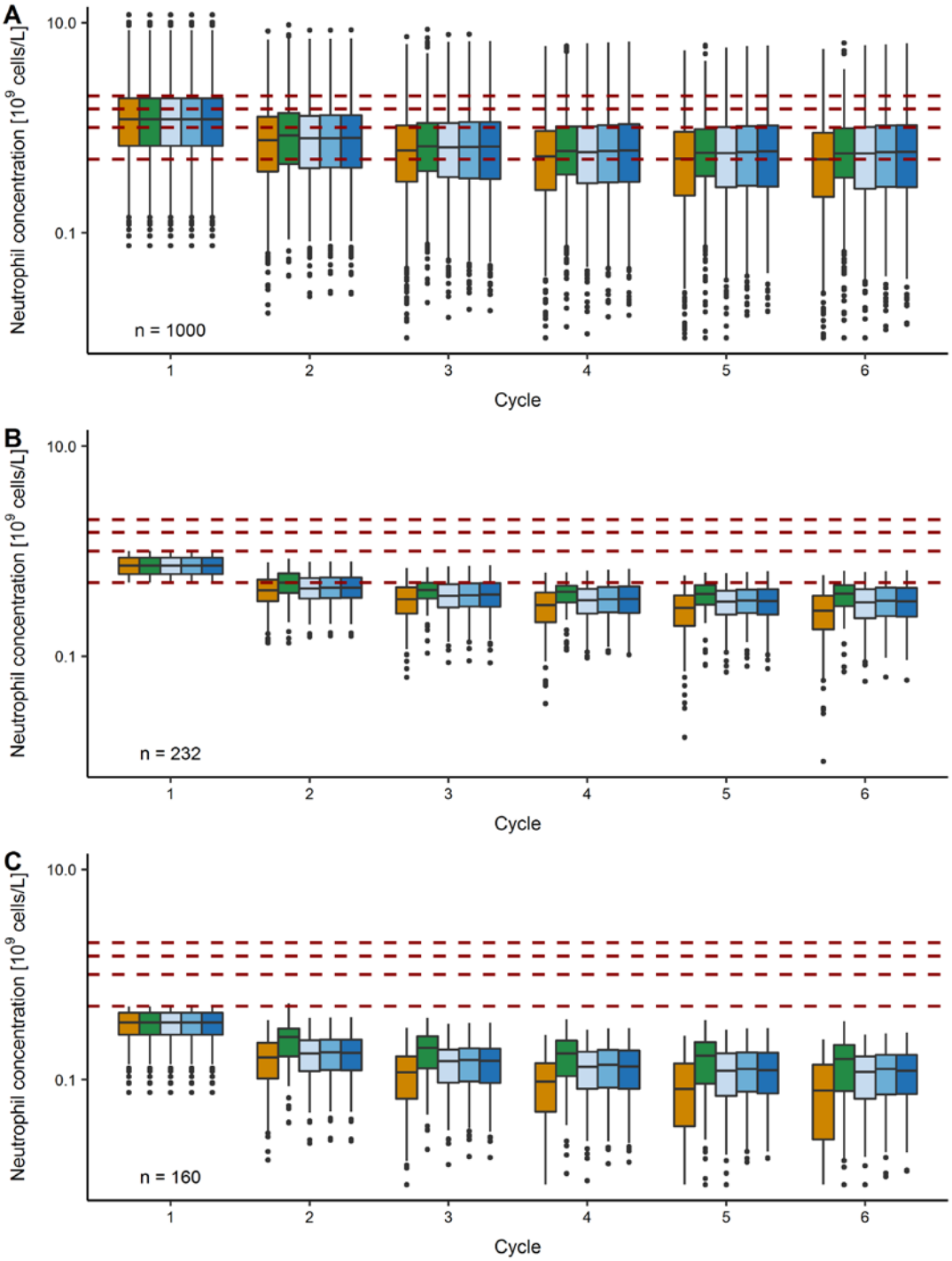

Figure 3.38: Simulated nadir neutropenia concentrations across different dosing scenarios and selected patient populations.
Panel A: whole simulated population (n = 1000 patients); Panel B: patients with grade 3 neutropenia in 1st cycle (n = 232 from 1000 patients); Panel C: patients with grade 4 neutropenia in 1st cycle (n = 160 from 1000 patients).
Colours: orange: Scenario 1 (no dose adaptation across cycles); green: Scenario 2 (dose adaptation across cycles); light blue: Scenario 3A (increased dosing interval: + 3 days); middle blue: Scenario 3B (increased dosing interval: + 5 days); dark blue: Scenario 3C (increased dosing interval: + 7 days).
Boxes: interquartile range (IQR), including median; whiskers: range from box hinge to highest/lowest value within 1.5•IQR; points: data beyond whiskers; red dashed lines: thresholds for grading neutropenia from grade 0 to 4.

Table 3.14: Proportion of patients experiencing a respective grade of neutropenia in treatment cycle 1 and 6.

Grade	*Cycle 1**	*Cycle 6*				
	S1-S3C	*S1*	*S2*	*S3A*	*S3B*	*S3C*
0	23.0%	3.84%	4.48%	4.62%	5.25%	5.35%
1	13.2%	4.69%	5.31%	6.15%	6.77%	6.94%
2	24.6%	12.7%	14.5%	14.5%	14.1%	14.6%
3	23.2%	28.6%	34.3%	29.8%	30.5	29.6%
4	16.0%	50.2%	41.4%	44.9%	43.4	43.2%

S: Scenario.
S1 (no dose adaptation across cycles); S2 (dose adaptation across cycles); S3A (increased dosing interval: + 3 days); S3B (increased dosing interval: + 5 days); S3C (increased dosing interval: + 7 days).
* Same prediction for all dosing scenarios in cycle 1.

When evaluating only those patients who experienced grade 3 or 4 neutropenia (Figure 3.38, Panel B and Panel C, respectively), none of the investigated treatment strategies was able to sufficiently prevent severe toxicity in the following cycles. For patients with grade 4 neutropenia in the first cycle, none of the dosing strategies was able to reduce toxicity to at least grade 3 neutropenia in the subsequent cycles. For patients with grade 3 neutropenia in the first cycle, > 75% of the patients experienced grade 4 neutropenia in cycle 6 for all investigated dosing scenarios.

In Scenario 1, from the patients who experienced grade 4 neutropenia in cycle 6, 243 patients had grade ≤ 3 neutropenia in the first cycle. This number was lower for the other scenarios (178 patients in Scenario 2, 203 patients in Scenario 3A, 194 patients in Scenario 3B, 183 patients in Scenario 3C). Hence, grade 4 neutropenia was prevented for 65 patients (6.5% of the total investigated population) with Scenario 2 and 60 patients (6.0%) with Scenario 3C compared to the fixed dose in Scenario 1.

3.5.3 Efficacy outcome

3.5.3.1 Tumour growth

For evaluating the treatment efficacy outcome of the different dosing scenarios, the tumour size development over time was evaluated for time points every 6 weeks, similar to the sampling schedule in the CEPAC-TDM study (Figure 3.39, Panel A). No significant difference was observed between the dosing scenarios. Differences, especially for Scenario 3, in which the dosing interval was increased, might have resulted from the difference in time after last dose. For the tumour assessment after 12 weeks, the time after last dose was the same for

Scenario 1, 2 and 3C, however, for Scenario 1 and 2, four doses were given until then, while for Scenario 3C, three doses had been administered.

Scenario 3C with three doses after 12 weeks showed an increased tumour size compared to the other dosing scenarios. However, after 30 weeks, when therapy was completed for all scenarios, the longer treatment period in Scenario 3A – C resulted in reduced tumour sizes (Figure 3.39, Panel A).

Time span elapsed after last dose had also an impact the evaluation on the relative change in tumour size at week 8 (RS_8, Figure 3.39, Panel B). RS_8, which was used to inform overall survival, was slightly higher in dosing Scenario 3C. The tumour growth evaluation for this scenario took place at the beginning of the infusion of the third dose, while for Scenario 1 and 2, the third dose was already administered 2 weeks before. Thus, the time after last dose varied between 2 weeks (Scenario 1 and 2) and 4 weeks (Scenario 3C), which influences the interpretability of the tumour assessment data.

Finally, the time until tumour progression compared to the last tumour assessment was evaluated (Figure 3.39, Panel C). All patients, in all simulated scenarios, that did not have an event of death before week 30 were diagnosed with progression within the first 30 weeks. For patients in Scenario 1, 2 and 3A, progression was diagnosed in week 24 almost exclusively. Treatment stopped after 18 weeks in Scenario 1 and 2, while in Scenario 3A treatment ended after 20 weeks and 4 days. In the following tumour assessment, at week 24, tumour growth was detected for those patients, since re-growth occurred directly after the end of therapy. In Scenario 3B and 3C treatment was stopped after 26 weeks and 28 weeks, respectively. Tumour growth for those patients was detected between week 18 and 30. Detection of tumour growth within the treatment period might again result from the fact, that tumour size evaluation in the simulation was no longer synchronised with dosing.

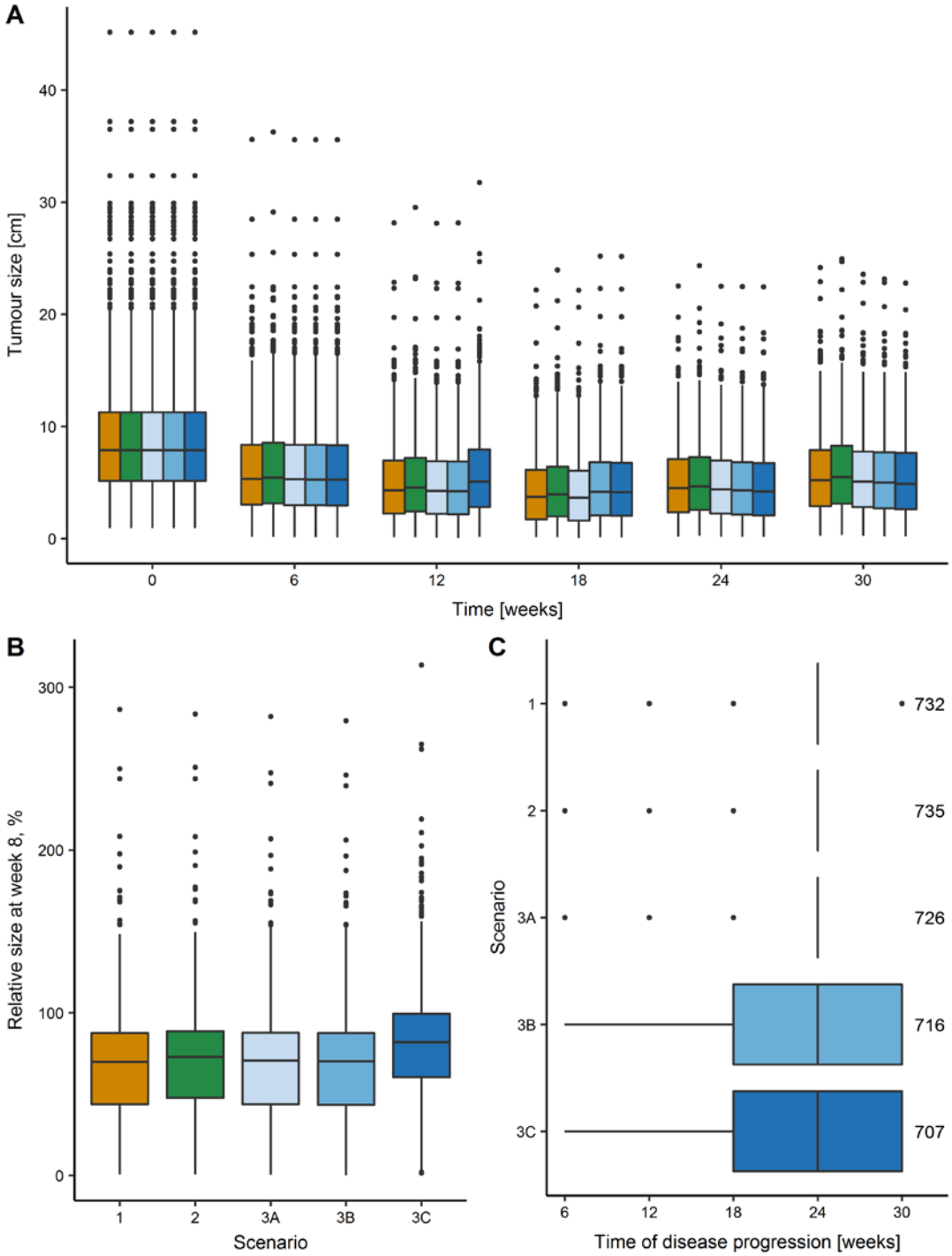

Figure 3.39: Outcome of simulated tumour growth inhibition across different dosing scenarios.
Panel A: Tumour size development; Panel B: Relative change in tumour size at week 8 as it was used to predict overall survival; Panel C: time to tumour disease progression, meaning that tumour size increased compared to the previous assessment.
Colours: orange: Scenario 1 (no dose adaptation across cycles); green: Scenario 2 (dose adaptation across cycles); light blue: Scenario 3A (increased dosing interval: + 3 days); middle blue: Scenario 3B (increased dosing interval: + 5 days); dark blue: Scenario 3C (increased dosing interval: + 7 days).
Boxes: interquartile range (IQR), including median; whiskers: range from box hinge to highest/lowest value within 1.5•IQR; points: data beyond whiskers; red dashed lines: thresholds determining grades of neutropenia.

3.5.3.2 Overall survival

No significant difference was also observed regarding the overall survival outcome between the dosing scenarios (Figure 3.40). The median survival time (overall survival = 0.5) was approximately 45 weeks = 10.5 month, in all scenarios. After the end of the two-year observation period, 25% of the patients survived.

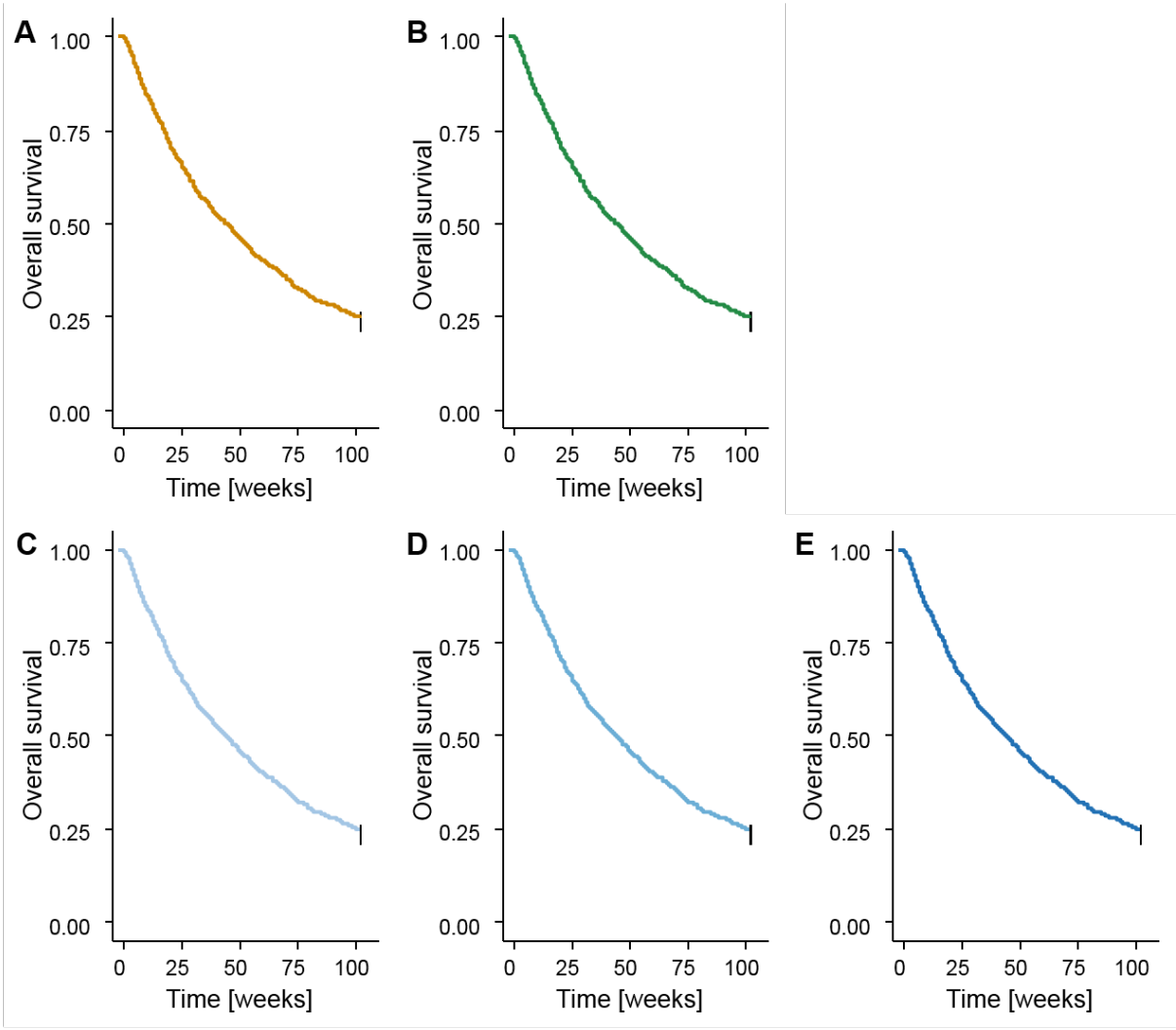

Figure 3.40: Simulated overall survival across different dosing scenarios.
Panel A: Scenario 1 (no dose adaptation across cycles); Panel B: Scenario 2 (dose adaptation across cycles); Panel C: Scenario 3A (increased dosing interval: + 3 days); Panel D: Scenario 3B (increased dosing interval: + 5 days); Panel E: Scenario 3C (increased dosing interval: + 7 days).

3.5.3.3 Drop-out

Finally, the number of drop-outs during the study treatment was determined (Figure 3.41). This evaluation, similar to the pharmacokinetic target and neutropenia analyses, was based on treatment cycles. Comparable rates of drop-out were observed for the different dosing scenarios, which were informed by tumour re-growth and death. Over all treatment cycles, the highest number of drop-outs was observed in Scenario 3C (30.8%) and the lowest for Scenario 1 (29.7%).

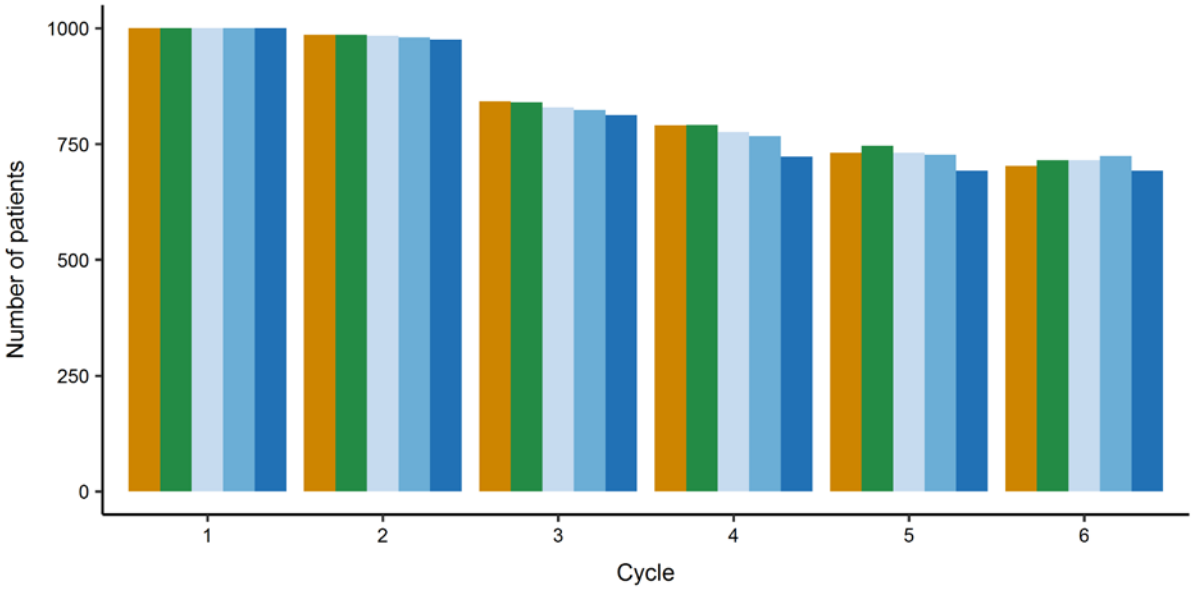

Figure 3.41: Simulated drop-out
Colours: orange: Scenario 1 (no dose adaptation across cycles); green: Scenario 2 (dose adaptation across cycles); light blue: Scenario 3A (increased dosing interval: + 3 days); middle blue: Scenario 3B (increased dosing interval: + 5 days); dark blue: Scenario 3C (increased dosing interval: + 7 days).

4 Discussion

4.1 Numerical and graphical data analysis

The CEPAC-TDM trial was a large prospective study with 365 patients evaluating the impact of a model-based dosing algorithm on neutropenia and efficacy (PFS and OS). Further, the CEPAC-TDM study was the largest oncology study investigating therapeutic drug monitoring [139]. Doses were overall lower for patients in Arm B. This was already the case in the first cycle and the difference increased over the study duration. Nevertheless, the algorithm allowed for increased doses for some patients and led to a broadening of the dose range.

Adherence to the protocol including dose adjustments to toxicities and the suggested dosing algorithm was good for the first cycle, in which dosing decision was only based on the patient characteristics, beside of the cisplatin overdosing. For the following cycles, where drug exposure (only for paclitaxel in Arm B) and toxicity were considered, the adherence decreased with a trend to overdosing of paclitaxel, especially in Arm A. This means that dose reductions were not applied as suggested by the protocol and higher doses were administered. The overdosing of cisplatin was constant for the following cycles. The evaluation of the adherence reveals that, even though the protocol was followed in general, an investigation considering the actual treatment should be done in addition to the “intended to treat” statistical analysis performed in [139].

Concentration measurements of paclitaxel were unfortunately only performed for Arm B. In addition, very sparse sampling of only one sample per patient and cycle was collected. However, sampling times were spread over a time range of approximately 13 h. This spread allowed to “borrow” information between the patients for PK parameter estimation within the nonlinear mixed-effects modelling framework (see section 2.1.1.1). Nevertheless, considering the complex PK of paclitaxel in combination with the sparse sampling, development of a PK model only based on the concentration measurements from the CEPAC-TDM study would not be possible. Thus, prior knowledge was included in Project 1.

The paclitaxel concentration measurements were used to determine the $T_{C>0.05}$ as a marker for drug exposure. Due to the sampling time close to the threshold, this estimation is relatively precise (root squared mean error: 0.5%) [138], even though only one sample was available. Evaluating the determined $T_{C>0.05}$, it was seen that the target range of 26 – 31 h was not met for the majority of the analysed treatment cycles/patients (Figure 3.3). While overdosing regarding the target range was reduced over the cycles, underdosing increased. This suggests

that dose reductions due to toxicities or high drug exposure were too strong to meet the PK target.

Toxicity was evaluated in terms of neutropenia. It must be considered that the neutrophil concentrations measured on day 15 ± 2 were obtained after the nadir, which is typically between day 11 and 12 [138]. Thus, neutropenia in both arms was underestimated. Nevertheless, no statistically significant reduction of severe neutropenia was found for the dose adaption in Arm B compared to Arm A [139]. This finding confirms that further improvement in the algorithm is needed to reduce grade 3 and especially grade 4 neutropenia. Nevertheless, the variability in the neutrophil concentration measurements was reduced, despite the increasing range in the doses administered. This shows the impact of the dosing algorithm on neutropenia and displays that with further adjustments of the dosing algorithm it might be possible to bring the majority of the patients to grade 2 or grade 3 neutropenia. Further, a cumulative pattern was found for both study arms, meaning a worsening of neutropenia over the treatment cycles despite the dose reductions (at least for patients in Arm B). This pattern was previously described for the combination therapy of paclitaxel with carboplatin [188] and was also seen for the thrombocyte and erythrocyte concentrations (Figure 3.5). This reduction of neutrophil concertation is not described by the Friberg *et al.* [119] model, that was used to develop the dosing algorithm [138]. Hence, adaptations in the PK/PD model describing neutropenia were needed to account for the cumulative neutropenia pattern to achieve reliable model predictions (Project 2).

Further, efficacy was evaluated as it defines the lower bound of the therapeutic window. Here again, no significant difference between the two study arms was reported [139], even though significantly lower doses were administered in Arm B. Modelling of efficacy was not considered when the dosing algorithm was developed. Still, it is important to investigate both toxicity and efficacy for dose adaptations since both define success of a treatment. In this case, further dose reductions might be preferable regarding the neutropenia, however, at the same time, efficacy may than be compromised. Thus, a tumour growth inhibition model was developed and linked to overall survival in Project 3.

Regarding the development of tumour size, the data showed substantial drop-out rate, which was not at random. Patients with growing tumour size were more likely to die and therefore drop-out. Therefore, the tumour growth inhibition modelling approach only considered the first 30 weeks after the 1st paclitaxel administration, since at later time points the data became very sparse, in terms of the number of individuals observed, and biased due to the high drop-out. Development of resistance will be investigated in the modelling process as well, but might not be the major reason for patients having disease progression after initial response. Further, tumour regrowth might also result from end of treatment.

Death was not the only relevant factor for drop-out, but tumour progression was influencing early end of treatment, before finishing cycle 6 significantly. Hence, model predicted tumour progression and death were used to inform drop-out in Project 4.

The here presented exploratory analysis of the covariates was mainly focussing on the covariates used in the following projects. The correlations between covariates were used to generate a realistic virtual population in Project 4, that does not include unrealistically extreme combinations of covariates. Further, it was observed that concomitant anticancer treatment was administered for some patient in parallel to the study treatment or in the follow-up phase, which potentially influences neutropenia and efficacy outcome.

In summary, a need to further improve the dosing algorithm was found. The performed data exploration was a prerequisite to develop a strategy for the following modelling activities. The following model-based analyses further had the advantage to use the information of the actual study procedure and not as “intended to treat”, since deviations from the protocol were observed for dosing, sampling time points and the administration of concomitant treatment in parallel to the study medication.

4.2 Project 1: Pharmacokinetic modelling of paclitaxel

This project aimed to evaluate the applicability of a published PK model [138] for the newly obtained CEPAC-TDM paclitaxel concentration measurements. Further, potential misspecifications identified in the external model evaluation were tackled in the model optimisation step.

4.2.1 External PK model evaluation using the CEPAC-TDM data

To evaluate whether the two studies, the one on which the previous PK model was built and the CEPAC-TDM study, and therefore their results are comparable, the differences and equalities will be summarised (Table 4.1): Both studies included a high number of patients (> 250). While the original study included different cancer types (mainly ovarian cancer), the CEPAC-TDM study included non-small cell lung cancer exclusively. Hence, the distribution of sex is different in the two studies, since lung cancer is more frequent in man than in woman due to different smoking habits in the relevant age group [28,189]. The original study included a wide dose range from 100 to 250 mg/m² and intense sampling for up to 3 treatment cycles. These attributes of the study in combination with the high number of patients makes it an ideal learning study to develop a PK model with broad applicability. Further, paclitaxel PK is schedule-dependent, explicitly the PK depends on the infusion duration [68,190], which was similar in both studies. To conclude, the study design was different for the original study (upper

left part of Figure 1.6) compared to the CEPAC-TDM study, especially in terms of sampling times, which makes the original study an ideal learning study, while the CEPAC-TDM study was designed to be a confirming study and has, due to the sparse sampling, limited applicability for learning. The study population was slightly different due to the differences in the included cancer type. Nevertheless, the PK model developed on the original study should be able to predict the paclitaxel concentrations measured in the CEPAC-TDM study.

Table 4.1: Comparison of the previous study and the CEPAC-TDM study

	Original study	***CEPAC-TDM study***
Number of patients included	273	**Arm A**: n = 182 **Arm B**: n = 183
Cancer type	Ovarian cancer: (n = 145) NSCLC (n = 102) Various other solid tumours (n = 26)	NSCLC
Dose paclitaxel [mg/m²]	175: n = 225 100-250: n = 48 <175/>200: n = 40	Starting dose: Arm A: 200 Arm B: 168 (98 – 201)
Comedication	Carboplatin (n = 197) 92 patients: 300 – 400 mg 105 patients: AUC 5 mg/mL • min Monotherapy (n = 76)	Carboplatin (n = 304) Cisplatin (n = 61)
Infusion duration	3 h infusion (n = 261) 24 h infusion (n = 12)	3 h infusion
PK samples	1.5 h after start of infusion, end of infusion 0.75, 2, 6, 9, 12, 24 h after infusion	Arm A: none Arm B: 24 h after start of infusion
Neutrophil samples	For 104 patients, 314 samples Only for the 1st cycle	Day 1 and 15 ± 2 of each cycle
Efficacy	Not mentioned	According to RECIST

n: number of patients

The external model evaluation showed that prediction of the CEPAC-TDM data is overall possible. An almost perfect prediction was observed for the individually predicted data. However, this prediction results from the combination of the sparse sampling with the high interindividual variability in many of the parameters, which caused the high shrinkage and the "overfitting". Therefore, the results from the individual prediction should not be exaggerated, but the population prediction and the pcVPC should be evaluated. Here, an underprediction was observed, which was less severe for females. This can be explained by the fact, that more females were included in the original study. Considering that the samples were taken in the terminal phase of the concentration-time profile and the resulting low concentration range, in which the PK measurements were available (up to approximately 0.3 µmol/L, see Figure 3.2) compared to the maximum concentration (approximately 6 µmol/L, see Figure 3.13), the

misspecification was not severe. Nevertheless, a model optimisation was performed to tackle the misspecification described.

4.2.2 Model optimisation combining prior knowledge and the CEPAC-TDM data

For model optimisation, the frequentist prior approach was used, since an estimation of all parameters in the complex PK model would not be possible with the sparse sampling in the CEPAC-TDM study. Furthermore, the misspecification was not high, thus the information from the previous study could be combined with the one from the CEPAC-TDM study. Therefore, two variants of the frequentist prior were investigated, including only the diagonal elements of the variance-covariance matrix Γ (Model I) or the full matrix (Model II). The second approach is more restrictive, since it does not only limit the flexibility for the estimation of each fixed-effects parameter, but in addition constrains certain combinations of fixed-effects parameters due to the incorporation of the covariance terms.

Both approaches provided stable estimation with high precision as expected, since the precision in the original model was already high (RSE ≤ 10% for most parameters, exceptions were only seen for the covariate effects and interindividual variability on k_{21}). Interestingly, the precision and stability of the estimation in Model I were better than for Model II. Since the restriction of parameter estimation was higher for Model II, higher precision was expected for this model.

The changes in the parameter estimates for Model I and II compared to the original model were low (≤ ± 16%), beside of the covariate effect of bilirubin on VM_{EL} (-41.1% and -45.2% for Model I and II, respectively). Thus, changes in the concentration-time profile, evaluated by deterministic simulations were also small and only visible on a semi-logarithmic scale. As expected, changes in the concentration-time profile, due to the change in the parameter estimates, were small and occurred only in the terminal phase. Changes in earlier phases of the concentration-time profile were not supported by the CEPAC-TDM study data and also in the later phases, strong changes were not needed, as seen in the external model evaluation. Since Model II allowed for more flexibility, it lead to greater changes in the profile than Model I and also increased $T_{C>0.05}$ more.

Although the changes in the parameter estimates were small, these changes lead to an improved prediction to the observed data compared to the original model for both approaches (Model I and II), even a though slight misspecification was still observed in the goodness-of fit plots. The greater changes in the parameter estimates for Model II increased in the quality of the prediction compared to the observed data more than for Model I.

Overall, the greater flexibility allowed in parameter estimation of Model I was needed to improve the prediction sufficiently and also resulted in a more stable and precise parameter

estimation. Therefore, Model I was chosen for the following modelling steps. Further investigations on the impact of the off-diagonal elements of Γ on the parameter estimation using the frequentist prior approach are needed to explore and understand the behaviour in parameter precision and stability. General conclusion shall not be made by this investigation, since the model was complex and therefore the estimation process difficult.

Comparing the optimised PK model parameters with literature values (Table 4.2), the total volume of distribution was higher than reported in most of the PK analyses, nevertheless, similar rages were reported as well [68]. The same is true for clearance, which was a bit smaller in most publications. Clearance was reduced in the optimised model compared to the original model, which brings overall clearance more in line with literature. However, models with saturable processes are difficult to compare with values arising from linear assumption. Hence, variations from common literature values do not necessarily imply physiological implausibility.

Table 4.2: Comparison of volume of distribution (V) and clearance (CL) between literature, the original and the optimised PK model

Analysis	*V [L/m²]*	*CL [L/h/m²]*	*Study information*
Wiernik, 1987 [61]	119	21.6	Dosing: 200 - 275 mg/m² Infusion duration: 24 h 9 patients
Wiernik, 1987 [191]	60.1	8.04	Dosing: 175 - 275 mg/m² Infusion duration: 6 h 12 patients
Brown, 1991 [65]	48.6	13.9	Dosing: 175 - 275 mg/m² Infusion duration: 6 h 31 patients
Huizing, 1993 [68]	199	18.0	Dosing: 135 - 175 mg/m² Infusion duration: 3 h – 24 h 18 patients
Ohtsu, 1995 [190]	36.9	5.89	Dosing: 105 - 270 mg/m² Infusion duration: 3 h – 24 h 27 patients
Gianni, 1995 [56]	75.3	4.30	Dosing: 135 - 175 mg/m² Infusion duration: 3 h – 24 h 30 patients
Van Zylen, 2001 [192] *	254	41.8	Dosing: 135 – 225 mg/m² Infusion duration: 3 h 7 patients
Henningson, 2001 [193] *	816	252	Dosing: 135 – 225 mg/m² Infusion duration: 3 h 20 patients
Joerger, 2012 [138] (original model)	234	36.6	Dosing: 100 - 250 mg/m² Infusion duration: 3 h 273 patients
Model I (optimised model)	232	31.6	Dosing: 58.3 - 251 mg/m² Infusion duration: 3 h 168 patients

V: total volume of distribution; CL: clearance
For saturable processes, (intercompartmental), clearance was calculated for the linear phase of the respective process.
Parameters reported not per body surface area were divided by the typical value of 1.7 m²
For volume of distribution the sum of all compartment (if compartmental analysis) is reported.
* unbound

For further improvement, tackling the remaining misspecifications seen in the goodness-of fit plots a denser sampling would be needed to account for further mechanisms of the complex PK as the influence of cremophor EL (see section 1.2.3.1) or binding to blood cells, as implemented in [192,193].

Further improvement in the parameter estimation was also not needed, since the prediction was good considering the sparse data situation. For the following modelling steps precision of

the EBEs and thus the individual concentration-time profile was more important than the population prediction. Minor changes in the population parameters would probably not result in significant changes in these profiles. To conclude, PK model "fit-for-purpose" (see section 1.1.3.1) of the following steps was successfully developed.

4.2.3 Evaluation of the impact of the optimised model

To understand the impact on the individual concentration-time profile and exposure, the new parameter estimates of Model I were compared to the original model. Here, the major changes were seen for V_3 and Q, which also changed comparably strong (9.45% and 7.69%). The strong change in the bilirubin and the other covariates on VM_{EL}, on the other hand, did not bias the original individual value of VM_{EL} compared to Model I (bias: -3.33%). In this comparison, the absolute value of bias and imprecision did not vary significantly from each other, meaning that deviation of the original individual parameter from the newly estimated one typically went in the same direction. This results from the strong dependency of the individual parameter on the population parameter due to the high shrinkage, even though interindividual variability was high.

Further, the original model was underestimating $T_{C>0.05}$ (bias: -5.82%), taking Model I as reference. When comparing $T_{C>0.05}$ over the treatment cycles for the two models, it was seen that the number of patients estimated to be underdosed decreased by applying the optimised model, while the opposite trend was seen for overdosing. Overall, the percentage of patients not reaching the target range was estimated to be higher for the optimised model. This result was expected, since the dosing algorithm was based on the original model. Nevertheless, the proportion of patients being either over- or underdosed was more equally distributed for the optimised model and the median of $T_{C>0.05}$ was closer or more often within the target range. This means that patients in general were estimated to be closer to the target range applying the optimised PK model, even when they were estimated to be outside this range.

When further comparing the simulated $T_{C>0.05}$ with the ones obtained by simulations for Arm B, the variability was lower for the exposure obtained by *post-hoc* estimation, which was expected due to the high shrinkage. Further, the median $T_{C>0.05}$ decreased more for the simulated exposure than for the ones obtained by *post-hoc* estimation over the cycles, which led to an increasing discrepancy between the $T_{C>0.05}$ derived by the two approaches. No such difference was obvious in the first cycle. *Post-hoc* estimations further showed a decrease in the variability, which was similar for the simulations. These differences between simulations and *post-hoc* estimations show that the dosing-algorithm did successfully select patients with high and low exposure and adapted them accordingly. For the simulation, no such selection is performed, but each individual dosing regimen is simulated 1000 times, representing the whole range of

individual PK parameters and resulting exposure. This example nicely shows how adaptive dosing can influence exposure and shows that simulations and simulation-based diagnostics can be misleading, when this aspect is not considered. Thus, prediction-correction in the VPCs is essential and NPDE analysis should be assessed with caution. Also, correlations between drug exposure and outcome (e.g. drug exposure or variables describing toxicity/efficacy such as the nadir of neutropenia) must not be done if the outcome influenced the dose. Hence, correlations between dose, $T_{C>0.05}$ and neutropenia based on exploratory or statistical analysis must be avoided in this project due to the adaptive dosing in the CEPAC-TDM study (Figure 1.5). A possible solution is to apply the same dose adjustments and drop-outs in the simulations [194], which is in this project very complex, since many factors in addition to drug exposure and neutropenia, such as neuropathy, influenced dosing and end of study treatment. Hence, a model for each of these factors would be needed to be developed and to be considered.

Since drug exposure was not considered in the dose finding for patients in Arm A and no complex adaptive dosing was performed, simulations of Arm A can be compared to drug exposure in Arm B derived by *post-hoc* estimation. Here, the median trend showed that drug exposure in Arm A was higher than in Arm B, as expected due to the higher doses. Since doses did not change to a high extent for patients in this conventional study arm, also drug exposure did not change substantially but did decrease slightly as the doses.

Applying the optimised PK model does slightly change the interpretation of the exploratory data analysis. The percentage of patients underdosed is less severe than assumed, which might explain partly why there was no significant change in the efficacy outcome. On the other hand, the number of patients being overdosed was underestimated using the original model, which might then again partly explain why there was no significant difference in the outcome of adverse events in terms of neutropenia. Nevertheless, the number of patients reaching the exposure target range was low over all cycles (24.6% – 36.4%, applying the optimised PK model). But a clear influence of the adaptive dosing was seen when comparing simulations and *post-hoc* estimation of exposure in Arm B. Hence, further optimisation of the dosing algorithm is needed if the target range shall be reached. Still, it must be considered that reaching the PK target is not the primary goal. Exposure is a surrogate parameter that cannot fully predict treatment outcome in terms of toxicity and efficacy due to the interindividual variability, observed in the PK/PD models for neutropenia and tumour growth.

4.2.4 Evaluation of limited sampling strategy applied in the CEPACT-TDM study

The optimised PK model described the data from the CEPAC-TDM study well. Nevertheless, for the following steps, the PK/PD modelling, the whole individual concentration-time profile

was used to inform the drug effect. Thus, precision and bias of the EBEs determining the individual concentration-time profile were investigated. The simulations showed only minor bias and sufficient precision. This is in line with previous investigations [138,195,196] and results from the sampling time which was planned to determine $T_{C>0.05}$ and was therefore set to a time after dose when concentrations are typically close to the threshold. From this perspective, the sampling strategy is well planned for the study purpose, determination of $T_{C>0.05}$ for dose individualisation.

On the other hand, EBEs were estimated with low bias but high imprecision, up to 43%. This high imprecision results from the combination of firstly high interindividual variability and secondly the sparse sampling, which causes high shrinkage. Imprecision is especially high for parameters determining the early phases of the concentration-time profile as Km_{TR} and Q, that drive the distribution processes, since sampling was only performed in the terminal phase of the concentration-time profile.

In conclusion, there is little bias but considerable imprecision in the estimation of the individual concentration-time profile. Thus, the sampling strategy is suboptimal for the sequential PK/PD modelling approach, but cannot be solved in a simultaneous PK/PD analysis either. One of the exposure parameters, $T_{C>0.05}$ or AUC, could have been chosen to inform the drug effect, but this would result in a high loss of mechanistic character in the neutropenia PD model. Further, $T_{C>0.05}$ and AUC are not constant over the cycles within one patient, cycle length varies between patients and finally at the end of therapy also the drug effect has to end and assumptions would be needed for the follow-up period, especially for the tumour growth inhibition PD model. It must be considered that interindividual variability in the PK/PD models might be overestimated due to the shrinkage in the individual PK concentration-time profiles. Despite this bias, the sequential modelling strategy, this is the best approach available.

4.3 Project 2: Modelling of paclitaxel-induced long-term neutropenia

The aim of this project was to evaluate the appropriateness of the original model using the gold standard Friberg *et al.* [119] structural model for the neutrophil data from the CEPAC-TDM study. Further, the model structure was to be optimised to be able to describe and predict the cumulative neutropenia pattern observed in the exploratory data analysis. Finally, in order to allow for dose adaptation simulations, the neutropenic drug effect was analysed, differentiating between the impact of paclitaxel and the platinum-based drugs.

4.3.1 External model evaluation

In the first step, the external model evaluation, the observed CEPAC-TDM study data (only patients of experimental study Arm B) were compared with the prediction of the original PK/PD model (with optimised PK part, see Project 1). Both, the goodness-of-fit plots, as well as the pcVPC showed that the cumulative neutropenia pattern, leading to decreasing neutrophil concentrations over the cycles, was not captured by the original PK/PD model. This was expected, since the gold standard structural model which was used in the original PK/PD model, predicts approximately the same neutrophil concentration-time profile for each treatment cycle (Figure 3.21, Panel A), if dose and dosing interval were not changed. In the CEAC-TDM study it was observed that on the one hand, the neutrophil concentration decreased over the cycles, while on the other hand, doses were reduced for the majority of the patients (see Figure 3.1). Thus, the original model predicted increasing neutrophil concentrations, while the observed data showed an opposite trend.

Since the previous study [138] only investigated neutrophil concentrations of the 1st treatment cycle (Table 4.1), the cumulative pattern was not included in the original model, which resulted in the misspecification observed in the external model evaluation. Due to the repeated number of treatment cycles, the CEPAC-TDM study gave the opportunity to investigate the cumulative behaviour in more detail, since clinical trials rarely investigate neutropenia over such a long study period.

A second finding of the external model evaluation was, that for the population prediction and the pcVPC the neutrophil concentrations on day 15 ± 2 were underpredicted. This pointed towards a misspecification of the slope parameter estimate of the original model. On the individual level, this misspecification did not become obvious as the individual slope parameters were estimated (*post-hoc* estimation) in a way that day 15 ± 2 neutrophil concentrations at approximately the middle of the therapy (cycle 2 - 3) were well described.

These results indicated that parameter re-estimation with the gold standard model structure could improve the model prediction, especially for the day 15 ± 2 neutrophil concentrations. However, the structural model was expected to inadequately describe the cumulative neutropenia over the treatment cycles.

4.3.2 Comparison and evaluation of re-estimation of the original model compared to Model A – C

Based on the results of the external model evaluation, it was investigated whether the prediction of the model could be improved by re-estimating the parameters of the gold standard

structural model. Further, different approaches were studied to describe the observed cumulative neutropenia.

For the re-estimation of the PD parameters in the gold standard structural model, the slope factor was estimated to be higher than in the original model. Thus, the 1st cycle in the population prediction was well described. However, due to the model structure, predicting approximately the same nadir concentration for each cycle in case of unchanged dosing, parameter re-estimation did not cover the cumulative neutropenia pattern adequately.

Residual variability, resulting from measurement errors but also potential model misspecifications, was approximately 2 times higher than originally estimated. This was expected considering the negative ε-shrinkage in this parameter in the external model evaluation. Negative ε-shrinkage indicates that the standard deviation of the individual weighted residuals ($IWRES$) was higher than the one predefined by the original PK/PD model. Thus, negative ε-shrinkage in the external model evaluation pointed towards the need of a higher residual variability parameter for this structural model, which was confirmed in the model re-estimation.

On the other hand, considerable η-shrinkage on the mean maturation time (MMT) was observed in the external model evaluation, indicating that a lower interindividual variability would be quantified in the re-estimation step. Indeed, the CV% decreased from 44.8% to < 10% and was finally excluded from the model.

To be able to describe cumulative neutropenia, three different structural models were investigated (Model A – C). While Model A and B were identified from literature and adapted for this application, Model C was developed as a semi-physiological alternative. Since the aim was to describe and predict neutropenia over repeated treatment cycles to ultimately simulate different dosing scenarios, physiological plausibility was a main model selection criterion, increasing the ability for extrapolations in the simulations.

Model A (adapted from [121]) used a rather empirical mechanism: by decreasing $BASE_{tot}(t)$ time dependently, the feedback effect on the proliferation and therewith the capacity of the system to recover from neutropenia was reduced. Model B (adapted from [122]) was not initially intended to describe cumulative myelosuppression, but thrombocytopenia after different dosing schedules. Nevertheless, a more mechanistic approach was used for Model B by implementing quiescent cells not harmed by the drug and accounting for progenitor cells that are resting (G_0 phase of the cell cycle). Finally, Model C was developed implementing cumulative neutropenia as a physiologically rational consequence of damage of also early primitive bone marrow stem cells, such as pluripotent long-term haematopoietic stem cells (LT-HSC) [111]. By accounting for this bone marrow exhaustion (BME) hypothesis, a physiologically plausible semi-mechanistic approach was followed.

In all three models, the slope factor was higher than originally estimated, though high variation between the 3 models was observed. This was due to differences in neutrophil concentrations in the respective proliferation compartments. E.g. for Model B, the concentration in this compartment was increased (Figure 3.21, Panel C). However, as in this model cells can also become quiescent cells, the proportion of cells entering the maturation chain was reduced compared to the re-estimated gold standard model. Interindividual variability on the slope factor was high for all investigated models (> 40%). This might result from the high η-shrinkage in the PK model (Project 1), since the individually predicted paclitaxel concentration-time profiles informed the drug effect of the neutropenia model, but were shrunk to the population prediction. If variability in the slope factor is overestimated due to misspecification in the individual PK prediction, this might lead to more extreme predictions in simulations of neutropenia (as in Project 4), meaning that percentages of grade 4 and 0 neutropenia might be overestimated.

Regarding cumulative neutropenia, all three models were able to account for this pattern to a certain extent but the best prediction regarding AIC (Table 3.7) and pcVPC (Figure 3.20) was found for Model C, followed by Model A (prediction similarly well) and B (significantly lower predictive performance), respectively. For Model A, the parameter estimate k_{depl} of the time-dependent second drug effect is specific for the cycle length of the underlying data. Thus, extrapolations to other cycle lengths than 3 weeks would be misleading. Further, predictions of the recovery of patients strongly depend on the assumptions made for E_{drug2} after the last treatment cycle. Hence, the lack of physiological plausibility and the empirical implementation of the additional time-dependent drug effect E_{drug2}, excluded Model A even though predictive performance in the pcVPC was comparable to Model C. Model A should not be used for simulations extrapolating the dosing schedule, especially the dosing interval.

Model B used a more physiological approach compared to Model A. Resting quiescent cells were implemented and were not affected by the drug effect. Nevertheless, for Model B, due to the higher estimate of γ and thus the short time the system needs to recover, increased cycle lengths (longer than time to recover) would not result in cumulative neutropenia. This reduced recovery time, moreover, led to the prediction of neutrophil concentrations (nadir and peak values) that mainly dropped in the first two cycles and thereafter did than not change further (Figure 3.21), since the system reaches a “steady state” with the regular dosing. This observation does not correspond to the observed cumulative neutropenia pattern with increasing neutrophil concentrations also in the later cycles. Further, the prediction of the model (AIC, pcVPC) was inferior to Model A and C.

Model C was newly developed and implemented the BME hypothesis by including an additional stem cell compartment in front of the maturation chain mimicking pluripotent

LT-HSC, while the proliferating cell compartment (Prol) represented the progenitor cells. Proliferation of these stem cells was affected by the same drug effect as the progenitor cells (i.e. same mathematical function with the same slope factor SL and drug concentration), following the underlying assuming that the cytotoxic effect depends on the proliferation rate [197] which is slower for the LT-HSC than for progenitor cells [198]. Damage of these stem cells occurs in particular for the second and the following administrations of cytotoxic drugs, since induced haematopoietic stress from the first cycle stimulates the proliferation of the stem cells and makes them more vulnerable for the following doses [199,200]. Further, the same feedback mechanism as for the progenitor cells was influencing the proliferation of the cells in the stem cell compartment, since cytokines are regulating the proliferation of these pluripotent stem cells as well, even though the type of cytokines differ from the ones influencing progenitor cells [102]. Including this modelling approach, Model C was able to describe the decreasing neutrophil concentrations over the cycles in a semi-mechanistic way. This resulted in an approximately exponential decline of the nadir and the peak values of the neutrophil concentrations over the cycles. Nadir values were more affected than peak values (Table 3.8), which was supported by the data. The lacking ability of the stem cell compartment to recover within a cycle mimicked the aforementioned hypothesis that long-term stem cells are damaged. This hypothesis is also supported by the fact that thrombocyte and erythrocyte concentrations showed the same decreasing pattern over time (Figure 3.5). This is plausible as stem cells common for neutrophils, thrombocytes and erythrocytes are disturbed (Figure 1.3). Furthermore, the model predicted a long time (approx. half a year after last dose administration) for the stem cells to fully recover after treatment over 6 cycles. Since no neutrophil measurements were available for such a long time period, predictions for the time after the 6th cycle are extrapolations that need further validation. Nevertheless, a long time for full recovery seems plausible, since previous chemotherapy was found as covariate on baseline using the gold standard model [201], supporting the assumption that the bone marrow is still disturbed and needs a long time to recover. However, an alternative hypothesis is plausible as well, which relates the damage of stem cells to an induction of senescence, i.e. a reduction of the self-renewal capacity [202]. In this case, the damage in the stem cell compartment would not result from a loss of cells but a limited number of replications, which could be implemented by a change in k_{stem} or decreased number of cells in stem that actually replicate. However, it is difficult to distinguish the two hypotheses, since the effect is only measured in the circulating cell compartment and difference might only be observed in the time to recover, since permanent, and not a temporary, damage of self-renewal capacity would destruct the homeostasis of the haematopoietic system and would thus not allow for full recovery compared to Model C. Hence, further evaluation of neutrophil data after the end of chemotherapy, potentially in combination with more complex system pharmacology models, is

needed to increase the understanding of the long-term effect of cytotoxic drugs on the bone marrow.

In comparison to Model B, the system-related parameters (MMT and γ) of Model A and C, were in good agreement with the respective parameters of the original/re-estimated gold standard model (Table 3.7). This indicated, that previous knowledge gained from the gold standard modelling approach, could be used as prior information on system-related parameters for Model C.

Overall, the best description of the neutrophil data was obtained using Model A and Model C. Model A used a non-physiological explanation for the BME effect by implementing a time-dependent second drug effect. Model C, on the other hand, gave the most physiological explanation of the drug effect and has the potential to describe long-term treatment with paclitaxel. Thus, Model C gave further evidence on the BME hypothesis that destruction of pluripotent haematopoietic stem cells causes cumulative myelotoxicity. Further, due to the semi-mechanistic modelling approach the comprehensive PK/PD modelling framework can be possibly used to describe the effect of other myelotoxicity drugs.

4.3.3 Differentiation of drug effects of paclitaxel and platinum-based drugs

To allow for reliable simulation of dose modifications, it is necessary to distinguish between the drug effect of paclitaxel and carboplatin/cisplatin, since dose reduction of one of the drugs does not necessarily reduce the drug effect of the concomitant drug to the same extent. This is especially necessary for carboplatin, since of the two platinum-based drugs, carboplatin has stronger myelotoxicity [30]. Two different approaches were investigated within the framework of Model C: the additive drug effect model and the general PD interaction model.

Since PK of carboplatin and cisplatin was not measured in the CEPAC-TDM study, the population prediction based on two published PK models were implemented. For cisplatin the one-compartment PK model of De Jongh *et al.* [75] was utilised, which was built based on data from 285 patients with weekly or 3-weekly cisplatin dosing of 50 - 100 mg/m² (combination therapy with different chemotherapeutic drugs). This PK model for cisplatin was chosen due to the high number of patients on which the model was originally built on, similar study inclusion criteria (ECOG performance status ≥ 2 and creatinine clearance ≥ 60 mL/min for the cisplatin patients), similar dosing schedule and the intensive covariate analysis performed [75]. The implemented carboplatin PK model was built on data from 69 patients treated with high-dose combination chemotherapy [185]. Doses were higher (1500 mg/m² or AUC 20 – 22 mg/mL) than in the CEPA-TDM study but included 500 mg/m² (≙ target AUC of 5.86 mg • min/L for a patient with 1.7 m² BSA and 120 mL/min GFR, similar to the target AUC of 6 mg • min/L in the CEPAC-TDM study) as consecutive doses for 3 days as well. Furthermore, PK of carboplatin

is linear for doses up to 2400 mg • min/m² [82]. The two-compartment carboplatin PK model comprised several covariates (creatinine clearance and body height on clearance, body weight on the central volume of distribution and age and body height on the intercompartmental clearance), which allowed for a comprehensive population prediction for each patient.

By implementing the population PK prediction for carboplatin and cisplatin, no PK interaction between paclitaxel and platinum-based drugs was assumed. For cisplatin, this assumption holds not true when cisplatin is administered preceded paclitaxel (leading to 25% decrease in paclitaxel clearance) [78]. However, this can be avoided by inverting the sequence of drug administration, as done in the CEPAC-TDM study [78]. For carboplatin, no evidence for a pharmacokinetic interaction had been reported [90,188,203]. Hence, the assumption of no PK interaction is plausible.

In the additive drug effect model, the parameter estimates (Table 3.9) of the slope factors of paclitaxel (5.18 L/µmol) and carboplatin (0.997 L/mg) were approximately twice as high as reported in literature for monotherapy estimated with the gold standard model (for paclitaxel: from 1.85 L/µmol [71] to 2.21 L/µmol [119]; for carboplatin: 0.460 L/mg [186]). A published analysis of an additive drug effect on neutropenia using the gold standard neutropenia model found lower slope factors for both drugs, paclitaxel and carboplatin [204], which is not in line with the severe neutropenia observed in the CEAPC-TDM study. The parameter estimate of SL_{cis} was higher than expected. Thus, for each of the 3 drugs, AUC_{0-24h} of the drug effect was evaluated and confirmed the implausibility. Cisplatin AUC_{0-24h} was significantly higher than for carboplatin considering that, as above mentioned, cisplatin is known to be less or equally neutropenic. Reliable estimation of the cisplatin effect was not possible given that only 30 patients in study Arm B were treated with cisplatin. Comparing paclitaxel and carboplatin, AUC_{0-24h} of paclitaxel was higher, which is in line with literature reporting neutropenia as dose-limiting toxicity for paclitaxel, but not for carboplatin, which predominantly causes thrombocytopenia.

Due to the sparse PD sampling in the CEPAC-TDM study, the general PD interaction model had to be simplified (see section 2.4.2.2). Consequently, this model results in an additive model as soon as both drugs are present in at least a low concentration. Since paclitaxel and cisplatin/carboplatin were administered shortly after each other, paclitaxel is acting as a single drug only during the 3 h infusion. Afterwards, the platinum-based drug was added and elimination of all 3 drugs took place in a comparable time frame (Figure 3.23).

Using the reduced general PD interaction model, the paclitaxel SL_{PTX} of the additive model was equivalent to $\frac{SL_{PTX}}{1+INT}$ = 5.06 L/µmol of the general PD interaction model and comparably also SL_{carbo} of the additive model was equivalent to $\frac{SL_{carbo}}{1+INT}$ = 1.05 L/mg of the general PD

interaction model. These values were within the 95% confidence interval of the respective parameter in the additive model. Thus, the two approaches, general PD interaction model and additive model, are in alignment with each other, resulting in a similar prediction and indicating a synergism between paclitaxel and carboplatin of approximately 50%.

The synergism between carboplatin and paclitaxel was intensively discussed in literature. Synergistic drug interaction was found for different cancer cell lines for simultaneous drug administration *in vitro* [205,206]. On the other hand, decreased thrombocytopenia was observed for this combination therapy *in vitro* as well as in clinical studies [207–209]. Nevertheless, this antagonistic drug effect on the thrombocytes was not seen for neutropenia, but additive to synergistic effects were observed in a clinical trial [209]. The mechanism of the synergism seen in some cell lines is not fully understood yet. However, it was suggested, that due the cell cycle arrest in the G_2/M phase caused by paclitaxel, cells return to a pseudo G_1 phase and therefore the proportion of cells in this phase of the cell cycle increases [210]. Since cells in the G_1 phase of the cell cycle are more sensitive to carboplatin, synergism is plausible [205].

Overall, both modelling approaches did improve the PK/PD model in terms of AIC compared to Model C, but both models do not give a mechanistic or drug concentration-dependent explanation for the observed synergism. The generalised PD interaction model is a good option to understand and quantify drug-drug interactions, but due to the sparse data situation in the CEPAC-TDM study it was not possible to estimate all interaction parameters within this framework, which lead to a model comparable to the additive effect model but quantified the synergism. Overall the difference between the two models was negligible (ΔAIC = 2), but parameter estimation was more stable for the additive model, especially estimation of standard errors, thus, the additive modelling approach was chosen. However, further analyses with dense sampling including monotherapy data applying the generalised PD interaction model could increase the understanding of the complex PD interaction taking place in different cell lines. In addition, data assessment with other dose combinations of paclitaxel and carboplatin or even monotherapy should be performed to allow for reliable parameter estimation using the general PD interaction model.

4.3.4 Covariate model building

A covariate analysis was performed to identify risk factors for severe neutropenia, that should be considered for dose selection. Since no relevant interindividual variability was identified on MMT and γ, covariate effects were not investigated on these parameters.

From the covariates investigated in the graphical analysis, only previous therapy in general and more specifically previous chemotherapy and radiotherapy showed a significant trend on

the individual variability of the slope factor of paclitaxel ($\eta_{SL,i}$, Figure 10.3). Thus, surgery was excluded from the following covariate analysis, and previous chemo- and radiotherapy were summarised as one binary categorical covariate. This covariate was implemented on E_{drug}, since the same trend, even though not significant, was observed for carboplatin ($\eta_{SLcarbo,i}$). Furthermore, it is physiologically more plausible to increase the sensitivity to chemotherapy in general than only to paclitaxel. However, neither the additive nor the multiplicative implementation of the previous chemo-/radiotherapy was statistically significant (α = 0.05, but a trend was observed in Figure 10.3), even though and it was a significant covariate on SL before [211], and can be considered as physiologically plausible underlying the bone marrow exhaustion theory. Assuming that the stem cells recover slowly, the concentration of the neutrophils and progenitor cells after previous chemo-/radiotherapy might already be within the physiological range, even though decreased, but the stem cell compartment is still severely disturbed. This might then lead to an increased sensitivity to the following therapy and explain a potential influence. The reason why this covariate was not identified to be significant in this analysis might be the low number of patients (11.0%) with previous therapy (Table 3.2) since the study was planned for newly diagnosed NSCLC patents. Further studies, including a higher proportion of patients with previous therapy, are needed to elucidate the influence on the drug effect as well as on baseline neutrophil concentrations.

Similarly to the previous chemo-/radiotherapy, concomitant chemo-/radiotherapy was investigated as a binary, but time-varying, covariate. Even though an increase of the drug effect is plausible, this influence was not significant in this study. The reason might be, similarly to the one for the previous therapy, the low number (6.85%) of patients with concomitant therapy (Table 3.4). Furthermore, the drugs used for concomitant chemotherapy were not reported for all patients and might include additionally targeted, non-cytotoxic treatment.

Finally, supportive G-CSF therapy was a significant covariate with an additive effect on E_{drug}. This way of implementation was chosen since E_{drug} then summarises all administered drugs. G-CSF increases the proliferation and enhances the maturation within the granulopoiesis [212]. Nevertheless, the effect on the stem cell proliferation, compared to the progenitor cell proliferation, is probably lower [102]. Different modelling approaches captured this biological effect of G-CSF more physiologically by increasing the proliferation and transition rate constants [213,214]. Even though this analysis used a simplified implementation of the G-CSF effect and could only explain a minor part of the interindividual variability in SL (0.735%) and SL_{Carbo} (1.35%), it was shown that the impact is high (ΔOFV = 22.5, with only 9 patients receiving this supportive treatment) and should be considered. Since not enough data is available to implement or develop a more physiological approach, simulations in Project 4 will not include patients with supportive G-CSF therapy. Overall, this model was

successfully evaluated for patients in treatment Arm A who received the standard dosing of paclitaxel and did not undergo PK sampling. The slight misspecification in the 5th percentile of the neutrophil concentration-time profile might result from an overprediction in the variability in the slope factors due to η-shrinkage in the PK, as discussed before (section 4.3.2.)

4.3.5 Impact of the optimised PK/PD model on the study results

Time to nadir was analysed and compared to the sampling time of the CEPAC-TDM study. This comparison revealed that the planned sampling time (day 15 ± 2) did capture the nadir for only 5.85% of the occasions. The median time to nadir was approximately 11 days, which is supported by prior analyses [138,215,216]. Sampling was planned after the real nadir and thus severity of neutropenia was underpredicted in both study arms. Sampling on day 10 – 12 after the last drug administration, a range that covers approximately 90% of the nadir occurrences, can in future improve the interpretability of the neutropenia results. This would not only shift the sampling time, but also decrease the possible sampling time span, which would reduce variability in the neutrophil measurements for statistical analysis.

Even though the model predicted nadir is an estimate of the individual nadir, it gives a more precise and accurate measure of neutropenia than the sampling on day 15 ± 2. The estimated nadir corrects the underprediction of neutropenia and is therefore a more meaningful parameter for dose adaptations. Evaluating the model predicted nadir, variability was lower for Arm B (Figure 3.28), as it was seen for the day 15 ±2 study data. As just described, the results showed more severe neutropenia as suggested by the day 15 ± 2 measurements. Comparing nadir values between the two study arms, grade 4 neutropenia was reduced for patients in Arm B while the proportion of patients experiencing grade 3 neutropenia was elevated. Since grade 3 neutropenia is sometimes seen as acceptable toxicity that at the same time indicates efficacy [217], this result indicates that the treatment schedule in Arm B is superior compared to the standard dosing. Nevertheless, in cycle 3 to 6 more than 25% of the patients in Arm B suffered from life-threating grade 4 neutropenia, which emphasises the need of further improvement of the dosing algorithm. Different dosing strategies based on the here developed model were explored in a simulation study in Project 4.

4.4 Project 3: Efficacy modelling: Tumour size and overall survival

The aim of Project 3 was to describe tumour size development over time and overall survival as treatment efficacy measure.

4.4.1 Tumour size modelling

The structure of the tumour growth inhibition model comprised a linear tumour growth and a linear drug effect term. Linear tumour growth as simplified model is plausible if the diameter of a single lesion is evaluated as tumour metrics. Then, the cubic law is followed, in which the tumour volume is proportional to t^3 and the tumour diameter is proportional to time t [218]. However, the sum of diameters of up to 5 target lesions was evaluated. Hence, the hypothesis of the cubic law is not fully applicable. However, linear tumour growth of the sum of diameters was also reported by Stein *et al.* [219] for patients with metastatic renal cell carcinoma. The growth rate found by Stein *et al.* ($1.92 \cdot 10^{-3}$ cm/h) was approximately three-fold larger compared to growth rate k_g in the here developed model. This difference resulted probably from the different tumour entities. Doubling times of tumour volume of adenocarcinoma and squamous-cell carcinoma of the lung was reported to be 72 and 146 days in humans, respectively [220]. Thus, for a tumour diameter of d_0 = 8.30 cm (median baseline tumour size for patients in Arm B), the tumour grows within the first hour by $1.60 \cdot ^{-3}$ cm and $7.90 \cdot 10^{-4}$ cm ($d_{1h} - d_0$) for adenocarcinoma and squamous-cell carcinoma, respectively, assuming the tumour volume at time t ($\mathrm{V(t)}$) to be a perfect sphere (Eq. 4.1 - Eq. 4.3). The estimated growth rate ($6.26 \cdot 10^{-4}$ cm/h, Table 3.12) was close to that and also show the high variability in tumour growth that was also described in literature [220].

$$\mathrm{V(t=0)} = \frac{1}{6} \cdot \pi \cdot {d_0}^3 \qquad \textbf{Eq. 4.1}$$

$$\mathrm{V(t=1h)} = \frac{1}{6} \cdot \pi \cdot {d_{1h}}^3 = \frac{1}{6} \cdot \pi \cdot {d_0}^3 \cdot e^{(1/doubling\ time) \cdot 1h} \qquad \textbf{Eq. 4.2}$$

$$d_{1h} - d_0 = d_0 \cdot \left(e^{(1/doubling\ time) \cdot 1h \cdot (1/3)} - 1\right) \qquad \textbf{Eq. 4.3}$$

More mechanistic growth models had been developed, e.g. accounting for quiescent tumour cells [16]. Such a sophisticated approach was not within the scope of this work due to the sparse data situation and the absence of a placebo group to investigate tumour growth without drug influence which would be unethical in patients.

The drug effect in the developed tumour growth inhibition model was linear. Unfortunately, distinguishing between anticancer effects of paclitaxel and carboplatin by estimating two separate drug effects was technically not possible. This is not unexpected since the sampling was sparse and delayed with respect to the drug administration. Similarly, this sparse data problem was faced before by Tham *et al.* [221] with the combination therapy of gemcitabine and carboplatin. However, to differentiate between the two drug effects, data from preclinical experiments in combination with the well-established modelling framework of Simeoni *et al.* [1] was used to determine a factor correlating the drug effect of carboplatin to the one of paclitaxel.

This approach included the assumption that the ratio of the effect of carboplatin and paclitaxel from mice is transferable to human. Further, the PK profile was determined from tumour tissue in mice as target-site, while plasma concentrations were used in the developed human PK model. Hence, it was assumed that the ratio of the AUC of the two drugs is similar in the tumour of the mice and the plasma in humans. Finally, as in the neutropenia model an additive drug effect was assumed, knowing that synergism was described before [205,206] (see section 4.3.3). Thus, as well as for the neutropenia model, extrapolations outside the investigated paclitaxel/carboplatin concentration ranges are probably not reliable. Nevertheless, the factor relating paclitaxel and carboplatin drug effect (r_{effect}) was similar to the ratio of SL_{carbo}/SL = 0.192 in the neutropenia PK/PD model (1.40 times higher than r_{effect}), which gave further evidence on the plausibility of the parameter estimate r_{effect}.

With integrating more data, which might also come from preclinical experiments, more complex and mechanistic models of the combination effect can be developed. Such models can increase the understanding of the synergism and can be use this knowledge to optimise the sequence and dosing of the two drugs [22]. Further, preclinical PK/PD models reported describe tumour growth inhibition by including a delay in the drug effect, since this is typically seen in tumour size shrinkage as well [1,222]. Such a mechanism can potentially increase the reliability of predictions regarding changes in dose or cycle length.

The developed tumour growth inhibition model did not include a resistance term, since the estimation of such an effect was not successful, probably due to the sparse sampling (tumour size measurements approximately every 6 weeks). Hence, simulations of largely increased dosing intervals should be regarded with care, since this might increase the probability of resistance development [223], which is captured by the developed model. The lack of a resistance mechanism further led to unreliable predictions of drop-out in Project 4 (see section 3.5.3.3 and 4.5), in which this model underpredicted drop-out compared to the CEPAC-TDM study. Nevertheless, the model was able to predict tumour size at week 8 sufficiently well for both study arms ultimately inform overall survival.

Large interindividual variability was identified for both model parameters, k_g and β_{PTX}, and was also found for other tumour growth inhibition models for tumour growth rates, which might also yield from variability in resistance development [16,126,164]. The covariate analysis could explain parts of the high interindividual variability (19.3% of the interindividual variability of k_g and 23.2% of the interindividual variability of β_{PTX}) with two prognostic factors: tumour histology on the response to paclitaxel and age on the tumour growth rate. Three groups of tumour histology were defined for the analysis and patients with adenocarcinoma showed the worst response, followed by the patients with unknown tumour histology. Patients with squamous-cell carcinoma had the best response, with a resulting drug effect being 132% higher than the

typical patient with adenocarcinoma. Even though literature does not report differences in the sensitivity to paclitaxel treatment for the different tumour histologies, significantly better prognosis for patients with squamous-cell carcinoma histology of non-small cell lung cancer (stage II) had been reported [224]. Furthermore, altering survival depending on tumour histology and treatment had been observed as well [225]. Hence, an influence of tumour histology on the treatment response is plausible but the extent of the difference in effect cannot be compared to literature. Further, the effect could also result from different growth rates [220], but tumour histology was not a significant covariate on this parameter.

The second significant covariate effect, decreasing tumour growth rate with increasing age (5.06% per year of age), was also identified in different clinical trials with other tumour entities [226–228]. Geedes *et al.* [229] suggested that one reason might be that slowly growing tumours are detected later, thus, in older patients. Only a linear relationship between growth rate and age was investigated but other models, e.g. exponential relationship, might be possible. However, the linear relationship described the tumour size over age sufficiently for both treatment groups (Figure 3.32 and Figure 3.33). Based on the parameter estimate young patients would profit more from the therapy, since the cancer cells are due to the higher proliferation rate constant more vulnerable to the cytotoxic therapy.

Overall, the tumour size was well described for both study arms, even though a tendency for overprediction for Arm B and underprediction for Arm A was observed (Figure 3.30, Figure 3.32). Tumour size at week 8 was well described for all patient groups, despite the small groups of patients with unknown tumour histology or squamous-cell carcinoma in Arm A (Figure 3.33). Thus, tumour size at week 8 was therefore used as predictor for overall survival. For the performed simulation investigation, it has to be considered that drug concentrations and dosing should not be chosen outside the here investigated range and that also significant changes in the cycle length must be regarded with care.

In general, modelling of tumour size in humans is difficult due to sparse sampling, high interindividual variability in the response and lack of placebo tumour growth data. Thus, typically empirical models are developed in the clinical drug development stage [127]. Nevertheless, modelling of treatment efficacy on tumour size can help to guide study designs and strategies of treatment individualisation based on clinically relevant covariates [125,127].

4.4.2 Linking tumour size to overall survival

A parametric modelling approach was chosen in this project, since different dosing scenarios were simulated in Project 4. A log-normal distribution of the individual survival times was assumed as described previously in [164]. Other distributions had been applied in literature describing oncologic treatment outcome of survival, such as the Weibull distribution [230,231],

but log-normal distribution had successfully described large clinical trials [126,164] and had been reported to be superior in a direct comparison for patients with hepatocellular carcinoma [232].

The log-normal distribution model was able to successfully describe the observed survival data. The median survival time for a patient with ECOG performance status ≤ 1 (RS_8 = 69.3%, LDH = 230 U/L) was 342 days. Wang *et al.* [164] had estimated a very similar median survival time of 354 days (ECOG performance status = 1, RS_8 = 69.3%). The standard deviation of the distribution was higher in this analysis (95% prediction interval: 33 – 3524 days) compared to Wang *et al*. (95% prediction interval: 166 – 2683 days). Wang *et al*., compared to this analysis, included also patients with less advanced tumour stages and different treatments, and did not analyse patients who died within the first 8 weeks, which might explain the differences in the distribution of survival times.

Wang *et al*. further chose, dependent on the treatment regimen, a different setting of the reference patient with respect to the ECOG performance status, thus the influence of the ECOG performance status is not fully comparable to the here developed model. However, the influence of the ECOG performance status was less profound in the analysis of Wang *et al*. (difference in the median survival time for Wang *et al*.: 82 days comparing ECOG performance status 0 to 1; developed model: 199 days comparing ECOG performance status 2 to ≤ 1), while the influence of change in tumour size at week 8 was higher (median survival time of 667 days in case of 90% tumour reduction and ECOG performance status = 1). Unfortunately, the parameter estimate of the paclitaxel carboplatin combination, which included LDH as covariate, had not been reported in [164]. As discussed before, the studies are not fully comparable and might explain the differences in the detected covariate influences.

ECOG performance status was the covariate with the most prominent influence on the median survival time in the analysis presented here and had been identified to be influential in different analyses [231,233]. Future investigations could include ECOG performance status not only as a dichotomous covariate, differentiating between a performance status of ≤ 1 and 2, but also characterise differences in the survival between performance status 0 and 1, since those two stages included the majority of the patients (48.2% and 44.7% respectively, Figure 3.10).

The influence of tumour size at week 8 on the distribution of survival times was rather small (almost complete response, RS_8 = 10% only prolongs median survival time by 29 days compared to the typical patient), but evidence on the influence is given by several studies which identified tumour size at week 6, 7 or 8 to be predictive for overall survival [234]. Nevertheless, this approach has some drawbacks, since a patient might have good response until week 8 but might develop resistance soon afterwards [234], which might also explain the low magnitude of influence, thus, low clinical relevance. Nevertheless, the possibility of a false

inclusion (Type I error) of the covariate has to be considered, since high shrinkage (> 30%) was observed in the tumour growth model (Table 3.12) and since the time span of observations of tumour growth was limited to 30 weeks [235]. Besides, the relative change in tumour size at a certain time point, time to tumour growth and the tumour regrowth rate had been investigated as covariates influencing survival [236] and might be worth to examine in future. Similarly, the individual estimate of the drug effect parameter β_{PTX} could be further investigated, since it quantifies the response of the patient to the treatment.

Lactate dehydrogenase (LDH), which was also a significant covariate in this analysis, is often used as a tumour marker. LDH catalyses the formation of lactic acid and oxidation of nicotinamide adenine dinucleotide under anaerobic conditions. Hence, LDH concentrations increases in case of hypoxia and cell damage, which are seen in tumour tissue, and stimulates angiogenesis. The prognostic ability was shown in several clinical trials, e.g. [237–239]. Thus, LDH is a plausible covariate. Further investigations could be performed on the implementation of LDH in the overall survival model, since currently lower LDH concentrations even within the physiological range result in increased survival. Instead, a hockey stick model could be investigated, with decreased survival in case of elevated LDH concentrations higher than the physiological range.

This analysis was focusing on the covariates identified to be significant in [164] for the paclitaxel carboplatin combination in patients with non-small cell lung cancer. Nevertheless, other potential covariates might be worth to investigate in a next step: This should include covariates describing drug exposure and should consider the additional radio- and chemotherapeutic treatment, that was administered especially in the follow-up phase of the CEPAC-TDM study. Further, the ratio between neutrophil and lymphocyte concentration is currently intensively discussed as a prognostic factor for overall survival and was found in a recent meta-analysis to be significant for patient with lung cancer [240]. Hence, an evaluation of this ratio as covariate could potentially contribute to the current discussion.

Overall, the model was able to describe the observed survival sufficiently well for the whole populations and for the investigated subgroups. Survival *after* two years was not well predicted, most likely due to the low number of patient in this late phase. Nevertheless, predictions should not be made for more than two years after the first dose. Therefore, simulations in Project 4 only covered this time frame. Since in Project 4 the different scenarios investigated different dosing schedules but for the same population, a significant difference between the scenarios was not expected due to the limited clinical relevance of the relative change in tumour size on survival. Further steps should thus investigate a direct influence of drug exposure on survival or, as discussed before, other metrics resulting from the tumour growth inhibition model as time to tumour growth or the tumour growth rate.

4.5 Project 4: Evaluation of dosing strategies for paclitaxel cancer therapy

In Project 4, the PK, PK/PD and time-to-event models for toxicity and efficacy developed in Project 1 – 3 were used to simulate different dosing scenarios. The aim of this investigation was to evaluate the question, whether it is better to reduce the dose or increase the dosing interval in case of severe toxicity. As a starting point the first dose in all dosing scenarios was adjusted as suggested in the dosing algorithm, since this dose showed less overdosing with respect to the target exposure range and less toxicity in the CEPAC-TDM study [139]. In Scenario 1, this dose was continuously administered every 3 weeks, thus serving as reference scenario, while in Scenario 2, the dose for the following cycles was adjusted as suggested in the dosing algorithm. According to the algorithm, doses were reduced in case of grade 3 or 4 neutropenia. In Scenario 3, the influence of an increased cycle length was investigated.

For the pharmacokinetics, it was observed that the dosing based on sex and age, as it was performed in the first cycle for all scenarios, led to overdosing for the majority of the patients (64.9%). Only in Scenario 2, in which the doses were modified over the cycles, a reduction of exposure was observed. Nevertheless, only 15% of these patients finally reached the target range in cycle 6. The high interindividual variability in PK resulted in extremely low and high drug exposure compared to [56], in which the minimum $T_{C>0.05}$ was 13 h and maximum $T_{C>0.05}$ was 45 h with comparable infusion duration and doses. This suggests, that correlations between the PK parameters describing interindividual variability might be needed to avoid unrealistic extreme values. Such an analysis was not possible with data from the CEPAC-TDM study, due to the sparse sampling, but could potentially be done with the data of the clinical trials, from which the original model originates from [138]. Another reason why dose adaptation in the CEPAC-TDM study as well as in this simulation did not result in a higher proportion of patients being within the target range, might be due to interoccasion variability. Since therapeutic drug monitoring cannot account for interoccasion variability (CV, % for V_1 and VM_{EL} was 37.3% and 15.2%, respectively, [138]), drug exposure for the following dose cannot be predicted precisely [241]. Hence, it has to be considered, that therapeutic drug monitoring can only have limited success.

For neutropenia, the major adverse event, the first cycle resulted in considerable grade 4 neutropenia for all dosing scenarios (16.0%, Table 3.14). The percentage of patients with grade 4 neutropenia in the first cycle was higher than the one for patients in Arm B of the CEPAC-TDM study (considering the estimated nadir not day 15 ± 2 measurements, 4.92%, Figure 3.28). The increased percentage of patients with grade 4 neutropenia results probably from the high variability in the PK and the absence of shrinkage in the simulations. Hence, this

result further indicates the need for correlations between the interindividual variability parameters. Due to the overestimation of interindividual variability in the PK, the percentage of patients in the respective grades of neutropenia must be regarded with care. However, comparison of neutrophil concentrations between the dosing scenarios are possible, since they are influenced by the same potential bias.

Further, it was seen that none of the investigated dosing strategies was able to prevent grade 4 neutropenia sufficiently. Using the dosing algorithm or the increased cycle length only prevented 65 or 60 patients (6.5 and 6.0% of the total simulate population, respectively) from grade 4 neutropenia, respectively, compared to the constant dosing in Scenario 1. Furthermore, for patients with grade 3 or 4 neutropenia in the first cycle, none of the dosing strategies led to a sufficient improvement in the subsequent cycles. Although, Scenario 1 resulted in the lowest nadir concentration compared to the other dosing scenarios, the improvement by the other scenarios did not lead to significantly lower grades of neutropenia. From the perspective of toxicity, further dosing strategies should be evaluated: Besides of further reducing the dose or increasing the cycle length, a combination of both components should be evaluated. Further, the carboplatin dose should be taken into consideration as well for the dose adaptation. Both methods, combined dose reduction with increased cycle length and reduced dosing are already done in clinical practice as well as in the CEAPC-TDM study but are typically based on empirical recommendations or physicians experience. Thus, a systematic evaluation of these strategies is needed to improve evidence-based medicine. Further, as for the pharmacokinetic model, estimation of correlations between PD parameters, specifically between the slope factor of paclitaxel and the one for carboplatin should be further investigated to avoid unrealistically high or low response to drug exposure.

In a next step, the effect of the different dosing scenarios on tumour size was evaluated. While for the pharmacokinetics and neutropenia the evaluation was by treatment cycle, tumour size was analysed over time since first dose. Overall, no significant differences were seen for the tumour size over time. Since the predicted tumour size immediately shrank after drug administration and then slowly regrows during the dosing interval, this analysis was influenced by the time after last dose. In this analysis, fixed evaluation time points every 6 weeks were chosen for analysis to be close to what is done in clinical practice, evaluation based on the cycle length should be considered in future. Another approach would be to further improve the tumour growth inhibition model structure and account for the typically observed time delay in the response of the tumour size to drug administration. This time delay might have pharmacokinetic or pharmacodynamic reasons as e.g. the removal of death tumour cells [221].

Further, it was observed that overall the onset of tumour growth was detected relatively late (at week 24 in median). This did also lead to the low number of drop-outs (approximately 30%)

during the study treatment (Figure 3.41), which was significantly lower than in the CEPAC-TDM study (approximately 65%, Figure 3.8). This points towards the need of the inclusion of a resistance term. This resistance would lead to a faster onset of tumour growth in some patients and would lead to a more realistic prediction of drop-outs. The commonly used time-dependent resistance term [124], on the other hand, is not able to account for differences in the onset of resistances due to different dosing schedules, especially increased cycle length due to its empirical character.

Overall, regarding tumour growth inhibition, no significant differences were observed between the dosing scenarios. Nevertheless, those results must be regarded with care and further steps in the model development are needed, to give more reliable answers to the question how dosing and dosing intervals influence tumour size. This includes modelling a description of the time delay in response as well as a resistance term. Further, parameters of the neutropenia model and the tumour growth inhibition model should be estimated simultaneously and a correlation between the response on the bone marrow and on the tumour size (correlation between SL and β_{PTX}) should be investigated. Adverse events as metrics, e.g. change of from baseline (which could be change of neutrophil concentrations from baseline), for efficacy modelling have been suggested [234] and a correlation between adverse events and efficacy was seen for sorafenib [242]. Furthermore, neutropenia and overall survival in patients with advanced small-cell lung cancer treated with classical anticancer drugs were correlated [243]. Even though such correlations may result from drug exposure, investigations of correlations could increase the understanding of the drug action and improve predictive performance of modelling.

Further, for overall survival no significant difference was seen between the dosing scenarios, as well. This was expected, since pharmacokinetics or drug exposure did not directly influence overall survival and the influence of the relative change in tumour size at week 8 was low. The predicted median survival time (10.5 month) was within the range of median survival reported for paclitaxel-carboplatin combination therapy for patients with advance non-small cell lung cancer (8.1 – 10.3 month) [244–246] and the CEPAC-TDM study (9.5 – 10.1 month) [139]. Nevertheless, it is expected that a different treatment would result in a different survival outcome, which was not seen in this analysis. Hence, further influential factors on overall survival such as drug exposure or other tumour size response metrics should be investigated.

Overall, the result of the simulation exercise showed that neither the investigated dose reduction nor the investigated dose interval incensement did sufficiently reduce severe neutropenia. No significant difference, i.e. no compromise, was observed for efficacy, but the results should be regarded with care. Hence, other treatment schedules, as combination of

dose reduction and interval prolongation should be investigated and the model for tumour growth and overall survival should be further improved.

5 Conclusions and perspectives

The overall aim of this work was to contribute to the optimisation of the dose individualisation of paclitaxel/carboplatin combination chemotherapy. NLME modelling was applied to characterise the pharmacokinetics of paclitaxel as well as its toxicity and efficacy in a combination therapy. Toxicity was described as cumulative neutropenia and efficacy was investigated as tumour growth inhibition and overall survival. Finally, simulations combining all developed models were used to investigate how dose reduction compared to increased cycle lengths influenced toxicity and efficacy of the anticancer combination treatment with paclitaxel and carboplatin.

To characterise the pharmacokinetics of paclitaxel, prior modelling knowledge was combined with the CEPAC-TDM study data. This was required since an underprediction of paclitaxel concentrations was found in the external model evaluation. This prior approach allowed to optimise the PK model by re-estimating all PK model parameters. Thus, the model was adjusted for the difference between the CEPAC-TDM study population and the original study population. Without prior information, adequate description of paclitaxel PK would not have been possible due to the sparse PK sampling in the CEPAC-TDM study. Simulations showed that the variability in the optimised PK model was very high, which was also the case in the original model. In combination with the sparse PK sampling, the high variability led to high shrinkage in the individual PK parameter estimates. Thus, individual PK parameters were estimated with low bias but high imprecision. To further optimise the PK model, estimation of correlations between interindividual variability parameters is need in future to avoid predictions of unrealistically high or low exposure. For this step, denser sampling will be needed than had been applied in the original PK study.

In the external model evaluation of the original neutropenia model, using the gold standard model structure, did not adequately describe the observed cumulative neutropenia pattern across the 6 cycles. However, a semi-mechanistic characterisation of the cumulative neutropenia pattern was needed to allow for reasonable predictions of the repeated treatment cycles. Thus, three different model structures, two from literature and a newly developed one, were investigated for their applicability to the CEPAC-TDM neutrophil data and for their physiological plausibility. While, Model A used a time-dependent reduction of the feedback mechanism which was responsible for the recovery of the neutrophil concentrations, to characterise neutropenia, Model B implemented a quiescent cell cycle that was not affected by the chemotherapy. Finally, the newly developed Model C considered the bone marrow exhaustion hypothesis semi-mechanistically by adding at the beginning of the maturation chain

a compartment with slowly proliferating cells affected by both, chemotherapy and feedback. Model C gave the best description of the data as well as the most physiological explanation for the cumulative pattern of neutropenia: The developed model structure gave further evidence on the hypothesis that damage of stem cells causes the cumulative pattern often seen for haematological toxicities in cytotoxic anticancer therapy. Due to the semi-mechanistic character of the model, it can potentially be used to characterise cumulative haematological toxicity on neutrophils and other blood cells caused by different cytotoxic drugs.

The developed neutropenia PK/PD model distinguished between the drug effects of paclitaxel and carboplatin. Since both drugs influence neutropenia, simulations of dose adaptations were more realistic when accounting for the effect of both drugs. However, an additive effect of the drugs was assumed even though synergism was identified and quantified (approximately 50%). Unfortunately, a mechanistic implementation of the combination effect more complex than additive was not possible due to sparse sampling and the lack of carboplatin PK samples. However, model evaluation using the data from the conventional study revealed that the model was sufficient for the prediction of neutropenia, after exposure with doses/drug concentrations used in the CEPAC-TDM study. Hence, simulations within the broad range of the evaluated dosing regimen should be reliable.

To further optimise and evaluate the developed neutropenia PK/PD model, denser neutrophil sampling and PK sampling of all involved drugs would be needed. In addition, neutrophil samples after the end of therapy would be required to characterise the long-term recovery of the patients. By evaluation of such samples, a better understanding of potential causes of cumulative neutropenia could be gained and the bone marrow exhaustion hypothesis implemented in the developed neutropenia model could be evaluated.

Since toxicity only covers one side of the therapeutic window, efficacy was additionally characterised in a PK/PD model for tumour growth inhibition and a time-to-event model for overall survival. The tumour growth inhibition model was rather empirical due to the sparse sampling in the study and included a linear growth of the tumour size and a linear drug-induced decay of tumour size. As seen in simulations, an additional resistance term would be needed to allow for plausible predictions of tumour size development, but was not supported by the CEPAC-TDM study data. Thus, the developed tumour growth inhibition model was only a first step towards adequate description of the development of the tumour size during and after paclitaxel-carboplatin combination therapy. One challenge in further model optimisation is that, for ethical reasons, no placebo study arm is typically available to precisely characterise tumour growth without drug influence. Further, the sparse sampling scheme makes a semi-mechanistic model development difficult. Hence, implementation of prior knowledge from

animal experiments, which typically include denser sampling, might be needed to improve the model.

The second model developed to describe efficacy was an overall survival model. It used the ECOG performance status, the lactate dehydrogenase (LDH) concentration and the relative change in tumour size at week 8 (RS_8) derived from the tumour growth inhibition model as predictors for survival. While the ECOG performance status showed a high influence on survival, which more than doubles the median survival time for patients with better general health, LDH and RS_8 showed lower impact. Investigation of covariates on survival is important to individually plan cancer therapy and to decide on a curative or palliative treatment aim. Thus, further covariates should be investigated, as e.g. the ratio between neutrophil and lymphocyte concentration. Covariate model development should also focus on the chemotherapeutic effect by either implementing PK characteristics (drug concentration-time profile or exposure markers) or tumour response characteristics (e.g. time to tumour growth). While the developed model well described survival resulting from the CEPAC-TDM treatment, further covariates could potentially improve the predictivity for other dosing regimens and populations.

The simulations in Project 4 aimed to investigate the impact of dose reductions based on the dosing algorithm compared to increased dosing intervals. Although these simulations are not yet suitable for concrete dose recommendations, they revealed further steps needed in the characterisation of PK, toxicity and efficacy of the combination chemotherapy with paclitaxel and carboplatin. Additionally, the simulations indicated that both dosing strategies alone are not sufficient to prevent life-threating grade 4 neutropenia for patients with severe toxicity during the first cycle. Thus, after further model optimisation, a combination of both strategies, reduced dose and increased cycle length, should be investigated.

Overall, PK, cumulative neutropenia, tumour growth inhibition and overall survival for the patients in the CEPAC-TDM study were characterised. For this work, a confirmatory phase IV study was not only used for confirmation of a potential improvement of therapy by using the dosing algorithm, but also for additional learning, as suggested by Lewis Sheiner [14]. While the models for efficacy need further optimisation and correlations between interindividual PK parameters should be investigated, the developed semi-mechanistic neutropenia model can potentially help to optimise paclitaxel and other cytotoxic chemotherapies in the future.

6 Abstract/Zusammenfassung

6.1 Abstract

The objective of this thesis was to improve the model-informed treatment of the first-line combination therapy of paclitaxel and carboplatin for patients with advanced non-small cell lung cancer (NSCLC). Further, the aim was to increase the understanding of the relation between pharmacokinetics and the systems dynamics of neutropenia and tumour growth, respectively. Dose individualisation is needed, since paclitaxel in combination with carboplatin, both cytotoxic anticancer drugs, has a narrow therapeutic window with cumulative neutropenia as the dose-limiting toxicity. In addition, high interindividual variability in the pharmacokinetics of paclitaxel increases the risk of exceeding the narrow therapeutic window. A previous analysis has developed a paclitaxel-neutropenia PK/PD model (original model) and a dose individualisation algorithm based on this model [138]. This algorithm was compared in the CEPAC-TDM study, a multicentre, prospective, open-label, randomised, parallel-group study, against a standard body surface area adjusted dosing approach. However, the dosing algorithm has not been able to significantly reduce grade 4 neutropenia. Thus, the data of the CEPAC-TDM study was used in the present work to externally evaluate the original PK/PD model and to optimise and to extend it. The developed PK/PD models should increase understanding of the system dynamics by implementing a coherent and physiologically plausible modelling framework. The aim was then to use these developed models to investigate different dosing strategies with respect to toxicity and efficacy.

In Project 1, the original PK model was externally evaluated using the CEPAC-TDM data, and an underprediction of paclitaxel concentrations was found. This misspecification was corrected by re-estimation of all PK parameters using the prior approach, i.e. considering the information gained in the original PK analysis. The individually predicted PK concentration-time profiles were used to predict the drug effects on neutropenia and tumour growth. In Project 2, cumulative neutropenia was described in a newly developed semi-mechanistic model by considering the bone marrow exhaustion hypothesis, which states that the damage of slowly proliferating haematopoietic stem cells causes the cumulative toxicity pattern. This was an important step towards an optimal and individualised cytotoxic chemotherapy, since the current gold standard model (used in the original model) was not able to describe this pattern.

To optimise therapy based on both sides of the therapeutic window, tumour growth inhibition and overall survival were characterised in Project 3. However, due to the infrequent tumour assessment, tumour size development was described in a rather empirical way. Furthermore,

the influence of the tumour size development (i.e. relative change in tumour size at week 8) on survival was limited but ECOG performance status was identified an important predictor.

Finally, all four developed models were combined to evaluate the impact of dose reduction or increase of the dosing interval on toxicity and efficacy in Project 4. Due to the empirical character of the efficacy model, dose recommendations should be avoided. However, the simulation suggested that none of the investigated strategies sufficiently prevented grade 4 neutropenia yet, but did also not compromise efficacy, thus, a combination of both dosing strategies should be investigated.

6.2 Zusammenfassung

Das Ziel dieser Arbeit war die Verbesserung der modellbasierten Therapie mit der Erstlinienkombination von Paclitaxel und Carboplatin für Patienten mit fortgeschrittenem nichtkleinzelligem Lungenkarzinom. Des Weiteren war das Ziel, das Verständnis über die Pharmakokinetik und des dynamischen Systems von Neutropenie und Tumorwachstum zu verbessern. Dosisindividualisierung ist erforderlich, da Paclitaxel in Kombination mit Carboplatin, beides zytotoxische Arzneistoffe, ein enges therapeutisches Fenster mit kumulativer Neutropenie als dosislimitierende Toxizität aufweist. Zusätzlich unterliegt die Pharmakokinetik von Paclitaxel einer hohen interindividuellen Variabilität, was das Risiko erhöht, das enge therapeutische Fenster zu verlassen. Eine vorherige Datenanalyse hat ein Paclitaxel/Neutropenie-PK/PD-Modell (Originalmodell) und darauf basierend einen Dosisindividualisierungsalgorithmus entwickelt [138]. Dieser Algorithmus wurde in der CEPAC-TDM-Studie mit einer körperoberflächenbasierten Standardmethode verglichen. Dieser Dosisalgorithmus war jedoch nicht in der Lage, Grad-4-Neutropenie signifikant zu reduzieren. Daher wurden die Daten der CEPAC-TDM-Studie, einer multizentrischen, prospektiven, nicht verblindeten, randomisierten Studie mit parallelen Gruppen, in der vorliegenden Arbeit genutzt, um das originale PK/PD-Modell extern zu evaluieren, zu optimieren und zu erweitern. Die entwickelten PK/PD-Modelle sollten das Verständnis über das dynamische System durch die Implementierung einer schlüssigen und physiologisch plausiblen Struktur erweitern. Das Ziel war schließlich, die so entwickelten Modelle zu nutzen, um verschiedene Dosisstrategien in Bezug auf Toxizität und Wirksamkeit zu untersuchen.

In Projekt 1 wurde das Original-PK-Modell mittels der Daten der CEPAC-TDM-Studie extern evaluiert und eine Unterschätzung der Paclitaxelkonzentrationen gefunden. Diese Missspezifikation wurde durch Neuschätzung aller PK-Parameter mittels des „Prior-Ansatzes“ korreliert, d.h., dass die Informationen, die in der originalen PK-Analyse gewonnen wurden, berücksichtigt wurden. Die individuell vorhergesagten PK-Konzentrations-Zeitprofile wurden genutzt, um den Arzneistoffeffekt auf die Neutropenie und das Tumorwachstum vorherzusagen. In Project 2 wurde die kumulative Neutropenie mittels eines neu entwickelten, semimechanistischen Modells unter Berücksichtigung der Hypothese der Knochenmarksdepression, welche besagt, dass die Schädigung der sich langsam teilenden hämatopoetischen Stammzellen kumulative Toxizitätsmuster verursacht, beschrieben. Dies war ein bedeutender Schritt in Richtung einer optimalen und individualisierten zytotoxischen Chemotherapie, da das derzeitige Goldstandardmodell (welches im Originalmodell genutzt wurde) nicht in der Lage war, dieses Muster zu beschreiben.

Um die Therapie basierend auf beiden Grenzen des therapeutischen Fensters zu optimieren, wurden die Tumorwachstumsinhibition und das Gesamtüberleben in Projekt 3 charakterisiert.

Auf Grund der seltenen Tumorgrößenbestimmung wurde die Entwicklung der Tumorgröße jedoch eher empirisch beschrieben. Der Einfluss der Tumorgrößenentwicklung (d.h. der relativen Änderung der Tumorgröße in Woche 8) auf das Überleben war begrenzt, aber der ECOG-Performance-Status wurde als wichtiger Prädiktor identifiziert.

Schlussendlich wurden alle vier entwickelten Modelle kombiniert, um den Einfluss von Dosisreduktion oder verlängertem Dosisintervall auf Toxizität und Wirksamkeit in Projekt 4 zu untersuchen. Aufgrund des empirischen Charakters des Wirksamkeitsmodells sollten Dosisempfehlungen vermieden werden. Die Simulationen zeigten dennoch, dass keine der untersuchten Dosierungsstrategien eine Grad-4-Neutropenie bis jetzt ausreichend verhindern konnte, aber auch die Wirksamkeit der Therapie nicht einschränkten; daher sollte eine Kombination beider Dosierungsstrategien untersucht werden.

7 References

[1] M. Simeoni, P. Magni, C. Cammia, G. De Nicolao, V. Croci, E. Pesenti, M. Germani, I. Poggesi, M. Rocchetti. Predictive pharmacokinetic-pharmacodynamic modeling of tumor growth kinetics in xenograft models after administration of anticancer agents. Cancer Res., 64: 1094–1101 (2004).

[2] P.J. Williams, A. Desai, E. Ette. The role of pharmacometrics in cardiovascular drug development. In: Cardiac drug development guide. Humana Press, New York, New York, 1st ed.: 365–387 (2003).

[3] S.F. Marshall, R. Burghaus, V. Cosson, S.Y.A. Cheung, M. Chenel, O. DellaPasqua, N. Frey, B. Hamrén, L. Harnisch, F. Ivanow, T. Kerbusch, J. Lippert, P.A. Milligan, S. Rohou, A. Staab, J.L. Steimer, C. Tornøe, S.A.G. Visser. Good Practices in Model-Informed Drug Discovery and Development: Practice, Application, and Documentation. CPT Pharmacometrics Syst. Pharmacol., 5: 93–122 (2016).

[4] Food and Drug Administration. Challenge and opportunity on the critical path to new medical products. Silver Spring, Maryland: 1–31 (2004).

[5] T. Shepard. Role of modeling and simulation in regulatory decision maing in Europe. http://www.ema.europa.eu/docs/en_GB/document_library/Presentation/2011/11/WC500118262.pdf, London (2012).

[6] L.B. Sheiner, S.L. Beal. Evaluation of methods for estimating population pharmacokinetics parameters. I. Michaelis-Menten model: routine clinical pharmacokinetic data. J. Pharmacokinet. Biopharm., 8: 553–571 (1980).

[7] L.B. Sheiner, S.L. Beal. Evaluation of methods for estimating population pharmacokinetic parameters. II. Biexponential model and experimental pharmacokinetic data. J. Pharmacokinet. Biopharm., 9: 635–651 (1981).

[8] E. Ette, P. Williams. Pharmacometrics: the science of quantitative pharmacology. John Wiley & Sons, Inc, Hoboken, New Jersey, 1st ed. (2007).

[9] G. Levy, L.E. Hollister. Inter- and intrasubject variations in drug absorption kinetics. J. Pharm. Sci., 53: 1446–1452 (1964).

[10] L.B. Sheiner, B. Rosenberg, K.L. Melmon. Modelling of individual pharmacokinetics for computer-aided drug dosage. Comput. Biomed. Res., 5: 441–459 (1972).

[11] L.B. Sheiner, S.L. Beal. Evaluation of methods for estimating population pharmacokinetic parameters. III. Monoexponential model: routine clinical

pharmacokinetic data. J. Pharmacokinet. Biopharm., 11: 303–319 (1983).

[12] P.L. Bonate. Pharmacokinetic-pharmacodynamic modeling and simulation. Springer Science+Business Media, New York, New York, 2nd ed. (2011).

[13] R. Bies, S. Cook, S. Duffull. The pharmacometrician's dilemma: the tension between mechanistic and empirical approaches in mathematical modelling and simulation - a continuation of the age-old dispute between rationalism and empiricism? Br. J. Clin. Pharmacol., 82: 580–582 (2016).

[14] L.B. Sheiner. Learning versus confirming in clinical drug development. Clin. Pharmacol. Ther., 61: 275–291 (1997).

[15] J. V Gobburu, P.J. Marroum. Utilisation of pharmacokinetic-pharmacodynamic modelling and simulation in regulatory decision-making. Clin. Pharmacokinet., 40: 883–892 (2001).

[16] B. Ribba, G. Kaloshi, M. Peyre, D. Ricard, V. Calvez, M. Tod, B. Čajavec-Bernard, A. Idbaih, D. Psimaras, L. Dainese, J. Pallud, S. Cartalat-Carel, J.Y. Delattre, J. Honnorat, E. Grenier, F. Ducray. A tumor growth inhibition model for low-grade glioma treated with chemotherapy or radiotherapy. Clin. Cancer Res., 18: 5071–5080 (2012).

[17] W.E. Evans, M. V. Relling, J.H. Rodman, W.R. Crom, J.M. Boyett, C.-H. Pui. Conventional compared with individualized chemotherapy for childhood acute lymphoblastic leukemia. N. Engl. J. Med., 338: 499–505 (1998).

[18] D.R. Mould, G. D'Haens, R.N. Upton. Clinical decision support tools: the evolution of a revolution. Clin. Pharmacol. Ther., 99: 405–418 (2016).

[19] S.B. Duffull, D.F.B. Wright. What do we learn from repeated population analyses? Br. J. Clin. Pharmacol., 79: 40–47 (2015).

[20] M. Hay, D.W. Thomas, J.L. Craighead, C. Economides, J. Rosenthal. Clinical development success rates for investigational drugs. Nat. Biotechnol., 32: 40–51 (2014).

[21] A. Felici, J. Verweij, A. Sparreboom. Dosing strategies for anticancer drugs: the good, the bad and body-surface area. Eur. J. Cancer, 38: 1677–1684 (2002).

[22] J. Gabrielsson, F.D. Gibbons, L.A. Peletier. Mixture dynamics: Combination therapy in oncology. Eur. J. Pharm. Sci., 88: 132–146 (2016).

[23] A.S. Zandvliet, J.H.M. Schellens, J.H. Beijnen, A.D.R. Huitema. Population pharmacokinetics and pharmacodynamics for treatment optimization in clinical oncology. Clin. Pharmacokinet., 47: 487–513 (2008).

[24] World Health Organization. Global health risks: Mortality and burden of disease attributable to selected major risks. Geneva: 1–62 (2009).

[25] Robert Koch Institute. Cancer in Germany 2009/2010. Berlin, 9th ed.: 1–144 (2014).

[26] R.L. Siegel, K.D. Miller, A. Jemal. Cancer statistics. CA Cancer J Clin, 66: 7–30 (2016).

[27] International Agency for Research on Cancer, World Health Organization. World cancer report 2014. Lyon: 1–630 (2014).

[28] A. Jemal, F. Bray, M.M. Center, J. Ferlay, E. Ward, D. Forman. Global cancer statistics. CA. Cancer J. Clin., 61: 69–90 (2011).

[29] M. Ezzati, A.D. Lopez. Estimates of global mortality attributable to smoking in 2000. Lancet, 362: 847–852 (2003).

[30] S. Peters, A.A. Adjei, C. Gridelli, M. Reck, K. Kerr, E. Felip. Metastatic non-small-cell lung cancer (NSCLC): ESMO Clinical Practice Guidelines for diagnosis, treatment and follow-up. Ann. Oncol., 23 Suppl 7: vii56-vii64 (2012).

[31] American Cancer Society. Cancer facts & figures 2016. Atlanta, Georgia: 1–9 (2016).

[32] A.S. Narang, D.S. Desai. Anticancer drug development. In: Pharmaceutical perspectives of cancer therapeutics. Springer US, New York, New York, 1st ed.: 49–92 (2009).

[33] D. Hanahan, R.A. Weinberg. The Hallmarks of Cancer. Cell, 100: 57–70 (2000).

[34] D. Hanahan, R.A. Weinberg. Hallmarks of cancer: The next generation. Cell, 144: 646–674 (2011).

[35] National Cancer Institute. Common terminology criteria for adverse events (CTCAE) version 4.03. Bethesda, Maryland: 1–194 (2010).

[36] M.M. Oken, R.H. Creech, D.C. Tormey, J. Horton, T.E. Davis, E.T. McFadden, P.P. Carbone. Toxicity and response criteria of the Eastern Cooperative Oncology Group. Am. J. Clin. Oncol., 5: 649–655 (1982).

[37] D. Cross, J.K. Burmester. The promise of molecular profiling for cancer identification and treatment. Clin. Med. Res., 2: 147–50 (2004).

[38] Deutsche Gesellschaft für Hämatologie und Medizinische Onkologie. Leitlinie Lungenkarzinom, nicht-kleinzellig (NSCLC). Berlin: 1–48 (2010).

[39] G. D'Addario, E. Felip. Non-small-cell lung cancer: ESMO clinical recommendations for diagnosis, treatment and follow-up. Ann. Oncol., 20 Suppl 4: 68–70 (2009).

[40] J. Vansteenkiste, L. Crinò, C. Dooms, J.Y. Douillard, C. Faivre-Finn, E. Lim, G. Rocco,

S. Senan, P. van Schil, G. Veronesi, R. Stahel, S. Peters, E. Felip, K. Kerr, B. Besse, W. Eberhardt, M. Edelman, T. Mok, K. O'Byrne, S. Novello, L. Bubendorf, A. Marchetti, P. Baas, M. Reck, K. Syrigos, L. Paz-Ares, E.F. Smit, P. Meldgaard, A. Adjei, M. Nicolson, W. Weder, D. de Ruysscher, C. Le Pechoux, P. de Leyn, V. Westeel. 2nd ESMO consensus conference on lung cancer: Early-stage non-small-cell lung cancer consensus on diagnosis, treatment and follow-up. Ann. Oncol., 25: 1462–1474 (2014).

[41] W.E.E. Eberhardt, D. De Ruysscher, W. Weder, C. Le Péchoux, P. De Leyn, H. Hoffmann, V. Westeel, R. Stahel, E. Felip, S. Peters, Panel Members. 2nd ESMO Consensus Conference in Lung Cancer: locally advanced stage III non-small-cell lung cancer. Ann. Oncol. Off. J. Eur. Soc. Med. Oncol., 26: 1573–1588 (2015).

[42] G.A. Orr, P. Verdier-Pinard, H. McDaid, S.B. Horwitz. Mechanisms of taxol resistance related to microtubules. Oncogene, 22: 7280–7295 (2003).

[43] S.B. Horwitz, L. Lothstein, J.J. Manfredi, W. Mellado, J. Parness, S.N. Roy, P.B. Schiff, L. Sorbara, R. Zeheb. Taxol: mechanisms of action and resistance. Ann. N. Y. Acad. Sci., 466: 733–744 (1986).

[44] M.A. Jordan, L. Wilson. Microtubules as a target for anticancer drugs. Nat. Rev. Cancer, 4: 253–265 (2004).

[45] J.E. Liebmann, J. a Cook, C. Lipschultz, D. Teague, J. Fisher, J.B. Mitchell. Cytotoxic studies of paclitaxel (Taxol) in human tumour cell lines. Br. J. Cancer, 68: 1104–1109 (1993).

[46] E.A. Eisenhauer, W.W. ten Bokkel Huinink, K.D. Swenerton, L. Gianni, J. Myles, M.E. van der Burg, I. Kerr, J.B. Vermorken, K. Buser, N. Colombo. European-Canadian randomized trial of paclitaxel in relapsed ovarian cancer: high-dose versus low-dose and long versus short infusion. J. Clin. Oncol., 12: 2654–2666 (1994).

[47] T.-C. Huang, T.C. Campbell. Comparison of weekly versus every 3 weeks paclitaxel in the treatment of advanced solid tumors: a meta-analysis. Cancer Treat. Rev., 38: 613–617 (2012).

[48] T.M. Mekhail, M. Markman. Paclitaxel in cancer therapy. Expert Opin. Pharmacother., 3: 755–766 (2002).

[49] R.Z. Yusuf, Z. Duan, D.E. Lamendola, R.T. Penson, M. V Seiden. Paclitaxel resistance: molecular mechanisms and pharmacologic manipulation. Curr. Cancer Drug Targets, 3: 1–19 (2003).

[50] R.T. Dorr. Pharmacology and toxicology of Cremophor EL diluent. Ann. Pharmacother., 28: S11–S14 (1994).

[51] R.B. Weiss, R.C. Donehower, P.H. Wiernik, T. Ohnuma, R.J. Gralla, D.L. Trump, J.R. Baker, D. a Van Echo, D.D. Von Hoff, B. Leyland-Jones. Hypersensitivity reactions from taxol. J. Clin. Oncol., 8: 1263–1268 (1990).

[52] A. Sparreboom, L. van Zuylen, E. Brouwer, W.J. Loos, P. de Bruijn, H. Gelderblom, M. Pillay, K. Nooter, G. Stoter, J. Verweij. Cremophor EL-mediated alteration of paclitaxel distribution in human blood: clinical pharmacokinetic implications. Cancer Res., 59: 1454–1457 (1999).

[53] A.J. ten Tije, J. Verweij, W.J. Loos, A. Sparreboom. Pharmacological effects of formulation vehicles: implications for cancer chemotherapy. Clin. Pharmacokinet., 42: 665–85 (2003).

[54] D. Kessel. Properties of cremophor EL micelles probed by fluorescence. Photochem. Photobiol., 56: 447–451 (1992).

[55] L. van Zuylen, L. Gianni, J. Verweij, K. Mross, E. Brouwer, W.J. Loos, A. Sparreboom. Inter-relationships of paclitaxel disposition, infusion duration and cremophor EL kinetics in cancer patients. Anticancer. Drugs, 11: 331–337 (2000).

[56] L. Gianni, C.M. Kearns, A. Giani, G. Capri, L. Viganó, A. Lacatelli, G. Bonadonna, M.J. Egorin. Nonlinear pharmacokinetics and metabolism of paclitaxel and its pharmacokinetic/pharmacodynamic relationships in humans. J. Clin. Oncol., 13: 180–190 (1995).

[57] J.J. Manfredi, J. Parness, S.B. Horwitz. Taxol binds to cellular microtubules. J. Cell Biol., 94: 688–696 (1982).

[58] H.J. Kuh, S.H. Jang, M.G. Wientjes, J.L. Au. Computational model of intracellular pharmacokinetics of paclitaxel. J. Pharmacol. Exp. Ther., 293: 761–770 (2000).

[59] E. Brouwer, J. Verweij, P. De Bruijn, W.J. Loos, M. Pillay, D. Buijs, A. Sparreboom. Measurement of fraction unbound paclitaxel in human plasma. Drug Metab. Dispos., 28: 1141–1145 (2000).

[60] G.N. Kumar, U.K. Walle, K.N. Bhalla, T. Walle. Binding of taxol to human plasma, albumin and alpha 1-acid glycoprotein. Res. Commun. Chem. Pathol. Pharmacol., 80: 337–344 (1993).

[61] P.H. Wiernik, E.L. Schwartz, A. Einzig, J.J. Strauman, R.B. Lipton, J.P. Dutcher. Phase I trial of taxol given as a 24-hour infusion every 21 days: responses observed in metastatic melanoma. J. Clin. Oncol., 5: 1232–1239 (1987).

[62] O. van Tellingen, M.T. Huizing, V.R. Panday, J.H. Schellens, W.J. Nooijen, J.H. Beijnen. Cremophor EL causes (pseudo-) non-linear pharmacokinetics of paclitaxel in patients.

Br. J. Cancer, 81: 330–335 (1999).

[63] M.D. Wild, U.K. Walle, T. Walle. Extensive and saturable accumulation of paclitaxel by the human platelet. Cancer Chemother. Pharmacol., 36: 41–44 (1995).

[64] S.M. Longnecker, R.C. Donehower, A.E. Cates, T.L. Chen, R.B. Brundrett, L.B. Grochow, D.S. Ettinger, M. Colvin. High-performance liquid chromatographic assay for taxol in human plasma and urine and pharmacokinetics in a phase I trial. Cancer Treat. Rep., 71: 53–59 (1987).

[65] T. Brown, K. Havlin, G. Weiss, J. Cagnola, J. Koeller, J. Kuhn, J. Rizzo, J. Craig, J. Phillips, D. Von Hoff. A phase I trial of taxol given by a 6-hour intravenous infusion. J. Clin. Oncol., 9: 1261–1267 (1991).

[66] N.F. Smith, M.R. Acharya, N. Desai, W.D. Figg, A. Sparreboom. Identification of OATP1B3 as a high-affinity hepatocellular transporter of paclitaxel. Cancer Biol. Ther., 4: 815–818 (2005).

[67] B. Monsarrat, E. Mariel, S. Cros, M. Garès, D. Guénard, F. Guéritte-Voegelein, M. Wright. Taxol metabolism. Isolation and identification of three major metabolites of taxol in rat bile. Drug Metab. Dispos., 18: 895–901 (1990).

[68] M.T. Huizing, A.C.F. Keung, H. Rosing, V. van der Kuij, W.W. ten Bokkel Huinink, I.M. Mandjes, A.C. Dubbelman, H.M. Pinedo, J.H. Beijnen. Pharmacokinetics of paclitaxel and metabolites in a randomized comparative study in platinum-pretreated ovarian cancer patients. J. Clin. Oncol., 11: 2127–2135 (1993).

[69] A. Sparreboom, M.T. Huizing, J.J. Boesen, W.J. Nooijen, O. van Tellingen, J.H. Beijnen. Isolation, purification, and biological activity of mono- and dihydroxylated paclitaxel metabolites from human feces. Cancer Chemother. Pharmacol., 36: 299–304 (1995).

[70] M. Joerger, A.D.R. Huitema, D.H.J.G. van den Bongard, J.H.M. Schellens, J.H. Beijnen. Quantitative effect of gender, age, liver function, and body size on the population pharmacokinetics of paclitaxel in patients with solid tumors. Clin. Cancer Res., 12: 2150–2157 (2006).

[71] M. Joerger, A.D.R. Huitema, M.T. Huizing, P.H.B. Willemse, A. de Graeff, H. Rosing, J.H.M. Schellens, J.H. Beijnen, J.B. Vermorken. Safety and pharmacology of paclitaxel in patients with impaired liver function: a population pharmacokinetic-pharmacodynamic study. Br. J. Clin. Pharmacol., 64: 622–633 (2007).

[72] D.S. Sonnichsen, Q. Liu, E.G. Schuetz, J.D. Schuetz, A. Pappo, M. V Relling. Variability in human cytochrome P450 paclitaxel metabolism. J. Pharmacol. Exp. Ther., 275: 566–575 (1995).

[73] C. Rodríguez-Antona. Pharmacogenomics of paclitaxel. Pharmacogenomics, 11: 621–623 (2010).

[74] A. Andersson, J. Fagerberg, R. Lewensohn, H. Ehrsson. Pharmacokinetics of cisplatin and its monohydrated complex in humans. J. Pharm. Sci., 85: 824–827 (1996).

[75] F.E. de Jongh, J.M. Gallo, M. Shen, J. Verweij, A. Sparreboom. Population pharmacokinetics of cisplatin in adult cancer patients. Cancer Chemother. Pharmacol., 54: 105–112 (2004).

[76] S. Dasari, P. Bernard Tchounwou. Cisplatin in Cancer therapy: Molecular mechanisms of action. Eur. J. Pharmacol., 740: 364–378 (2014).

[77] R.C. DeConti, B.R. Toftness, R.C. Lange, W.A. Creasey. Clinical and Pharmacological Studies with cis-Diamminedichloroplatinum(II). Cancer Res., 33: 1310–1315 (1973).

[78] E.K. Rowinsky, M.R. Gilbert, W.P. McGuire, D.A. Noe, L.B. Grochow, A.A. Forastiere, D.S. Ettinger, B.G. Lubejko, B. Clark, S.E. Sartorius. Sequences of taxol and cisplatin: a phase I and pharmacologic study. J. Clin. Oncol., 9: 1692–1703 (1991).

[79] E. Wong, C.M. Giandomenico. Current status of platinum-based antitumor drugs. Chem. Rev., 99: 2451–2466 (1999).

[80] A.H. Calvert, D.R. Newell, L.A. Gumbrell, S. O'Reilly, M. Burnell, F.E. Boxall, Z.H. Siddik, I.R. Judson, M.E. Gore, E. Wiltshaw. Carboplatin dosage: prospective evaluation of a simple formula based on renal function. J. Clin. Oncol., 7: 1748–1756 (1989).

[81] D.W. Cockcroft, Gault M.H. Prediction of creatinine clearance from serum creatinine. Nephron, 16: 31–41 (1979).

[82] W.J. van der Vijgh. Clinical pharmacokinetics of carboplatin. Clin. Pharmacokinet., 21: 242–261 (1991).

[83] D.A. Van Echo, M.J. Egorin, M.Y. Whitacre, E.A. Olman, J. Aisner. Phase I clinical and pharmacologic trial of carboplatin daily for 5 days. Cancer Treat. Rep., 68: 1103–1114 (1984).

[84] A.J. Wagstaff, A. Ward, P. Benfield, R.C. Heel. Carboplatin. A preliminary review of its pharmacodynamic and pharmacokinetic properties and therapeutic efficacy in the treatment of cancer. Drugs, 37: 162–190 (1989).

[85] T.C. Shea, M. Flaherty, A. Elias, J.P. Eder, K. Antman, C. Begg, L. Schnipper, E. Frei, W.D. Henner. A phase I clinical and pharmacokinetic study of carboplatin and autologous bone marrow support. J. Clin. Oncol., 7: 651–661 (1989).

[86] G.A. Curt, J.J. Grygiel, B.J. Corden, R.F. Ozols, R.B. Weiss, D.T. Tell, C.E. Myers, J.M.

Collins. A phase I and pharmacokinetic study of diamminecyclobutane-dicarboxylatoplatinum (NSC 241240). Cancer Res., 43: 4470–4473 (1983).

[87] S.J. Harland, D.R. Newell, Z.H. Siddik, R. Chadwick, A.H. Calvert, K.R. Harrap. Pharmacokinetics of cis-diammine-1,1-cyclobutane dicarboxylate platinum(II) in patients with normal and impaired renal function. Cancer Res., 44: 1693–1697 (1984).

[88] J.M. Koeller, D.L. Trump, K.D. Tutsch, R.H. Earhart, T.E. Davis, D.C. Tormey. Phase I clinical trial and pharmacokinetics of carboplatin (NSC 241240) by single monthly 30-minute infusion. Cancer, 57: 222–225 (1986).

[89] R.E. Sanborn. Cisplatin versus carboplatin in NSCLC: is there one “best” answer? Curr. Treat. Options Oncol., 9: 326–342 (2008).

[90] M.T. Huizing, G. Giaccone, L.J. van Warmerdam, H. Rosing, P.J. Bakker, J.B. Vermorken, P.E. Postmus, N. van Zandwijk, M.G. Koolen, W.W. ten Bokkel Huinink, W.J. van der Vijgh, F.J. Bierhorst, A. Lai, O. Dalesio, H.M. Pinedo, C.H. Veenhof, J.H. Beijnen. Pharmacokinetics of paclitaxel and carboplatin in a dose-escalating and dose-sequencing study in patients with non-small-cell lung cancer. The European Cancer Centre. J. Clin. Oncol., 15: 317–329 (1997).

[91] A.I. de Vos, K. Nooter, J. Verweij, W.J. Loos, E. Brouwer, P. de Bruijn, E.J. Ruijgrok, M.E. van der Burg, G. Stoter, A. Sparreboom. Differential modulation of cisplatin accumulation in leukocytes and tumor cell lines by the paclitaxel vehicle cremophor EL. Ann. Oncol., 8: 1145–1150 (1997).

[92] K.C. Micetich, D. Barnes, L.C. Erickson. A comparative study of the cytotoxicity and DNA-damaging effects of cis-(diammino)(1,1-cyclobutanedicarboxylato)-platinum(II) and cis-diamminedichloroplatinum(II) on L1210 cells. Cancer Res., 45: 4043–4047 (1985).

[93] M. Kondo, A.J. Wagers, M.G. Manz, S.S. Prohaska, D.C. Scherer, G.F. Beilhack, J.A. Shizuru, I.L. Weissman. Biology of hematopoietic stem cells and progenitors: implications for clinical application. Annu. Rev. Immunol., 21: 759–806 (2003).

[94] S.N. Catlin, L. Busque, R.E. Gale, P. Guttorp, J.L. Abkowitz. The replication rate of human hematopoietic stem cells in vivo. Blood, 117: 4460–4466 (2011).

[95] D. Dingli, A. Traulsen, J.M. Pacheco. Compartmental architecture and dynamics of hematopoiesis. PLoS One, 2: e345 (2007).

[96] B.E. Shepherd, P. Guttorp, P.M. Lansdorp, J.L. Abkowitz. Estimating human hematopoietic stem cell kinetics using granulocyte telomere lengths. Exp. Hematol., 32: 1040–1050 (2004).

[97] B.I. Lord. Myeloid cell kinetics in response to haemopoietic growth factors. Baillieres Clin Haematol, 5: 533–550 (1992).

[98] C.A. Finch, L.A. Harker, J.D. Cook. Kinetics of the formed elements of human blood. Blood, 50: 699–707 (1977).

[99] J.T. Dancey, K.A. Deubelbeiss, L.A. Harker, C.A. Finch. Neutrophil kinetics in man. J. Clin. Invest., 58: 705–715 (1976).

[100] G.E. Cartwright, J.W. Athens, M.M. Wintrobe. The kinetics of granulopoiesis in normal man. Blood, 24: 780–803 (1964).

[101] M.R. Howard, P.J. Hamilton. Haematology an illustrated colour text. Elsevier Ltd., 4th ed. (2013).

[102] Y. Oki, J.-P. Issa. Hematopoietic growth factors in oncology. Springer US, Boston, Maryland, 1st ed. (2011).

[103] R.E. Parchment, M. Gordon, C.K. Grieshaber, C. Sessa, D. Volpe, M. Ghielmini. Predicting hematological toxicity (myelosuppression) of cytotoxic drug therapy from in vitro tests. Ann. Oncol. Off. J. Eur. Soc. Med. Oncol., 9: 357–364 (1998).

[104] V.C. Nock. Processes in the haematopoietic system and blood: Leukocyte progenitor proliferation and maturation in vitro and in cancer Patients and erythrocyte ageing. Freie Universität Berlin (2013).

[105] I.F. Tannock. Experimental chemotherapy and concepts related to the cell cycle. Int. J. Radiat. Biol. Relat. Stud. Phys. Chem. Med., 49: 335–355 (1986).

[106] R.B. Weiss, B.F. Issell. The nitrosoureas: carmustine (BCNU) and lomustine (CCNU). Cancer Treat. Rev., 9: 313–330 (1982).

[107] P.J. O'Brien. Molecular mechanisms of quinone cytotoxicity. Chem. Biol. Interact., 80: 1–41 (1991).

[108] N. Touroutoglou, D. Gravel, M.N. Raber, W. Plunkett, J.L. Abbruzzese. Clinical results of a pharmacodynamically-based strategy for higher dosing of gemcitabine in patients with solid tumors. Ann. Oncol., 9: 1003–1008 (1998).

[109] D.S. Alberts. Protection by amifostine of cyclophosphamide-induced myelosuppression. Semin. Oncol., 26: 37–40 (1999).

[110] A.M. Mauer, E.H. Kraut, S.A. Krauss, R.H. Ansari, K. Kasza, L. Szeto, E.E. Vokes. Phase II trial of oxaliplatin, leucovorin and fluorouracil in patients with advanced carcinoma of the esophagus. Ann. Oncol., 16: 1320–1325 (2005).

[111] P. Mauch, L. Constine, J. Greenberger, W. Knospe, J. Sullivan, J.L. Liesveld, H.J. Deeg.

Hematopoietic stem cell compartment: acute and late effects of radiation therapy and chemotherapy. Int. J. Radiat. Oncol. Biol. Phys., 31: 1319–1339 (1995).

[112] R. Maze, T. Moritz, D.A. Williams. Increased survival and multilineage hematopoietic protection from delayed and severe myelosuppressive effects of a nitrosourea with recombinant interleukin-11. Cancer Res., 54: 4947–4951 (1994).

[113] R. van Os, S. Robinson, T. Sheridan, J.M. Mislow, D. Dawes, P.M. Mauch. Granulocyte colony-stimulating factor enhances bone marrow stem cell damage caused by repeated administration of cytotoxic agents. Blood, 92: 1950–1956 (1998).

[114] L.E. Friberg, M.O. Karlsson. Mechanistic models for myelosuppression. Invest. New Drugs, 21: 183–194 (2003).

[115] H. Minami, Y. Sasaki, N. Saijo, T. Ohtsu, H. Fujii, T. Igarashi, K. Itoh. Indirect-response model for the time course of leukopenia with anticancer drugs. Clin. Pharmacol. Ther., 64: 511–521 (1998).

[116] L.E. Friberg, C.J. Brindley, M.O. Karlsson, A.J. Devlin. Models of schedule dependent haematological toxicity of 2'-deoxy-2'-methylidenecytidine (DMDC). Eur. J. Clin. Pharmacol., 56: 567–574 (2000).

[117] L.E. Friberg, A. Freijs, M. Sandström, M.O. Karlsson. Semiphysiological model for the time course of leukocytes after varying schedules of 5-fluorouracil in rats. J. Pharmacol. Exp. Ther., 295: 734–740 (2000).

[118] W.C. Zamboni, D.Z. D'Argenio, C.F. Stewart, T. MacVittie, B.J. Delauter, A.M. Farese, D.M. Potter, N.M. Kubat, D. Tubergen, M.J. Egorin. Pharmacodynamic model of topotecan-induced time course of neutropenia. Clin. Cancer Res., 7: 2301–2308 (2001).

[119] L.E. Friberg, A. Henningsson, H. Maas, L. Nguyen, M.O. Karlsson. Model of chemotherapy-induced myelosuppression with parameter consistency across drugs. J. Clin. Oncol., 20: 4713–4721 (2002).

[120] L.E. Friberg, M. Sandström, M.O. Karlsson. Scaling the time-course of myelosuppression from rats to patients with a semi-physiological model. Invest. New Drugs, 28: 744–753 (2010).

[121] B.C. Bender, F. Schaedeli-Stark, R. Koch, A. Joshi, Y.-W. Chu, H. Rugo, I.E. Krop, S. Girish, L.E. Friberg, M. Gupta. A population pharmacokinetic/pharmacodynamic model of thrombocytopenia characterizing the effect of trastuzumab emtansine (T-DM1) on platelet counts in patients with HER2-positive metastatic breast cancer. Cancer Chemother. Pharmacol., 70: 591–601 (2012).

[122] V. Mangas-Sanjuan, N. Buil-Bruna, M.J. Garrido, E. Soto, I.F. Trocóniz.

Semimechanistic cell-cycle type-based pharmacokinetic/pharmacodynamic model of chemotherapy-induced neutropenic effects of diflomotecan under different dosing schedules. J. Pharmacol. Exp. Ther., 354: 55–64 (2015).

[123] E.A. Eisenhauer, P. Therasse, J. Bogaerts, L.H. Schwartz, D. Sargent, R. Ford, J. Dancey, S. Arbuck, S. Gwyther, M. Mooney, L. Rubinstein, L. Shankar, L. Dodd, R. Kaplan, D. Lacombe, J. Verweij. New response evaluation criteria in solid tumours: revised RECIST guideline (version 1.1). Eur. J. Cancer, 45: 228–247 (2009).

[124] B. Ribba, N.H.G. Holford, P. Magni, I.F. Trocóniz, I. Gueorguieva, P. Girard, C. Sarr, M. Elishmereni, C. Kloft, L.E. Friberg. A review of mixed-effects models of tumor growth and effects of anticancer drug treatment used in population analysis. CPT Pharmacometrics Syst. Pharmacol., 3: e113 (2014).

[125] D.R. Mould, A.-C. Walz, T. Lave, J.P. Gibbs, B. Frame. Developing exposure/response models for anticancer drug treatment: Special considerations. CPT Pharmacometrics Syst. Pharmacol., 4: 1–16 (2015).

[126] L. Claret, P. Girard, P.M. Hoff, E. Van Cutsem, K.P. Zuideveld, K. Jorga, J. Fagerberg, R. Bruno. Model-based prediction of phase III overall survival in colorectal cancer on the basis of phase II tumor dynamics. J. Clin. Oncol., 27: 4103–4108 (2009).

[127] A.A. Suleiman, L. Nogova, U. Fuhr. Modeling NSCLC progression: recent advances and opportunities available. AAPS J., 15: 542–550 (2013).

[128] H. Gurney. Dose calculation of anticancer drugs: a review of the current practice and introduction of an alternative. J. Clin. Oncol., 14: 2590–2611 (1996).

[129] S.D. Baker, J. Verweij, E.K. Rowinsky, R.C. Donehower, J.H.M. Schellens, L.B. Grochow, A. Sparreboom. Role of body surface area in dosing of investigational anticancer agents in adults, 1991-2001. J. Natl. Cancer Inst., 94: 1883–1888 (2002).

[130] S.A. Kaestner, G.J. Sewell. Chemotherapy dosing part I: scientific basis for current practice and use of body surface area. Clin. Oncol., 19: 23–37 (2007).

[131] S.D. Baker, R.B. Diasio, S. O'Reilly, V.S. Lucas, S.P. Khor, S.E. Sartorius, R.C. Donehower, L.B. Grochow, T. Spector, J.A. Hohneker, E.K. Rowinsky. Phase I and pharmacologic study of oral fluorouracil on a chronic daily schedule in combination with the dihydropyrimidine dehydrogenase inactivator eniluracil. J. Clin. Oncol., 18: 915–926 (2000).

[132] J.S. de Bono, J. Stephenson, S.D. Baker, M. Hidalgo, A. Patnaik, L.A. Hammond, G. Weiss, A. Goetz, L. Siu, C. Simmons, J. Jolivet, E.K. Rowinsky. Troxacitabine, an L-stereoisomeric nucleoside analog, on a five-times-daily schedule: a phase I and

pharmacokinetic study in patients with advanced solid malignancies. J. Clin. Oncol., 20: 196–109 (2002).

[133] C.H. Smorenburg, A. Sparreboom, M. Bontenbal, G. Stoter, K. Nooter, J. Verweij. Randomized cross-over evaluation of body-surface area-based dosing versus flat-fixed dosing of paclitaxel. J. Clin. Oncol., 21: 197–202 (2003).

[134] S.A. Kaestner, G.J. Sewell. Chemotherapy Dosing Part II: Alternative Approaches and Future Prospects. Clin. Oncol., 19: 99–107 (2007).

[135] K. Venkatakrishnan, L.E. Friberg, D. Ouellet, J.T. Mettetal, A. Stein, I.F. Trocóniz, R. Bruno, N. Mehrotra, J. Gobburu, D.R. Mould. Optimizing oncology therapeutics through quantitative translational and clinical pharmacology: challenges and opportunities. Clin. Pharmacol. Ther., 97: 37–54 (2015).

[136] A.A. Miller, G.L. Rosner, M.J. Egorin, D. Hollis, S.M. Lichtman, M.J. Ratain. Prospective evaluation of body surface area as a determinant of paclitaxel pharmacokinetics and pharmacodynamics in women with solid tumors: Cancer and Leukemia Group B Study 9763. Clin. Cancer Res., 10: 8325–8331 (2004).

[137] H.J.G.D. van den Bongard, R.A.A. Mathôt, O. van Tellingen, J.H.M. Schellens, J.H. Beijnen. A population analysis of the pharmacokinetics of Cremophor EL using nonlinear mixed-effect modelling. Cancer Chemother. Pharmacol., 50: 16–24 (2002).

[138] M. Joerger, S. Kraff, A.D.R. Huitema, G. Feiss, B. Moritz, J.H.M. Schellens, J.H. Beijnen, U. Jaehde. Evaluation of a pharmacology-driven dosing algorithm of 3-weekly paclitaxel using therapeutic drug monitoring: a pharmacokinetic-pharmacodynamic simulation study. Clin. Pharmacokinet., 51: 607–617 (2012).

[139] M. Joerger, J. von Pawel, S. Kraff, J.R. Fischer, W. Eberhardt, T.C. Gauler, L. Mueller, N. Reinmuth, M. Reck, M. Kimmich, F. Mayer, H.-G. Kopp, D.M. Behringer, Y.-D. Ko, R.A. Hilger, M. Roessler, C. Kloft, A. Henrich, B. Moritz, M.C. Miller, S.J. Salamone, U. Jaehde. Open-label, randomized study of individualized, pharmacokinetically (PK)-guided dosing of paclitaxel combined with carboplatin or cisplatin in patients with advanced non-small-cell lung cancer (NSCLC). Ann. Oncol. Off. J. Eur. Soc. Med. Oncol., 27: 1895–902 (2016).

[140] A. Henrich, M. Joerger, S. Kraff, U. Jaehde, W. Huisinga, C. Kloft, Z.P. Parra-Guillen. Semimechanistic bone marrow exhaustion pharmacokinetic/pharmacodynamic model for chemotherapy-induced cumulative neutropenia. J. Pharmacol. Exp. Ther., 362: 347–358 (2017).

[141] S.L. Beal. Population pharmacokinetic data and parameter estimation based on their

first two statistical moments. Drug Metab. Rev., 15: 173–193 (1984).

[142] S.B. Duffull, D.F.B. Wright, H.R. Winter. Interpreting population pharmacokinetic-pharmacodynamic analyses - a clinical viewpoint. Br. J. Clin. Pharmacol., 71: 807–814 (2011).

[143] M. Frank. Population pharmacokinetic modelling and simulation of nevirapine in pregnant women and newborns for dosing strategies to prevent HIV-1 transmission in resource-constrained countries. Freie Universität Berlin (2011).

[144] J.S. Owen, J. Fiedler-Kelly. Introduction to population pharmacokinetic/ pharmacodynamic analysis with nonlinear mixed effects models. John Wiley & Sons, Inc., Hoboken, New Jersey, 1st ed. (2014).

[145] D. Fisher, S. Shafer. Fisher/Shafer NONMEM workshop pharmacokinetic and pharmacodynamic analysis with NONMEM - basic concepts. Het Pand, Ghent: 1–111 (2007).

[146] L. Gibiansky. Parameter estimates of population models: Comparison of NONMEM versions and estimation methods. 17th PAGE Meeting, abstract 1268. Marseille: 1–1 (2008).

[147] R.M. Savic, M.O. Karlsson. Importance of shrinkage in empirical bayes estimates for diagnostics: problems and solutions. AAPS J., 11: 558–569 (2009).

[148] E.N. Jonsson, M.O. Karlsson. Automated covariate model building within NONMEM. Pharm. Res., 15: 1463–1468 (1998).

[149] J. Ribbing, J. Nyberg, O. Caster, E.N. Jonsson. The lasso - a novel method for predictive covariate model building in nonlinear mixed effects models. J. Pharmacokinet. Pharmacodyn., 34: 485–517 (2007).

[150] R.J. Bauer, S. Guzy, C. Ng. A survey of population analysis methods and software for complex pharmacokinetic and pharmacodynamic models with examples. AAPS J., 9: E60–E83 (2007).

[151] S.L. Beal, L.B. Sheiner. NONMEM users guide - Part VII conditional estimation methods. San Francisco, California: 1–20 (1998).

[152] E.L. Plan, A. Maloney, F. Mentré, M.O. Karlsson, J. Bertrand. Performance comparison of various maximum likelihood nonlinear mixed-effects estimation methods for dose-response models. AAPS J., 14: 420–432 (2012).

[153] Y. Wang. Derivation of various NONMEM estimation methods. J. Pharmacokinet. Pharmacodyn., 34: 575–593 (2007).

[154] M. Lindstrom, D. Bates. Nonlinear mixed effects models for repeated measures data. Biometrics, 46: 673–687 (1990).

[155] L. Zhang, S.L. Beal, L.B. Sheiner. Simultaneous vs. sequential analysis for population PK/PD data I: best-case performance. J. Pharmacokinet. Pharmacodyn., 30: 387–404 (2003).

[156] L. Zhang, S.L. Beal, L.B. Sheinerz. Simultaneous vs. sequential analysis for population PK/PD data II: robustness of methods. J. Pharmacokinet. Pharmacodyn., 30: 405–416 (2003).

[157] B.D. Lacroix, L.E. Friberg, M.O. Karlsson. Evaluation of IPPSE, an alternative method for sequential population PKPD analysis. J. Pharmacokinet. Pharmacodyn., 39: 177–193 (2012).

[158] J.R. Wade, M.O. Karlsson. Combining PK and PD data during population PK/PD analysis. 8th PAGE Meeting, abstract 139. Saintes: 1–1 (1999).

[159] C. Dansirikul, H.E. Silber, M.O. Karlsson. Approaches to handling pharmacodynamic baseline responses. J. Pharmacokinet. Pharmacodyn., 35: 269–283 (2008).

[160] P.O. Gisleskog, M.O. Karlsson, S.L. Beal. Use of prior information to stabilize a population data analysis. J. Pharmacokinet. Pharmacodyn., 29: 473–505 (2002).

[161] J.R. Wade, A.W. Kelman, C.A. Howie, B. Whiting. Effect of misspecification of the absorption process on subsequent parameter estimation in population analysis. J. Pharmacokinet. Biopharm., 21: 209–222 (1993).

[162] R.J. Bauer. NONMEM user guide - introduction to NONMEM 7.3.0. Hanover, Maryland: 1–210 (2014).

[163] N.H.G. Holford. A time to event tutorial for pharmacometricians. CPT Pharmacometrics Syst. Pharmacol., 2: e43 (2013).

[164] Y. Wang, C. Sung, C. Dartois, R. Ramchandani, B.P. Booth, E. Rock, J. Gobburu. Elucidation of relationship between tumor size and survival in non-small-cell lung cancer patients can aid early decision making in clinical drug development. Clin. Pharmacol. Ther., 86: 167–174 (2009).

[165] Food and Drug Administration. Guidance for Industry Population Pharmacokinetics. Silver Spring, Maryland: 1–31 (1999).

[166] E.B. Roecker. Prediction error and its estimation for subset-selected models. Technometrics, 33: 459–468 (1991).

[167] K. Brendel, C. Dartois, E. Comets, A. Lemenuel-Diot, C. Laveille, B. Tranchand, P.

Girard, C.M. Laffont, F. Mentré. Are population pharmacokinetic and/or pharmacodynamic models adequately evaluated? A survey of the literature from 2002 to 2004. Clin. Pharmacokinet., 46: 221–234 (2007).

[168] D.R. Mould, R.N. Upton. Basic concepts in population modeling, simulation, and model-based drug development-part 2: introduction to pharmacokinetic modeling methods. CPT Pharmacometrics Syst. Pharmacol., 2: e38 (2013).

[169] M.O. Karlsson, R.M. Savic. Diagnosing model diagnostics. Clin. Pharmacol. Ther., 82: 17–20 (2007).

[170] A.C. Hooker, C.E. Staatz, M.O. Karlsson. Conditional weighted residuals (CWRES): a model diagnostic for the FOCE method. Pharm. Res., 24: 2187–2197 (2007).

[171] N.H.G. Holford, M.O. Karlsson. A tutorial on visual predictive checks. 17th PAGE Meeting, abstract 1434. Marseille: 1–17 (2008).

[172] D.D. Wang, S. Zhang. Standardized visual predictive check versus visual predictive check for model evaluation. J. Clin. Pharmacol., 52: 39–54 (2013).

[173] M. Bergstrand, A.C. Hooker, J.E. Wallin, M.O. Karlsson. Prediction-corrected visual predictive checks for diagnosing nonlinear mixed-effects models. AAPS J., 13: 143–151 (2011).

[174] K. Brendel, E. Comets, C. Laffont, C. Laveille, F. Mentré. Metrics for external model evaluation with an application to the population pharmacokinetics of gliclazide. Pharm. Res., 23: 2036–2049 (2006).

[175] E. Comets, K. Brendel, F. Mentré. Computing normalised prediction distribution errors to evaluate nonlinear mixed-effect models: The npde add-on package for R. Comput. Methods Programs Biomed., 90: 154–166 (2008).

[176] K. Tunblad, L. Lindbom, L. McFadyen, E.N. Jonsson, S. Marshall, M.O. Karlsson. The use of clinical irrelevance criteria in covariate model building with application to dofetilide pharmacokinetic data. J. Pharmacokinet. Pharmacodyn., 35: 503–526 (2008).

[177] R. Keizer, D. Pastoor, R. Savic. New open source R libraries for simulation & visualization: PKPDsim and vpc. 24th PAGE Meeting, abstract 3636. Hersonissos: 1–1 (2015).

[178] L. Zufía López, A. Aldaz Pastor, J.M. Aramendia Beitia, J. Arrobas Velilla, J. Giraldez Deiró. Determination of docetaxel and paclitaxel in human plasma by high-performance liquid chromatography: validation and application to clinical pharmacokinetic studies. Ther. Drug Monit., 28: 199–205 (2006).

[179] European Medicines Agency. Guideline on bioanalytical method validation. London: 1–23 (2012).

[180] J. Gabrielsson, B. Meibohm, D. Weiner. Pattern recognition in pharmacokinetic data analysis. AAPS J., 18: 47–63 (2016).

[181] J. Gabrielsson, S. Hjorth. Pattern recognition in pharmacodynamic data analysis. AAPS J., 18: 64–91 (2016).

[182] B. Efron, R. Tibshirani. Bootstrap methods for standard errors, confidence intervals, and other measures of statistical accuracy. Stat. Sci., 1: 54–77 (1986).

[183] L.B. Sheiner, S.L. Beal. Some suggestions for measuring predictive performance. J. Pharmacokinet. Biopharm., 9: 503–512 (1981).

[184] S. Wicha, C. Chen, O. Clewe, U. Simonsson. A general pharmacodynamic interaction (GPDI) model. 25th PAGE Meeting, abstract 5946. Lisbon: 1–28 (2016).

[185] A. Lindauer, C. Eickhoff, C. Kloft, U. Jaehde. Population pharmacokinetics of high-dose carboplatin in children and adults. Ther. Drug Monit., 32: 159–168 (2010).

[186] A. Schmitt, L. Gladieff, C.M. Laffont, A. Evrard, J.-C. Boyer, A. Lansiaux, C. Bobin-Dubigeon, M.-C. Etienne-Grimaldi, M. Boisdron-Celle, M. Mousseau, F. Pinguet, A. Floquet, E.M. Billaud, C. Durdux, C. Le Guellec, J. Mazières, T. Lafont, F. Ollivier, D. Concordet, E. Chatelut. Factors for hematopoietic toxicity of carboplatin: refining the targeting of carboplatin systemic exposure. J. Clin. Oncol., 28: 4568–4574 (2010).

[187] R.S. Herbst, H. Takeuchi, B.A. Teicher. Paclitaxel/carboplatin administration along with antiangiogenic therapy in non-small-cell lung and breast carcinoma models. Cancer Chemother. Pharmacol., 41: 497–504 (1998).

[188] M.T. Huizing, L.J. van Warmerdam, H. Rosing, M.C. Schaefers, A. Lai, T.J. Helmerhorst, C.H. Veenhof, M.J. Birkhofer, S. Rodenhuis, J.H. Beijnen, W.W. ten Bokkel Huinink. Phase I and pharmacologic study of the combination paclitaxel and carboplatin as first-line chemotherapy in stage III and IV ovarian cancer. J. Clin. Oncol., 15: 1953–1964 (1997).

[189] J.E. Harris. Cigarette smoking among successive birth cohorts of men and women in the United States during 1900-80. J. Natl. Cancer Inst., 71: 473–479 (1983).

[190] T. Ohtsu, Y. Sasaki, T. Tamura, Y. Miyata, H. Nakanomyo, Y. Nishiwaki, N. Saijo. Clinical pharmacokinetics and pharmacodynamics of paclitaxel: a 3-hour infusion versus a 24-hour infusion. Clin. Cancer Res., 1: 599–606 (1995).

[191] P.H. Wiernik, E.L. Schwartz, J.J. Strauman, J.P. Dutcher, R.B. Lipton, E. Paietta. Phase

I clinical and pharmacokinetic study of taxol. Cancer Res., 47: 2486–2493 (1987).

[192] L. van Zuylen, M.O. Karlsson, J. Verweij, E. Brouwer, P. de Bruijn, K. Nooter, G. Stoter, A. Sparreboom. Pharmacokinetic modeling of paclitaxel encapsulation in Cremophor EL micelles. Cancer Chemother. Pharmacol., 47: 309–318 (2001).

[193] A. Henningsson, M.O. Karlsson, L. Viganò, L. Gianni, J. Verweij, A. Sparreboom. Mechanism-based pharmacokinetic model for paclitaxel. J. Clin. Oncol., 19: 4065–4073 (2001).

[194] B. Ribba, E. Watkin, M. Tod, P. Girard, E. Grenier, B. You, E. Giraudo, G. Freyer. A model of vascular tumour growth in mice combining longitudinal tumour size data with histological biomarkers. Eur. J. Cancer, 47: 479–490 (2011).

[195] S. Kraff, A. Lindauer, M. Joerger, S.J. Salamone, U. Jaehde. Excel®-Based Tool for Pharmacokinetically-Guided Dose Adjustment of Paclitaxel. Ther. Drug Monit., 37: 725–732 (2015).

[196] S. Kraff, A.J.M. Nieuweboer, R.H.J. Mathijssen, F. Baty, A.-J. de Graan, R.H.N. van Schaik, U. Jaehde, M. Joerger. Pharmacokinetically based dosing of weekly paclitaxel to reduce drug-related neurotoxicity based on a single sample strategy. Cancer Chemother. Pharmacol., 75: 975–983 (2015).

[197] M.C. Berenbaum. In vivo determination of the fractional kill of human tumor cells by chemotherapeutic agents. Cancer Chemother. reports, 56: 563–571 (1972).

[198] R.A. Steinman. Cell cycle regulators and hematopoiesis. Oncogene, 21: 3403–3413 (2002).

[199] D.E. Harrison, C.P. Lerner. Most primitive hematopoietic stem cells are stimulated to cycle rapidly after treatment with 5-fluorouracil. Blood, 78: 1237–1240 (1991).

[200] A. Trumpp, M. Essers, A. Wilson. Awakening dormant haematopoietic stem cells. Nat. Rev. Immunol., 10: 201–209 (2010).

[201] C. Kloft, J. Wallin, A. Henningsson, E. Chatelut, M.O. Karlsson. Population pharmacokinetic-pharmacodynamic model for neutropenia with patient subgroup identification: comparison across anticancer drugs. Clin. Cancer Res., 12: 5481–5490 (2006).

[202] L. Shao, Y. Wang, J. Chang, Y. Luo, A. Meng, D. Zhou. Hematopoietic stem cell senescence and cancer therapy-induced long-term bone marrow injury. Transl. Cancer Res., 2: 397–411 (2013).

[203] M.S. Lam, R.J. Ignoffo. A guide to clinically relevant drug interactions in oncology. J.

Oncol. Pharm. Pract., 9: 45–85 (2003).

[204] M. Joerger, A.D.R. Huitema, D.J. Richel, C. Dittrich, N. Pavlidis, E. Briasoulis, J.B. Vermorken, E. Strocchi, A. Martoni, R. Sorio, H.P. Sleeboom, M.A. Izquierdo, D.I. Jodrell, H. Calvert, A. V Boddy, H. Hollema, R. Féty, W.J.F. Van der Vijgh, G. Hempel, E. Chatelut, M. Karlsson, J. Wilkins, B. Tranchand, A.H.G.J. Schrijvers, C. Twelves, J.H. Beijnen, J.H.M. Schellens. Population pharmacokinetics and pharmacodynamics of paclitaxel and carboplatin in ovarian cancer patients: a study by the European organization for research and treatment of cancer-pharmacology and molecular mechanisms group and new drug development group. Clin. Cancer Res., 13: 6410–6418 (2007).

[205] P. Engblom, V. Rantanen, J. Kulmala, S. Grènman. Carboplatin-paclitaxel- and carboplatin-docetaxel-induced cytotoxic effect in epithelial ovarian carcinoma in vitro. Cancer, 86: 2066–2073 (1999).

[206] G. Konecny, M. Untch, D. Slamon, M. Beryt, S. Kahlert, M. Felber, E. Langer, S. Lude, H. Hepp, M. Pegram. Drug interactions and cytotoxic effects of paclitaxel in combination with carboplatin, epirubicin, gemcitabine or vinorelbine in breast cancer cell lines and tumor samples. Breast Cancer Res. Treat., 67: 223–233 (2001).

[207] A.D. Guminski, P.R. Harnett, A. DeFazio. Carboplatin and paclitaxel interact antagonistically in a megakaryoblast cell line--a potential mechanism for paclitaxel-mediated sparing of carboplatin-induced thrombocytopenia. Cancer Chemother. Pharmacol., 48: 229–234 (2001).

[208] C.M. Kearns, M.J. Egorin. Considerations regarding the less-than-expected thrombocytopenia encountered with combination paclitaxel/carboplatin chemotherapy. Semin. Oncol., 24: S2.91-S2.96 (1997).

[209] L.J. van Warmerdam, M.T. Huizing, G. Giaccone, P.E. Postmus, W.W. ten Bokkel Huinink, N. van Zandwijk, M.G. Koolen, T.J. Helmerhorst, W.J. van der Vijgh, C.H. Veenhof, J.H. Beijnen. Clinical pharmacology of carboplatin administered in combination with paclitaxel. Semin. Oncol., 24: S2.97-S2.104 (1997).

[210] B.H. Long, C.R. Fairchild. Paclitaxel inhibits progression of mitotic cells to G1 phase by interference with spindle formation without affecting other microtubule functions during anaphase and telephase. Cancer Res., 54: 4355–4361 (1994).

[211] F. Puisset, J. Alexandre, J.-M. Treluyer, V. Raoul, H. Roché, F. Goldwasser, E. Chatelut. Clinical pharmacodynamic factors in docetaxel toxicity. Br. J. Cancer, 97: 290–296 (2007).

[212] B.I. Lord, G. Molineux, Z. Pojda, L.M. Souza, J.J. Mermod, T.M. Dexter. Myeloid cell kinetics in mice treated with recombinant interleukin-3, granulocyte colony-stimulating factor (CSF), or granulocyte-macrophage CSF in vivo. Blood, 77: 2154–2159 (1991).

[213] M.L. Pastor, C.M. Laffont, L. Gladieff, A. Schmitt, E. Chatelut, D. Concordet. Model-Based Approach to Describe G-CSF Effects in Carboplatin-Treated Cancer Patients. Pharm. Res., 30: 2795–2807 (2013).

[214] O. Vainas, S. Ariad, O. Amir, W. Mermershtain, V. Vainstein, M. Kleiman, O. Inbar, R. Ben-Av, A. Mukherjee, S. Chan, Z. Agur. Personalising docetaxel and G-CSF schedules in cancer patients by a clinically validated computational model. Br. J. Cancer, 107: 814–822 (2012).

[215] J.B. Bulitta, P. Zhao, R.D. Arnold, D.R. Kessler, R. Daifuku, J. Pratt, G. Luciano, A.-R. Hanauske, H. Gelderblom, A. Awada, W.J. Jusko. Multiple-pool cell lifespan models for neutropenia to assess the population pharmacodynamics of unbound paclitaxel from two formulations in cancer patients. Cancer Chemother. Pharmacol., 63: 1035–1048 (2009).

[216] H. Minami, Y. Sasaki, T. Watanabe, M. Ogawa. Pharmacodynamic modeling of the entire time course of leukopenia after a 3-hour infusion of paclitaxel. Japanese J. cancer Res., 92: 231–238 (2001).

[217] J.E. Wallin, L.E. Friberg, M.O. Karlsson. Model-based neutrophil-guided dose adaptation in chemotherapy: evaluation of predicted outcome with different types and amounts of information. Basic Clin. Pharmacol. Toxicol., 106: 234–242 (2010).

[218] W. V. Mayneord. On a law of growth of Jensen's rat sarcoma. Cancer Res., 16: 841–846 (1932).

[219] A. Stein, W. Wang, A.A. Carter, O. Chiparus, N. Hollaender, H. Kim, R.J. Motzer, C. Sarr. Dynamic tumor modeling of the dose-response relationship for everolimus in metastatic renal cell carcinoma using data from the phase 3 RECORD-1 trial. BMC Cancer, 12: 311 (2012).

[220] K.M. Kerr, D. Lamb. Actual growth rate and tumour cell proliferation in human pulmonary neoplasms. Br. J. Cancer, 50: 343–349 (1984).

[221] L.S. Tham, L. Wang, R.A. Soo, S.C. Lee, H.S. Lee, W.P. Yong, B.C. Goh, N.H.G. Holford. A pharmacodynamic model for the time course of tumor shrinkage by gemcitabine + carboplatin in non-small cell lung cancer patients. Clin. Cancer Res., 14: 4213–4218 (2008).

[222] N.L. Jumbe, Y. Xin, D.D. Leipold, L. Crocker, D. Dugger, E. Mai, M.X. Sliwkowski, P.J.

Fielder, J. Tibbitts. Modeling the efficacy of trastuzumab-DM1, an antibody drug conjugate, in mice. J. Pharmacokinet. Pharmacodyn., 37: 221–242 (2010).

[223] J. Foo, F. Michor. Evolution of acquired resistance to anti-cancer therapy. J. Theor. Biol., 355: 10–20 (2014).

[224] Y. Ichinose, T. Yano, H. Asoh, H. Yokoyama, I. Yoshino, Y. Katsuda. Prognostic factors obtained by a pathologic examination in completely resected non-small-cell lung cancer: An analysis in each pathologic stage. J. Thorac. Cardiovasc. Surg., 110: 601–605 (1995).

[225] G.V. Scagliotti, P. Parikh, J. Von Pawel, B. Biesma, J. Vansteenkiste, C. Manegold, P. Serwatowski, U. Gatzemeier, R. Digumarti, M. Zukin, J.S. Lee, A. Mellemgaard, K. Park, S. Patil, J. Rolski, T. Goksel, F. De Marinis, L. Simms, K.P. Sugarman, D. Gandara. Phase III study comparing cisplatin plus gemcitabine with cisplatin plus pemetrexed in chemotherapy-naive patients with advanced-stage non-small-cell lung cancer. J. Clin. Oncol., 26: 3543–3551 (2008).

[226] K. Breur. Growth rate and radiosensitivity of human tumours. I. Growth rate of human tumours. Eur. J. Cancer, 2: 157–171 (1966).

[227] P.G. Peer, J. a van Dijck, J.H. Hendriks, R. Holland, a L. Verbeek. Age-dependent growth rate of primary breast cancer. Cancer, 71: 3547–3551 (1993).

[228] Y. Tanaka, K. Hongo, T. Tada, K. Sakai, Y. Kakizawa, S. Kobayashi. Growth pattern and rate in residual nonfunctioning pituitary adenomas: correlations among tumor volume doubling time, patient age, and MIB-1 index. J. Neurosurg., 98: 359–365 (2003).

[229] D.M. Geddes. The natural history of lung cancer: A review based on rates of tumour growth. Br. J. Dis. Chest, 73: 1–17 (1979).

[230] E.K. Hansson, G. Ma, M. a Amantea, J. French, P. a Milligan, L.E. Friberg, M.O. Karlsson. PKPD modeling of predictors for adverse effects and overall survival in sunitinib-treated patients with GIST. CPT Pharmacometrics Syst. Pharmacol., 2: e85 (2013).

[231] C. Zecchin, I. Gueorguieva, N.H. Enas, L.E. Friberg. Models for change in tumour size, appearance of new lesions and survival probability in patients with advanced epithelial ovarian cancer. Br. J. Clin. Pharmacol., 82: 717–727 (2016).

[232] N. Muszbek, N. Kreif, A. Valderrama, A. Benedict, J. Ishak, P. Ross. Modelling survival in hepatocellular carcinoma. Curr. Med. Res. Opin., 28: 1141–1153 (2012).

[233] E. Rapp, J.L. Pater, A. Willan, Y. Cormier, N. Murray, W.K. Evans, D.I. Hodson, D.A. Clark, R. Feld, A.M. Arnold, J.I. Ayoub, K.S. Wilson, J. Latreille, R.F. Wierzbicki, D.P.

Hill. Chemotherapy can prolong survival in patients with advanced non-small-cell lung cancer--report of a Canadian multicenter randomized trial. J Clin Oncol, 6: 633–641 (1988).

[234] B.C. Bender, E. Schindler, L.E. Friberg. Population pharmacokinetic-pharmacodynamic modelling in oncology: a tool for predicting clinical response. Br. J. Clin. Pharmacol., 79: 56–71 (2015).

[235] B. Ribba, N. Holford, F. Mentré. The use of model-based tumor-size metrics to predict survival. Clin. Pharmacol. Ther., 96: 133–135 (2014).

[236] L. Claret, M. Gupta, K. Han, A. Joshi, N. Sarapa, J. He, B. Powell, R. Bruno. Evaluation of tumor-size response metrics to predict overall survival in Western and Chinese patients with first-line metastatic colorectal cancer. J. Clin. Oncol., 31: 2110–2114 (2013).

[237] W. Wulaningsih, L. Holmberg, H. Garmo, H. Malmstrom, M. Lambe, N. Hammar, G. Walldius, I. Jungner, T. Ng, M. Van Hemelrijck. Serum lactate dehydrogenase and survival following cancer diagnosis. Br. J. Cancer, 113: 1389–1396 (2015).

[238] S. Diem, B. Kasenda, L. Spain, J. Martin-Liberal, R. Marconcini, M. Gore, J. Larkin. Serum lactate dehydrogenase as an early marker for outcome in patients treated with anti-PD-1 therapy in metastatic melanoma. Br. J. Cancer, 114: 256–261 (2016).

[239] L. Faloppi, M. Bianconi, R. Giampieri, A. Sobrero, R. Labianca, D. Ferrari, S. Barni, E. Aitini, A. Zaniboni, C. Boni, F. Caprioni, S. Mosconi, S. Fanello, R. Berardi, A. Bittoni, K. Andrikou, M. Cinquini, V. Torri, M. Scartozzi, S. Cascinu, Italian Group for the Study of Digestive Tract Cancer (GISCAD). The value of lactate dehydrogenase serum levels as a prognostic and predictive factor for advanced pancreatic cancer patients receiving sorafenib. Oncotarget, 6: 35087–35094 (2015).

[240] Y. Yin, J. Wang, X. Wang, L. Gu, H. Pei, S. Kuai, Y. Zhang, Z. Shang. Prognostic value of the neutrophil to lymphocyte ratio in lung cancer: A meta-analysis. Clinics, 70: 524–530 (2015).

[241] M.O. Karlsson, L.B. Sheiner. The importance of modeling interoccasion variability in population pharmacokinetic analyses. J. Pharmacokinet. Biopharm., 21: 735–750 (1993).

[242] A. Granito, S. Marinelli, G. Negrini, S. Menetti, F. Benevento, L. Bolondi. Prognostic significance of adverse events in patients with hepatocellular carcinoma treated with sorafenib. Therap. Adv. Gastroenterol., 9: 240–249 (2016).

[243] M. Di Maio, C. Gridelli, C. Gallo, F. Shepherd, F.V. Piantedosi, S. Cigolari, L. Manzione,

A. Illiano, S. Barbera, S.F. Robbiati, L. Frontini, E. Piazza, G. Pietro Ianniello, E. Veltri, F. Castiglione, F. Rosetti, V. Gebbia, L. Seymour, P. Chiodini, F. Perrone. Chemotherapy-induced neutropenia and treatment efficacy in advanced non-small-cell lung cancer: a pooled analysis of three randomised trials. Lancet. Oncol., 6: 669–677 (2005).

[244] J.H. Schiller, D. Harrington, C.P. Belani, C.J. Langer, A.B. Sandler, J. Krook, J. Zhu, D.H. Johnson. Comparison of four chemotherapy regimens for advanced non-small-cell lung cancer. N. Engl. J. Med., 346: 92–98 (2002).

[245] A.B. Sandler, R. Gray, M.C. Perry, J.R. Brahmer, J.H. Schiller, A. Dowlati, R. Lilenbaum, D.H. Johnson. Paclitaxel-carboplatin alone or with bevacizumab for non-small-cell lung cancer. N. Engl. J. Med., 355: 2542–2550 (2006).

[246] J.A. Treat, R. Gonin, M.A. Socinski, M.J. Edelman, R.B. Catalano, D.M. Marinucci, R. Ansari, H.H. Gillenwater, K.M. Rowland, R.L. Comis, C.K. Obasaju, C.P. Belani. A randomized, phase III multicenter trial of gemcitabine in combination with carboplatin or paclitaxel versus paclitaxel plus carboplatin in patients with advanced or metastatic non-small-cell lung cancer. Ann. Oncol., 21: 540–547 (2010).

[247] M. Joerger, J. Von Pawel, S. Kraff, J.R. Fischer, W. Eberhardt, T.C. Gauler. Open-label, randomised study of individualized, pharmacokinetically (PK)-guided dosing of paclitaxel combined with carboplatin or cisplatin in patients with advanced non-small cell lung cancer (NSCLC). Ann. Oncol.,: 1–22 (2016).

8 Publications

Original Papers

- A. Henrich, M. Joerger, S. Kraff, U. Jaehde, W. Huisinga, C. Kloft, Z.P. Parra-Guillén.
  Semi-mechanistic bone marrow exhaustion pharmacokinetic/pharmacodynamic model for chemotherapy-induced cumulative neutropenia.
  J. Pharmacol. Exp. Ther. 362: 347-358 (2017).
  doi: 10.1124/jpet.117.240309

- M. Joerger, J. von Pawel, S. Kraff, J.R. Fischer, W. Eberhardt, T.C. Gauler, L. Mueller, N. Reinmuth, M. Reck, M. Kimmich, F. Mayer, H.G. Kopp, D.M. Behringer, Y.D. Ko, R.A. Hilger, M. Roessler, C. Kloft, A. Henrich, B. Moritz, M.C. Miller, S.J. Salamone, U. Jaehde.
  Open-label, randomised study of individualized, pharmacokinetically (PK)-guided dosing of paclitaxel combined with carboplatin or cisplatin in patients with advanced non-small cell lung cancer (NSCLC).
  Ann. Oncol. 27: 1895-1902 (2016).
  doi: 10.1093/annonc/mdw290

Presentations

- A. Henrich, M. Joerger, W. Huisinga, Z.P. Parra-Guillen, C. Kloft.
  Semi-mechanistic PK/PD modelling to characterise long-term deterioration of neutropenia in cancer patients.
  Annual Meeting of the Central European Society of Anticancer Drug Research (CESAR), Munich, Germany, 08-10 September 2016.
  Abstractbook, 16, (2016).

- A. Henrich, C. Kloft.
  Damit nicht mehr alles grau erscheint - Wichtiges in der Behandlung von Depressionen.
  Lange Nacht der Wissenschaften, Berlin, Germany, 10 May 2014.

Conference abstracts

- F.W. Ojara, A. Henrich, N. Hartung, M. Joerger, M. Roessler, J.V. Pawel, W. Huisinga, C. Kloft.
  Examining the relationship between paclitaxel exposure and peripheral neuropathy in non-small cell lung cancer.
  26th Population Approach Group Europe (PAGE), Budapest, Hungary, 06-09 June 2017.
  PAGE 26: 7278 [www.page-meeting.org/default.asp?abstract=7278], (2017)

- F.W. Ojara, A. Henrich, M. Joerger, C. Kloft.
  Evaluating predictors of paclitaxel-associated peripheral neuropathy: a pharmacodynamic modelling approach.
  6th International Pharmaceutical Federation Pharmaceutical Sciences World Congress (FIP PSWC), Stockholm, Sweden, 21-24 May 2017.
  https://www.fip.org/abstracts?page=abstracts&action=item&item=18157, (2017).

- A. Henrich, M. Joerger, W. Huisinga, C. Kloft, Z.P. Parra-Guillen.
  Characterisation of bone marrow exhaustion and long-term neutropenia by applying PK/PD modelling.
  Annual Meeting of the Deutsche Pharmazeutische Gesellschaft (DPhG), Munich, Germany, 04-07 October 2016.
  www.dphg.de/fileadmin/downloads/DPhG2016_ConferenceBook_final.pdf, 119, (2016).

- A. Henrich, M. Joerger, S. Kraff, U. Jaehde, W. Huisinga, C. Kloft, Z.P. Parra-Guillen.
  PK/PD model extension to characterise bone marrow exhaustion in cancer patient making use of a prior paclitaxel PK model.
  25th Population Approach Group Europe (PAGE), Lisbon, Portugal, 07-10 June 2016.
  PAGE 25: 5879 [www.page-meeting.org/?abstract=5879], (2016).

- M. Joerger, J. von Pawel, S. Kraff, J.R. Fischer, T. Gauler, L. Mueller, N. Reinmuth, M. Reck, M. Kimmich, M. Frank, H.G. Kopp, D. Behringer, Y.D. Ko, H. Ralf, M. Roessler, C. Kloft, A. Henrich, B. Moritz, U. Jaehde.
  Pharmacokinetically (PK)-guided dosing of paclitaxel in combination with carboplatin in advanced non-small cell lung cancer (NSCLC) is gender dependent: Updated results of the randomized CEPAC-TDM study.
  The European Cancer Congress 2015, Vienna, Austria, 25-29 September 2015.
  http://scientific.sparx-ip.net/ecco2015/#/page/646-647/dp, 51, (2015).

- A. Henrich, M. Joerger, W. Huisinga, C. Kloft, Z. P. Parra-Guillen.
  Dose-individualisation of paclitaxel in patients with advanced non-small cell lung cancer: exploiting modelling and simulation to refine dosing algorithm.
  Annual Meeting of the Central European Society of Anticancer Drug Research (CESAR), Innsbruck, Austria, 17-19 September 2015.
  http://link.springer.com/article/10.1007/s12254-015-0224-6, 51, (2015).

- A. Henrich, M. Joerger, W. Huisinga, C. Kloft, Z. P. Parra-Guillen.
  External evaluation of a PK/PD model describing the time course of paclitaxel and eutropenia in patients with advanced non-small cell lung cancer.
  24th Population Approach Group Europe (PAGE), Hersonissos, Greece, 02-05 June 2015.
  PAGE 24: 3460 [www.page-meeting.eu/default.asp?abstract=3460], (2015).

- A. Henrich, Z. Parra-Guillen, C. Kloft.
  Comparison of three pharmacokinetic/toxicity models describing neutropenia caused by topotecan in cancer patients.
  Annual Meeting of the Deutsche Pharmazeutische Gesellschaft (DPhG), Frankfurt, Germany, 24-26 September 2014.
  Abstractbook, 136, (2014).

- A. Henrich, Z. Parra-Guillen, C. Kloft.
  Comparison of three PK/PD models for describing neutropenia in cancer patients treated with topotecan.
  Annual Meeting of the Central European Society of Anticancer Research (CESAR), Bonn, Germany, 26-28 June 2014.
  Abstractbook, 42, (2014).

9 Curriculum vitae

Der Lebenslauf ist in der Online-Version
aus Gründen des Datenschutzes nicht enthalten

10 Appendix

10.1 Dataset preparation

Table 10.1: Identification of patient- and time-associated information

Data label	*Description and characteristics*	*Derived based on*	*Unit*	*Possible values (type)*	*Changes, imputations, assumptions, comments*
SID	Study patient identifier xx Study centre yyy ID within study centre Example: 06/007	---	---	xx/yyy (natural/ natural, both > 0)	• 1 patient was ignored: This patient was enroled in the study with the histopathological diagnosis of adenocarcinoma of the lung. After six cycles of treatment histopathological evaluation was revised to an epithelial pleura mesothelioma. This was a violation of inclusion criteria. This lead to the overall patient number of 365.
ID	Patient identifier xx Study centre + 10 yyy ID within study centre Example: 16007	SID	---	xxyyy (natural, > 0)	---
CENT	Study centre 1 Kantonspital St. Gallen 2 Eberhard-Karls-Universität Tübingen 3 Askepios-Fachkliniken München-Gauting 4 Augusta Krankenanstalt GmbH 6 Klinik Löwenstein GmbH 7 Onkologische Schwerpunktpraxis Leer 8 Universitätsklinikum Essen 9 Klinikum Schillerhöhe 10 Krankenhaus Großhansdorf 11 Evangelische Kliniken Bonn gGmbH	---	---	1, 2, 3,… 11	---

Data label	*Description and characteristics*	*Derived based on*	*Unit*	*Possible values (type)*	*Changes, imputations, assumptions, comments*
DATE	Date yyyy year mm month dd day	---	---	yyyy-mm-dd	• For 1 patient (≙ 0.27%), one follow-up visit date contained obviously a typo in year; 2014 was changed to 2013 and was flagged (FLGTIME = 6). • For 3 patients (≙ 0.82%), day of date of study visits was unknown, thus middle of the month assumed (FLGTIME = 8). • For 46 patients (≙ 12.6%), end of study visits after death, date of death taken as date of end of study visit. • For 1 patient (≙ 0.27%), comments reported an addition cisplatin dose on day 8 for 2 cycles, thus additional rows were added (FLGTIME = 4).
CLOCKT	Clock time hh hour mm minute	---	---	hh:mm	• Except for drug administration and paclitaxel concentration measurements, there was not clock time reported. Thus, the most frequent clock time was imputed for all other events, e.g. complete blood count, tumour assessment or covariate assessment. • For the administration of the platinum-based drugs dose administration was assumed to take place 3 h after start of paclitaxel infusion. • For 3 patients (≙ 0.82%), comments stated that order between paclitaxel and platinum-based drug was changed in one cycle. For these occasions, 1 h before start of paclitaxel infusion was assumed (FLGTIME = 3).
OCC	Occasion/treatment cycle 1 Cycle 1 including screening/baseline 2 - 6 Cycle 2 - 6 7 Starting from 3 weeks after last dose 8 Starting from end of observation	TIME (for occasion 7 and 8)	---	1 - 6 (natural)	• If OCC/DAY and date were not consistent, date was assumed to be correct and OCC/DAY were adapted accordingly.

Data label	*Description and characteristics*	*Derived based on*	*Unit*	*Possible values (type)*	*Changes, imputations, assumptions, comments*
DAY	Day of the study cycle (this is used as a marker and does NOT correspond to actual dates) 1 1st day of cycle (drug administration), OCC > 6 2 2nd day of cycle (PK measurement) 2.5 All events between day 2 and 3 3 100 h after the paclitaxel dose, for calculation of $T_{C>0.05}$ in NONMEM 7 All events between day 3 and 15 8 Neutrophil measurement before day 15 (if end of study visit was before) 15 Day 15 of the cycle (neutrophil measurement) 20 All events between day 15 and next dose 21 Marker for dummy events	TIME	---	x - y (natural, > 0)	• If OCC/DAY and date were not consistent, date was assumed to be correct and OCC/DAY were adapted accordingly.
TIME	Relative time elapsed from start of 1st paclitaxel administration.	DATE CLOCKT	h	x.xx - y.yy (real, ≥ 0)	• All events before 1st administration were set to 0.00.
TALD	Time after last dose: relative time elapsed from last paclitaxel administration.	DATE CLOCKT LASTD	h	x.xx - y.yy (real, ≥ 0)	• All events before 1st administration were set to 0.00.

Table 10.2: Dosing information

Data label	*Description and characteristics*	*Derived based on*	*Unit*	*Possible values (type)*	*Changes, imputations, assumptions, comments*
ARM	Study arm 1 Conventional (Arm A) 2 Experimental (Arm B)	---	---	1, 2	---
DOSE	Actual administered dose of each drug	---	mg	x - y (natural, ≥ 0)	• Cisplatin dose was either planned to be given as one dose on day 1 of the cycle or split in two doses administered on day 1 and 2. Information whether the dose was split was not available, thus administration as a single dose was assumed. • For 1 occasion (≙ 0.07%), carboplatin dose was reported as 0 but comment stated: "Patient received carboplatin 600 mg due to polyneuropathy". Thus, DOSE and DRUG were adapted accordingly. • For 12 occasions (≙ 0.83%) comment stated that the platinum-based drug was changed to carboplatin and no dose was reported. These doses were reported in an interim data and thus taken from there (FLGDOSE = 4). • For 1 occasion (≙ 0.07%): date of drug administration was changed to one day later because of a respective comment in AE dataset, stating that an allergic reaction was reported and that the drug administration was therefore stopped and administered one day later. DATE was adopted accordingly. • For 2 occasions (≙ 0.14%) chemotherapy was stopped due to an allergic reaction. Those dosing records were deleted because there is no information how much of the infusion was administered. Thus, all following events were ignored (FLGPK = 2).

Data label	*Description and characteristics*	*Derived based on*	*Unit*	*Possible values (type)*	*Changes, imputations, assumptions, comments*
AMT	Amount: dose of paclitaxel for modelling activities transformed in µmol. Platinum-based drugs still in mg	DOSE	µmol or mg	x.xx - y.yy (real, ≥ 0)	---
DUR	Infusion duration: Paclitaxel: actual infusion duration (planned duration: 3 h) Carboplatin: planned duration (0.5 h, actual infusion duration not documented) Cisplatin: planned duration (2 h, actual infusion duration not documented)	---	h	x.xx - y.yy (real, ≥ 0)	• For 86 occasions (≙ 5.91%), start (and stop time) was missing or reported as “00:00”. For these events, a duration of 3 h as planned in the protocol was assumed and start time was set to 10:00 (FLGTIME = 1). • For 1 occasion (≙ 0.07%), infusion duration was missing, because of missing stop time. Infusion duration of 3 h was assumed (FLGTIME = 2). • For 1 occasion (≙ 0.07%), infusion duration was reported to be 1 min this not possible because of toxicity, thus 3 h were assumed (FLGTIME = 2). • Carboplatin, cisplatin: planned infusion duration assumed.
RATE	Infusion rate: amount administered in 1 h (= AMT / DUR)	AMT DUR	mg/h or µmol/h	x.xx - y.yy (real, ≥ 0)	---
DRUG	Drug administered 1 Cisplatin 2 Carboplatin 3 Paclitaxel	---	---	1, 2, 3	• Carboplatin doses < 250 mg were assumed to be cisplatin, this occurred for 5 of cisplatin doses (≙ 2.06%) (FLGDOSE = 1). • Cisplatin doses > 400 mg were assumed to be carboplatin, this occurred for 2 of carboplatin doses (≙ 1.15%) (FLGDOSE = 2).
LASTD	Time point of last dose calculated as time since 1st dose	TIME	h	x.xx - y.yy (real, ≥ 0)	---
CURRENTP	Concomitant platinum-based chemotherapy for the current cycle 0 Cisplatin 1 Carboplatin	DRUG	---	0, 1	---

Data label	*Description and characteristics*	*Derived based on*	*Unit*	*Possible values (type)*	*Changes, imputations, assumptions, comments*
PLATIN	Concomitant platinum-based therapy at the beginning of the 1st cycle 0 Cisplatin 1 Carboplatin	DRUG	---	0, 1	---
DOSEG	Dose groups according to average paclitaxel dose/m² based on typical doses administered in clinical practice 1 < 175 mg/m² 2 175 - < 200 mg/m² 3 ≥ 200 mg/m²	DOSEAV BSA MAXOCC	---	1, 2, 3	---
DOSEG2	Dose groups according to absolute average paclitaxel dose based on the 25th ($P_{0.25}$), 50th ($P_{0.5}$) and 75th ($P_{0.75}$) percentiles 1 < $P_{0.25}$ 2 $P_{0.25}$ - < $P_{0.5}$ 3 $P_{0.5}$ - < $P_{0.75}$ 4 ≥ $P_{0.75}$ $P_{0.25}$ = 281 mg, $P_{0.5}$ = 335 mg, $P_{0.75}$ = 372 mg	DOSEAV MAXOCC	---	1, 2, 3, 4	---
MAXOCC	Number of cycles a patient received in total during the study	OCC	---	1 - 6 (natural)	---
DOSEP	Planned dose according to algorithm and toxicity for all 3 drugs (raw data was searched for entities regarding ototoxicity and hearing problems)	GRADEN TC SEX AGE DOSE BSA NHEMMAX NEURMAX GRADEP CLCR	mg	x - y (natural, ≥ 0)	---

Data label	*Description and characteristics*	*Derived based on*	*Unit*	*Possible values (type)*	*Changes, imputations, assumptions, comments*
DOSEALG	Planned dose according to algorithm (Figure 1.5) not considering additional toxicity for all 3 drugs	GRADEN TC SEX AGE DOSE BSA CLCR	mg	x - y (natural, ≥ 0)	---
CHANGE	Cisplatin should have been changed to carboplatin but was not? 0 No, no change needed or performed accordingly 1 Yes, change to carboplatin should have been performed but was not	CLCR NEURMAX	---	0, 1	---
DOSECUM	Cumulative paclitaxel dose up to the respective time point	DOSE OCC	mg	x - y (natural, ≥ 0)	---
DOSETOT	Total dose of paclitaxel a patient received over all cycles (sum of doses in all 6 cycles)	DOSE OCC	mg	x - y (natural, ≥ 0)	---
DOSEAV	Average paclitaxel dose a patient received (= DOSETOT/MAXOCC)	DOSETOT MAXOCC	mg	x - y (natural, ≥ 0)	---
DDIFALG	Deviation of given dose to algorithm (= DOSE – DOSEALG) > 0: overdosed < 0: underdosed	DOSE, DOSEALG	mg	x - y (natural, ≥ 0)	---
DDIFPLAN	Deviation of given dose to planned dose (= DOSE – DOSEP) > 0 overdosed < 0 underdosed	DOSE, DOSEP	mg	x - y (natural, ≥ 0)	---
DIFPLAL	Deviation between planned dose and dose based on the algorithm (= DOSEP – DOSEALG)	DOSEP, DOSEALG	mg	x - y (natural, ≥ 0)	---
PREM	Was premedication administered per protocol? 0 No 1 Yes 2 Yes plus additional medication	---	---	0, 1, 2	---

Table 10.3: Information about PK measurements

Data label	*Description and characteristics*	*Derived based on*	*Unit*	*Possible values (type)*	*Changes, imputations, assumptions, comments*
CONC	Paclitaxel plasma concentration	---	ng/mL	x.x - y.y (real, ≥ 0)	• For 3 measurements (≙ 0.45%), 0 was reported, being below the lower limit of quantification. Due to the low number of occurrences, these were assumed to be missing (FLGPK = 1). • 4 measurements (≙ 0.57%) were reported to be taken before drug administration, thus 24 h were added to the sampling time (FLGTIME = 7). • For 2 measurements (≙ 0.29%), very short time intervals between drug administration and sampling time (< 2 h) were reported. Thus, 24 h were added to the sampling time (FLGTIME = 7). • For 2 measurements (≙ 0.29%), very long time intervals between drug administration and sampling time (> 40 h) were reported. Thus, 24 h were subtracted from the sampling time (FLGTIME = 7).
LNCONC	Natural logarithm of paclitaxel plasma concentration	CONC	ln(µmol/L)	x.x - y.y (real)	---
TC	Time above the threshold of 0.05 µmol/L ($T_{C>0.05}$) estimated during the CEPAC-TDM study with the respective cycle Target range: 26 - 31 h	---	h	x.x - y.y (real, ≥ 0)	---

Table 10.4: Complete blood count data information

Data label	*Description and characteristics*	*Derived based on*	*Unit*	*Possible values (type)*	*Changes, imputations, assumptions, comments*
NGA	Absolute neutrophil concentration Concentrations were either reported as relative or absolute neutrophil concentration. If relative concentrations were reported, the absolute were derived as follows: NGA = relative neutrophil count/WBC Reference interval: 2.4 - 8.2	• WBC	• 10^9 cells/L	• x.xx - y.yy (real, ≥ 0)	• For 13 measurements (≙ 0.39%), 0 was reported, being below the lower limit of quantification. To be able to compute the logarithm the minimum of all values was imputed ($0.01 \cdot 10^9$ cells/L), these values were ignored for the analysis (FLGN = 1).
LNEU	Natural logarithm of absolute neutrophils	NGA	ln(10^9 cells/L)	x.xx - y.yy (real)	---
BSL	Baseline of neutrophil concentration: only 1st measurement was considered	NGA	10^9 cells/L	x.xx - y.yy (real, ≥ 0)	---
BSLM	Mean baseline of neutrophil concentration: median of all measurements before the 1st dose was computed: often measurements were available for the baseline visit and day 1 of the 1st cycle.	NGA	10^9 cells/L	x.xx - y.yy (real, ≥ 0)	---
WBC	Concentration of white blood cells Reference interval: 4.4 – 11.3	---	10^9/L	x.xx - y.yy (real, ≥ 0)	---
PLAT	Concentration of thrombocytes Reference interval: 150 – 300	---	10^9/L	x.x - y.y (real, ≥ 0)	---
LCA	Absolute concentration of lymphocytes Concentration were either reported as relative or absolute lymphocyte concentration. If relative concentrations were reported, the absolute were derived as follows: LCA = relative lymphocyte concentration/WBC Reference interval: 1.4 – 4	---	10^9 cells/L	x.xx - y.yy (real, ≥ 0)	---

Data label	*Description and characteristics*	*Derived based on*	*Unit*	*Possible values (type)*	*Changes, imputations, assumptions, comments*
RBC	Concentration of red blood cells Reference interval female: 4.1 – 5.4 Reference interval female: 4.5 – 6.0	---	10^6/µL	x.xx - y.yy (real, ≥ 0)	---
HC	Haematocrit Reference interval female: 40 – 54 Reference interval male: 36 – 48	---	%	x.xxx - y.yyy (real, ≥ 0)	---
HB	Haemoglobin Reference interval female: 11.5 – 16.4 Reference interval male: 13.5 – 18.0	---	g/dL	x.x - y.y (real, ≥ 0)	---

Table 10.5: Efficacy measurement information

Data label	*Description and characteristics*	*Derived based on*	*Unit*	*Possible values (type)*	*Changes, imputations, assumptions, comments*
SUMDIA	Sum of diameters of target lesions according to RECIST (= LUNGDIA + LIVERDIA + BRAINDIA + LYMPDIA +OTHERDIA)	LUNGDIA LIVERDIA BRAINDIA LYMPDIA OTHERDIA	cm	x.xx - y.yy (real, ≥ 0)	• For 1 tumour assessment date (≙ 0.05%), the year was implausible and therefore adapted (FLGTIME = 6).
PROG	Tumour progression 0 No progression detected yet 1 Time when progression was detected 2 Time after detection of progression	---	---	0, 1, 2	• For 3 patients (≙ 0.82%), tumour progression was reported as adverse events but not reported in the progression dataset. The respective events were added in the progression dataset and not considered as adverse events. (FLGPROS = 1).
DEATH	Death 0 Patient alive 1 Time of death	---	---	0, 1	• For 4 patients (≙ 1.09%), day of the month of death was unknown, thus middle of the month was assumed (FLGTIME = 9). • For 6 patients (≙ 1.64%), reason of study end was “death” but no date was reported, thus date of end of study was imputed (FLGTIME = 10).
HIST	Histology determined at screening/baseline visit 0 Carcinoma, not otherwise specified 1 Adenocarcinoma 2 Bronchioalveolar carcinoma 3 Squamous-cell carcinoma	---	---	0, 1, 2, 3	---
STAGE	Most recent tumour staging determined at screening/baseline visit 0 IIIB 1 IV	---	---	0, 1	---
DIAG	Time between diagnose and 1st study dose	Date of diagnose DATE	days	x - y (natural, ≥ 0)	• For 16 patients (≙ 4.38%), median (20 days) of whole population was imputed for incomplete date of diagnosis (FLGCOV = 8).
PFST	Progression-free survival time, calculated from 1st dose administration	PROG DATE	days	x - y (natural, ≥ 0)	---
OST	Overall survival time, calculated from 1st dose administration	DEATH DATE	days	x - y (natural, ≥ 0)	---

Data label	*Description and characteristics*	*Derived based on*	*Unit*	*Possible values (type)*	*Changes, imputations, assumptions, comments*
NTARG	Number of target lesions max: 5 according to RECIST	---	---	0 - 5 (natural)	---
NNTARG	Number of non-target lesions	---	---	x - y (natural, ≥ 0)	---
TARGRES	Response of target lesions according to RECIST 0 NE: not evaluable 1 PD: progressive disease 2 SD: stable disease 3 PR: partial response 4 CR: complete response	---	---	0 - 4 (natural)	---
NTARGRES	Response of non-target lesions according to RECIST 0 NE: not evaluable 1 PD: progressive disease 2 SD: stable disease 3 PR: partial response 4 CR: complete response	---	---	0 - 4 (natural)	---
NEWLES	Have new lesions been detected? 0 No 1 Yes	---	---	0, 1	---
ORESI	Overall response according to investigator 0 NE: not evaluable 1 PD: progressive disease 2 SD: stable disease 3 PR: partial response 4 CR: complete response	---	---	0 - 4 (natural)	---
ORESC	Overall response calculated 0 NE: not evaluable 1 PD: progressive disease 2 SD: stable disease 3 PR: partial response 4 CR: complete response	---	---	0 - 4 (natural)	---

Data label	*Description and characteristics*	*Derived based on*	*Unit*	*Possible values (type)*	*Changes, imputations, assumptions, comments*
LIVERL	Were liver lesions detected? 0 No 1 Yes	---	---	0, 1	• Imputation by last observation carried forward, for time points between tumour assessment.
BRAINL	Were brain lesions detected? 0 No 1 Yes	---	---	0, 1	• Imputation by last observation carried forward, for time points between tumour assessment.
LYMPL	Were lymph lesions detected? 0 No 1 Yes	---	---	0, 1	• Imputation by last observation carried forward, for time points between tumour assessment.
BONEL	Were bone lesions detected 0 No 1 Yes	---	---	0, 1	• Imputation by last observation carried forward, for time points between tumour assessment.
OTHERL	Were other lesions (beside lung, liver, brain, lymph nodes and bones) detected? 0 No 1 Yes	---	---	0, 1	• Imputation by last observation carried forward, for time points between tumour assessment.
LUNGDIA	Sum of diameters of lesions at the target site lung	---	cm	x.xx - y.yy (real, ≥ 0)	---
LIVERDIA	Sum of diameters of lesions at the target site liver	---	cm	x.xx - y.yy (real, ≥ 0)	---
BRAINDIA	Sum of diameters of lesions at the target site brain	---	cm	x.xx - y.yy (real, ≥ 0)	---
LYMPDIA	Sum of diameters of lesions at the target site lymph nodes	---	cm	x.xx - y.yy (real, ≥ 0)	• For 3 tumour measurements (≙ 0.16%), very long diameters (> 16 cm) were reported. For these it was assumed that these values were reported in mm instead of cm, thus they were divided by 10 (FLGTUM = 1).
OTHERDIA	Sum of diameters of other target sites (besides lung, liver, brain and lymph nodes)	---	cm	x.xx - y.yy (real, ≥ 0)	---

Table 10.6: Information on further patient-related covariates

Data label	*Description and characteristics*	*Derived based on*	*Unit*	*Possible values (type)*	*Changes, imputations, assumptions, comments*
AGE	Age at screening/baseline visit	---	years	x - y (natural, > 0)	---
AGEG	Age group based on the categorisation of the dosing algorithm 1 ≤ 45 years 2 > 45 - 50 years 3 > 50 - 55 years 4 > 55 - 60 years 5 > 60 - ≤ 65 years 6 > 65 years	AGE	---	1 - 6 (natural)	---
SEX	Sex 0 Female 1 Male	---	---	0, 1	---
SMOK	Smoking status at screening/baseline visit 1 Never 2 Former 3 Current	---	---	1, 2, 3	---
HT	Body height at screening/baseline visit	---	cm	x - y (natural, > 0)	---
BSA	Body surface area Calculated by the DuBois-DuBois-formula: $0.007184 \cdot HT^{0.725} \cdot WT^{0.425}$	HT WT	m^2	x.xx - y.yy (real, > 0)	• Missing values were imputed by applying the DuBois-DuBois-formula.
WT	Body weight determined at the beginning of each cycle	---	kg	x - y (natural, > 0)	• Imputation by last observation carried forward, for time points between measurements.

Data label	*Description and characteristics*	*Derived based on*	*Unit*	*Possible values (type)*	*Changes, imputations, assumptions, comments*
ECOG	ECOG performance status determined at the beginning of each cycle 0 Fully active 1 Restricted in physically strenuous activity but ambulatory 2 Ambulatory and capable of all self-care but unable to carry out any work activities 3 Capable of only limited self-care 4 Completely disabled 5 Dead	---	---	0, 1, 2,… 5	• Imputation by last observation carried forward, for time points between measurements.

Table 10.7: Clinical chemistry information

Data label	*Description and characteristics*	*Derived based on*	*Unit*	*Possible values (type)*	*Changes, imputations, assumptions, comments*
BILI	Total bilirubin concentration Reference interval: < 19 µmol/L	---	µmol/L	x.xx - y.yy (real, ≥ 0)	• Linear regression over time was used to impute bilirubin values between the time points of measurement.
BILIG	Bilirubin group, divided based on the 25th ($P_{0.25}$), 50th ($P_{0.5}$) and 75th ($P_{0.75}$) percentiles of baseline bilirubin concentration 1 <$P_{0.25}$ 2 $P_{0.25}$ - < $P_{0.5}$ 3 $P_{0.5}$ - < $P_{0.75}$ 4 ≥ $P_{0.75}$ $P_{0.25}$ = 5 µmol/L, $P_{0.5}$ = 7 µmol/L, $P_{0.75}$ = 9 µmol/L	BILI	---	1, 2, 3,4	---
CREA	Creatinine concentration determined at the beginning of each cycle Reference interval female: 0.8 – 1.2 Reference interval male: 0.9 – 1.4	---	mg/dL	x.xx - y.yy (real, ≥ 0)	• Imputation by last observation carried forward, for time points between measurements.
CLCR	Creatinine clearance as predictor for glomerular filtration rate (GFR) Calculated using the Cockroft-Gault formula [81] CLCR = Sex related factor * ((140 - AGE) / (CREA)) * (WT / 72) Sex related factor: male = 1, female = 0.85) Reference interval female: 98 – 156 Reference interval male: 95 – 160	SEX AGE CREA WT	mL/min	x.xx - y.yy (real, ≥ 0)	---
AST	Concentration of aspartate aminotransferase at screening/baseline visit (also called glutamic oxaloacetic transaminase (GOT)) Reference interval female: <35 reference interval male: <50	---	U/L	x - y (natural, ≥ 0)	---
ALT	Concentration of alanine aminotransferase at screening/baseline visit (also called glutamate-pyruvate transaminase (GPT)) Reference interval female: <35 Reference interval male: <50	---	U/L	x - y (natural, ≥ 0)	---

Data label	*Description and characteristics*	*Derived based on*	*Unit*	*Possible values (type)*	*Changes, imputations, assumptions, comments*
GGT	Concentration of gamma-glutamyl transpeptidase at screening/baseline visit Reference interval female: 4 – 18 Reference interval male: 10 – 71	---	U/L	x - y (natural, ≥ 0)	• For 1 patient (≙ 0.27%), median of whole population (47 U/L) was imputed for missing values (FLGCOV = 4).
ALP	Concentration of alkaline phosphatase at screening/baseline visit Reference interval female: 60 – 170 Reference interval male: 70 – 175	---	U/L	x - y (natural, ≥ 0)	---
LDH	Concentration of lactate dehydrogenase at screening/baseline visit Reference interval: 120 – 240	---	U/L	x - y (natural, ≥ 0)	---
PROT	Total protein concentration at screening/baseline visit Reference interval: 6.6 – 8.3	---	g/dL	x.x - y.y (real, ≥ 0)	---
GLU	Blood glucose concentration at screening/baseline visit Reference interval fasted: 70 – 110 Reference interval 2 h after meal: < 140	---	mg/dL		• For 2 patients (≙ 0.55%), median of whole population (106 mg/dL) was imputed for missing values (FLGCOV = 4 and 5).
CA	Calcium concentration at screening/baseline visit Reference interval: 2.20 – 2.65	---	mmol/L	x.xx - y.yy (real, ≥ 0)	• ---
CL	Chloride concentration at screening/baseline visit Reference interval: 95 – 110	---	mmol/L	x - y (natural, ≥ 0)	• For 3 patients (≙ 0.82%), median of whole population (102 mmol/L) was imputed for missing values (FLGCOV = 1).
K	Potassium concentration at screening/baseline visit Reference interval: 3.6 – 5.2	---	mmol/L	x.xx - y.yy (real, ≥ 0)	---
NA	Sodium concentration at screening/baseline visit Reference interval: 135 – 148	---	mmol/L	x - y (natural, ≥ 0)	---

Data label	*Description and characteristics*	*Derived based on*	*Unit*	*Possible values (type)*	*Changes, imputations, assumptions, comments*
APTT	Activated partial thromboplastin time at screening/baseline visit Reference interval: 28-38 seconds	---	s	x.xx - y.yy (real, ≥ 0)	• For 3 patients (≙ 0.82) values < 5 or > 70 (0.73; 0.98; 91 s, respectively) were reported and deleted due to implausibility median of whole population (30 s) was imputed for missing values (FLGCOV = 2).

Table 10.8: Pretreatment information

Data label	*Description and characteristics*	*Derived based on*	*Unit*	*Possible values (type)*	*Changes, imputations, assumptions, comments*
PRETRE	Pre-Treatment Has any pretreatment been performed 0 No 1 Yes	PRER PREC PRES	---	0, 1	• For 1 patient (≙ 0.27%), description says radio-chemotherapy, closest to radiotherapy For 1 patient (≙ 0.27%), descript.ion says photodynamic therapy, closest to surgery (only local effect) (for both, FLGCOV = 3).
PREC	Pre-therapy with chemotherapy Time difference between last day of pre-therapy and first day of paclitaxel administration within the CEPAC-TDM Study	End of pre-therapy DATE	days	x - y (natural, ≥ 0)	---
PRER	Pre-therapy with radiotherapy Time difference between last day of pre-therapy and first day of paclitaxel administration within the CEPAC-TDM Study	End of pre-therapy DATE	days	x - y (natural, ≥ 0)	---
PRES	Pre-therapy with surgery Time difference between last day of pre-therapy and first day of paclitaxel administration within the CEPAC-TDM Study	End of pre-therapy DATE	days	x - y (natural, ≥ 0)	---

Table 10.9: Information about concomitant therapy, supportive treatment and other comedication

Data label	*Description and characteristics*	*Derived based on*	*Unit*	*Possible values (type)*	*Changes, imputations, assumptions, comments*
CMNP	Comedication causing neutropenia (probability of effect) 0 No effect known 1 Very rare adverse events < 0,01% 2 Rare adverse events 0,01% - 0,1% 3 Occasional adverse events 0,1% - 1% 4 Common adverse events 1% - 10% 5 Very common adverse events > 10%	---	---	0 - 5 (natural)	• Each active ingredient of a medication reported as comedication, cotherapy or in the follow-up was graded based on the probability to cause an effect, based on the information from the summary of product characteristics. • Radiotherapy and surgery were treated separately and are not represented in this column. • Medications already started at least one day before study start were ignored, since it was assumed that they might influence the baseline neutrophil concentration but not the effect of the chemotherapy on neutropenia. Missing start date of comedication: Medication was assumed to be taken at least one year before study start. • If chemotherapeutic agent was known, it was treated as any other medication; if not it was assumed to have neutropenia as a very common side effect. • Medications for which an end date was not known were assumed to be taken until study end and further (1983 of 5718). • For medications without full date was available (day of the date or day and month missing), mid of the month/year (121 and 12 occasions, respectively) was assumed. • For one patient one medication only stated in the comments of the adverse events dataset was added (AUGEMNTAN). • Medications administered via a locally acting route of administration (e.g. creams, …) were assumed not to have any influence.

Data label	*Description and characteristics*	*Derived based on*	*Unit*	*Possible values (type)*	*Changes, imputations, assumptions, comments*
					• Start clock times were set to 10:00 and end clock times were set to 23:59. • The following probabilities were assigned to frequency grades grade: 0 probability: 0 grade: 1 probability: 0.005 grade: 2 probability: 0.05 grade: 3 probability: 0.5 grade: 4 probability: 5 grade: 5 probability: 10 • For each time point the probabilities of the currently taken medications were summed up. • Afterwards the resulting probabilities were back-transformed to grades.
CMGLUC	Comedication with glucocorticoids (in addition to the premedication) administered at the respective time point? 0 No 1 Yes	---	---	0, 1	• Start clock times were set to 10:00 and end clock times were set to 23:59.
CMGCSF	Comedication with G-CSF administered at the respective time point? 0 No 1 Yes	---	---	0, 1	• Start clock times were set to 10:00 and end clock times were set to 23:59.
CHEMO	Concomitant chemotherapy administered at the respective time point? 0 No 1 Yes	---	---	0, 1	• Start clock times were set to 10:00 and end clock times were set to 23:59. • Day of date was unknown, middle of the month was assumed.

Data label	*Description and characteristics*	*Derived based on*	*Unit*	*Possible values (type)*	*Changes, imputations, assumptions, comments*
RADIO	Concomitant radiotherapy administered at the respective time point? 0 No 1 Yes	---	---	0, 1	• Start clock times were set to 10:00 and end clock times were set to 23:59. • Day of date was unknown, middle of the month was assumed. • For 1 concomitant therapy, the whole start date of radiotherapy was missing; assume same date as end of therapy.
SURG	Surgery performed at the respective time point? 0 No 1 Yes	---	---	0, 1	• Start clock times were set to 10:00 and end clock times were set to 23:59 of the same day. • In the comments of the efficacy report, 2 surgeries were reported and were thus added to this column.
CMNP4ID	Patients receiving comedication with increasing influence on neutropenia, with an effect of ≥ 4 (i.e. common and very common side effect, see CMNP) 0 No 1 Yes	CMNP	---	0, 1	---
CMNP5ID	Patients receiving comedication with increasing influence on neutropenia, with an effect of ≥ 5 (very common side effect, see CMNP) 0 No 1 Yes	CMNP	---	0, 1	---
CMGLUCID	Patients with glucocorticoids as comedication 0 No 1 Yes	CMGLUC	---	0, 1	---
CMGCSFID	Patients with G-CSF as comedication 0 No 1 Yes	CMGCSF	---	0, 1	---
CHEMOID	Patients with concomitant chemotherapy 0 No 1 Yes	CHEMO	---	0, 1	---

Data label	*Description and characteristics*	*Derived based on*	*Unit*	*Possible values (type)*	*Changes, imputations, assumptions, comments*
RADIOID	Patients with concomitant radiotherapy 0 No 1 Yes	RADIO	---	0, 1	---
SURGID	Patients with concomitant surgery 0 No 1 Yes	SURG	---	0, 1	---
CHEMOIDS	Patients with concomitant chemotherapy, “yes” assigned from start of concomitant therapy until last event of the respective patient 0 No 1 Yes	CHEMO	---	0, 1	---
RRADIOIDS	Patients with concomitant radiotherapy, “yes” assigned from start of concomitant therapy until last event of the respective patient 0 No 1 Yes	RADIO	---	0, 1	---
SURGIDS	Patients with concomitant surgery, “yes” assigned from start of concomitant therapy until last event of the respective patient 0 No 1 Yes	SURG	---	0, 1	---

Table 10.10: Information about adverse events according to CTCAE4.0 criteria [35]

Data label	*Description and characteristics*	*Derived based on*	*Unit*	*Possible values (type)*	*Changes, imputations, assumptions, comments*
HEMMAX	Maximal haematological toxicity in the current treatment cycle according to CTCAE4.0 criteria 1 Mild 2 Moderate 3 Severe 4 Life-threatening 5 Death	---	---	1 - 5 (natural)	• As for the statistical analysis in [247], adverse events reported as following were grouped: "anaemia", "decreased granulocyte count", "decreased lymphocyte count", "decreased neutrophil count", "decreased thrombocyte count", "decreased WBC count", "febrile infection", "haematocrit decreased/low", "haemoglobinemia", "leukopenia", "neutropenia with or without sepsis/fever", "pancytopenia", "sepsis", "septic shock".
NEURMAX	Maximal neurological toxicity (peripheral neuropathy) in the current treatment cycle according to CTCAE4.0 criteria 1 Mild 2 Moderate 3 Severe 4 Life-threatening 5 Death	---	---	1 - 5 (natural)	• As for the statistical analysis in [247], adverse events reported as following were grouped: "burning feet", "diabetic polyneuropathy", "dysasthesia/parasthesia in hands and feet", "feet and hands polyneuropathy", "increasing pain in extremities", "legs and fingertips numbness", "myalgia (peripheral)", "numbness left hand", "numbness lower extremities both sides", "pain in lower extremities", "paresthesia", "(peripheral) dysesthesia", "peripheral (poly)neuropathy", "pnp", "polyneuropathia", "polyneuropathy", "polyneuropathy peripheral", "progressive polyneuropathy", "shooting pain".
NHEMMAX	Maximal non-haematological toxicity in the current treatment cycle according to CTCAE4.0 criteria 1 Mild 2 Moderate 3 Severe 4 Life-threatening 5 Death	---	---	1 - 5 (natural)	• As for the statistical analysis in [247], adverse events were grouped: all other adverse events that were not listed in HEMMAX or NEURMAX.

Data label	*Description and characteristics*	*Derived based on*	*Unit*	*Possible values (type)*	*Changes, imputations, assumptions, comments*
GRADEN	Grade of neutropenia according to CTCAE4.0 criteria 1 Mild 2 Moderate 3 Severe 4 Life-threatening 5 Death	NGA	---	1 - 5 (natural)	---
GRADEP	Grade of thrombocytopenia according to CTCAE4.0 criteria 1 Mild 2 Moderate 3 Severe 4 Life-threatening 5 Death	---	---	1 - 5 (natural)	---

Table 10.11: Information on flags

Data label	*Description and characteristics*	*Derived based on*	*Unit*	*Possible values (type)*	*Changes, imputations, assumptions, comments*
FLGTIME	Time flag 0 No imputation/change 1 Missing start (and stop) time of infusion 2 Very short infusion duration (< 1 h) or extreme high RATE (> 400 µmol/h) --> DUR = 3 3 Platinum-based drug administration before paclitaxel 4 Additional platinum-based drug dose on day 8 6 Probably wrong date for tumour assessment (year changed) 7 PK measurement before/less than 2 h after drug administration or more than 40 h after PTX administration 8 Day of date missing for end of study visit (15 imputed)	---	---	0 - 8 (natural)	---
FLGDOSE	Dose flag 0 No imputation/change 1 Carboplatin was reported, based on dose it was concluded that cisplatin must have been given 2 Cisplatin was reported, based on dose it was concluded that carboplatin must have been given 3 Carboplatin dose imputed from interims data, since the information was deleted in the final dataset and commented that the drug was changed from cisplatin to carboplatin	---	---	0 - 4 (natural)	---
FLGPK	PK flag 0 No imputation/change 1 Paclitaxel concentration measurement reported to be 0 2 Infusion stopped due to allergic reaction, influence on all following measurements	---	---	0 - 2 (natural)	---

Data label	*Description and characteristics*	*Derived based on*	*Unit*	*Possible values (type)*	*Changes, imputations, assumptions, comments*
FLGN	Neutrophil flag 0 No imputation/change 1 0 reported, LNEU --> ln(0.01)	---	---	0, 1	---
FLGTUM	Tumour assessment flag: 0 No imputation/change 1 Diameter of lymph nodes divided by 10 as wrong unit was assumed	---	---	0, 1	---
FLGCOV	Covariate flag 0 No imputation/change 1 Chloride concentration missing, imputed by median of whole population 2 APPT > 70 (deleted) or < 5, imputed by median of whole population 3 Changes in pretreatment 4 GGT and glucose concentration imputed by median of whole population 5 Diagnose imputed by median of whole population 8 Date of diagnose incomplete, imputed by median of whole population	---	---	0 - 8 (natural)	---
FLGPROS	Progression and survival flag 0 No imputation/change 1 Date of progression taken from comments from adverse events 2 End of study information imputed for day of death, because date unknown but reason for end of study was death 3 Day of date of death unknown (15 imputed)	---	---	0 - 3 (natural)	---
FLAG	Marker for events used for the PK analysis during the CEPAC-TDM study to determine the $T_{C>0.05}$. Only Paclitaxel dosing information, the PK measurement and TALD = 100 h were used. 0 Not used during the study 1 Used during the study	---	---	0, 1	---

10.2 Figures

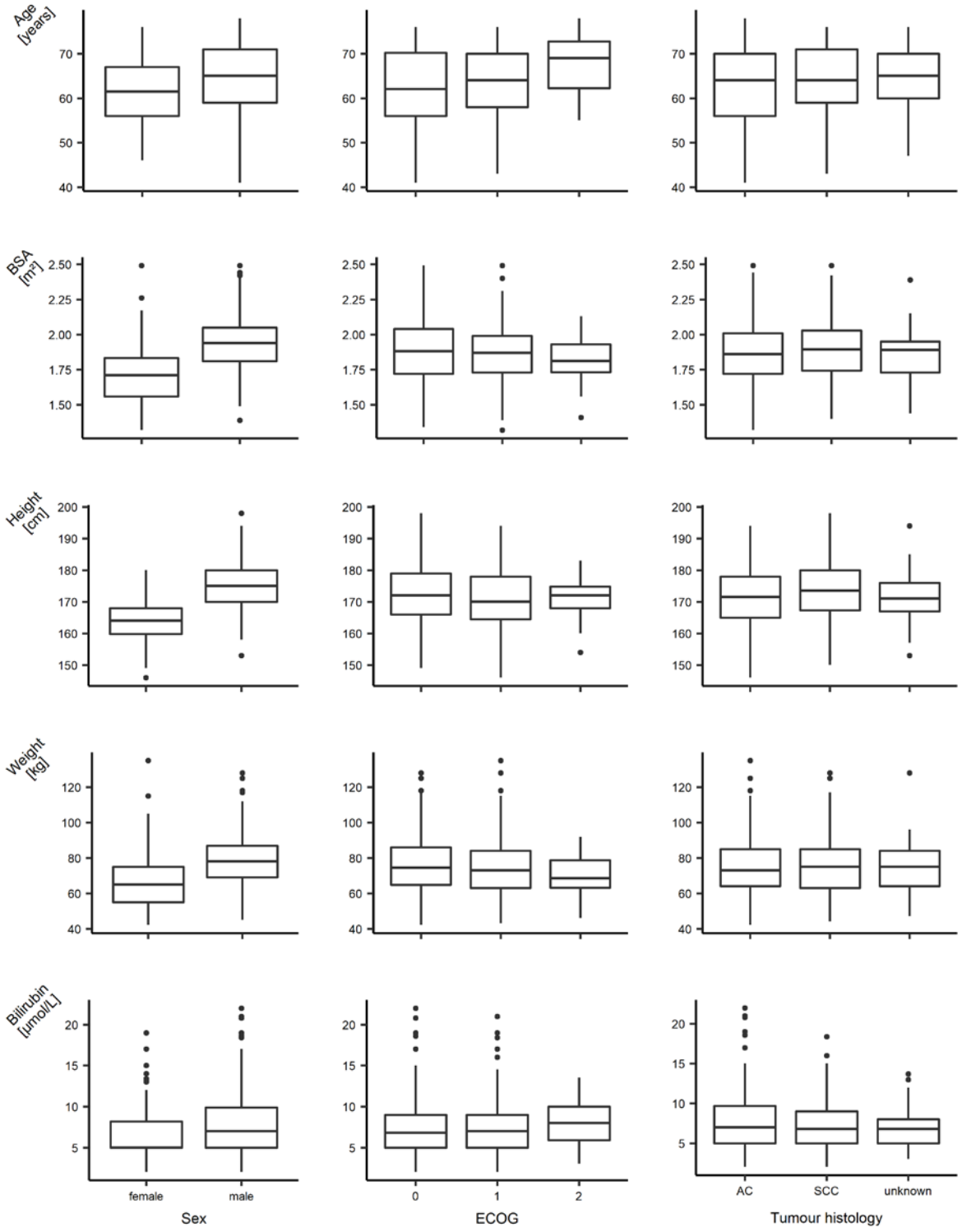

Figure 10.1: Exploration of continuous covariates over categorical covariates.
AC: adenocarcinoma; BSA: body surface area; BSL: neutrophil concentration at baseline; BSL_{SD}: baseline tumour size; CL_{CR}: creatinine clearance; LDH: lactate dehydrogenase; SCC: squamous-cell carcinoma.
Boxes: interquartile range (IQR), including median; whiskers: range from box hinge to highest/lowest value within 1.5•IQR; points: data beyond whiskers.

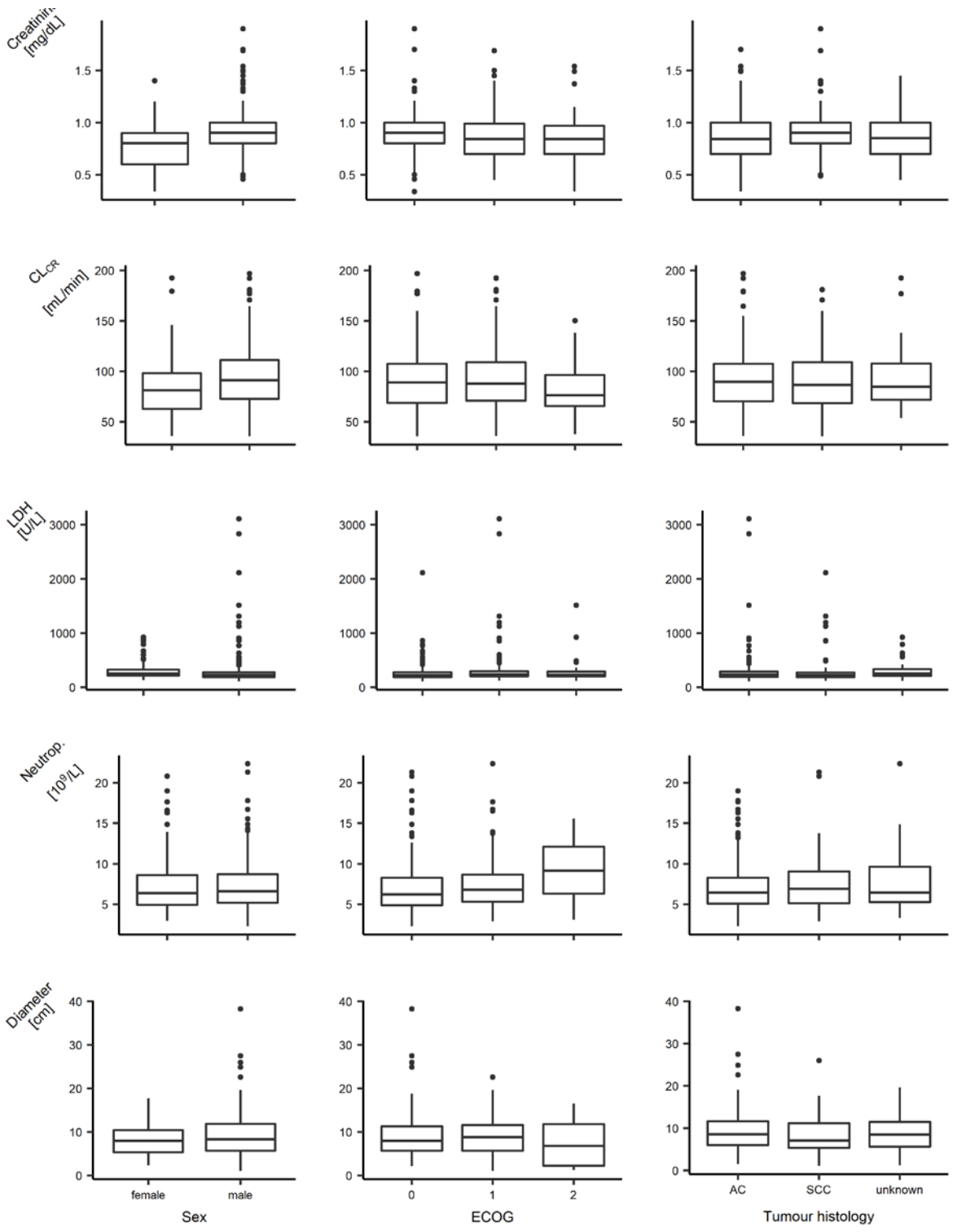

Figure 10.1 continued

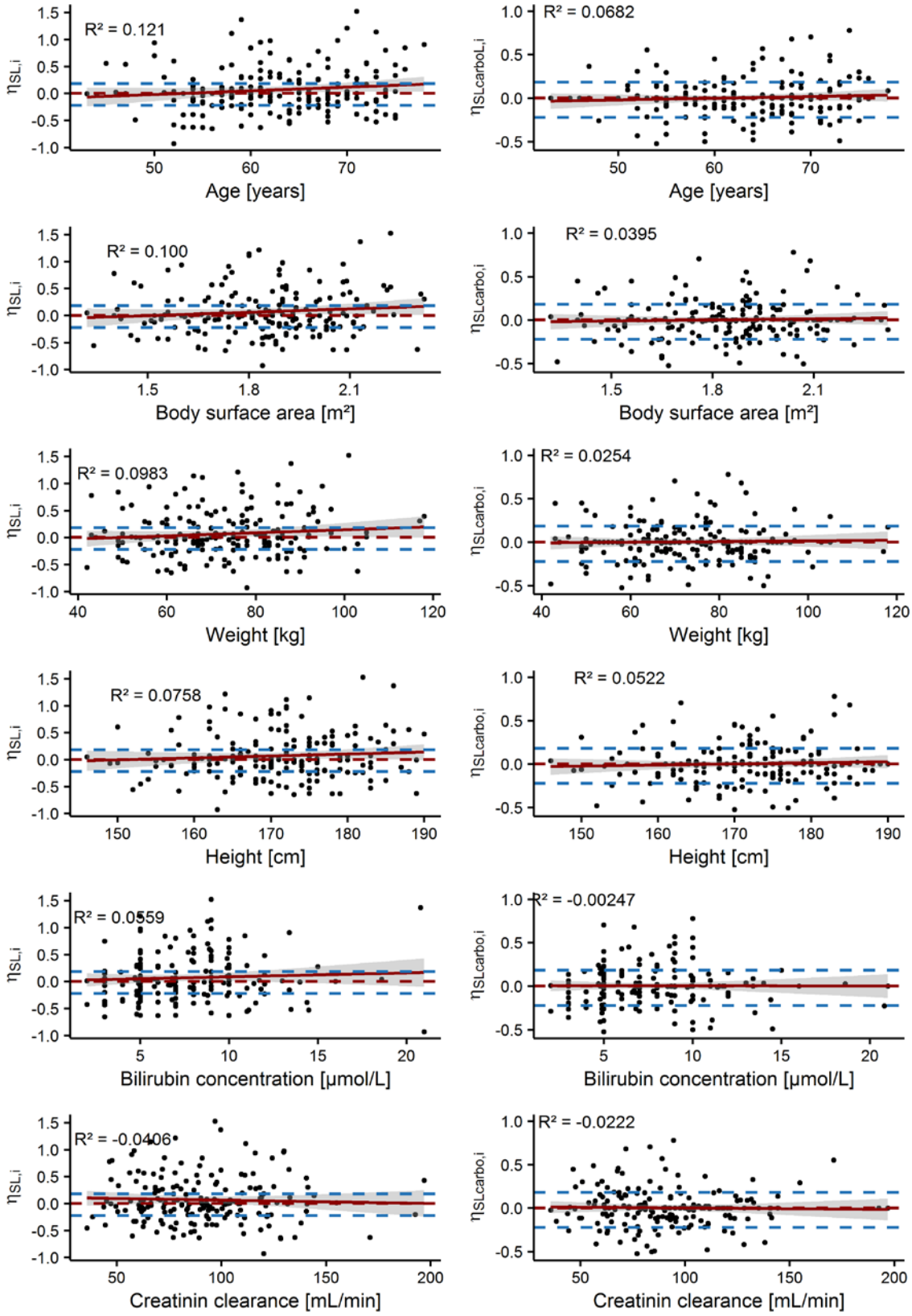

Figure 10.2: Visual inspection of potential influences of continuous covariates on the slope factor of paclitaxel and carboplatin respectively

$\eta_{SL,i}$ and $\eta_{SL_{carbo},i}$: individual variability parameter on the slope factor of paclitaxel and carboplatin, respectively; R²: Pearson's correlation coefficient.

Red dashed line: no effect of the individual variability parameter; blue dashed lines: natural logarithm of 0.8 and 1.2, respectively determining 20% change in the individual parameter estimate; solid red line: linear regression; grey shaded area: 95% confidence interval of the linear regression.

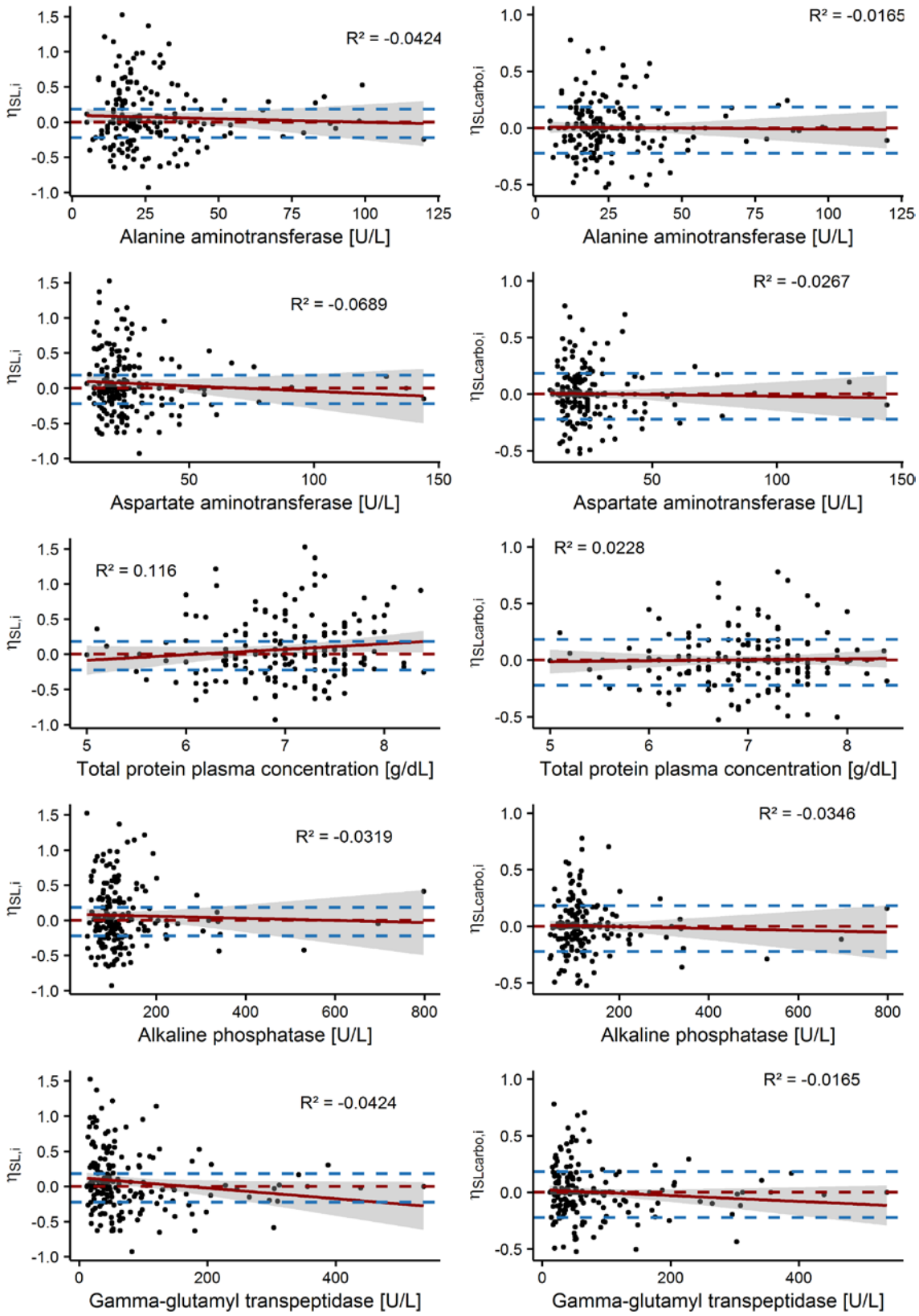

Figure 10.2 continued

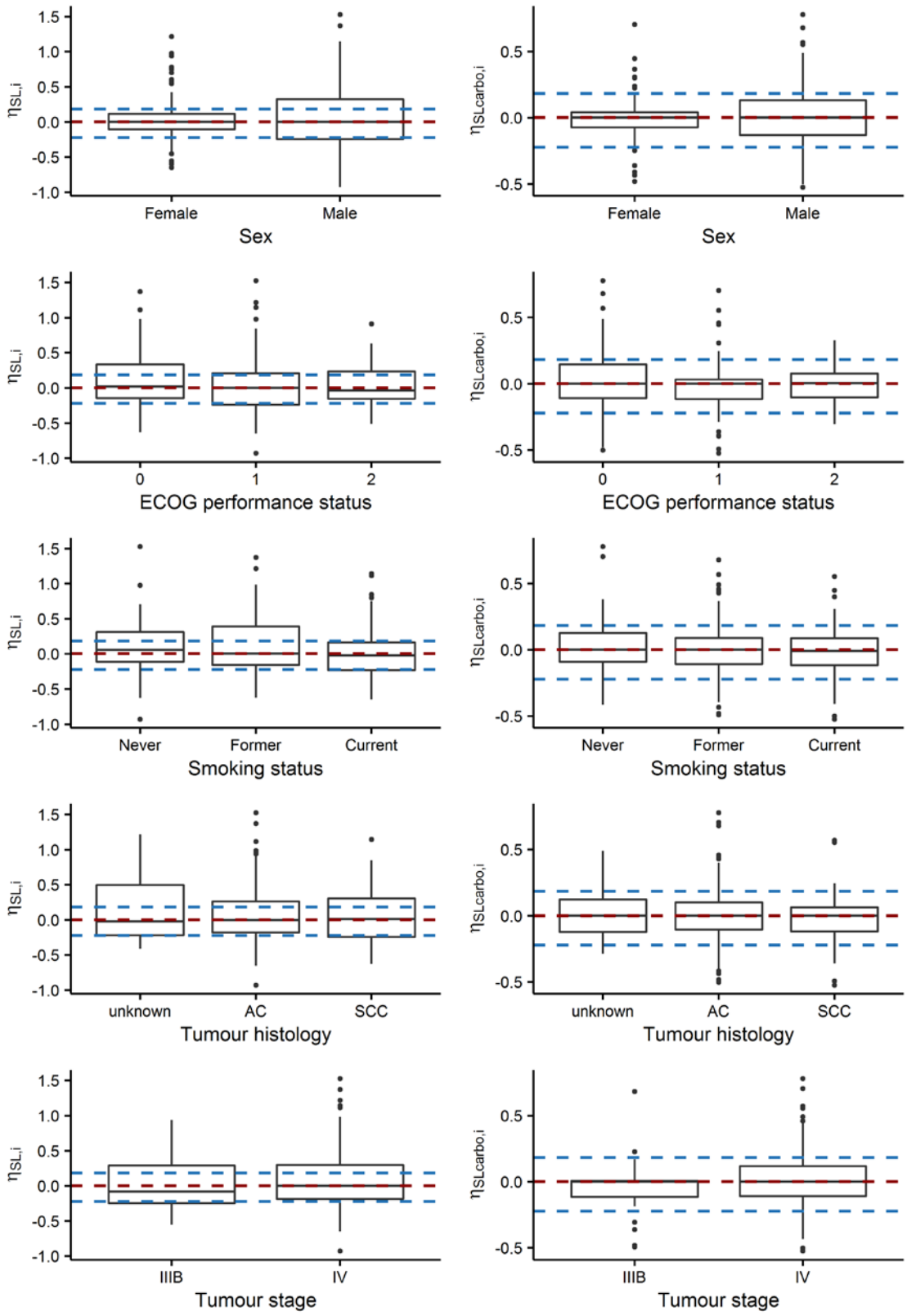

Figure 10.3: Visual inspection of potential influences of categorical covariates on the slope factor of paclitaxel and carboplatin respectively

$\eta_{SL,i}$ and $\eta_{SL_{carbo},i}$: individual variability parameter on the slope factor of paclitaxel and carboplatin, respectively; AC: adenocarcinoma; SCC: squamous-cell carcinoma.

Red dashed line: no effect of the individual variability parameter; blue dashed lines: natural logarithm of 0.8 and 1.2, respectively determining 20% change in the individual parameter estimate.

Boxes: interquartile range (IQR), including median; whiskers: range from box hinge to highest/lowest value within 1.5•IQR; points: data beyond whiskers.

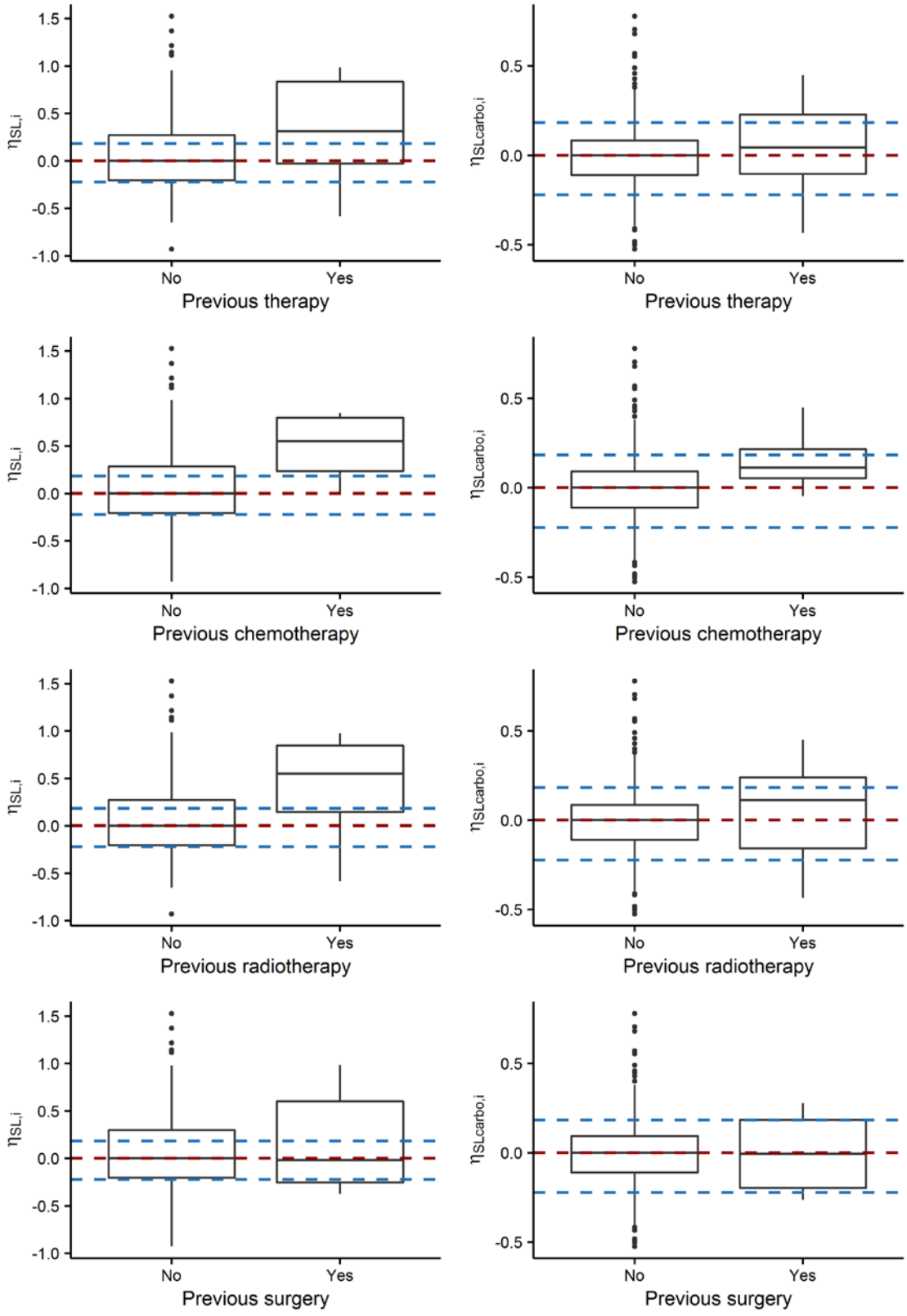

Figure 10.3 continued

10.3 NONMEM model code

10.3.1 Project 1: PK Model I

```
$SIZES LVR = 60          ; Number of possible ETA estimates was increased due to the prior function

$PROBLEM PK Paclitaxel Model I

$INPUT  ID TIME2 TIME OCC DAY AMT DOSE DRUG RATE DUR DV CONC TC CMT EVID MDV
        FLGTIME FLGDOSE FLGPK FLGCOV FLAG AGE SEX BSA BILI CURRENTP PLATIN
        DOSEG DOSEG2 AGEG BILIG MAXOCC
   ; TIME2 = TIME and TIME = TALD → the modelling is performed on the TALD scale, which requires
        EVID 4 for each dosing event which resets all compartments at the same time
   ; DV = LNCONC

$DATA    PacliPK6.2subs.csv    IGNORE = #

$SUBROUTINES ADVAN6 TOL=4

$PRIOR NWPRI          ; Normal inverseWishart distribution

$MODEL      COMP = (CENTRAL, DEFDOSE)  ; Central paclitaxel compartment
            COMP = (PER1)              ; First peripheral compartment
            COMP = (PER2)              ; Second peripheral compartment
            COMP = (THR)               ; Dummy compartment for calculation of T_C>0.05
            COMP = (AUC)               ; Dummy compartment for calculation of AUC

$PK

   FLG1     = 0
   FLG2     = 0
   FLG3     = 0
   FLG4     = 0
   FLG5     = 0
   FLG6     = 0
   IF(OCC.EQ.1) FLG1 =1
   IF(OCC.EQ.2) FLG2 =1
   IF(OCC.EQ.3) FLG3 =1
   IF(OCC.EQ.4) FLG4 =1
   IF(OCC.EQ.5) FLG5 =1
   IF(OCC.EQ.6) FLG6 =1

   TVV1     = THETA(1)
   IOVV1    = FLG1*ETA(7) + FLG2*ETA(8) + FLG3*ETA(9) + FLG4*ETA(10) + FLG5*ETA(11)
              + FLG6*ETA(12)
   V1       = TVV1*EXP(IOVV1)
   TVKM1    = THETA(2)
   KM1      = TVKM1                  ; Km_EL
```

```
    TVVM1   = THETA(3) * (BSA/1.8)**THETA(9) * THETA(10)**SEX * (AGE/56)**THETA(11)
              * (BILI/7)**THETA(12)
    IOVVM1  = FLG1*ETA(13) + FLG2*ETA(14) + FLG3*ETA(15) + FLG4*ETA(16) + FLG5*ETA(17) +
              FLG6*ETA(18)
    VM1     = TVVM1 * EXP(ETA(1)+IOVVM1)          ; VM_EL
    TVKM2   = THETA(4)
    KM2     = TVKM2*EXP(ETA(2))                   ; Km_TR
    TVVM2   = THETA(5)
    VM2     = TVVM2*EXP(ETA(3))                   ; VM_TR
    TVK21   = THETA(6)
    K21     = TVK21*EXP(ETA(4))
    TVV3    = THETA(7)
    V3      = TVV3*EXP(ETA(5))
    TVQ     = THETA(8)
    Q       = TVQ*EXP(ETA(6))
    K13     = Q/V1
    K31     = Q/V3
    S1      = V1
    S3      = V3

$DES
    C1      = A(1)/S1             ; C_PTX(t)
    DADT(1) = -C1*VM1/(KM1+C1) + K21*A(2) - C1*VM2/(KM2+C1) + K31*A(3) - K13*A(1)
    DADT(2) = C1*VM2/(KM2+C1) - K21*A(2)
    DADT(3) = K13*A(1) - K31*A(3)

    SLOP    = 0           ; Calculation of T_C>0.05
    IF(C1.GE.0.05) SLOP=1
    DADT(4) = SLOP
    THR     = A(4)        ; THR = T_C>0.05 resulting from new model; TC = T_C>0.05 from original
                          model calculated during the CEPAC-TDM study

    DADT(5) = C1          ; Calculation of AUC
    AUC     = A(5)

$ERROR
    IF(F.GT.0) IPRED = LOG(F)
    Y       = IPRED + EPS(1)
    W       = IPRED
    IRES    = DV - IPRED
    IWRES   = IRES/W

$THETA
    10.8    ;1: V_1
    0.576   ;2: Km_EL
    35.8    ;3: VM_EL
    1.43    ;4: Km_TR
    177     ;5: VM_TR
    1.11    ;6: k_21
```

```
   275       ;7: V3
   15.6      ;8: Q
   1.30      ;9: BSA on VMEL
   1.16      ;10: SEX on VMEL
   -0.449    ;11: AGE on VMEL
   -0.159    ;12: BILI on VMEL

$OMEGA 0.0318          ;1: IIV VMEL                ; IIV: interindividual variability
$OMEGA 0.487           ;2: IIV KmTR
$OMEGA 0.0821          ;3: IIV VMTR
$OMEGA 0.00864         ;4: IIV k21
$OMEGA 0.213           ;5: IIV V3
$OMEGA 0.210           ;6: IIV Q

$OMEGA BLOCK(1) 0.139 FIX      ;7 : IOV V1 OCC1      ; IOV: interoccasion variability
$OMEGA BLOCK(1) SAME           ;8 : IOV V1 OCC2
$OMEGA BLOCK(1) SAME           ;9 : IOV V1 OCC3
$OMEGA BLOCK(1) SAME           ;10: IOV V1 OCC4
$OMEGA BLOCK(1) SAME           ;11: IOV V1 OCC5
$OMEGA BLOCK(1) SAME           ;12: IOV V1 OCC6

$OMEGA BLOCK(1) 0.0232 FIX     ;13: IOV VMEL OCC1
$OMEGA BLOCK(1) SAME           ;14: IOV VMEL OCC2
$OMEGA BLOCK(1) SAME           ;15: IOV VMEL OCC3
$OMEGA BLOCK(1) SAME           ;16: IOV VMEL OCC4
$OMEGA BLOCK(1) SAME           ;17: IOV VMEL OCC5
$OMEGA BLOCK(1) SAME           ;18: IOV VMEL OCC6

$SIGMA
   0.1       ;EPS

$THETAP       ; Prior information for THETAs
   10.8      FIX      ;1: V1
   0.576     FIX      ;2: KmEL
   35.8      FIX      ;3: VMEL
   1.43      FIX      ;4: KmTR
   177       FIX      ;5: VMTR
   1.11      FIX      ;6: k21
   275       FIX      ;7: V3
   15.6      FIX      ;8: Q
   1.30      FIX      ;9: BSA on VMEL
   1.16      FIX      ;10: SEX on VMEL
   -0.449    FIX      ;11: AGE on VMEL
   -0.159    FIX      ;12: BILI on VMEL

$THETAPV      ; Prior information for precision of THETAs
   0.169     FIX      ;1: V1
   0.00191   FIX      ;2: KmEL
```

```
   2.84     FIX     ;3: VM_EL
   0.0147   FIX     ;4: Km_TR
   33.2     FIX     ;5: VM_TR
   0.00146  FIX     ;6: k_21
   230      FIX     ;7: V_3
   0.632    FIX     ;8: Q
   0.0168   FIX     ;9: BSA on VM_EL
   0.00192  FIX     ;10: SEX on VM_EL
   0.00858  FIX     ;11: AGE on VM_EL
   0.00102  FIX     ;12: BILI on VM_EL

$OMEGAP     ; Prior information for OMEGAs
   0.0318   FIX     ;1: IIV VM_EL
   0.487    FIX     ;2: IIV Km_TR
   0.0821   FIX     ;3: IIV VM_TR
   0.00864  FIX     ;4: IIV k_21
   0.213    FIX     ;5: IIV V_3
   0.210    FIX     ;6: IIV Q

$OMEGAPD    ; Prior information for precision of OMEGAs (degrees of freedom)
   62.0     FIX     ;1: IIV VM_EL
   70.5     FIX     ;2: IIV Km_TR
   84.6     FIX     ;3: IIV VM_TR
   2.50     FIX     ;4: IIV k_21
   88.5     FIX     ;5: IIV V_3
   141      FIX     ;6: IIV Q

$SIGMAP     0.0334  FIX     ; Prior information for SIGMA

$SIGMAPD    1000    FIX     ; Prior information for precision of SIGMA (degrees of freedom)

$ESTIMATION PRINT=5 MAXEVAL=99999 METHOD=1 NOABORT POSTHOC SIGDIG=2
        MSFO=MSF002

$TABLE  ID OCC DAY TIME2 TIME AMT DOSE DRUG RATE DUR DV MDV EVID CONC TC CMT
        PRED IPRED RES WRES CWRES IRES IWRES CIWRES
        NOPRINT ONEHEADER FILE=sdtab002

$TABLE  ID TIME2 TIME V1 THR AUC KM1 TVVM1 VM1 KM2 VM2 K21 V3 Q EVID ETA1 ETA2 ETA3
        ETA4 ETA5 ETA6 ETA7 ETA8 ETA9 ETA10 ETA11 ETA12 ETA13 ETA14 ETA15 ETA16
        ETA17 ETA18
        NOPRINT ONEHEADER FILE=patab002

$TABLE  ID TIME2 TIME BSA AGE BILI
        NOPRINT ONEHEADER FILE=cotab002

$TABLE  ID TIME2 TIME SEX FLGTIME FLGDOSE FLGPK FLGCOV FLAG MAXOCC PLATIN
        CURRENTP DOSEG DOSEG2 AGEG BILIG MAXOCC
        NOPRINT ONEHEADER FILE=catab002
```

10.3.2 Project 2: Neutropenia Model C including combination therapy and G-CSF as covariate

```
$SIZES PD = -100        ; to allow for more input variables

$PROBLEM PD Neutropenia Model C, additive combination, covariates

$INPUT   ID OCC DAY TIME TALD AMT DOSE DRUG RATE DUR CMT EVID MDV LASTD LNEU=DV
         NGA=DROP BSLM FLGTIME FLGDOSE FLGPK FLGN FLGCOV CENT AGE SEX SMOK
         HT BSA WT BILI CURRENTP PLATIN ECOG V1 V3 KM1 TVVM1 VM1 KM2 VM2 K21 Q AUC
         THR DOSEG DOSEG2 AGEG BILIG MAXOCC PRETRE PREC PRER PRES PREM HIST
         STAGE PFST=DROP OST=DROP CMNP CMGLUC CMGCSF CHEMO RADIO CMNP4ID
         CMNP5ID CMGLUCID CMGCSFID CHEMOID RADIOID CHEMOIDS RRADIOIDS AST ALT
         GGT ALP PROT BONEL CLCR

   ; V1 V3 KM1 TVVM1 VM1 KM2 VM2 K21 Q AUC THR are the EBEs/exposure parameters extracted
         from the PK model

$DATA    PacliPDprior6.5Subs3.csv      IGNORE = #
         IGNORE = (FLGN.EQ.1)          ; ignore sample below lower limit of quantification

$SUBROUTINES ADVAN6 TOL=5

$MODEL       COMP = (CENTRAL, DEFDOSE)  ; 1 Central paclitaxel compartment
             COMP = (PER1)              ; 2 First peripheral paclitaxel compartment
             COMP = (PER2)              ; 3 Second peripheral paclitaxel compartment
             COMP = (STEM)              ; 4 Stem cell compartment
             COMP = (PROL)              ; 5 Compartment of proliferating cells
             COMP = (TRANS1)            ; 6 Transit compartment 1
             COMP = (TRANS2)            ; 7 Transit compartment 2
             COMP = (TRANS3)            ; 8 Transit compartment 3
             COMP = (CIRC)              ; 9 Compartment of circulating neutrophils
             COMP = (TTN)               ; 10 Dummy compartment, time to nadir
             COMP = (NADIR)             ; 11 Dummy compartment, nadir
             COMP = (CARBOC)            ; 12 Central carboplatin compartment
             COMP = (CARBOP)            ; 13 Peripheral compartment carboplatin
             COMP = (CIS)               ; 14 Cisplatin compartment

$PK

   ; Paclitaxel pharmacokinetics
   K13     = Q/V1
   K31     = Q/V3
   S1      = V1

   ; Influence of platinum-based drugs and G-CSF
   IF(CURRENTP.EQ.1)SLOPE2 = THETA(6) * EXP(ETA(6))   ; carboplatin
   IF(CURRENTP.EQ.0)SLOPE2 = THETA(7) * EXP(ETA(7))   ; cisplatin
   RED     = 0                                        ; G-CSF
   IF(CMGCSF.EQ.1) RED = THETA(8)
```

```
    ; Neutrophils (pharmacodynamics)
    MTT     = THETA(1) * EXP(ETA(1))
    SLOPE   = THETA(2) * EXP(ETA(2))
    BASE    = EXP(LOG(BSLM) + THETA(3)*ETA(3))
    GAMMA   = THETA(4) * EXP(ETA(4))
    X       = THETA(5) * EXP(ETA(5))                ; ftr
    KTR     = 4/MTT
    KPROL   = X * KTR
    KSTEM   = (1-X) * KTR

    A_0(4)  = BASE
    A_0(5)  = BASE
    A_0(6)  = BASE
    A_0(7)  = BASE
    A_0(8)  = BASE
    A_0(9)  = BASE

    ; Carboplatin pharmacokinetics
    CAV1    = 20.4 * (WT/70)**0.806
    CAQ     = 0.834 * (AGE/31)**(-0.311) * (HT/176)**2.33
    CACL    = 6.588 * (CLCR/103.1)**0.57 * (HT/176)**1.43
    CAV2    = 32.3
    CAK10   = CACL/CAV1
    CAK12   = CAQ/CAV1
    CAK21   = CAQ/CAV2

    ; Cisplatin pharmacokinetics
    CICL    = 51.7 + 26.3 * (BSA - 1.86)
    CIV     = 41.4 + 24.6 * (BSA - 1.86)
    CIK10   = CICL/CIV

$DES

    ; Carboplatin pharmacokinetics
    DADT(12)  = - CAK12 * A(12) + CAK21 * A(13) - CAK10 * A(12)
    DADT(13)  = CAK12 * A(12) - CAK21 * A(13)
    CAC1      = A(12)/CAV1          ; C_Carbo(t)

    ; Cisplatin pharmacokinetics
    DADT(14)  = - CIK10 * A(14)
    CIC       = A(14)/CIV           ; C_Cis(t)

    ; Paclitaxel pharmacokinetics
    C1      = A(1)/S1               ; C_PTX(t)
    DADT(1) = - C1*VM1/(KM1+C1) + K21*A(2) - C1*VM2/(KM2+C1) + K31*A(3) - K13*A(1)
    DADT(2) = C1*VM2/(KM2+C1) - K21*A(2)
    DADT(3) = K13*A(1) - K31*A(3)
```

```
    ; Neutrophils (pharmacodynamics)
    EFFPTX  = SLOPE*C1
    IF(CURRENTP.EQ.1) EFFPL = SLOPE2 * CAC1     ; carboplatin
    IF(CURRENTP.EQ.0) EFFPL = SLOPE2 * CIC      ; cisplatin
    EFF     = EFFPTX + EFFPL – RED              ; additive drug effect
    FEEDB   = (BASE/A(9))**GAMMA

    DADT(4) = KSTEM*(1-EFF)*FEEDB*A(4) - KSTEM*A(4)
    DADT(5)  = KPROL*A(5)*(1-EFF)*FEEDB - KTR*A(5) + KSTEM*A(4)
    DADT(6)  = KTR*A(5) - KTR*A(6)
    DADT(7)  = KTR*A(6) - KTR*A(7)
    DADT(8)  = KTR*A(7) - KTR*A(8)
    DADT(9)  = KTR*A(8) - KTR*A(9)

    ; Calculating nadir (NADIR), time to nadir (TTN)
    B       = KTR*A(8) - KTR*A(9)
    IF(B.GT.0.AND.TALD.GT.100) THEN     ; TALD>100 is needed to be after the peak, which
                                        appears to be after the dosing due to the time delay
                                        caused by the transit compartments
      DADT(10)      = 1
      DADT(11)      = KTR*A(8) - KTR*A(9)   ; Same derivative as neutrophil compartment as
                                            soon as nadir was passed
    ELSE
      DADT(10)      = 0
      DADT(11)      = 0
    ENDIF
; To calculate nadir and time to nadir for each cycle compartment 10 and 11 are reset and restarted at
        each dosing event using additional rows in the dataset (CMT = -10 and CMT= -11 for reset
        and CMT = 10 and CMT= 11 for restart, EVID = 2 for each of these rows)

$ERROR

    ; Output of amounts
    AA1     = A(1)
    AA2     = A(2)
    AA3     = A(3)
    AA4     = A(4)
    AA5     = A(5)
    AA6     = A(6)
    AA7     = A(7)
    AA8     = A(8)
    AA9     = A(9)
    AA10    = A(10)
    AA11    = A(11)
    AA12    = A(12)
    AA13    = A(13)
    AA14    = A(14)
```

```
    ; Calculating nadir (NADIR), time to nadir (TTN)
    BX      = KTR*A(8) - KTR*A(9)     ; New name needed in $ERROR
    FLG     = 0
    IF(BX.GE.0.AND.TALD.GT.100) FLG = 1
    TTN     = 0
    TTN2    = 0
    NADIR   = 0
    IF(FLG.EQ.1) TTN = TIME - A(10)          ; Time to nadir since first dose
    TTN2    = TTN – LASTD                    ; Time to nadir since last dose
    IF(FLG.EQ.1) NADIR = A(9) - A(11)        ; Nadir neutrophil concentration

    ; Residual variability
    IPRED   = 0.0001
    IF(A(9).GT.0) IPRED = LOG(A(9))
    W       = THETA(3)
    Y       = IPRED + W *EPS(1)
    IRES    = DV - IPRED
    IWRES   = IRES/W

$THETA
    140             ;1 MMT
    5.18            ;2 SL
    0.501           ;3 residual variability
    0.270           ;4 γ
    (0, 0.722, 1)   ;5 ftr
    1.01            ;6 SL_carbo
    32.1            ;7 SL_cis
    (0, 0.506)      ;8 G-CSF on E_drug

$OMEGA
    0   FIX     ;1 IIV MMT              ; IIV = interindividual variability
    0.446       ;2 IIV SL
    1   FIX     ;3 IIV baseline variability
    0   FIX     ;4 IIV γ
    0   FIX     ;5 IIV ftr
    0.193       ;6 IIV SL_carbo
    0   FIX     ;7 IIV SL_cisis

$SIGMA
    1   FIX     ; residual variability

$ESTIMATION PRINT=5 MAXEVAL=99999 METHOD=1 INTER NOABORT POSTHOC SIGDIG=3
            MSFO=MSF067

$COVARIANCE PRINT=E
```

```
$TABLE  ID OCC DAY TIME TALD DOSE DRUG AMT RATE DUR DV CMT EVID MDV PRED IPRED
        RES IRES WRES IWRES CWRES CIWRES C1 AA1 AA2 AA3 AA4 AA5 AA6 AA7 AA8 AA9
        AA10 AA11 AA12 AA13 AA14
        NOPRINT ONEHEADER NOAPPEND FILE=sdtab067

$TABLE  ID OCC DAY TIME TALD MTT SLOPE BASE GAMMA X EFF FEEDB KTR KPROL KSTEM
        EFFPTX EFFPL B FLG TTN TTN2 NADIR CAV1 CAQ CACL CAV2 CAK10 CAK12 CAK21
        CAC1 CIC CICL CIV CIK10 ETA1 ETA2 ETA3 ETA6
        NOPRINT ONEHEADER NOAPPEND FILE=patab067

$TABLE  ID OCC DAY TIME TALD BSA AGE HT WT CLCR BILI AST ALT GGT ALP PROT LASTD
        BSLM V1 V3 KM1 VM1 KM2 VM2 K21 Q
        NOPRINT ONEHEADER NOAPPEND FILE=cotab067

$TABLE  ID TIME SEX SMOK CENT CURRENTP PLATIN ECOG FLGTIME FLGDOSE FLGPK
        FLGN FLGCOV DOSEG DOSEG2 AGEG BILIG MAXOCC PRETRE PREC PRER PRES
        PREM HIST STAGE CMNP CMGLUC CMGCSF CHEMO RADIO CMNP4ID CMNP5ID
        CMGLUCID CMGCSFID CHEMOID RADIOID CHEMOIDS RRADIOIDS BONEL
        NOPRINT ONEHEADER NOAPPEND FILE=catab067
```

10.3.3 Project 3: Tumour growth inhibition model including combination therapy and covariates

```
$SIZES PD=-100                ; to allow for more input variables

$PROBLEM PD Tumour growth inhibition, additive combination, covariates

$INPUT  ID OCC DAY TIME TALD AMT DOSE DRUG RATE DUR SUMDIA DV BSLSD CMT EVID
        MDV LASTD CLCR FLGTIME FLGDOSE FLGPK FLGTUM FLGCOV CENT AGE SEX SMOK
        HT BSA WT BILI CURRENTP PLATIN ECOG LDH V1 V3 KM1 TVVM1 VM1 KM2 VM2 K21
        Q AUC THR DOSEG DOSEG2 AGEG BILIG MAXOCC PRETRE PREC PRER PRES PREM
        HIST STAGE PFST OST CHEMO RADIO CHEMOID RADIOID CHEMOIDS RRADIOIDS
        SURGIDS NTARG NNTARG TARGRES NTARGRES NEWLES ORESI ORESC LIVERL
        BRAINL LYMPL BONEL OTHERL LUNGDIA LIVERDIA BRAINDIA LYMPDIA OTHERDIA
   ; DV = natural logarithm of SUMDIA
   ; BSLSD = sum of diameter at baseline (BSL_SD)
   ; V1 V3 KM1 TVVM1 VM1 KM2 VM2 K21 Q AUC THR are the EBEs/exposure parameters extracted
         from the PK model

$DATA PacliTGprior3Subs3.csv IGNORE=I

   IGNORE(PLATIN.EQ.0)
   IGNORE(CHEMOIDS.EQ.1, RRADIOIDS.EQ.1, SURGIDS.EQ.1)
   IGNORE(TIME.GT.5040)                                  ; 30 weeks

$SUBROUTINES ADVAN6 TOL=5

$MODEL      COMP = (CENTRAL, DEFDOSE)  ; 1 Central paclitaxel compartment
            COMP = (PER1)              ; 2 First peripheral paclitaxel compartment
            COMP = (PER2)              ; 3 Second peripheral paclitaxel compartment
            COMP = (CARBOC)            ; 4 Central carboplatin compartment
            COMP = (CARBOP)            ; 5 Peripheral compartment carboplatin
            COMP = (CIS)               ; 6 Cisplatin compartment
            COMP = (SD)                ; 7 Sum of diameters
            COMP = (TTNX)              ; 8 Time to nadir of tumour diameter
            COMP = (NADIRX)            ; 9 Nadir of tumour diameter
            COMP = (PROG)              ; 10 time to disease progression
            COMP = (SIZE8)             ; 11 Tumour size at week 8

$PK

   ; Paclitaxel pharmacokinetics
   K13      = Q/V1
   K31      = Q/V3
   S1       = V1

   ; Covariate effects
   NLES         = NTARG + NNTARG
   PRE          = 0
   IF(PRETRE.GT.0) PRE = 1
```

```
CHIST       = 1
IF(HIST.EQ.0) CHIST = 1+THETA(4)
IF(HIST.EQ.2) CHIST = 1+THETA(4)
IF(HIST.EQ.3) CHIST = 1+THETA(5)
CAGE        = THETA(6)

; Sum of diameters
GR          = THETA(1) * (1+CAGE*(AGE-65)) * EXP(ETA(1))    ; Growth rate (k_g)
BETA        = THETA(2) * CHIST * EXP(ETA(2))                ; Drug-induced decay (β)
BASE        = EXP(LOG(BSLSD)+THETA(3)*ETA(3))               ; Baseline

A_0(7)      = BASE
A_0(11)     = BASE

IF(NEWIND.LE.1) PD = BSLSD/100*130    ; progressive disease (see RESIST criteria)
IF(NEWIND.LE.1) PROGE = 0             ; progression event

; Platinum concentration on β
BETA2 = (THETA(2) * 0.137)            ; carboplatin

; Carboplatin pharmacokinetics
CAV1        = 20.4 * (WT/70)**0.806
CAQ         = 0.834 * (AGE/31)**(-0.311) * (HT/176)**2.33
CACL        = 6.588 * (CLCR/103.1)**0.57 * (HT/176)**1.43
CAV2        = 32.3
CAK10       = CACL/CAV1
CAK12       = CAQ/CAV1
CAK21       = CAQ/CAV2

; Cisplatin pharmacokinetics
CICL        = 51.7 + 26.3 * (BSA - 1.86)
CIV         = 41.4 + 24.6 * (BSA - 1.86)
CIK10       = CICL/CIV

$DES

; Paclitaxel pharmacokinetics
C1          = A(1)/S1                 ; C_PTX(t)
DADT(1)     = - C1*VM1/(KM1 + C1) + K21*A(2) - C1*VM2/(KM2+C1) + K31*A(3) - K13*A(1)
DADT(2)     = C1*VM2/(KM2 + C1) - K21*A(2)
DADT(3)     = K13*A(1) - K31*A(3)

; Carboplatin pharmacokinetics
DADT(4)     = - CAK12 * A(4) + CAK21 * A(5) - CAK10 * A(4)
DADT(5)     = CAK12 * A(4) - CAK21 * A(5)
CAC1    = A(4)/CAV1               ; C_Carbo(t)
```

```
; Cisplatin pharmacokinetics
DADT(6)     = - CIK10 * A(6)
CIC         = A(6)/CIV              ; C_Cis(t)

; Sum of diameters
EFFPTX      = BETA * C1
EFFPL       = BETA2 * CAC1
EFF         = EFFPTX + EFFPL        ; additive drug effect
DADT(7)     = GR - EFF * A(7)
CT          = A(7)

; Output of time to progression
SLOP        = 1
IF(CT.GE.PD) SLOP=0
DADT(10)    = SLOP
TPD         = A(10)

; Output of week 8 size
IF(T.LT.1344) SLOP2 = GR - EFF * A(7)    ; 8*7*24=1344 h
IF(T.GE.1344) SLOP2 = 0
DADT(11) = SLOP2

; Calculating nadir (NADIR), time to nadir (TTN) (explanation see neutropenia model code)
B           = GR - EFF * A(7)
IF(B.GT.0.AND.TALD.GT.100) THEN
   DADT(8)  = 1
   DADT(9)  = GR - EFF * A(7)
ELSE
   DADT(8)  = 0
   DADT(9)  = 0
ENDIF

$ERROR

; Output of amounts
AA1         = A(1)
AA2         = A(2)
AA3         = A(3)
AA4         = A(4)
AA5         = A(5)
AA6         = A(6)
AA7         = A(7)
AA8         = A(8)
AA9         = A(9)
AA10        = A(10)
AA11        = A(11)
```

```
    ; Relative change of size at week 8
    SIZE        = AA11
    RS8         = 100/BSLSD*SIZE

    IF(AA7.GT.PD)PROGE = 1

    ; Calculating Nadir (NADIR), time to nadir (TTN)
    C1X         = A(1)/S1
    CAC1X       = A(4)/CAV1
    CICX        = A(6)/CIV
    EFFPTXX     = BETA * C1X
    EFFPLX      = BETA2 * CAC1X
    EFFX        = EFFPTXX + EFFPLX
    BX          = GR - EFFX * A(7)
    FLG         = 0
    IF(BX.GE.0.AND.TALD.GT.100) FLG = 1
    TTN         = 0
    TTN2        = 0
    NADIR       = 0
    IF(FLG.EQ.1) TTN = TIME - A(8)
    TTN2        = TTN - LASTD
    IF(FLG.EQ.1) NADIR = A(7) - A(9)

    ; Residual error
    IPRED       = 0.0001
    IF(A(7).GT.0) IPRED = LOG(A(7))
    W           = THETA(3)
    Y           = IPRED + W *EPS(1)
    IRES        = DV-IPRED
    IWRES       = IRES/W

$THETA
    (0, 0.00064)        ; 1 k_g
    (0, 0.00426)        ; 2 β
    (0, 0.17)           ; 3 residual variability
    (1.02)              ; 4 HIST on β
    (1.37)              ; 5 HIST on β
    -0.0522             ; 6 AGE on k_g

$OMEGA
    0.518               ; 1 IIV k_g
    1.59                ; 2 IIV β
    1 FIX               ; 3 IIV baseline variability

$SIGMA
    1 FIX                ; residual variability
```

```
$ESTIMATION PRINT=5 MAXEVAL=99999 METHOD=0 NOABORT POSTHOC SIGDIG=3
        MSFO=MSF251

$COVARIANCE PRINT=E

$TABLE  ID OCC DAY TIME TALD DOSE DRUG AMT RATE DUR DV SUMDIA CMT EVID MDV
        BSLSD LASTD PRED IPRED RES IRES WRES IWRES CWRES CIWRES C1 AA1 AA2 AA3
        AA7 AA4 AA5 AA6 AA8 AA9 AA10 AA11
        NOPRINT ONEHEADER NOAPPEND FILE=sdtab251

$TABLE  ID OCC DAY TIME TALD GR BETA BASE EFF PD PROGE SLOP SLOP2 SIZE RS8 TPD B
        FLG TTN TTN2 NADIR BETA2 EFFPTX EFFPL CAV1 CAQ CACL CAV2 CAK10 CAK12
        CAK21 CAC1 CIC CICL CIV CIK10 ETA1 ETA2 ETA3
        NOPRINT ONEHEADER NOAPPEND FILE=patab251

$TABLE  ID OCC DAY TIME TALD AGE HT BSA WT BILI LDH DPLATIN NLES V1 V3 KM1 VM1 KM2
        VM2 K21 Q AUC THR PFST OST LUNGDIA LIVERDIA BRAINDIA LYMPDIA OTHERDIA
        NOPRINT ONEHEADER NOAPPEND FILE=cotab251

$TABLE  ID TIME CENT SEX SMOK DOSEG DOSEG2 AGEG BILIG MAXOCC FLGTIME FLGDOSE
        FLGPK FLGN FLGCOV FLGTUM PREM HIST STAGE CURRENTP PLATIN ECOG PRETRE
        PREC PRER PRES CHEMO RADIO CHEMOID RADIOID CHEMOIDS RADIOIDS NTARG
        NNTARG TARGRES NTARGRES NEWLES ORESI ORESC LIVERL BRAINL LYMPL
        BONEL OTHERL
        NOPRINT ONEHEADER NOAPPEND FILE=catab251
```

10.3.4 Project 3: Overall survival time-to-event model including covariates

```
$SIZES PD=-100

;Sim_start        ; comment mode switched for simulation
;$SIZES NO=500 LIM6=5000
;Sim_end

$PROBLEM Overall survival

$INPUT  ID OCC TIME TALD CMT DV EVID MDV SIMFLG ARM AGE SEX SMOK HT BSA WT BILI
        PLATIN=DROP ECOG BSLSD MAXOCC PREC PRER PRES HIST STAGE CREA CLCR
        LDH RS FLGPROS
   ; SIMFLAG = 0 for dummy rows needed for simulation (1 row per day), otherwise SIMFLAG = 1
   ; BSLSD = baseline of sum of diameters
   ; RS = relative tumour size at week 8
   ; PLATIN=DROP: patients receiving cisplatin combination therapy were deleted from the dataset
        before

$DATA PacliOS1.csv    IGNORE = I

   ;Sim_start
   IGNORE = (SIMFALG.LE.0)
   ;Sim_end

$SUBROUTINES ADVAN6 TOL=3

$MODEL        COMP = (OS)                    ; 1 Overall survival

$PK

   BASE     = THETA(1) * EXP(ETA(1))     ; μ     ; one ETA needed for NONMEM (fixed to 0)

   ; Covariates
   CECOG  = 0                             ; θ_μ,ECOG=2
   IF(ECOG.LE.1) CECOG = THETA(2)         ; θ_μ,ECOG<2
   CLDH     = THETA(3)                    ; θ_μ,LDH      median LDH = 230 L/U
   CSEX     = 0                           ; θ_μ,male
   IF(SEX.EQ.0) CSEX = THETA(4)           ; θ_μ,female
   CPRES = 0                              ; θ_μ,without
   IF(PRESG.EQ.1) CPRES = THETA(5)        ; θ_μ,with
   CRS      = THETA(6)                    ; θ_μ,RS8      median RS_8 = 69.259
   CBSL     = THETA(7)                    ; θ_μ,BSL median BSL_SD = 7.9

   MU       = BASE + CECOG + CLDH*(LDH-230) + CSEX + CPRES + CRS*(RS-69.259) +
      CBSL*(BSLSD -7.9)       ; μ_g
   SD       = THETA(8)          ; standard deviation ρ
   TX       = EXP(MU)           ; PRED (Survival time)
```

```
    IF(ICALL.EQ.4) THEN                    ; only called during the simulation step
      IF(NEWIND.LE.1) THEN                 ; new individual
            CALL RANDOM (2, R)             ; generate random number
            UEVT = R                       ; save random number
            ALIVE = 1                      ; patient alive
      ENDIF
    ENDIF

$DES
    PDF     = 0                            ; probability density function
    IF(T.GT.0) PDF = 1/(SQRT(2*3.142*SD**2)*T) * EXP(-0.5*((LOG(T)-MU)/SD)**2)
    DADT(1) = PDF
    S       = 1-A(1)                       ; survival function

$ERROR
    AA1     = A(1)
    ST      = 1 - A(1)                     ; survival function (renamed)
    PDFT    = 0                            ; probability density function (renamed)
    IF(TIME.GT.0) PDFT = 1/(SQRT(2*3.142*SD**2)*TIME) * EXP(-0.5*((LOG(TIME)-MU)/SD)**2)
    H       = PDFT/ST                      ; hazard

    IF(DV.EQ.0) Y = ST          ; drop-out event (right censoring)
    IF(DV.EQ.1) Y = PDFT        ; death event

    IF(ICALL.EQ.4) THEN         ; only called during the simulation step
      DV = 0
      TTE = 0
      IF(UEVT.GE.ST.AND.ALIVE.EQ.1) THEN          ; death event
            DV=1
            TTE = 1
            ALIVE = 0
      ENDIF
    ENDIF

$THETA
    (8.14)        ; μ
    (0.87)        ; 2 ECOG on μ
    (-0.00102)    ; 3 LDH on μ
    (0) FIX       ; 4 SEX on μ
    (0) FIX       ; 5 PRES on μ
    (-0.00295)    ; 6 RS_8 on μ
    (0) FIX       ; 7 BSL_SD on μ
    (0, 1.19)     ; 8 Standard deviation ρ

$OMEGA
     0 FIX        ; dummy variable
```

```
;Sim_start : add/remove for simulation
;$SIMULATION (123456789) (12345 UNIFORM) ONLYSIM NOPREDICTION SUB=1000
$ESTIMATION MAXEVAL=99999 METHOD=0 LIKE PRINT=1 SIGL=6 SIGDIG=3 NOABORT
            MSFO=MSF017
$COVARIANCE PRINT=E
;Sim_end

$TABLE  ID OCC TIME TALD CMT DV EVID MDV SIMFLG
            NOPRINT ONEHEADER NOAPPEND FILE=sdtab017

$TABLE  MU SD TX AA1 ST PDFT
            ;Sim_start : add/remove for simulation
            ;TTE ALIVE UEVT
            ;Sim_end
            NOPRINT ONEHEADER NOAPPEND FILE=patab017

$TABLE  HT BSA WT BILI AGE BSLSD CREA CLCR LDH RS
            NOPRINT ONEHEADER NOAPPEND FILE=cotab017

$TABLE  ARM SEX SMOK ECOG MAXOCC PREC PRER PRES HIST STAGE
            NOPRINT ONEHEADER NOAPPEND FILE=catab017
```

11 Acknowledgements

The Graduate Research Training Program PharMetrX - Pharmacometrics and computational disease modelling is gratefully acknowledged for its financial support and the opportunity to expand knowledge in the field of pharmacometric modelling and simulation by fostering the collaboration between academia and industry.

I would like to express my sincere gratitude to:

my supervisor Professor Charlotte Kloft for the exciting project, the freedom to develop it into the direction of my interest, the fruitful discussions where she gave me valuable input, ideas and comments, her long-standing support and encouragement for the project work and beyond,

Professor Wilhelm Huisinga for his valuable insights from the mathematical perspective, his interest and curiosity in my projects,

PD Dr Markus Joerger for regular telephone conferences in which he gave the clinical focus on the project, and his speedily responses to all e-mails,

Professor Ulrich Jaehde, Dr Stefanie Kraff for their input on the project and related publications,

Dr Zinnia Parra-Guillen for her technical and methodological support especially in the beginning of the project,

Dr Niklas Hartung for his discussions giving me the mathematical understanding of the usage of prior information and time-to-event modelling,

the Central European Society of Anticancer Drug Research (CESAR) for providing me with the clinical study data, in particular Max Roessler who helped cleaning the dataset,

Valerie Nock, my industry mentor within the PharMetrX program, for discussions neutropenia, and modelling and simulation in industry,

my colleagues, especially Lena Klopp-Schulze, for scientific discussions and proof reading,

above all I would like to thank my family, friends from Ludwigsburg, Frankfurt and Berlin, and colleagues who all became dear friends, for being always there for me when I needed them, their phone calls and visits, distracting me from work if needed, chocolate supply, in particular Robert Mende for making Berlin a great experience for me and ironing my blouses for conferences, and Danila Burau for saving me from eating convenience food on a daily basis.